UNIVERSIDAD AUTONOMA DE MADRID

Facultad de Ciencias
Departamento de Biología Molecular

Role of SNX27 in protein transport and lipid signaling in cell models of polarized trafficking

María Tello Lafoz

Madrid, September 2016

A dissertation submitted for the degree of Ph.D. in
Molecular Biosciences with international mention

The research presented in this memory was carried out
at the Centro Nacional de Biotecnología/CSIC under the
direction of Isabel Mérida Ph.D.

To my parents

Whatever you do will be insignificant, but
it is very important that you do it.

Mahatma Gandhi

Summary
Resumen

SUMMARY

Sorting nexin 27 (SNX27) belongs to the SNX family of proteins that control intracellular protein trafficking. SNX27 bears a PX (Phox homology) domain that regulates its endosomal localization, a unique PDZ (PSD-95, Dlg1, ZO-1) domain and an atypical FERM (4.1, ezrin, radixin, moesin) domain, which bind short peptide sequence motifs in the cargo protein cytoplasmic domains. SNX27 recycles PDZ-interacting receptors at the neuronal synapse, and its low expression is associated with impaired synaptic function and neurological diseases. T lymphocyte antigen recognition leads to the formation of a highly organized structure termed immune synapse (IS), by analogy with the nervous synapse. SNX27-positive endosomes polarize to the IS, but the role of SNX27 during T cell activation remains unknown.

In this study we investigated SNX27 dynamics and functions during IS formation. We characterized a previously unidentified FERM domain lipid-binding site that enhances SNX27 endosomal localization, and showed that a fraction of SNX27 accumulates at the IS in a PDZ ligand-dependent manner. We used proteomics to identify the SNX27 interactome in IS-forming T cells; a comparative interactome analysis of SNX27 WT and a mutant deficient for PDZ ligand recognition identified various cargoes linked to signaling and cytoskeletal regulation. We demonstrated that SNX27 controls the signaling and trafficking of some of these cargoes including the lipid kinase diacylglycerol kinase ζ (DGKζ) and the epithelial cell-cell junction protein zona occludens-2 (ZO-2). Proteomic analyses also detected the retromer and the actin nucleator WASH complex, and we confirmed that SNX27 acts as a WASH adaptor for PDZ cargoes in T cells. Analysis of *Snx27*$^{-/-}$ mice supported our studies in human T cell lines, underscoring a putative role for SNX27 in sustaining the function of the metabolic regulator mTOR (mammalian target of rapamycin) in activated T cells. This study broadens our knowledge of the SNX27 function in integrating sorting events with endosomal lipid signaling in T lymphocytes, and suggests conservation in the pathways that delimit polarized structures in nervous and epithelial systems during IS formation.

For their migration and invasion, cancer cells also need to form highly organized structures. Cells assemble invadopodia to coordinate the signaling and trafficking that promote increased secretion and matrix degradation. The SNX27 partner WASH, assisted by the exocyst complex, controls integrin and metalloproteinase recycling at invadopodia. The role of SNX27 in invasive cell polarized recycling has nonetheless not been explored. We showed SNX27 localization to invadopodia in a cancer cell line, and addressed the effects of its downmodulation on invasive migration. We identified the phosphatidylinositol (4,5)-bisphosphate-synthesizing enzyme phosphatidylinositol 4-phosphate 5-kinase γ (PIP5K γ), a known modulator of exocyst function, as a SNX27 partner. Our results support a SNX27 function as an endosomal hub that assists lipid modulation in the recycling compartment, and suggest that the frequent amplification of SNX27 in human cancers promotes oncogenic traits in tumor cells.

RESUMEN

Sorting nexin 27 (SNX27) pertenece a la familia de SNX, moléculas que controlan el tráfico intracelular de proteínas; su dominio PX (Phox homology) permite su localización endosomal, mientras que sus dominios PDZ (PSD-95, Dlg1, ZO-1), y FERM (4.1, ezrin, radixin, moesin) atípico unen secuencias peptídicas cortas en los dominios citoplasmáticos de las proteínas cargo. En la sinapsis nerviosa, SNX27 recicla receptores unidos a su PDZ, y su baja expresión está asociada a una disfunción sináptica y a enfermedades neurológicas. Por analogía con dicha sinapsis, se llama sinapsis inmune (SI) a la estructura formada por los linfocitos T tras el reconocimiento antigénico. Los endosomas positivos para SNX27 polarizan a la SI, sin embargo, se desconoce el papel de esta proteína en la activación de las células T.

En este estudio investigamos las dinámicas y funciones de SNX27 durante la formación de la SI. Caracterizamos un sitio de unión a lípidos en el dominio FERM de SNX27 que promueve su localización endosomal, y demostramos que la acumulación de SNX27 en la SI es dependiente de su unión a ligandos de PDZ. Usando una aproximación proteómica identificamos las proteínas asociadas a SNX27 en la SI; comparamos el interactoma de la proteína WT con el de una mutante incapaz de unir ligandos de PDZ, y detectamos varios cargos que regulan la señalización y el citoesqueleto. Además, demostramos que SNX27 controla la señalización y el tráfico de algunos de ellos como la diacilglicerol quinasa ζ (DGKζ) y la proteína de las uniones intercelulares epiteliales zona occludens-2 (ZO-2). Nuestro análisis proteómico también detectó el retrómero y el complejo WASH, y confirmamos que, en células T, SNX27 dirige sus cargos de PDZ hacia el transporte mediado por WASH. Los datos obtenidos en ratones *Snx27*$^{-/-}$ apoyaron los obtenidos en la línea celular T humana Jurkat y pusieron de manifiesto el papel de SNX27 en la activación del regulador metabólico mTOR (mammalian target of rapamycin) en células T activadas. Este estudio amplia el conocimiento sobre la función de SNX27 en la integración del tráfico y la señalización lipídica endosomal en linfocitos T. Además, sugiere que los mecanismos que delimitan las estructuras polarizadas en los sistemas nervioso y epitelial están conservados en células T durante la formación de la SI.

Las células tumorales forman estructuras altamente organizadas para migrar e invadir tejidos; en los invadopodios se coordina la señalización y el tráfico facilitando la secreción así como la degradación de las matrices extracelulares. WASH, ayudado por el complejo del exocisto, recicla integrinas y metaloproteasas en estas estructuras. Sin embargo, no se ha explorado la función de SNX27 en el reciclaje polarizado en células tumorales. En este estudio usamos una línea celular de cáncer de mama para mostrar la localización de SNX27 a los invadopodios, y el efecto de su silenciamiento en la invasión celular. Además, identificamos la asociación de SNX27 con la enzima lipídica reguladora del exocisto fosfatidilinositol 4-fosfato 5-kinasa γ (PIP5K γ). Nuestros datos apoyan la hipótesis de que SNX27 facilita la modulación de lípidos endosomal y sugieren que su amplificación promueve un fenotipo invasivo.

Index

Abbreviations

I. ABBREVIATIONS

5-HT$_{4(a)}$R 5-hydroxytryptamine 4a receptor
ABC ATP-binding cassette
ACOT8 acyl CoA thioesterase 8
AD Alzheimer disease
AMPAR α-amino-3-hydroxy-5-methyl-4-isoxazolepropionic acid
AP-1 activator protein 1
APC Allophycocyanin (flow cytometry)
APC antigen-presenting cell
APPL adaptor protein containing PH domain, PTB domain and leucine zipper motif
AR adrenergic receptor
Arf ADP-ribosylation factor
AU Arbitrary units
Aβ β-amyloid
BAR Bin, amphiphysin, Rvs
BARS brefeldin-A ADP-ribosylated substrate
BIM Bisindolylmaleimide
CASP cytohesin-associated scaffolding protein
CENPJ centromere associated protein J
CHX cycloheximide
CIA circular invasion assay
CIN85 85 kDa Cbl-interacting protein
CMAC 7-amino-4-chloromethylcoumarin
ConA concanavalin A
COPI coat protein complex I
CRIK citron Rho-interacting kinase
CTL cytotoxic T cells
Cx connexin
DAG diacylglycerol
DGK diacylglycerol kinase
DN double negative
Dok1 docking protein 1
DOX doxycycline
DP double positive
DS Down syndrome
ECM extracellular matrix
EEA1 early endosomal antigen 1
ER endoplasmic reticulum
ERC endocytic recycling compartment
ERK extracellular signal-regulated kinase
ERM ezrin/radixin/moesin
ESCRT endosomal sorting complex required for transport
FERM 4.1/ezrin/radixin/moesin
FRAP fluorescence recovery after photobleaching
FSC forward scatter
FYVE Fab1p, YOTB, Vac1, EEA1
FZD Frizzled
GEF guanine nucleotide exchange factor
GIRK G protein gated inward rectifying potassium channels
GIT G protein-coupled receptor kinase-interacting protein
GJ gap junction
GLUT1 glucose transporter 1
GMFI geometric mean fluorescence intensity
GO gene ontology
GPCR G protein-coupled receptor
GTPase small guanosine triphosphatases
HBSS Hank's balanced salt solution
HPV human papillomavirus
Hrs hepatocyte growth factor-regulated tyrosine kinase substrate
IFT intraflagellar transport system
IL interleukin
IS immune synapse
ITC isothermal titration calorimetry
Kidins220 kinase D-interacting substrate of 220 kDa

LAT transmembrane adaptor linker for activation of T cells
Lck lymphocyte-specific protein tyrosine kinase
LFA-1 lymphocyte function-associated antigen 1
LN lymph nodes
MAGUK membrane-associated guanylate kinase
MAPK mitogen-activated protein kinase
MARCKS myristoylated alanine-rich C-kinase substrate
MCT1 monocarboxylate transporter 1
MEK MAPK/ERK kinase
MFI mean fluorescence intensity
MHC major histocompatibility complex
MICAL-L1 microtubule-associated mono-oxygenase, calponin, and LIM domain containing-like 1
MMP matrix metalloproteinases
MRP4 multidrug resistance-associated protein 4
MT microtubule
MT1-MMP transmembrane type 1 MMP
MTM myotubularin
MTOC microtubule-organizing center
mTOR mammalian target of rapamycin
mTORC1 mTOR complex 1
MVB multivesicular bodies
NF-κB nuclear factor κB
NFAT nuclear factor of activated T cells
NHE3 Na^+/H^+ exchanger 3
NK natural killer
NLS nuclear localization signal
NMDAR N-methyl-D-aspartate receptors
NSF N-ethylmaleimide-sensitive factor
PA phosphatidic acid
PAK p21-activated kinase
PDK1 phosphoinositide-dependent kinase 1
PDZ PSD-95, Dlg1, ZO-1
PDZ-bm PDZ-binding motif
PE phycoerythrin
PFA paraformaldehyde
PH pleckstrin homology
PHLPP PH domain and leucine rich repeat protein phosphatase
PIK PtdIns kinase
PIPase PtdIns phosphatase
PIPK PtdInsP kinase
PIX p21-activated kinase-interactive exchange factor
PKC protein kinase C
PKD protein kinase D
PLC phospholipase C
PLD phospholipase D
PM plasma membrane
PMA phorbol 12 myristate 13-acetate
PS1 preselinin 1
PSD-95 postsynaptic density protein 95
PtdIns phosphatidylinositol
PtdInsP phosphatidylinositol phosphate
PTEN phosphatase and tensin homolog
PTHR parathyroid hormone receptor
PX phox homology
RA Ras association
Rab Ras-related in brain
RasGRP Ras guanyl nucleotide-releasing protein
RCP Rab-coupling protein
Rhod rhodamine
RLU relative luciferase units
RPMI Roswell Park Memorial Institute
Rps6 ribosomal protein S6
RT room temperature
S6K Ribosomal protein S6 kinase
SEE *Staphylococcus* enterotoxin E

SEM standard error of the mean

SH Src homology

SH3KBP1 SH3-domain kinase binding protein 1

SHIP SH2-containing Ins 5'-phosphatase

SHKBP1 SH3KBP1 binding protein 1

SMAC supramolecular activation clusters

SNARE soluble NSF attachment protein receptor

SNX sorting nexin

SOS son of sevenless

SP simple positive

SSTR5 somatostatin receptor subtype 5

TCR T cell receptor

Tf/TfR transferrin/ transferrin receptor

TGFβ transforming growth factor

TGN *trans*-Golgi network

TIRF total internal reflection fluorescence

Tks5 Tyr kinase substrate with five SH3 domains

VAMP7 vesicle-associated membrane 7

VPS vacuolar protein sorting-associated protein

WASH WASP and SCAR homologue

WASP Wiskott-Aldrich syndrome protein

XPR1 xenotropic and polytropic murine leukemia virus receptor

ZO zona occludens

Introduction

II. INTRODUCTION

1. LIPID MODULATION IN ENDOSOMAL COMPARTMENTS

1.1. Lipids and membrane trafficking

Intracellular membrane traffic comprises a network of pathways that distribute proteins and other macromolecules among different cell organelles, mostly by vesicular transport. A vast number of complex mechanisms regulate intracellular trafficking, which indicates the importance of this process for correct cell function. The cargo selection systems are coupled to the machinery for vesicle budding, scission, coating and fusion, and all are tightly regulated to ensure rapid, accurate delivery of cargo molecules. Rab (Ras-related in brain) GTPases (small guanosine triphosphatases) and lipids are important for the orchestration of cytoskeletal and membrane remodeling. Rab proteins are well-known molecular switches that regulate traffic between organelles, and lipids control physical properties of membranes directly and through the recruitment of curvature-generating or -sensing proteins, as well as by regulating cytoskeleton-associated molecules (reviewed in [8, 151]). Each intracellular organelle can be identified by the presence of a specific subset of lipids and Rab GTPases (reviewed in [75, 79]).

1.1.1. Phosphoinositides

Phosphoinositides are derived from the phosphorylation of phosphatidylinositol (PtdIns), and consist of a glycerol moiety with two fatty acid chains that allow insertion into lipid membranes, and an inositol headgroup that can be phosphorylated at D-3, D-4 and/or D-5 positions (Fig I1A, bottom). Although the exact subcellular distribution of the phosphoinositide species is not completely understood, the use of fluorescently tagged biosensors in cell imaging studies has contributed substantially to tracking their location in distinct subcellular compartments or domains within compartments (reviewed in [75, 79]) (Fig I1B).

PtdIns 4,5-bisphosphate (PtdIns(4,5)P_2), and PtdIns 3,4,5-triphosphate (PtdIns(3,4,5)P_3) are enriched at the plasma membrane (PM) and the endocytic recycling compartment (ERC), where they participate in nearly all events that involve membrane remodeling. PtdIns(4,5)P_2 promotes the recruitment and regulation of endocytic proteins such as the clathrin adaptors AP-2 and β-arrestin, the membrane fission regulator dynamin, or cytoskeleton-associated proteins involved in internalization and exocytosis including the Arp2/3 activator N-WASP (neural Wiskott-Aldrich syndrome protein) (reviewed in [79]).

Following endocytosis, PtdIns(4,5)P_2 and PtdIns(3,4,5)P_3 must be removed to allow the dissociation of endocytic factors. This function is carried out by PtdIns5-phosphatases (PI5Pase) such as synaptojanin or SHIP (SH2-containing Ins 5'-phosphatase), which generates the PtdIns(3,4)P_2 present in the early endocytic pathway (reviewed in [224]). Sequential dephosphorylation by PtdIns4-phosphatases (PI4Pase) generates PtdIns 3-phosphate (PtdIns3P), the phosphoinositide that characterizes the early endosomes [294]; the majority of this lipid is nonetheless produced by the class III PtdIns 3-kinase (PI3K) termed VPS34 (vacuolar

protein sorting-associated protein 34) [285] (Fig I1A,B). PtdIns3P-binding domains such as FYVE [Fab1, YOTB, Vac1, EEA1 (early endosomal antigen 1)] and PX (phox homology) are found in a variety of endosomal proteins that regulate membrane tethering and fusion, microdomain formation, cytoskeleton interaction and cargo transport; these include EEA1, Hrs [hepatocyte growth factor-regulated tyrosine kinase substrate, which is a component of ESCRT (endosomal sorting complex required for transport)], and the sorting nexins (SNX) (reviewed in [65, 66]). PtdIns3P effectors are also important for autophagosome formation and maturation (reviewed in [68]).

PtdIns3P can be dephosphorylated at the endosomal surface by members of the myotubularin (MTM) family (reviewed in [273]), degraded within the lumen of multivesicular bodies (MVB), or phosphorylated to PtdIns(3,5)P_2 by the PIKfyve kinase (reviewed in [223]). PtdIns(3,5)P_2 localizes to late endocytic compartments and to MVB, where it triggers vesicle budding and controls their size as well as protein sorting (reviewed in [295]) (Fig I1A,B).

PtdIns 4-phosphate (PtdIns4P) is generated in the secretory compartments, where it binds to proteins that control vesicle budding and membrane dynamics, and regulates vesicle-mediated export (reviewed in [127]); in the *trans*-Golgi network (TGN), PtdIns4P production by PtdIns 4-kinase (PI4K) facilitates cargo release from the retromer, which mediates protein transport from the endocytic compartment [185, 242] (Fig I1A,B).

1.1.2. Diacylglycerol and phosphatidic acid

Diacylglycerol (DAG) and phosphatidic acid (PA) are also important membrane constituents (Fig I1C). Both lipid species are major biosynthetic precursors of phospholipids and intermediates of the PtdIns cycle, but are also immediately implicated in membrane trafficking. Both are conical-shaped lipids and thus directly assist the negative membrane curvature necessary for vesicle fission and fusion; additionally, these lipids regulate intracellular transport indirectly by recruiting and/or activating proteins (reviewed in [44]). On the one hand, PA generation collaborates with membrane-binding proteins such as BARS (brefeldin-A ADP-ribosylated substrate) that bend membranes to promote vesicle fission [352]. PA also binds and/or activates proteins involved in membrane traffic control. These include Arf (ADP-ribosylation factor) family members, PIP5K (PtdIns4P 5-kinase), and NSF (N-ethylmaleimide-sensitive factor) [176, 205]. On the other hand, DAG controls the secretory pathway mainly by regulating the Ser/Thr kinase PKD (protein kinase D, also termed protein kinase C μ). PKD activation promotes vesicle formation and fission at the TGN [18, 191] as well as MVB maturation, which involves intraluminal exosome nanovesicle biogenesis and secretion [4, 215]. DAG is also needed at the *cis*-Golgi for the biogenesis of COPI (coat protein complex I)-coated vesicles [11, 99]. In addition, DAG participates in exocytosis through regulation of the membrane fusion steps that involve SNARE (soluble NSF attachment protein receptors) complex assembly. In neurons, direct DAG binding or DAG-dependent activation of PKC (protein kinase C) activates several components of the Munc family of proteins, and thus enhances vesicle priming and neurotransmitter release [17, 25, 265, 347].

Ordered lipid segregation in endosomal membranes drives directional vesicle and cargo trafficking from donor to acceptor membranes, facilitated by modification of physical membrane properties and recruitment of the budding and fusion machinery. Phospholipids can rapidly diffuse within, but not between, membranes, so their spatiotemporal restriction is mainly regulated by their interconversion through lipid kinases and phosphatases. The correct activation of lipid modifying enzymes is essential for membrane trafficking and their deregulation has been linked to a number of human diseases (reviewed in [28, 174, 333]).

Our group studies the DAG kinases (DGK), which phosphorylate DAG and transform it to PA (Fig I1C). DGK are potential drug targets for cancer, epilepsy, autoimmunity, cardiac hypertrophy, hypertension and type II diabetes. Ten mammalian DGK isoforms have been identified and classified into five different subtypes on the basis of their regulatory domains (reviewed in [221, 277]). Of all the DGK family components, the DGKα isoform accounts for most descriptions of these enzymes in the control of membrane and protein trafficking. PA generation by DGKα facilitates the biogenesis of tubular recycling endosomes and the recycling of class I MHC (major histocompatibility complex) molecules through MICAL-L1 interaction (microtubule-associated mono-oxygenase, calponin, and LIM domain containing-like 1) [348];

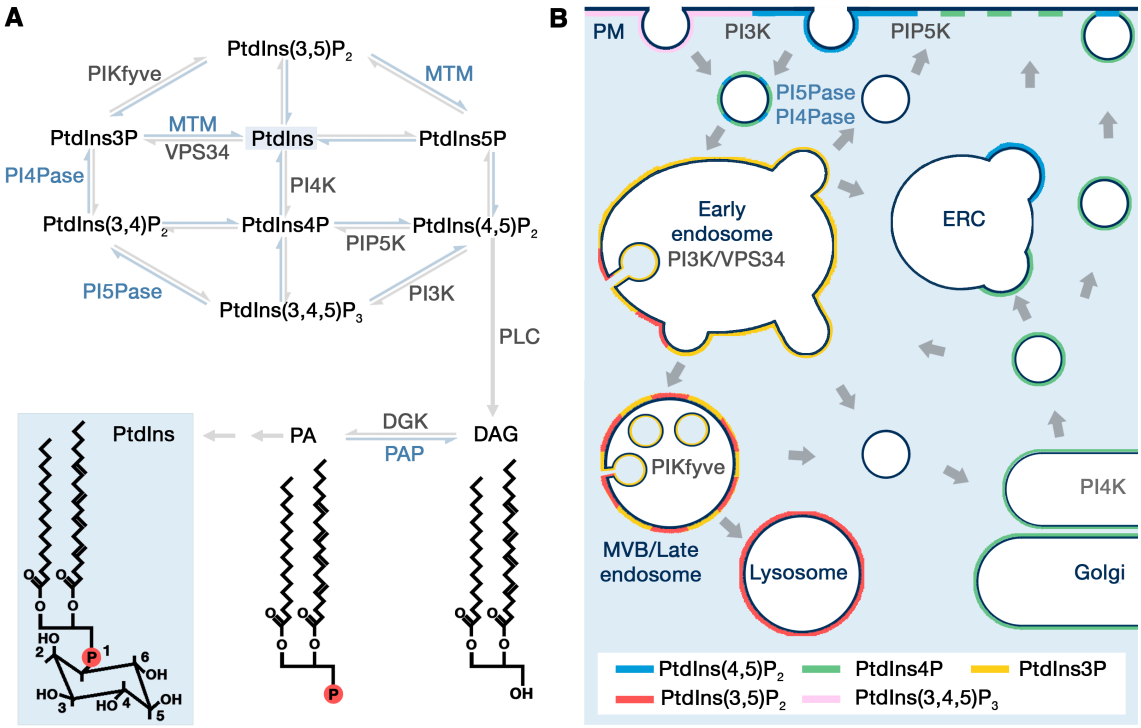

Fig I1. Phospholipid distribution in intracellular membrane organelles

(**A**) Phosphatidylinositol (PtdIns) is phosphorylated at distinct sites to generate phosphoinositide species (**B**) that segregate to the subcellular organelles (PM, plasma membrane; ERC, endocytic recycling compartment; MVB, multivesicular bodies). Lipid kinase (enzyme names in grey) and phosphatase activity (enzyme names in blue) maintain intracellular lipid distribution (see text for details). (A, bottom) Structure of PtdIns, diacylglycerol (DAG) and phosphatidic acid (PA). DAG and PA are interconverted by DAG kinase (DGK) and PA phosphatase (PAP) activity.

DGKα also regulates membrane tethering of the Rab11 effector RCP (Rab-coupling protein) and thus controls integrin recycling [263]. As a negative DAG modulator, DGKα in T lymphocytes limits MVB maturation and exosome secretion in part by controlling the DAG effector PKD [215]. The β, δ, and γ isoforms of DGK were identified as potential regulators of endocytosis and recycling in a large kinome screening [252]. In epithelial cells, DGKδ suppresses endoplasmic reticulum (ER) traffic to Golgi [233]. The DGKζ isoform controls transferrin receptor (TfR) trafficking [271] and was identified as a Golgi architecture regulator in an RNAi screening, DGKζ knockdown resulted in dramatic Golgi fragmentation [57].

1.2. Endosomal lipid signaling

Endocytosis was originally considered a mechanism for signal attenuation through internalization of unstimulated or ligand-associated cell surface receptors and their subsequent recycling or degradation. The endosomes are now also recognized as platforms that sustain cell signaling. The endocytosed ligand-associated receptors remain active throughout the endocytic pathway, where they converge with activated molecules from other routes to allow signal crosstalk. Receptor access to new substrates and scaffolds located exclusively in endosomal compartments constitutes endosome-specific signaling (reviewed by [286, 303]; for an extensive review, see [296]).

There is a growing list of pathways that involve protein localization to endosomes for the control of signal transduction. Several components of major signal transduction cascades are located at the endosomes, including those regulated by lipids such as the Akt, the PKC and the

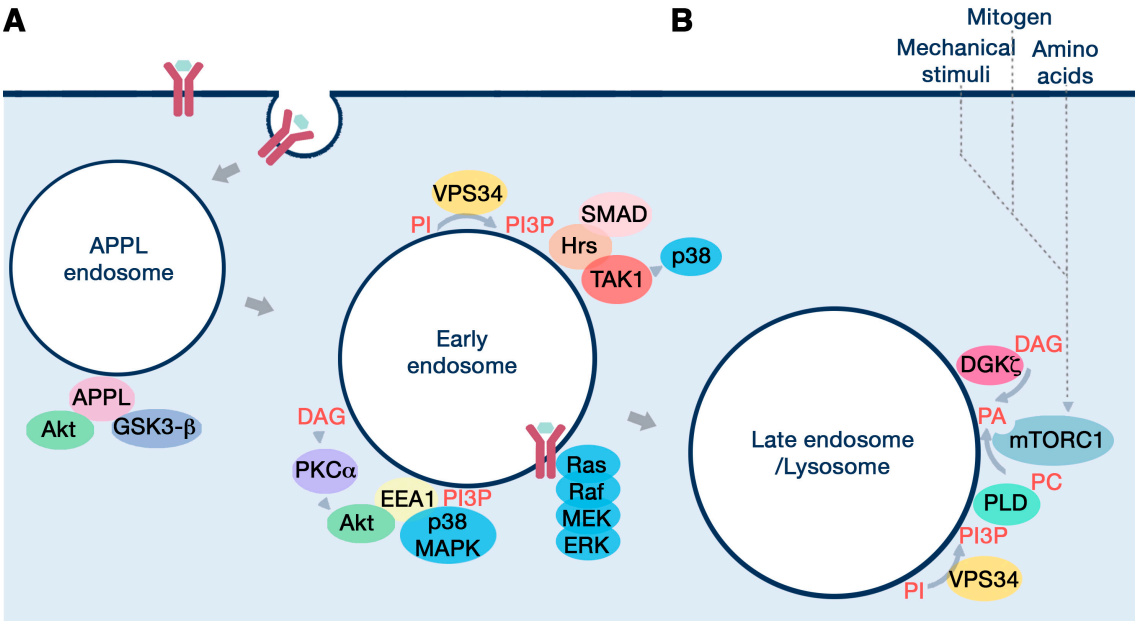

Fig I2. Signal crosstalk in endocytic compartments

(**A**) The APPL adaptors in pre-early endosomes, as well as PI3P-binding protein adaptors in early endosomes act as scaffolds for endosomal signaling and allow signal crosstalk (see text for details). (**B**) In response to serum, amino acid or mechanical stimulation, mTOR translocates to lysosomes. Phosphatidic acid (PA) generated by phospholipase D (PLD), and possibly by diacylglycerol kinase (DGK), activates mTOR at this compartment.

ERK (extracellular signal-regulated kinase) MAPK (mitogen-activated protein kinase) pathways (reviewed in [82, 303]) (Fig I2A). The spatiotemporal restriction of lipids is thus important for modulating local signaling. A subset of PtdIns3P-negative pre-early endosomes contains the APPL1/2 proteins (adaptor protein containing PH domain, PTB domain and leucine zipper motif 1 and 2), which are adaptors that interact with receptor and signaling molecules. They modulate signaling of pathways such as the Akt pathway [283, 343]. Although the APPL endosomes constitute a stable cargo-sorting compartment [167], a fraction of these vesicles serve as intermediates en route to the early endosomes. PtdIns3P generation by VPS34/PI3K promotes the switch from APPL1-dependent signaling to that controlled by PtdIns3P-binding scaffold proteins such as Hrs and EEA1 [367]. Hrs mediates crosstalk between the TGF-β (transforming growth factor β) and MAPK pathways [226], and EEA1 controls that between MAPK and Akt pathways [236] (reviewed in [247]) (Fig I2A).

The mTOR (mammalian target of rapamycin) Ser/Thr kinase acts as a signaling hub to control cell growth; it receives signals from growth factors and nutrients, and regulates the balance between protein synthesis and autophagy. Signal-mediated PI3K (class I)-dependent PtdIns(3,4,5)P_3 generation at the PM activates the classical mTOR complex 1 (mTORC1) pathway and inhibits autophagy, whereas pharmacological inhibition of mTORC1 by rapamycin treatment induces autophagy (reviewed in [171]). The lipid second messenger PA binds directly to the domain in mTOR that is targeted by rapamycin, and activates mTOR in response to serum and mechanical stimulation [93, 357] (Fig I3). During amino acid stimulation, mTORC1 localizes to lysosomes [104, 279](reviewed by [26]) and is activated in a VPS34/PI3K (class III)-dependent manner [38]. PA is generated in endosomal membranes by phospholipase D (PLD1), which bears a PI3P-binding PX domain [305, 356] (Fig I2B); studies nonetheless show that PLD1 inhibition prevents autophagosome formation [69]. The alternative source of PA, DGK, specifically the DGKζ isoform, activates PA-mTOR signaling in response to mechanical or serum stimuli and limits mTORC1 sensitivity to rapamycin treatment [12, 325, 358]. The *Drosophila* and *Caenorhabditis elegans* DGKζ homologs *rdgA* and *dgk-5* also control TOR function [190].

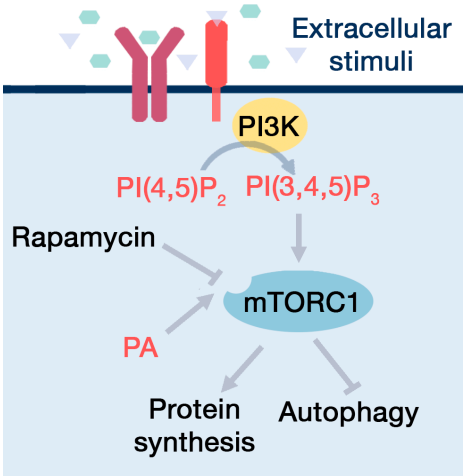

Fig I3. mTOR regulates protein synthesis and autophagy

The mTOR Ser/Thr kinase controls cell growth. Extracellular stimuli trigger PI3K-dependent PtdIns(3,4,5)P_3 generation at the plasma membrane and activation of the classical mTOR complex 1 (mTORC1) pathway leading to protein synthesis and autophagy inhibition. Production of phosphatdic acid (PA) also activates the mTOR pathway through its binding to the same domain in mTOR that is targeted by the pharmacological inhibitor rapamycin.

DGK also modulate cell signaling through DAG consumption (reviewed in [221]). Several DAG-responsive proteins localize in endomembranes, including components of the classical and the novel PKC subfamilies and the Ras guanine nucleotide exchange factor (GEF) termed RasGRP1 (Ras guanyl nucleotide-releasing protein 1). The classical PKCα and PKCβII and the novel PKCδ isoform localize to the ERC and control signaling of endocytosed receptors [5, 13, 23, 153, 261]. In smooth muscle cells, PKCα specifically regulates EEA1-dependent Akt signaling [236]. In cytotoxic T cells, PKCδ additionally localizes to secretory lysosomes and transduces signals necessary for polarized granule secretion [206]. DAG is present in bacteria-containing and rapamycin-induced autophagosomes and, although PKCδ localization to autophagosomes has not been studied, DAG-mediated activation of PKCδ induces autophagy [289]. RasGRP1, which is expressed in lymphocytes, keratinocytes and in some cells of the brain, is located at DAG-enriched membranes such as those of the ER and Golgi compartments. Stimulus-dependent DAG generation at the PM leads to RasGRP1 and PKC translocation to this site (reviewed in [164]). The control of RasGRP and PKC dynamics and activation by DGK has been previously examined in the context of the PM [119, 120, 183]. Further studies are nonetheless required to determine whether DGK modulates DAG/PKC/RasGRP signaling in endomembranes.

2. CELL MODELS OF POLARIZED TRAFFICKING

The correct function of the intracellular trafficking routes is of particular importance in polarized cells, which rely on formation of an active membrane traffic zone to carry out their specialized functions efficiently. In addition to the classical examples of neuron polarity and epithelial cell apicobasal polarity, other models of cell-cell or cell-extracellular matrix (ECM) contacts show a notable degree of polarization (reviewed in [84, 175, 345]).

2.1. T cell activation and immune synapse formation

T lymphocytes are cells specialized in pathogen recognition through the T cell receptor (TCR), which recognizes antigen-derived peptides bound to MHC proteins on the surface of antigen-presenting cells (APC). TCR stimulation triggers formation of a highly organized structure termed the immune synapse (IS) by analogy with chemical synapses in the nervous system [84].

2.1.1. Signaling at the immune synapse

After antigen recognition, the IS acts as a signaling platform; the TCR activates Src family kinases and recruits the adaptor molecules that lead to the activation of additional signaling molecules, including phospholipase C-γ1 (PLC-γ1) [50]. PLC-γ1 hydrolyzes PtdIns(4,5)P_2 in the PM to generate inositol 1,4,5-triphosphate (Ins(1,4,5)P_3) and DAG; soluble Ins(1,4,5)P_3 production leads to triggering of the Ca^{2+}/calcineurin/NFAT (nuclear factor of activated T cells) signaling pathway [131]. DAG generated at the PM stabilizes and activates various targets including components of the PKC family, regulators of the GTPases of the Ras and Rac families [44] such as RasGRP1 [86], which promotes Ras/ERK activation and AP-1 (activator protein 1)-dependent transcription. Although antigen-stimulated generation of Ca^{2+} and DAG drives a transcriptional program for the expression of activation-induced genes [159], costimulatory molecules such as CD28 are needed to trigger the full T cell activation program; CD28 binding of APC-presented B7 ligands activates signaling molecules such as PI3K or PKCθ, a PKC isoform that requires DAG generation for full competence. These in turn trigger the activation of the nuclear

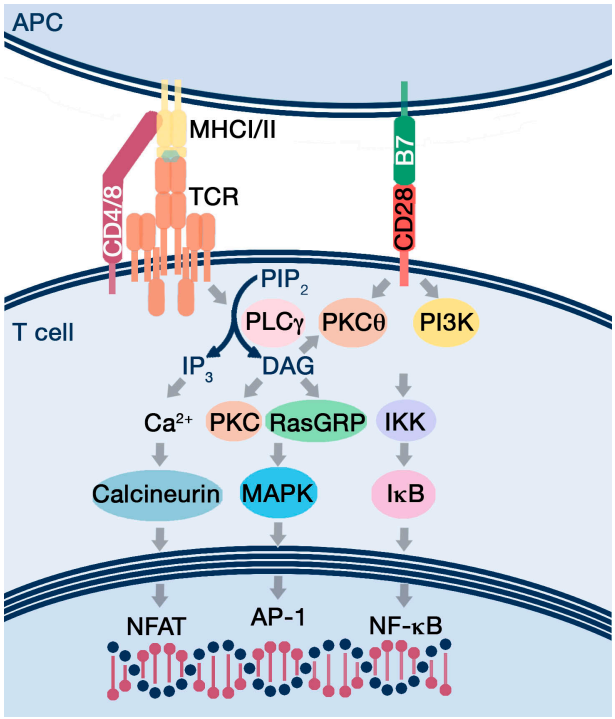

Fig I4. TCR-mediated signal transduction

Antigen-induced stimulation of the TCR triggers PLCγ-mediated hydrolysis of PtdIns(4,5)P_2 (PIP_2), which leads to Ins(1,4,5)P_3 (IP_3) and DAG generation. These two mediators stimulate the Ca^{2+}-NFAT and Ras-ERK-AP-1 pathways, resulting in target gene transcription. Costimulatory receptors such as CD28 promote activation of the PKCθ-NF-κB pathway.

factor κB (NF-κB) family of transcription factors [173, 269], which contribute to the immune response by allowing transition to a metabolically active state that permits cell proliferation and effector functions (reviewed in [108]) (Fig I4). DAG-regulated pathways are thus necessary for T cell function, and must be tightly controlled. DGKα and DGKζ are the two main DGK isoforms expressed in T cells, and both contribute to terminate DAG signaling downstream TCR activation by limiting the DAG-mediated recruitment of RasGRP1 to the PM. They are not fully redundant, with studies suggesting a dominant role for DGKζ in suppressing the Ras/ERK signaling pathway after antigen recognition. DGKζ indeed additionally controls the activation and the transient translocation to the IS of PKCα, another DAG effector that participates in Ras-ERK activation ([119, 120], reviewed in [220]).

2.1.2. Membrane and cytoskeletal remodeling

During IS formation, T cell signal transduction is facilitated through the reorganization of signaling molecules in supramolecular activation clusters (SMAC) [227], which are designated according to their location at the T cell-APC contact area. Clustered TCR and associated signaling proteins localize to the central zone (cSMAC) and are surrounded by cell-cell adhesion proteins that form a peripheral ring (pSMAC). The outermost region is termed distal SMAC (dSMAC) and was established as the site of proteins with large ectodomains, such as CD43 and CD45 (reviewed in [85]) (Fig I5A). Later studies nonetheless describe the dSMAC as a lamellipodium-like area of active membrane movement where new TCR microclusters form after antigen engagement and show centripetal movement towards the pSMAC and cSMAC [166, 331]. This relocation is an actin-dependent process reminiscent of retrograde actin flow during cell spreading and migration. Cytoskeletal rearrangement is indeed essential for mature IS formation; in addition to the centripetal flow of F-actin at the dSMAC, actin filaments are also found at the pSMAC, where they anchor to integrins to prevent filament movement and to

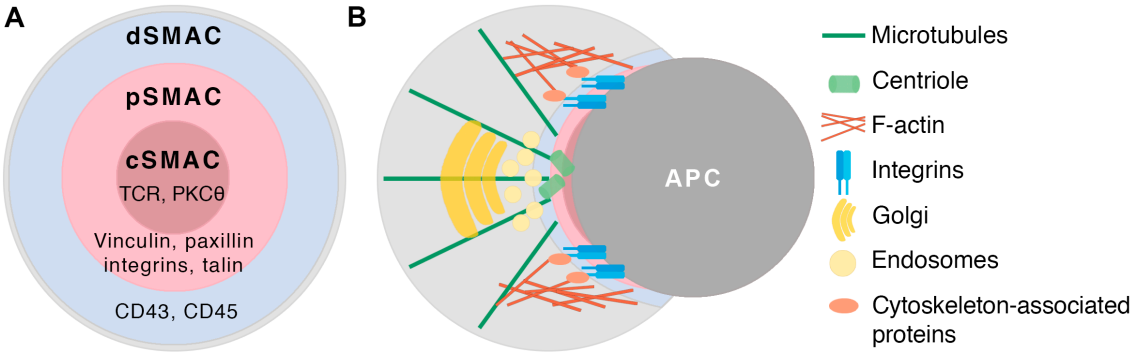

Fig I5. Immune synapse structure and polarization of intracellular organelles

(**A**) The immune synapse forms at the T cell-antigen presenting cell (APC) contact area, where signaling and adhesion molecules are reorganized in central, peripheral and distal supramolecular activation clusters (c-, p-, and dSMAC, respectively). (**B**) The T cell also reorients intracellular organelles towards the APC. These include the microtubule-organizing center (MTOC) and the recycling and secretory compartments.

sustain the adhesion ring (reviewed in [85]). Another type of F-actin organization structure termed actin foci were recently characterized in T cells as necessary scaffolds for Ca^{2+} and distal TCR signaling [177].

Cytoskeletal remodeling is necessary not only for redistribution of signaling receptors and molecules in the vicinity of the T cell-APC contact area, but also for polarization of intracellular organelles; the microtubule-organizing center (MTOC), the Golgi apparatus, and the endosomal compartments are reoriented towards the contact site [7, 71, 106, 178, 245] (Fig I5B). T cell reshaping during IS formation thus involves rapid changes in polarity and architecture of both the microtubule (MT) and actin cytoskeletons. Many scaffolds and signals involved in the control of T cell polarization have been elucidated and include some of the classical epithelial polarity proteins [175, 201]. Lipid signaling has a notable role in the coordination of cytoskeletal structure and polarity. Phospholipids such as PtdIns(4,5)P_2 or PtdIns(3,4,5)P_3 modulate T cell rigidity at the IS [314] and control actin architecture [181], respectively. DAG drives MTOC polarization, and DGK inhibition destabilizes synaptic DAG accumulation and impairs MTOC recruitment to the IS [262]. The activation and localization of these lipid modulatory enzymes are thought to sustain the membrane lipid gradient that drives T cell reorientation via a mechanism analogous to direction-sensing during migration of leukocytes and Dictyostelium ([262], reviewed in [148]).

Many lipid species are essential for T cell polarization and signal transduction. Similarly to epithelial cells, the reorganization of glycosphingolipids with cholesterol to form the membrane microdomains termed lipid rafts also participates in signaling and intracellular transport in T cells [3]. Although the participation of lipid rafts in PM micro- and nanodomain functions was debated, the role of membrane compartmentalization in the control of immune cell spatiotemporal responses and specialized functions continues to be studied [83, 188, 292]. Recent studies indicate that redirection of vesicular traffic to the T cell-APC contact area after TCR engagement assists in the formation of membrane signaling nanoterritories [302].

2.1.3. Vesicle trafficking at the immune synapse

Increasing evidence supports the relevance of the intracellular transport pathway for T cell activation. Vesicle fusion and continuous protein recycling cooperate to regulate signal intensity and duration ([302] reviewed in [245]), and endosomal transport of TCR to the IS is a major source of TCR replenishment after its exhaustion and endocytosis-mediated downregulation [71]. Other receptors and membrane-associated TCR signaling mediators are also partitioned between the PM and endocytic compartments during IS formation. These include the TfR [20], Lck (lymphocyte-specific protein tyrosine kinase) [87], and LAT (transmembrane adaptor linker for activation of T cells) [32], among others (see also review in [245]). The IS is thus used as a model to study the role and dynamics of different molecules in activation-induced polarized recycling. Although first applied to T and B cells of the adaptive immune system, the concept of the IS has expanded to cells of the innate immune system such as natural killer (NK) cells or phagocytes [21, 73]. The IS is not only considered a polarized model for recycling, but also for

secretion. APC-targeted exocytosis of cytokines by helper T cells and of cytotoxic granules by cytotoxic T cells (CTL) or NK cells, as well as T cell-APC information transfer through exosomes and microvesicles are crucial for their effector functions [7, 58, 128, 225].

While the prominent role of vesicle trafficking during IS formation is widely accepted, its regulatory mechanisms remain to be fully understood. Receptor-triggered signals elicit and sustain rapid endosomal polarization to the IS, which correlates with that of the MTOC, and is in fact MT polymerization-dependent in some cell types [71]. Although MT polymerization is needed for secretion by cytolytic cells [311], cytokine release by CD4 T cells requires local actin remodeling [53, 149, 310]. In addition to these cytoskeletal components, the endosomal machinery also participates in regulation of IS-directed trafficking. Most research efforts focus on determining the molecular mechanisms that drive TCR endosomal dynamics; the growing list of TCR trafficking regulators includes several members of the Rab GTPase family such as Rab4, Rab11 and Rab35, the endosomal actin nucleation-promoting factor WASH (WASP and SCAR homologue), some of the vesicle fusion mediators including SNARE, the UNC-119 adaptor, and even the intraflagellar transport system (IFT) ciliary protein IFT20 (reviewed in [245]). Further studies are needed to fully understand the complex network of pathways that facilitate trafficking not only of the TCR, but also of other proteins that contribute to T cell activation.

2.2. Cell migration and invasion

To carry out their physiological functions in response to pathogens or in inflammation, immune cells develop plasticity that allows the transition from a migratory to a static mode of action. Cytoskeletal rearrangement and membrane remodeling in these cells allow turnover of substrate adhesions and formation of transient, organized structures such as the IS or the podosome, a site of protease-dependent focal degradation linked to extravasation [43]. During migration and invasion, cancer cells exploit these mechanisms shared with untransformed cells to attain aggressive behavior.

In migrating cells, polarity is established by reorganization of cytoskeletal and membrane proteins [156, 332]. Signaling, polarity and adhesion protein traffic is directed to the cell leading edge, where large clusters of transmembrane receptors, integrins and cytosolic proteins connect the ECM with the actin cytoskeleton. These structures, termed focal adhesions, assemble continuously at the leading edge and disassemble at the trailing edge, making integrin trafficking particularly necessary for sustained migration (Fig I6A) [46, 48, 103, 266, 327]. Several components of the vesicular trafficking machinery are associated to the control of integrin traffic to the cell front, including Rab4, Rab11 and Rab25 [46, 48], some Rab GTPase-interacting proteins such as the Rab11 effector RCP [47], and the exocyst complex, which mediates docking of post-Golgi and endocytic recycling vesicles at the PM [192]. In this model of polarized trafficking, lipid modulation also coordinates cytoskeleton and membrane remodeling. PtdIns(4,5)P_2 production by PIP5Kγ facilitates exocyst complex assembly and promotes integrin trafficking in directionally migrating cells [322]. PA generation by DGKα regulates tethering of RCP to pseudopods in

migrating cancer cells and thus controls integrin recycling and tumor invasiveness [263]. Lipid rafts are also involved in adhesion protein internalization and recycling, as well as in regulation of focal adhesion disassembly [339, 340].

In tumors, some migrating cells with an invasive phenotype form invadopodia, PM protrusions that promote attachment to and degradation of the ECM and assist tumor aggressiveness (Fig I6B). During invadopodium formation, membranes and proteins reorganize into a bull's eye-structure, and metalloproteinases (MMP) are rapidly recycled and secreted at this site. Extracellular microenvironmental stimuli trigger intracellular signaling pathways, leading to localized F-actin remodeling and recruitment of several proteins including the actin regulators cortactin, cofilin and the Arp2/3 activator N-WASP, and adaptors such as Tks5 (Tyr kinase substrate with five SH3 domains). The actin core is surrounded by a ring containing integrins, paxillin and vinculin, among other adhesion proteins. These structures are not considered mature until functional accumulation of the transmembrane type 1 MMP (MT1-MMP) is observed at the core of the invadopodia (reviewed in [232]) (Fig I6C,D)

Mechanisms of MT1-MMP localization to invadopodia are still being studied, but intracellular trafficking is known to be major regulator of invadopodia maturation. Similarly to integrins, cell surface levels of MT1-MMP are regulated by clathrin- and caveola-mediated endocytosis and subsequent transport to endosomal or lysosomal compartments for recycling or degradation, respectively. MT1-MMP delivery to invadopodia is controlled by cortactin and several components of the exocytic machinery, including the SNARE protein vesicle-associated

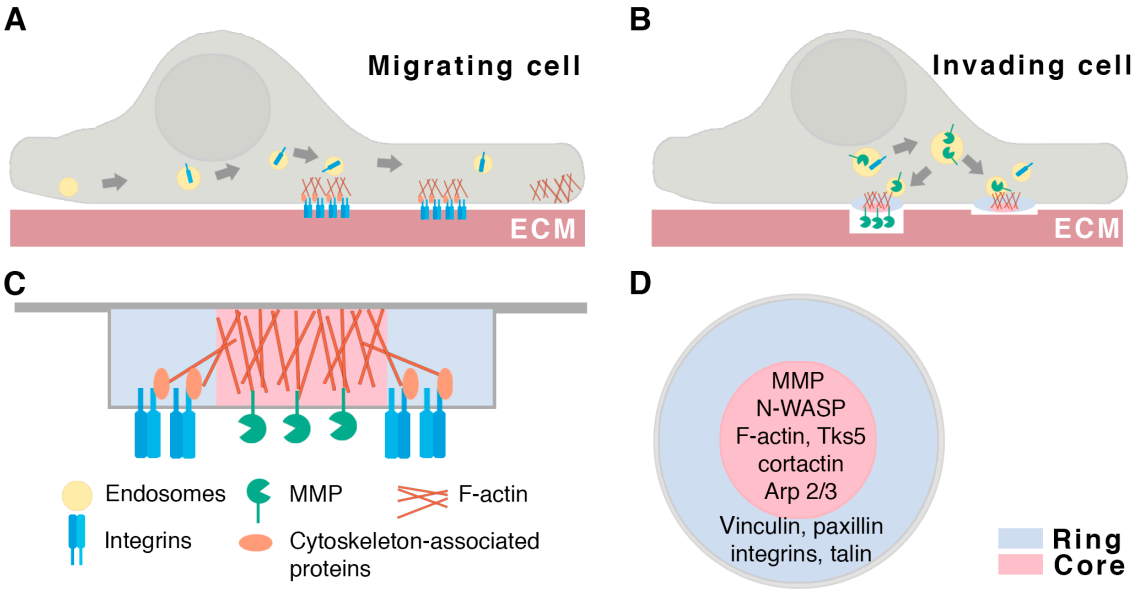

Fig I6. Polarized trafficking during migration and invadopodium formation

Polarized intracellular trafficking of signaling and adhesion molecules allows (**A**) adhesion site turnover during migration as well as (**B**) extracellular matrix (ECM) degradation during invasion. Invadopodium structures have a central core with functional molecules such as matrix metalloproteinases (MMP), surrounded by an integrin-enriched adhesive ring. (**C**) Front view; (**D**) top view.

membrane protein 7 (VAMP7) and the exocyst complex (reviewed in [257]). A recent report showed that this complex acts in concert with the WASH complex to target a sizable fraction of MT1-MMP stored in late endocytic compartments to the PM [228]. Actin polymerization is thus not only essential for N-WASP-dependent invadopodium formation, but also mediates vesicle exocytosis through WASH actin nucleation-promoting activity [228]. Cytoskeletal MT are also important for MMP transport to invadopodia, as they participate in a trafficking route analogous to that of proteins sorted to the apical domain of polarized cells [41]. MT disruption impairs matrix degradation and invadopodium elongation into basement membranes, which suggests impaired cargo delivery to the protruding tip [41, 168, 284].

With cytoskeleton remodeling, the modulation of membrane lipid composition in the invadopodium facilitates changes in membrane morphology and protein recruitment. PtdIns(4,5)P_2 patches are observed near invadopodia, where they activate actin-related proteins such as vinculin, talin, ezrin/radixin/moesin (ERM) proteins and N-WASP as well as other invadopodium components involved in endocytosis including dynamin-2. Local PtdIns(4,5)P_2 generation is associated with PIP5K accumulation, whereas class I PI3K uses PtdIns(4,5)P_2 as a substrate for PtdIns(3,4,5)P_3 production and regulates invadopodium formation, probably through PDK1 (phosphoinositide-dependent kinase 1) and Akt activation. PtdIns(3,4,5)P_3 is enriched in a ring around the invadopodium core, consistent with its conversion in the core to phosphatidylinositol-3,4-bisphosphate (PtdIns(3,4)P_2) by SHIP2 and synaptojanin phosphatases. This SHIP2-dependent PtdIns(3,4)P_2 generation is needed for recruitment of the key invadopodium scaffold protein Tks5 through its PX domain [291, 350, 351]. Lipid raft enrichment in membranes is also reported in invadopodia; several components involved in actin polymerization and membrane trafficking such as N-WASP, dynamin-2, and Arf6 localize to these rafts, which are also sites for caveolin-1-dependent trafficking of invadopodium components, including MT1-MMP (reviewed in [350]).

Invadopodium formation promotes the ECM remodeling necessary for cancer cell invasion and metastasis, the main cause of mortality in cancer patients. The abnormal arrangement of a similar structure termed podosome in specialized cells like osteoclasts, macrophages or smooth muscle cells is associated to developmental, vascular and immune diseases [36, 165, 232]. Further study is needed of the mechanisms that coordinate the cell-matrix and/or cell-cell contact signaling, cytoskeletal rearrangement, and polarized trafficking that are necessary for cell migration and invasion, for the development of therapeutic strategies.

3. SNX27: A UNIQUE SORTING NEXIN

3.1. The sorting nexin family

The SNX are molecules that regulate intracellular protein trafficking and endosomal signaling. All members of the SNX family have a PX domain that binds to PtdIns3P-enriched endosomal membranes. SNX are classified in subfamilies based on the presence of other structural domains: SNX-PX, SNX-BAR (Bin, amphiphysin, Rvs), SNX-FERM (4.1/ezrin/radixin/moesin), SNX-PXA-RGS-PXC and SNX-MIT (reviewed in [319]). Given their relevance in our studies, the SNX-BAR and SNX-FERM proteins will be detailed below.

The SNX-BAR have a BAR domain that forms a rigid curved structure with a membrane-binding surface that interacts preferentially with membranes of positive curvature, such as those of small vesicles or narrow-diameter membrane tubules. SNX-BAR acts as a scaffold for the remodeling of vesicular membranes to promote tubulation, and are best known for cooperation with the retromer in intracellular protein trafficking. The retromer, a heterotrimeric protein complex composed of VPS35, VPS29 and VPS26, regulates protein export from the endocytic compartment. In yeast, the retromer interacts strongly with the SNX-BAR subcomplex, whereas the association with the SNX-BAR mammalian homologue (SNX1 or SNX2 in complex with SNX5 or SNX6) appears to be less robust. Compared to yeast, the mammalian retromer binds a large number of additional proteins, and the SNX-BAR subcomplex therefore cannot be considered an integral retromer component. Members of the SNX-PX subfamily such as SNX3, as well as SNX27 of the SNX-FERM subfamily, are also important to retromer function (reviewed in [112]).

The SNX-FERM proteins have a C-terminal atypical FERM or 'FERM-like' domain, so termed by analogy with the canonical FERM domain; both the classical and the atypical FERM have F1, F2 and F3 subdomains, although their sequence similarity is low and the atypical SNX FERM domain has a notably smaller F2 module [117]. FERM domains generally mediate interactions of membranes or cytoskeletal elements with cytoplasmic proteins. SNX FERM domains are known to regulate endosomal cargo interactions and to act as scaffolds for signaling complexes; the F3 module binds cargoes bearing a NPxY/NxxY (Asn-Pro-Xaa-Tyr/Asn-Xaa-Xaa-Tyr) sequence [116], and the F1 contains a Ras-association (RA) domain, suggesting a role in Ras-mediated endosomal signal transduction [117].

The SNX-FERM subfamily has three components, SNX17, SNX27 and SNX31. SNX17 and SNX31 are similar, whereas SNX27 has a PDZ domain (PSD-95, Dlg1, ZO-1) in addition to the PX and FERM-like domains. In peptide array experiments, the FERM domains of SNX27, SNX17 and SNX31 share the ability to bind NPxY/NxxY sequences from a large variety of proteins, although SNX27 shows a preference for sequences phosphorylated at Y_0 [116]. *In vivo* studies nonetheless demonstrated a role only for SNX17 and SNX31 in preventing lysosomal degradation of transmembrane proteins with NPxY/NxxY sequences [246, 309, 326]. Studies of the FERM-RA domain showed H-Ras binding to all SNX-FERM proteins *in vitro* [117], but only linked

functionally the SNX27 RA domain to a specific Ras protein; it binds K-Ras [196] and regulates expression of GIRK potassium channels (G protein-coupled inwardly-rectifying potassium channels) [14]. SNX17, SNX27 and SNX31 FERM domains thus share similar cargo- and Ras-binding capacity *in vitro*, although cell biology studies reveal distinct binding properties for SNX27, suggesting evolutionary divergence of its FERM domain.

3.2. SNX27 is a core component of a multimeric protein complex

SNX27 is unique in the SNX family in that it has an N-terminal PDZ domain that binds proteins bearing a C-terminal class 1 PDZ-binding motif (PDZ-bm), a [Ser/Thr]-x-ϕ (ϕ = any hydrophobic residue) consensus motif [64]. The importance of the SNX27 PDZ lies in that it also mediates direct SNX interaction with the retromer complex, which increases SNX27 cargo binding affinity [111]. The retromer was originally characterized for its role in endosome-to-TGN transport and transcytosis in polarized cells; SNX27 association to the retromer thus broadens its functions to direct endosome-to-PM recycling (reviewed in [112]) (Fig I7A).

SNX27 directly binds the VPS26 retromer subunit, to which is also indirectly recruited via association with the SNX-BAR [308] and the WASH complex [308, 321], which induces actin polymerization at the endosomes and maintains endosomal and lysosomal network integrity [124, 125]. While an intact FERM-like domain is necessary to bind retromer SNX-BAR, the F3 FERM module interacts independently with the WASH complex through one of its core

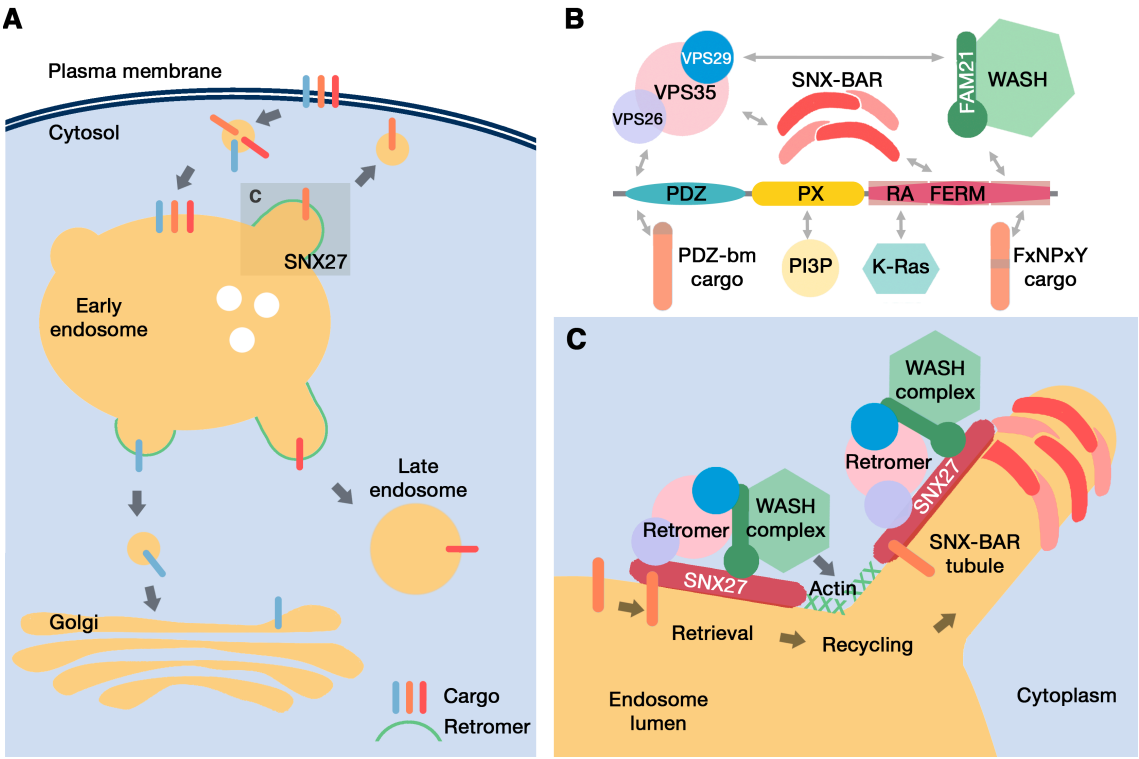

Fig I7. SNX27 localization and interactions in the intracellular trafficking pathway

(**A**) Intracellular transport routes. SNX27 participates mainly in endosome-to-plasma membrane protein recycling (expanded in **C**). (**B**) SNX27 protein structure. SNX27 domain interaction with different proteins and PtdIns3P (PI3P) lipid are detailed. Modified from [308].

components, FAM21 [185, 308]. FAM21 bridges SNX27 and the retromer subunit VPS35 via their respective interactions with the FAM21 globular or tail regions [137, 160, 185] (Fig I7B). Its protein domains thus facilitate the interactions that situate SNX27 as a core component of a multiprotein complex that directs endosome-to-PM protein recycling. The current model suggests that direct SNX27 association with the retromer and FAM21 prevents cargo transport to the lysosomes or to Golgi, respectively [185, 308]. SNX27 cargoes are then transported from early endosomes through SNX-BAR-decorated tubules, and coupled to F-actin-mediated endosomal trafficking as a result of SNX27/WASH interaction (Fig I7C). Recent findings identified additional accessory proteins that participate in SNX27-retromer-mediated protein recycling such as VARP (also known as ANKRD27) [144, 217], which controls the fusogenic state of VAMP7 and thus regulates late endosome-lysosome fusion [282].

3.3. SNX27 PDZ cargoes

The specific combination of the PDZ-PX-FERM structural domains, the singularity of FERM domain association to the WASH complex, and the differential binding to NPxY/NxxY and Ras compared to other SNX-FERM proteins all make SNX27 unique among SNX proteins and in need of further study.

SNX27 is known primarily for its PDZ-mediated contribution to the trafficking of type 1 PDZ-bm-bearing transmembrane proteins (see Table I1). These include G protein-coupled receptors (GPCR) such as β2AR (β2-adrenergic receptor) [180, 321], β1AR [234], PTHR (parathyroid hormone receptor) [51, 216], and SSTR5 (somatostatin receptor subtype 5) [22], ion channels and antiporters such as GIRK [15, 202, 231] and NHE3 (Na^+/H^+ exchanger 3) [300]. Others include proteins involved in neuron plasticity such as AMPAR (α-amino-3-hydroxy-5-methyl-4-isoxazolepropionic acid) [150, 196], NMDAR (N-methyl-D-aspartate) [40, 342] and 5-$HT_{4(a)}$R (5-hydroxytryptamine 4a receptors) [162], as well as the metabolic transporters GLUT1 (glucose transporter 1) and MCT1 (monocarboxylate transporter 1) [308].

The majority of these proteins use SNX27 as an adaptor for retromer-mediated transport from endosomes to the cell surface; SNX27-silenced or KO cells thus show decreased surface abundance and increased degradation of these cargoes. Several studies have nonetheless shown that SNX27 promotes internalization and lysosomal delivery of PDZ-bm-bearing cargoes such as Fzd7 (Frizzled 7) [313], 5-$HT_{4(a)}$R [162], GIRK [202], GluN2C (also termed NR2C) [40] and MRP4 (multidrug resistance-associated protein 4) [139]. Although some of these reports were based exclusively on experimental SNX27 overexpression [162, 202, 313], others showed that knockdown or KO of SNX27 indeed increases surface levels of cargo proteins [40, 139].

The SNX27 PDZ domain also binds non-transmembrane PDZ-bm-bearing cargoes involved in cytoskeleton rearrangement, including the tight junction protein ZO-2 (zona occludens-2) [366] and the Rho GEF β-PIX (p21-activated kinase-interactive exchange factor) [328] as well as in vesicle formation, such as CASP (cytohesin-associated scaffolding protein) [209]. Also noteworthy

Cargo	C-terminal sequence	SNX27 effect on cargo	References
AMPAR		SNX27 knockdown (KD) decreases surface and total levels	150
GluA1	PLGATGL	SNX27 KO leads to hydrocephalus and impaired long-term potentiation (LTP)	196
GluA2	GIESVKI		
GluA3	GTESVKI		
ATP7A	EDDDTAL	SNX27 KD decreases surface abundance and increases degradation	308
CASP	EEEESRF	SNX27 colocalizes at the endosomes	209
CD97	LRASESGI	SNX27 KD decreases surface abundance and increases degradation	308
DGKζ	EDQETAV	SNX27 KD increases Ras/ERK signaling	271 270
FZD 7	SKGETAV	SNX27 overexpression (OE) enhances endocytosis, promotes degradation and results in enhanced Wnt signaling	313
GIRK/ Kir 3.3	PESESKV	SNX27 OE reduces surface expression, increases degradation and results in smaller potassium currents	15 202
		SNX27 KO in dopamine neurons reduces GIRK currents and enhances cocaine response	231
GLUT1	LGADSQV	SNX27 KD decreases surface abundance and increases degradation	308
MCT1	PKEEESPV	SNX27 KD decreases surface abundance and increases degradation	308
MRP4	TIFETAL	SNX27 KD increases plasma membrane expression	139
NHE3	LPESTHM	SNX27 KD decreases its activity and reduces surface expression	300
NMDAR			
GluN1	PSVSTVV	SNX27 knockdown (KD) decreases cell surface and total levels, SNX27 KO in mice results in synaptic dysfunction and cognitive deficits	150 342
GluN2C/ NR2C	ISSLESEV	SNX27 KO in neurons increases expression, and impairs endocytosis	40
PS1	AFHQFYI	SNX27 KO increases γ-secretase Aβ generation	341
PTHR	EEWETVM	SNX27 KD and KO reduces cell surface levels, promotes lysosomal localization and augments PTHR signaling	51 216
		KO mice show reduced bone mineralization and skeletal defects	
SSTR5	LMQTSKL	SNX27 KD delays postendocytic recycling and enhances degradation	22
ZO-2	RYRDTEL	SNX27 KD decreases mobility at cell-cell contact regions and results in increased junctional permeability to large solutes	366
β-PIX	AWDETNL	SNX27 OE promotes endosomal localization, SNX27 KD decreases cell motility	328
β1AR	GFASESKV	SNX27 KD enhances lysosomal delivery	234
β2AR	CSTNDSLL	SNX27 KD decreases plasma membrane expression and reduces adrenergic signaling	180 321
5-HT_{4a}R	ESLESCF	SNX27 OE promotes endosomal localization	162

Table I1. Validated SXN27-PDZ cargoes The canonical type I consensus PDZ-binding motif is underlined; possible phosphorylation sites (pink) and positively charged amino acids (blue) are colored.

is the recent report of SNX27 PDZ domain interaction with the human papillomavirus 16 (HPV-16) L2 protein [255]. Although this association depends on the PDZ-bm-binding region of SNX27 PDZ, the L2 protein does not bear a C-terminal PDZ-bm. L2/SNX27 interaction is disrupted by deletion of a central part of L2, a previously unreported type of SNX27 PDZ interaction [255] that could be a mechanism for virus to perturb and exploit transport processes to complete their life cycle.

3.4. SNX27 in polarized cell models

SNX27 is ubiquitously expressed, but numerous SNX27 PDZ cargoes have prominent roles in neurons. Defective cargo trafficking is linked to synaptic dysfunction and cognitive defects in *Snx27* KO mice [196, 342], as well as to attenuation of neuropathic pain development after knockdown of spinal SNX27 expression in rats [189]. In humans, deleterious homozygous mutations in SNX27 are found in patients with myoclonic epilepsy [70]; in Down syndrome (DS) brain, an extra copy of the chromosome 21-encoded miR-155 leads to low SNX27 levels and contributes to the synaptic and cognitive deficits of DS patients [342]. SNX27 PDZ binding to the γ-secretase subunit PS1 (presenilin 1) is associated with Alzheimer disease (AD), in which SNX27 depletion results in enhanced γ-secretase-dependent β-amyloid (Aβ) production [341]. SNX27 overexpression in a Ts65Dn DS mouse model or AD transgenic mice rescues cognitive and synaptic impairments [342] and decreases Aβ generation [341], respectively. These fundamental discoveries thus identify a molecular mechanism for AD-like neurodegeneration in DS patients and illustrate the importance of neurological disorders associated with loss of SNX27 function.

Our group originally identified SNX27 in a proteomic screen for PDZ domain-containing interactors of DGKζ in T cells [271]. We and others showed that in APC-responsive T cells [270] and tumor-engaged NK cells [210] endosomal SNX27 undergoes rapid polarization to the IS. In T cells, SNX27 is sorted into two pools at the IS, where it is found at the PM and on TfR-positive vesicles [270]. PX and PDZ domains contribute to SNX27 recruitment to the T cell synapse; the PX domain binds to PtdIns3P-enriched endosomal membranes, driving SNX27 localization to the ERC, and the PDZ domain is necessary for its accumulation at the T cell-APC contact area [270]. The SNX27 FERM domain as well as the dual role for SNX27 PDZ domain in the recognition of PDZ-bm-containing cargoes and VPS26 were later identified [111, 117, 308]; determining their particular contribution to SNX27 IS localization was one of the objectives of the present study.

Localization studies suggest an important function of SNX27 at the IS that correlates with DGKζ translocation to the T cell-APC contact area. Moreover, attenuation of SNX27 expression mirrors the effect of DGKζ silencing on ERK activation during T cell activation, indicating that SNX27 interaction helps to regulate localized DGKζ-dependent DAG signaling [270]. SNX27 IS accumulation, however, is independent of DGKζ [270], which suggests the presence of other SNX27 PDZ cargoes at the IS. Further studies were thus required to fully characterize the

contribution of SNX27/DGKζ association to the control of DAG signaling and to identify additional SNX27 partners during T cell activation.

Besides providing a better understanding of the IS, the study of SNX27 dynamics and function in the T cell model offers interesting possibilities to extrapolate some findings to other models of intense polarized trafficking. As detailed above, from the neurological synapse to invadopodium formation, all are polarized cell-cell communication systems that share fundamental structures necessary for the correct rearrangement of actin, MT, adhesion molecules and lipids that facilitate vesicle trafficking. In invasive tumor cells, the SNX27 partner WASH mediates integrin [360] and MT1-MMP recycling [228]. Moreover, data from several web-based bioinformatics resources such as the cBioPortal for Cancer Genomics [49, 113] indicate that, in humans, SNX27 chromosome localization (1q21.3) is frequently amplified in different types of invasive cancer (see Appendix 1). SNX27 role in tumor cell polarized recycling, however, has not yet been explored.

Objectives

III. OBJECTIVES

SNX27 PDZ and FERM domains facilitate the intracellular trafficking of protein cargoes, and its PX domain assist in SNX27 endosomal localization. Using immune synapse (IS) formation as a model of polarized vesicle trafficking, our group identified SNX27 association with the PDZ-binding diacylglycerol kinase ζ (DGKζ). Later studies in neurons and epithelial cells identified additional interactors of SNX27, which is proving to be a critical hub for protein recycling in the nervous system. The precise function of SNX27 is not fully understood in other polarized cell systems. Our overall objective was to **determine the role of SNX27 during T cell activation and cancer cell invasion**, two situations when polarized intracellular trafficking is crucial for specialized cell function. To achieve this aim, we proposed the following specific objectives:

1. Determine the role of SNX27 during IS formation
    a. Assess the contribution of the SNX27 FERM and PDZ subdomains to SNX27 dynamics at the IS
    b. Identify the SNX27 PDZ-dependent and -independent interactome during IS formation
    c. Study the function of SNX27 interaction with partners identified in T cells

2. Assess the role of SNX27 during T cell activation
    a. Analyze the molecular details of SNX27/DGKζ association
    b. Examine the contribution of SNX27 in the control of T cell signaling
    c. Characterize the effects of SNX27 deficiency on mouse T cell development and function

3. Study the role of SNX27 during breast cancer cell invasion
    a. Examine SNX27 localization to invadopodia
    b. Analyze the effects of SNX27 silencing on invadopodium formation and invasion in breast cancer cells

Material and Methods

IV. MATERIAL AND METHODS

1. REAGENTS

The reagents used in the present study are detailed in Table M1. Remaining reagents were purchased as indicated.

Supplier	Reagents
Roche	Leupeptin, aprotinin
Sigma	Na_3VO_4, PMSF, β-glycerophosphate, NP-40, G418, poly-DL-lysine, methanol, paraformaldehyde (PFA), gelatin, cycloheximide (CHX), polybrene, BSA, doxycycline (Dox), phorbol 12-myristate 13-acetate (PMA), concanavalin A (ConA)
Calbiochem	Triton X-100, Tween 20, Gö6976, PD98059, MG-132
Life Technologies	Transferrin-rhodamine (Tf-Rhod), calcein-AM, BODIPY 630/650 succinimidyl ester, CMAC (7-amino-4-chloromethylcoumarin)
Invitrogen	LIVE/DEAD violet dead cell stain, Cell Trace Violet Cell Proliferation kit, AlexaFluor 647-phalloidin, rhodamine phalloidin

Table M1. Reagents used in this study

2. CONSTRUCTS

The constructs used in the present study for protein or shRNA expression are detailed in Table M2, or were generated as indicated in sections 2.1 and 2.2.

Plasmid	Supplier / Reference
pEGFP-C2-mSNX27a (WT/ΔPDZ)	E. Rincon [271]
pEGFP-C1-hSNX27 (WT/$L_{67\text{-}77A}$/H_{114}A)	P. Cullen [111, 308]
pmCherry-mSNX27	B. Collins [118]
pEGFP-N-SNX17	B. Collins [116]
pDsRed2-AKT-PH	M. Almena [118]
pmCherry-C2-2xFYVE	F. Meunier [344]
pEGFP-C3-ZO-2	M. Sudol Addgene #27422 [243]
pEGFP-ZO-1	A. Fanning Addgene # 30313 [95]
pEGFP-C1-CD63	G. Griffiths [29]
mRFP-Lifeact	R. Wedlich-Soldner [267]
pEFbos-GFP DGKζ (WT/ΔETAV)	T. Santos [281]
pSUPER.basic	Oligoengine (VEC-PBS-0001/0002)
pSUPER-shRNA mouse DGKα(Ctrl)	A. Ávila-Flores [271]
pSUPER-shRNA human DGKζ	A. Ávila-Flores [271]
PLKO-Tet-on-neo	D.Wiederschain/Addgene#21916 [346]
PLKO-shRNA mouse DGKα(Ctrl)	P. Torres-Ayuso, A. Ávila-Flores
MT1-MMP-mCherry	P. Chavrier [278]
pDMyc-SNX27 (FL/NT)	W. Hong [40]
pGEX4T1-GST-SNX27 FL	W. Hong [40]
pcDNA-GFP-PIPKγi2-FLAG	A. Huttenlocher [195]
pEGFP-C1-PIPKγi1	S. Mañes [179]
HA-PIP5KIβ	S. Mañes [211]

Table M2. Constructs used in this study

2.1. Mutagenesis

To generate the SNX27 FERM non-PtdInsP-binding mutant (pEGFP-C2-mSNX27a RRK/E) and SNX27 FERM non-NPxY-binding mutant (pEGFP-C2-mSNX27a W475A and pDMyc-SNX27 W475A), the sequences 5'-TCG AGG AGG AAG GGA-3', or 5'-GCA GCG AGC GGA CAC-3' were mutated to the sequences detailed in Table M3. The presence of the mutations was confirmed by sequencing using SeqSNX27400 primer (5'- TCA ACA TGC TAA GGA CCT GC-3'). To generate the DGKζ PDZ-bm mutants pEFbosGFP-DGKζ D924A, E926A, DE/A, T927D and T927A, then pEFbosGFP-DGKζ sequence 5'-GAC CAG GAG ACA GCT-3' was mutated to the sequence detailed in Table M3. The presence of the mutations was confirmed by sequencing using SeqDGKζCt primer (5'-GAG ACC TGT CTA CAC CAG GCA-3'). Site-directed mutagenesis was performed using the QuikChange mutagenesis kit (Agilent Technologies).

Generated mutant	Sequence (5'-3')
SNX27 RRK/E	TCG **GA**G **GA**G **G**AG GGA
SNX27 W475A	GCA **GC**G AGC GGA CAC
DGKζ D924A	G**C**C CAG GAG ACA GCT
DGKζ E926A	GAC CAG G**C**G ACA GCT
DGKζ DE/A	G**C**C CAG G**C**G ACA GCT
DGKζ T927D	GAC CAG GAG **GAT** GCT
DGKζ T927A	GAC CAG GAG **G**CA GCT

Table M3. Oligonucleotides used for mutagenesis
Nucleotides underlined encoded the modified amino acids

2.2. Cloning

2.2.1. pSUPER-derived shRNA plasmid

For SNX27 silencing, double strand oligonucleotides encompassing the 5'-CCA GGU AAU UGC AUU UGA A-3' interfering sequence [180] and a hairpin structure were cloned between the BglII and HindIII restriction sites of the pSUPER vector for transient shRNA expression. The presence of the inserts was confirmed by sequencing using the T7Seq primer (5'-AAT ACG ACT CAC TAT AG-3').

2.2.2. pLKO-derived shRNA plasmids

For SNX27 silencing, double strand oligonucleotides encompassing the 5'-CCA GGU AAU UGC AUU UGA A-3' interfering sequence [180] and a hairpin structure were cloned between the AgeI and EcoRI restriction sites of the pLKO-Tet-on vector for transient shRNA expression. The presence of the inserts was confirmed by sequencing using the pLKOSeq primer (5'-GGC AGG GAT ATT CAC CAT TAT CGT TTC AGA -3').

3. CELL CULTURE

3.1. Cell lines

Human leukemic Jurkat T cells and Raji human B lymphoma cells (American Type Culture Collection; ATCC) were maintained at subconfluence (<5 × 10^5 cells/ml) in RPMI-1640 medium

(BioWhittaker) supplemented with 10% FBS (Sigma or GBi Genycell Biotech) and 2 mM L-glutamine (Sigma or BioWhittaker) (37°C, 5% CO_2). Human epithelial HEK293T cells and breast cancer MDA-MB-231 cells (ATCC) were maintained at subconfluence in DMEM (BioWhittaker) supplemented as above (37°C, 5% CO_2).

3.2. Mouse-derived primary T cell culture

Snx27$^{+/-}$ mice were kindly provided by Dr. Brett Collins (Institute for Molecular Bioscience, University of Queensland, Australia), originally from Dr. Wanjin Hong (Institute of Molecular and Cell Biology, Singapore) [40]. Mice were housed in specific pathogen-free conditions and handled in accordance with the Australian Code of Practice for the Care and Use of Animals for Scientific Purposes. Experiments were approved by the Ethics Committee of the University of Queensland.

Thymus, spleen, or peripheral lymph nodes were dissected and mechanically disaggregated in PBS. Single-cell suspensions were obtained using a 40-μm cell strainer (BD Biosciences). Splenocytes were treated with red blood cell (RBC) lysis buffer (eBioscience) according to manufacturer's instructions. Cells were prepared for flow cytometry as described in section 7.3, or stimulated as indicated in section 4.2 and maintained in RPMI-1640 medium supplemented with 10% heat-inactivated FBS, 2 mM L-glutamine, penicillin/streptomycin (all from Gibco) and 50 mM β-mercaptoethanol (Sigma) (37°C, 5% CO_2).

3.3. Transient protein and shRNA expression

Jurkat T cells in logarithmic growth phase were transfected (1.2 x 10^7 cells in 400 μl complete medium) with 20 μg plasmid DNA by electroporation using a Gene Pulser (BioRad; 270 V, 975 mF) [271]. For transient protein expression in the MDA-MB-231 cell line, DNA plasmids were transfected using Lipofectamine 2000 or LTX (Life Technologies) or the Amaxa Nucleofector System (Lonza), both according to manufacturer's instructions. For nucleofection, cells were transfected (1-2 x 10^6 cells in 100 μl solution V (Lonza)) with 2 μg plasmid DNA by electroporation using a Nucleofector Device (program X-013). HEK293T cells were transfected using FuGENE (Roche) at a 3:1 v:w FuGENE:DNA ratio.

For all cell types, assays were generally performed 24 or 48 h post-transfection. For shRNA expression using pSUPER-derived plasmids, cells were assayed at 72-96 h post-transfection.

3.4. Generation of viral particles and transduction

Lentiviral particles were produced in human HEK293T cells by cotransfecting the lentiviral vector and the appropriate viral envelopes [pRSV-Rev, pMDL-g/pRRE, pVSV-G, all a kind gift from Dr John Stingl (Cambridge Research Institute, UK)]. DNA was used at a proportion of 2.5 μg/10^6 packaging cells, which were cultured in 10 cm^2 plates. After 48 h transfection, cell medium containing the viral particles was collected and centrifuged (1500 × *g*, 5 min, 33°C). The remaining supernatant was filtered through a low-protein-binding 0.45 μm filter (Pall Life Sciences).

Viral supernatant and complete medium were added at a 1:1 ratio to target cells, in the presence of 6 μg/ml polybrene to increase viral transduction efficiency. Cells were centrifuged in a 6-well plate (1500 × *g*, 90 min, 33°C) and incubated (3-4 h, 33°C). The virus-containing medium was then replaced with fresh medium. At 48 h post-infection, antibiotic (600 μg/ml G418) was added to growth medium to select efficiently transduced cells. Cells were maintained in antibiotic-containing medium for a minimum of 7 days.

3.5. Generation of stable shRNA-expressing cell lines

For loss-of-function analysis in MDA-MB-231 cells, we use the pPLKO-Tet-on-neo system for inducible expression of shRNAs. Cells were transduced with lentiviral particles containing shRNA-encoding plasmid pPLKO-Tet-on-neo against target sequences described in section 2.2.2. shRNA expression of MDA-MB-231-derived pLKO-Tet-on-neo cell lines was induced by doxycycline (Dox) treatment (1 μg/mL every 48 h). Protein silencing was effective after 72-96 h of Dox treatment.

4. ANALYSIS OF T CELL STIMULATION

4.1. T cell/APC conjugate formation

Raji B cells used as APC were pulsed with 1 μg/ml superantigen *Staphylococcus* enterotoxin E (SEE; Toxin Technology) at 10^7 cells/ml in medium containing 10 μM CMAC or 1 μM BODIPY 630/650 (1 h, 37ºC). For microscopy, CMAC-stained APC were washed and mixed 1:1 with Jurkat T cells for the times indicated. Flow cytometry-based conjugation assays were performed and analyzed as described [297], with minor modifications. Briefly, BODIPY-stained APC (red) and Jurkat cells stained with 4 nM calcein-AM (1 h, 37ºC) (green) were washed, resuspended to 10^6 cells/ml in medium and mixed 1:1 (37ºC) for indicated times. The relative proportion of red, green, and red/green events in each tube was determined by two-color flow cytometric analysis using a Cytomics FC500 analyzer (Beckman Coulter). The percentage of conjugation was calculated as the number of dual-labeled (red/green) events divided by the sum of the dual-labeled events and the unconjugated Jurkat cells (green events).

4.2. Anti-CD3 or anti-CD3/CD28 stimulation

The antibodies used for T cell stimulation are detailed in Table M4.

Antibody (anti-)	Supplier	Reference
Human CD3ε (clone HIT3a; mouse)	BD PharMingen	555336
Human CD28 (clone CD28.2; mouse)	BD PharMingen	555725
Mouse CD3ε (clone 145-2C11; hamster)	BD PharMingen	553058
Mouse CD28 (clone 37.51; hamster)	BD PharMingen	553295

Table M4. Antibodies used for T cell stimulation

4.2.1. Stimulation with antibody solution

Jurkat T cells were stimulated in complete medium (10^7 cells/ml) with soluble anti-CD3 or -CD3/CD28 antibodies (1 μg/ml) (Table M4) for the indicated times. Where indicated, cells

were pretreated for pharmacological inhibition with Gö6976 (100 nM) or PD98059 (50 μM) (37°C, 30 min) prior to stimulation.

4.2.2. Stimulation with plate-bound anti-CD3

Primary cells were stimulated in complete medium (2.5×10^6 cells/ml) with plate-bound anti-CD3 (plate coated with 2.5 μg/ml anti-CD3; 1 h, 37ºC) (Table M4); where indicated, medium was supplemented with anti-CD28 (1.25 μg/ml).

4.3. Proliferation assay

For staining, cells were incubated in pre-warmed Cell Trace Violet/PBS solution (5 μM; 5×10^6 cells/ml, 30 min, 37ºC). Unbound dye was quenched by adding 5 times the staining volume of complete culture medium (5 min, 37ºC). Cells were then washed in complete medium, cultured for indicated times and processed for flow cytometry (see section 7.3). The FlowJo Proliferation Platform (TreeStar) was used to track cell generations and calculate proliferation statistics.

4.4. Dual luciferase reporter assay

Jurkat cells were transfected with the indicated shRNA constructs as described in section 3.3. At 48 h post-transfection, cells were transfected with the indicated promoter construct (pGL2-AP-1 or pGL4-NF-κB plasmids with four or three transcription factor binding sites, respectively, were made in our laboratory by Raquel Arcos) and the 100 ng of *Renilla* luciferase vector pRL-TK (Promega) as internal control. After 24 h, cells were washed, allowed to recover (6 h), and stimulated as described in section 4.2.1. Cells were harvested and assayed for luciferase activity using the Dual-Luciferase Reporter Assay (Promega). Relative luciferase units (RLU) were calculated relative to *Renilla* luciferase values and, where indicated, normalized to the RLU of unstimulated control cells.

5. PROTEIN STABILITY ASSAYS

Cells were treated with 10 μg/ml cycloheximide (CHX) for the indicated times. Cells were processed as in section 7.1 to determine protein levels by quantitative western blot. Protein levels were normalized to GAPDH or tubulin. Results for each time point were also normalized to the untreated control, which was set to 1.

6. MIGRATION AND INVASION ASSAYS

6.1. Circular invasion assay

The circular invasion assay (CIA) was performed as described [359]. Cells were plated onto 35 mm micro-dishes using silicon inserts (both from Ibidi) to generate a cell-free space. After incubation (overnight, 37°) and removal of the insert, 250 μl 4.5-5.5 mg/ml Matrigel (BD Bioscience) diluted in DMEM at a 1:1 ratio was overlaid onto the cell monolayer and allowed to polymerize (2 h, 37°C). After addition of complete medium, cells were allowed to invade the Matrigel and imaged (24 h, 37°C). Cells were then fixed in 4% PFA and prepared for immunofluorescence analysis as in section 7.4. Time-lapse imaging was performed using a

phase-contrast microscope with a 20× objective, with image acquisition at 15 min intervals. The area covered by cells was measured using ImageJ Freehand Selection. The increase in cell-covered area was calculated for each time point and normalized to control cells at the final time point. Duplicates were analyzed for each sample and 3 time-lapse positions were measured for each replica in at least three independent experiments.

6.2. Inverted invasion assay

In a modification of traditional transwell-Matrigel inserts, inverted invasion assays were performed as described [143]. Briefly, 100 μl of 4.5-5.5 mg/ml Matrigel (BD Bioscience) were allowed to polymerize in transwell inserts (Corning) (1 h, 37°C). Inserts were then inverted, and 5 x 10^5 cells plated onto the outer side of the transfilter and allowed to adhere (3 h). Inserts were then washed in serum-free DMEM to remove unattached cells, and placed in 500 μl serum-free medium. To create a chemotactic gradient, 100 μl of 10% FBS-supplemented medium were added to the Matrigel-containing chamber. At 72 to 96 h post-seeding, cells were stained with calcein-AM (4 μM) in serum-free DMEM (1 h, 37°C). Cells that did not cross the transfilter were removed with a tissue and the invading cells were imaged on an FV1000 confocal laser-scanning microscope (Olympus) using a 40× objective. Serial optical sections were captured at 15-μm intervals. The area covered by cells was measured in each section using the ImageJ plugin "Area Calculator" in 8-bit images (threshold 30-50/255). Relative invasion was calculated as the area covered by cells that invaded 45 μm or more relative to total cell area of the Z-stack. At least three independent experiments in duplicate were performed for each sample.

7. IMMUNOASSAYS

The buffer solutions used for immunoassays are detailed in Table M5.

The antibodies used for immunoprecipitation, western blot and immunofluorescence are detailed in Table M6 and Table M7.

Buffer	Preparation
P70 glycerol /1% NP-40	10 mM HEPES pH 7.5, 15 mM KCl, 1 mM EDTA, 1 mM EGTA, 10% glycerol, 1% NP-40
RIPA	20 mM Tris-HCl pH 7.5, 300 mM NaCl, 2 mM EDTA, 1% Triton X-100, 0.1% SDS, 0.5% sodium deoxycholate, 10% glycerol
Sample buffer (5X)	312 mM Tris-HCl pH 6.8, 10% SDS, 25% β-mercaptoethanol, 50% glycerol, 0.1 mg/ml bromophenol blue
PBS staining buffer	1% FBS, 0.5% BSA, 0.01% sodium azide/PBS

Table M5. Buffer solutions used in this study

7.1. Western blot analysis

For western blot analysis, cells were washed in cold PBS and lysed (15 min, 4°C) in the indicated buffer solutions detailed in Table M5, containing protease and phosphatase inhibitors (20 μM leupeptin, 1.5 μM aprotinin, 1 mM PMSF, 1 mM Na_3VO_4, 40 mM β-glycerophosphate and 2 mM NaF); clarified lysates were quantified with the Pierce 660 nm Protein Assay (Thermo Scientific). An equivalent protein amount per sample was analyzed by SDS-PAGE. Proteins

were transferred to nitrocellulose membrane (Bio-Rad) and incubated with indicated primary antibodies. For HRP- or fluorescent-conjugated secondary antibodies, we used an ECL detection kit (Amersham Bioscience) or an Odyssey scanner (LI-COR), respectively. Densitometric analysis of proteins in western blots was performed using ImageJ.

7.2. Immunoprecipitation

For protein-protein interaction analysis by immunoprecipitation, cells were lysed as above. Lysates (500 μg - 1 mg) at a protein concentration of 1 μg/μl were incubated (1 h, 4°C) with the appropriate antibody, followed by incubation (30-60 min, 4°C) with 30-60 μl of 50% protein G-Sepharose slurry (GE Healthcare Life Sciences). Immunoprecipitates were washed three times in lysis buffer and eluted in sample buffer (Table M5). Immunoprecipitated proteins were analyzed by western blot (section 7.1) for validation and by 1D-gel-MS for protein identification (section 9).

7.3. Flow cytometry analysis

Cells were collected in ice-cold PBS and cell surface proteins stained with saturating concentrations of the indicated fluorophore-conjugated primary antibodies (Table M8) in PBS staining buffer as indicated in Table M5 (30 min, 4ºC). Cells were washed with the same buffer

Antibody (anti-)	Supplier	Reference
Akt	Cell Signaling	2910S
DGKζ	Abcam	ab105195
Drebrin	Abcam	ab12350
EEA1	BD Biosciences	610456
FLAG-tag	Cell Signaling	2368S
GAPDH	Santa Cruz	sc25778
GFP	Roche	11814460001
GFP (for IP)	Invitrogen	A11122
GLUT1 (for WB)	Abcam	ab15309
IκB-α	Cell Signaling	9242S
Kidins220	Kind gift from Dr Teresa Iglesias [154]	
MMP-14 (clone LEM-2/15.8)	Millipore	MAB3328
Myc-tag	Cell Signaling	2276S
p44/42 MAPK (ERK1/2)	Cell Signaling	4696S
P70 S6 kinase	Cell Signaling	2708
Phospho-(Ser) PKC substrate	Cell Signaling	2261L
Phospho-Akt (S473)	Cell Signaling	4060
Phospho-p44/42 MAPK (ERK1/2)(T202/Y204)	Cell Signaling	4370
Phospho-p70 S6 kinase (T389)	Cell Signaling	9206L
Phospho-PKD/PKCμ (S744/748)	Cell Signaling	2054L
Phospho-S6 ribosomal protein (S235/236)	Cell Signaling	2211S
PKCθ	BD Transduction	610090
PKCμ/PKD	Santa Cruz	sc-935
SNX27	Abcam	ab77799
Talin	Sigma	T3287
Transferrin receptor	Zymed	13-6800
WASH1 (for IF)	Atlas Antibodies	HPA002689
WASH1 (for WB)	Roche	11814460001
ZO-2	Zymed	71-1400
α-tubulin	Sigma	9026
β-actin	Sigma	A2228
β-PIX	Millipore	07-1450-I

Table M6. Primary antibodies used for western blot (WB), immunofluorescence (IF) and immunoprecipitation (IP)

and maintained at 4ºC for flow cytometry using Cytomics FC500 or Gallios cytometer (Beckman Coulter). Live cells were gated using forward and side scatter parameters. For fixed cells, LIVE/DEAD violet dead fixable cell stain (Invitrogen) was used. For primary cells, each sample was acquired for a minimum of 100,000 events. Data were analyzed using FlowJo software (TreeStar).

Antibody (anti-)	Supplier	Reference
Mouse IgG-AlexaFluor 680	Life Technologies	A-21057
Mouse IgG-Cy3	Jackson ImmunoResearch	115-166-071
Mouse IgG-HRP	Dako	P0447
Rabbit IgG light chain-specific-HRP	Jackson ImmunoResearch	211-032-171
Rabbit IgG-AlexaFluor 488	Life Technologies	A-11034
Rabbit IgG-Dylight 800	Thermo Scientific	SA5-35571
Rabbit IgG-HRP	Dako	P0448

Table M7. Secondary antibodies used for western blot and immunofluorescence

Antibody (anti-)	Supplier	Reference
Human CD11a-FITC (clone 25.3)	Immunotech	860
Human CD3ε-PC5	Beckman Coulter	A07749
Human CD69-PE	Beckman Coulter	IM1943
Human CD71-PE	Immunotech	2001
Human GLUT1-PE (also used for mouse)	R&D Systems	FAB1418P
Isotype control mouse IgG1-FITC	Beckman Coulter	PNIM0639
Isotype control mouse IgG1-PCy5	Beckman Coulter	A07798
Isotype control mouse IgG1-PE	BD PharMingen	556029
Mouse B220-FITC	Beckman Coulter	732154
Mouse CD11a-PE (clone 2D7)	PharMingen	553121
Mouse CD25-PE	PharMingen	553866
Mouse CD3ε-APC	eBioscience	17003183
Mouse CD4-PECy5	BioLegend	100434
Mouse CD44- FITC	Beckman Coulter	731957
Mouse CD69-FITC	PharMingen	553236
Mouse CD71-PE	PharMingen	553267
Mouse CD8-PeCy7	BioLegend	100722
Mouse TCRβ-APC	PharMingen	553174
Mouse TCRγδ–biotinylated	PharMingen	553176
Streptavidin- APC Cy7	BioLegend	405208

Table M8. Antibodies used for flow cytometry

7.4. Immunofluorescence

MDA-MB-231 cells were plated on 0.1% gelatin- or 10 μg/ml fibronectin-coated coverslips for the indicated times. Jurkat cells were plated on poly-DL-lysine-coated coverslips. Where indicated, transfected cells were pre-stained with Tf-Rhod (20 μg/ml, 15-30 min, 37°C). Jurkat T cells were washed and incubated with APC in complete medium for indicated times.

Cells were fixed and permeabilized (cold methanol (4 min) or 2% PFA (10 min) + 0.05% Triton X-100 (10 min)) and blocked in 10% goat serum/PBS (30 min). Cells were incubated with specific antibodies (3 h, RT), washed, and incubated with secondary antibodies (1 h, RT). Coverslips were washed and mounted on glass slides. An FV1000 confocal laser-scanning

microscope (Olympus) was used for imaging.

8. MICROSCOPY

8.1. Live cell imaging

For time-lapse experiments using MDA-MB-231 cells, an Andor spinning disc confocal system with Cairn Optsplit (for simultaneous GFP/RFP imaging) was used for imaging. Images were collected at 0.3-s intervals.

For time-lapse experiments, live Jurkat cells were imaged as described, with minor modifications [119]. Images were collected every 15 s, before, during and after addition of SEE-pulsed or unpulsed stained APC. Where indicated, transfected cells were pre-stained with Tf-Rhod (20 μg/ml, 15-30 min, 37°C). Cells were imaged on an FV1000 confocal laser-scanning microscope (Olympus).

8.2. Fluorescent recovery after photobleaching (FRAP)

Transfected cells were collected in HBSS, transferred to poly-DL-lysine-coated 8-chambered glass coverslips (Ibidi) and allowed to attach for at least 5 min (37ºC). Live-cell microscopy was performed at 37°C with a Leica SP5 TCS confocal scanning unit equipped with a PL APO lambda blue 63×/1.2-NA water immersion objective with the 488-nm Ar laser line for EGFP, and a pinhole setting of 5 AU. Within 30 min of T cell stimulation with APC, we bleached membrane areas of the T cell-APC contact site and on comparable areas of the PM of nonconjugated T cells. Laser power for bleaching was maximal but was reduced to 30% for imaging. At the optimal focal plane, the acquisition protocol was: 5 pre-bleach images, 5 bleach pulses and 90 images at 0.65 s intervals (512 × 512). Fluorescence recovery in the bleached region (5 μ^2) was measured as mean signal intensity. All recovery curves were generated from background-subtracted images. The fluorescence signal in the same region of interest was normalized using the mean prebleach signal as 1, and the intensity immediately following photobleach as 0. Curves were fitted by one-phase association exponential equations with GraphPad Prism. Statistical analyses were performed on the normalized data for each condition. The immobile fractions and half-recovery times were determined from the fitted curves.

8.3. Microscopy and image processing

Time-lapse phase contrast imaging was performed using:

- Nikon inverted fluorescence microscope TE 200 Wide Field fitted with a Nikon Plan-Fluor 10×/0.3NA objective. Imaging was performed using a CoolSnap HQ2 charge-coupled device camera (Photometrics) equipped with a Perfect Focus System device.
- Leica inverted fluorescence microscope DMI6000B with a Leica HC PL 10×0.3NA objective lens and 1.6× magnification, and fitted with a monochrome digital camera Orca R2, 12bit/16bit (Hamamatsu).

Confocal images were collected using:

- Fluoview FV1000 confocal laser-scanning microscope (Olympus) equipped with a uPlan-SApochromat 60×/1.35NA oil objective lens.

- Leica SP5 TCS confocal scanning unit equipped with a PL APO lambda blue 63×/1.2-NA water immersion objective.
- Zeiss Axiovert LSM 510-META inverted microscope equipped with a Zeiss PlanNeoFluar 20×/0.5NA and Zeiss Plan-Apochromat 63×/1.4NA oil objective lens.

Images were collected with Metamorph v.7.7.7 (Molecular Devices), FV10-ASW1.7 (Olympus), LAS AF v. 2.6.0. (Leica) or LaserSharp 2000v. 5.2 (Zeiss) acquisition software.

Images and videos were processed using ImageJ and Adobe Photoshop. We used ImageJ to quantify fluorescence signals or calculate areas of interest as described for each methods section, and to generate orthogonal and Z-projections. Pearson's correlation and Manders' overlap coefficients were calculated with ImageJ plugin JACoP (Just Another Co-localization Plugin) [30]. To quantify fluorescence immune synapse signals, we measured mean fluorescence intensity (MFI) ratios at the IS vs. other regions of interest using an ImageJ plugin developed in-house (COS Sorzano, CNB/CSIC) [270]. Ratio values were represented in graphs as dot plots, with each dot representing an individual cell.

9. PROTEOMICS ANALYSIS

9.1. Protein identification

We used standard procedures for protein identification. Briefly, eluted protein samples were separated by SDS-PAGE. Sixteen bands per sample were digested by automated in-gel digestion in a Proteineer DP (Bruker Daltonics); gel plugs were reduced (10 mM DTT) and alkylated (50 mM iodoacetamide), and digested with ~10 ng trypsin (Proteomics Grade Trypsin; Sigma-Aldrich) per gel plug (18 h). Tryptic peptides were extracted with 50% ACN, 1% TFA and dried by speed vac. Samples were pooled and analyzed by LC-MS/MS.

9.2. LC-MS/MS analysis

Tryptic peptides were analyzed by LC-MS/MS using a nano-HPLC system (Eksigent Technologies nanoLC Ultra 1D plus, AB SCIEX) coupled online to a TripleTOF 5600 mass spectrometer (AB SCIEX) with a nano-spray ionization source. The analytical column was a nano-Acquity UPLC column (1.7 μm, BEH 130 C18; Waters). The trap column was a nanoViper column Acclaim PepMap C18, 5 μm (Thermo Fisher Scientific). The loading pump delivered 0.1% formic acid in water at 2 μl/min; the nanopump provided a flow rate of 250 nl/min and was operated in gradient elution conditions with 0.1% formic acid in water as mobile phase A, and 0.1% formic acid in ACN as mobile phase B. Gradient elution was as follows: 98% A:2% B for 1 min, a linear increase to 30% B in 110 min and to 40% B in 10 min, then to 90% B in 5 min; isocratic conditions of 90% B for 5 min and return to initial conditions in 2 min. In general, one-third of the sample was processed by nanoLC-MS in a 5 μl injection volume.

Settings for TripleTOF were: ionspray voltage floating (ISVF) = 2800 V, curtain gas (CUR) = 20, interface heater temperature (IHT) = 150, ion source gas 1 (GS1) = 30, declustering potential (DP) = 85 V. Data were acquired in an information-dependent acquisition (IDA) mode with Analyst TF 1.7 software (AB SCIEX). For IDA parameters, a MS survey scan

(250 ms) in the mass range of 350-1250 *m/z* was followed by 25 MS/MS scans (100 ms) in the mass range of 100-1500 *m/z*. Switching criteria set to ions greater than *m/z* = 350 and smaller than *m/z* = 1250, with a charge state of 2-5, threshold >90 counts (cps) and dynamic exclusion of 20 s. Collision energy (CE) was set as rolling CE using a parameter script.

9.3. Data analysis

MS and MS/MS data for each sample fraction were processed using Analyst TF 1.7 Software. Raw data were translated to mascot general file (mgf) format using the PeakView program v.1.2 and a Uniprot database (2014-03-26) with human taxonomy restriction (NEWT 9606), containing 39,785 protein-coding genes and their reverse entries in an in-house Mascot Server v.2.5.1 (Matrix Science). Search parameters were as follows: fixed modification of carbamidomethyl cysteine; variable modifications oxidation of methionines and acetylation of the peptide N termini; peptide mass tolerance ±25 ppm; fragment mass tolerance ±0.05 Da; maximum of two trypsin digestion missed-cleavages. Accuracy of ±10 ppm was typically found for MS and MS/MS spectra. Criteria to accept individual spectra were based on Mascot ion score threshold (0.05) as the standard ion score threshold, and the identification certainty was established using false discovery rate criteria (FDR ≤1%) for peptide and protein matches using the Scaffold bioinformatic tool v.4.2.1 (Proteome Software). This cutoff value for protein identification corresponded to a Mascot score of protein identification of 25. A minimum of two peptides was required to identify a protein. The mass spectrometry proteomics data have been deposited in the ProteomeXchange Consortium via the PRIDE [336] partner repository with the dataset identifier PXD003628 and 10.6019/PXD003628.

9.4. Functional interpretation

To interpret the biological role of genes reported, Gene Ontology (GO) clustering analysis was performed by ClueGO (v.2.2.3), a Cytoscape plug-in (v.3.3.0). The PDZ-independent SNX27 interactome was clustered in molecular function GO categories with a 0.3 kappa score. The color code indicates the p value for enriched GO terms, and node size, the number of mapped genes. The CluePedia plug-in (v.1.2.3) was used to depict proteins associated with GO terms, and the STRING interaction database (v.10) to show reported interactions among transport-related proteins.

10. STATISTICAL ANALYSIS

Student's *t*-test was used to analyze differences between two conditions, using the paired two-tailed *t*-test when comparing data sets from each pair of WT and *Snx27*$^{-/-}$ mouse littermates. Two-way ANOVA with the Bonferroni post-hoc test was used for multiple comparisons, both with GraphPad Prism 5 software. Differences were considered not significant (ns) when $p > 0.05$, significant (*) when $p < 0.05$, very significant (**) when $p < 0.01$ and extremely significant (***) when $p < 0.001$.

Results

V. RESULTS

1. SNX27 DYNAMICS AND FUNCTION AT THE IMMUNE SYNAPSE

Our group examined the dynamics of SNX27 localization to the IS in T lymphocytes, and showed that SNX27 PX and PDZ domains are involved in IS recruitment [270]. Recent structural studies have revealed molecular details of SNX27 FERM and PDZ domains [111, 117, 308]. We investigated their particular contribution to SNX27 IS localization.

1.1. FERM domain contribution to SNX27 localization to the IS

1.1.1. NPxY/NxxY binding contribution to SNX27 localization

SNX-FERM proteins have an atypical FERM domain responsible for binding cargoes bearing the NPxY/NxxY motif for recycling [117]. In peptide array experiments, SNX27 bound preferentially to sequences phosphorylated at Y_0 in a large variety of transmembrane proteins [116]; these include proteins stimulated after T cell activation. To determine whether SNX27 binding to NPxY/NxxY motif-containing cargoes participates in its localization to the IS, we tested the ability of the non-NPxY/NxxY-binding mutant SNX27 (GFP-SNX27 W475A; Fig R1A) to accumulate at the T cell-APC contact area. Jurkat T cells were transfected with the GFP-tagged constructs (Fig R1A) and incubated with SEE-loaded Raji B cells as APC, to allow IS formation. Videomicroscopy showed that, compared to the WT protein, GFP-SNX27 W475A did not show localization defects (Fig R1B, C), demonstrating that impaired NPxY/NPxxY motif binding does not prevent SNX27 localization to the IS.

1.1.2. Lipid binding contribution to SNX27 localization

FERM domains show PtdInsP-binding activities in some proteins (reviewed in [16]). In collaboration with our colleagues from Dr. Brett Collins's group (Institute for Molecular Bioscience, University of Queensland, Australia), we examined SNX27 PtdIns-binding capacity, and identified a new PtdInsP-binding site with a clear preference for bi- and triphosphorylated PtdIns (see table in Appendix 2) [118]. Homology modeling identified the PtdInsP-binding site in the SNX27 FERM F3 subdomain. Sequence alignment comparison of the F3 subdomain of SNX17, SNX27 and SNX31 indicated the positively charged amino acids that constitute a basic patch on the SNX27 F3 module, which were absent in SNX17 and SNX31. The interaction was confirmed by biophysical, mutagenesis and modeling approaches (for more information see [118] in Appendix 4.1).

T cell-APC encounter triggers signaling processes such as PI3K activation, which increases local concentrations of PtdIns(3,4,5)P_3 ([63, 138, 181]). We thus hypothesized that the FERM PtdInsP-binding site plays a role in SNX27 recruitment to the IS, and therefore analyzed the localization of the SNX27 non-PtdInsP-binding mutant R435E/R436E/K437E (hereafter RRK/E)

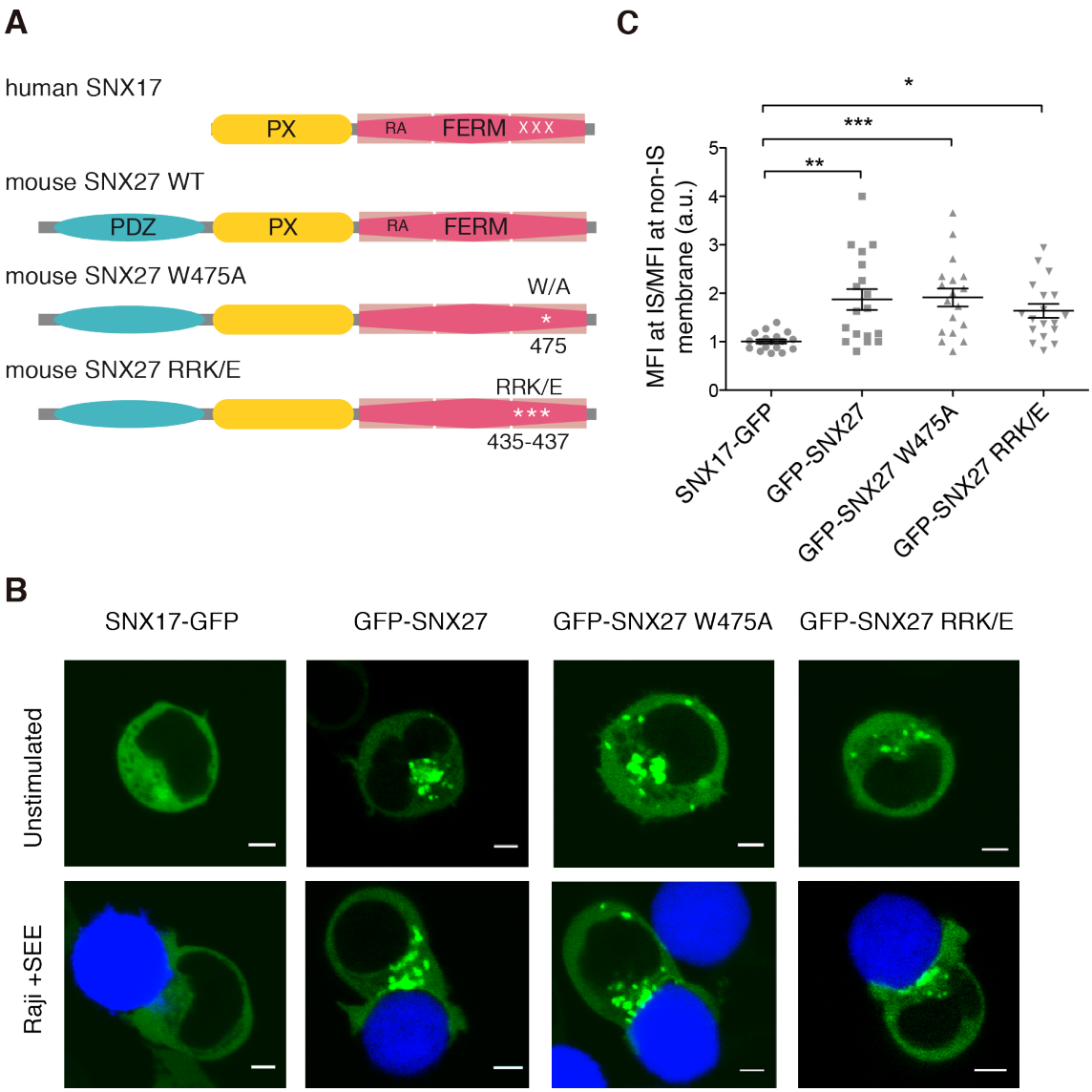

Fig R1. FERM domain interactions with PtdInsP lipids and NPxY/NxxY-motif are not necessary for SNX27 recruitment to the immune synapse

(**A**) Scheme of proteins used (GFP not shown). SNX27 W475A is the non-NPxY/NxxY-binding mutant, and SNX27 RRK/E is the non-PtdInsP-binding mutant. (**B**, **C**) For videomicroscopy, Jurkat T cells were transfected with the indicated GFP-tagged constructs (green) (**B**, top), and stimulated with SEE-pulsed Raji B cells (blue) (**B**, bottom). Representative images are shown. Bar: 3 μm. (**C**) Quantitative analysis of GFP-tagged protein accumulation at the immune synapse (IS). Each dot represents the synapse:cytosol intensity ratio for each protein after antigen presenting cell (APC) encounter. Data shown as mean ± SEM (*p<0.05, **p <0.01, ***p <0.001; one-way ANOVA/Bonferroni post test; n ≥ 19). a.u., arbitrary units. A representative experiment is shown (*n* = 3).

during IS formation. We compared its dynamics to those of GFP-SNX27 WT protein and SNX17-GFP, which lacks both the PtdInsP-binding pocket and the PDZ domain (Fig R1A). Whereas SNX17-GFP did not show IS localization, GFP-SNX27 RRK/E recruitment to the IS was similar to that in the WT protein (Fig R1B, C); this suggested that the FERM domain PtdInsP-binding site is not necessary for SNX27 localization to the T cell-APC contact area. The punctuate endosomal location of the RRK/E mutant in unstimulated Jurkat cells was nonetheless not well defined after APC engagement (Fig R1B). Since SNX17-GFP showed impaired endosomal and IS localization (Fig R1B, C), and PDZ deletion reduces SNX27 targeting to the ERC [271] and the IS [270], lack of the PDZ domain could explain SNX17 localization defects, but not those of the non-PtdInsP-binding mutant.

To better assess differences in endosomal localization for the RRK/E mutant during IS formation, we measured the overlap of our GFP-tagged constructs with internalized Tf (rhodamine-coupled Tf, Tf-Rhod) as an ERC marker. Videomicroscopy showed that in Jurkat cells, the GFP-SNX27 RRK/E colocalized with Tf-positive vesicles (Fig R2A, B). Quantitative analysis nonetheless demonstrated a significant decrease in Tf-Rhod colocalization with the GFP-SNX27 RRK/E mutant or SNX17-GFP compared with GFP-SNX27 WT protein, in basal and in polarized recycling conditions (Fig R2C). This defect was the result of reduced endosomal association, measured as the ratio of punctuate-to-cytosolic fluorescence (Fig R2D). Z-stack projections of confocal images showed the entire ERC and confirmed that after T cell stimulation, GFP-SNX27 maintains overlap with the polarized Tf-positive recycling organelles, and some labeling at the contact area (Fig R3A B, top). The non-PtdInsP-binding mutant was also found at the cell-cell contact site, but did not colocalize with the Tf-positive recycling compartment after IS formation (Fig R3A B, bottom).

Time-lapse imaging of Jurkat T cells cotransfected with cherry-SNX27 and GFP-SNX27 RRK/E further confirmed similar translocation dynamics, with loss of endosomal labeling of the FERM mutant (Fig R3C, Video 1; see links to all videos in Appendix 3). Whereas blocking FERM domain binding to PtdInsP did not grossly impair SNX27 localization to the IS, increased cytosolic fluorescence in GFP-SNX27(RRK/E)-expressing cells correlated with defective localization to the ERC. This coincides with results from Tseng *et al.*, who compared SNX27 vesicle-binding abilities to those of other SNX-FERM proteins, and suggested an additional lipid-binding site in SNX27 that was absent in both SNX17 and SNX31 [326].

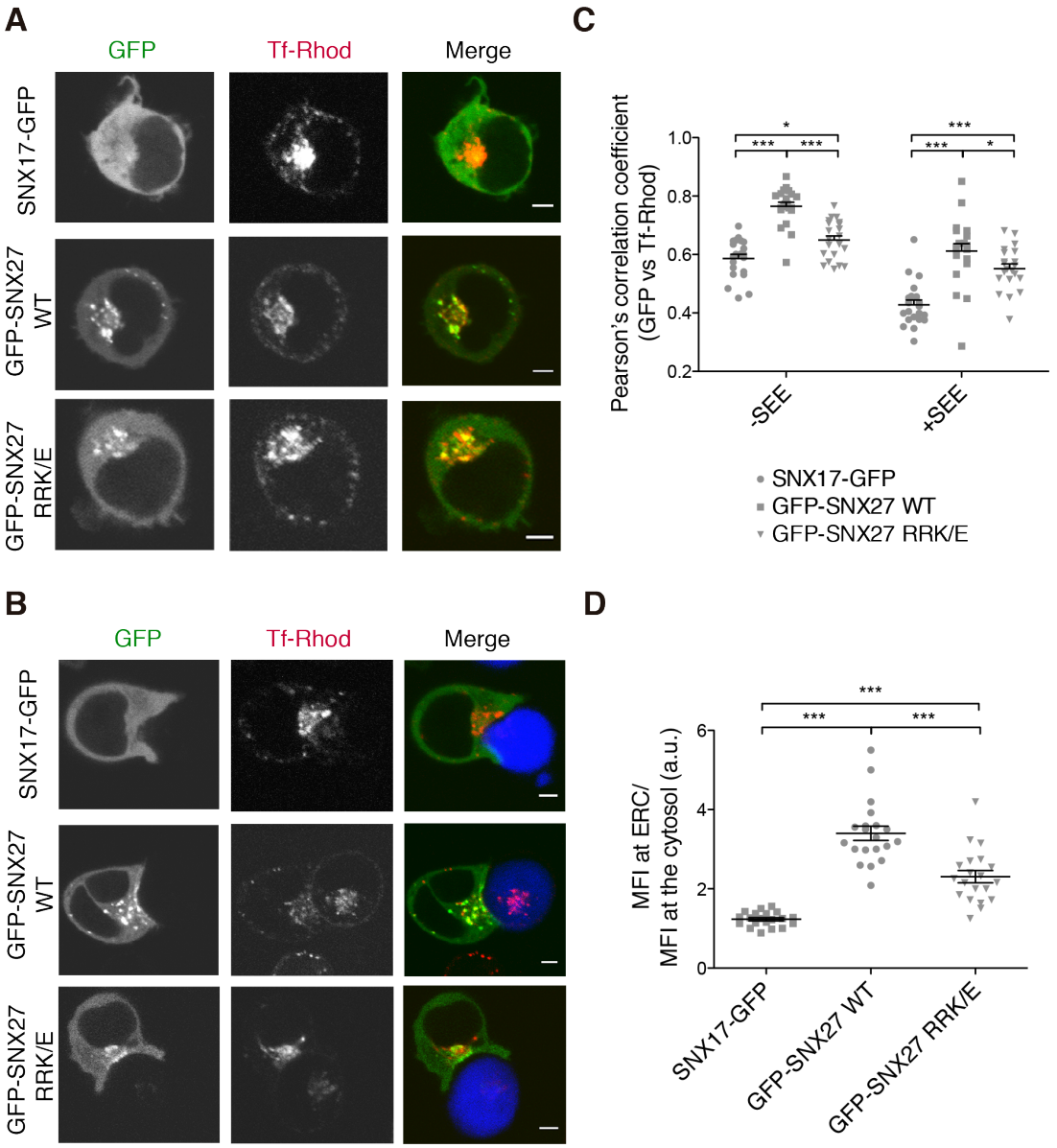

Fig R2. PtdInsP lipid interaction through the SNX27 FERM domain contributes to its recruitment to the endocytic recycling compartment

Jurkat T cells were transfected with GFP-tagged constructs (green), incubated with Tf-Rhod (rhodamine-coupled transferrin; red) to visualize Tf-positive recycling endosomes by videomicroscopy (**A**), and stimulated with SEE-pulsed Raji B cells (blue) (**B**). Bar: 3 μm. WT and PtdInsP-binding mutant (RRK/E) GFP-SNX27 colocalization with Tf-Rhod (**C**). Measurement of the punctuate-to-cytosolic fluorescence intensity ratio (**D**) suggested that this defect is the result of reduced GFP-SNX27 RRK/E endosomal association. (C, D) Pearson's correlation coefficient and ratio values are represented as dot plots, with each dot representing an individual cell. Data shown as mean ± SEM. *p <0.05, ***p <0.001; two-way ANOVA; n ≥ 15; a representative experiment is shown.

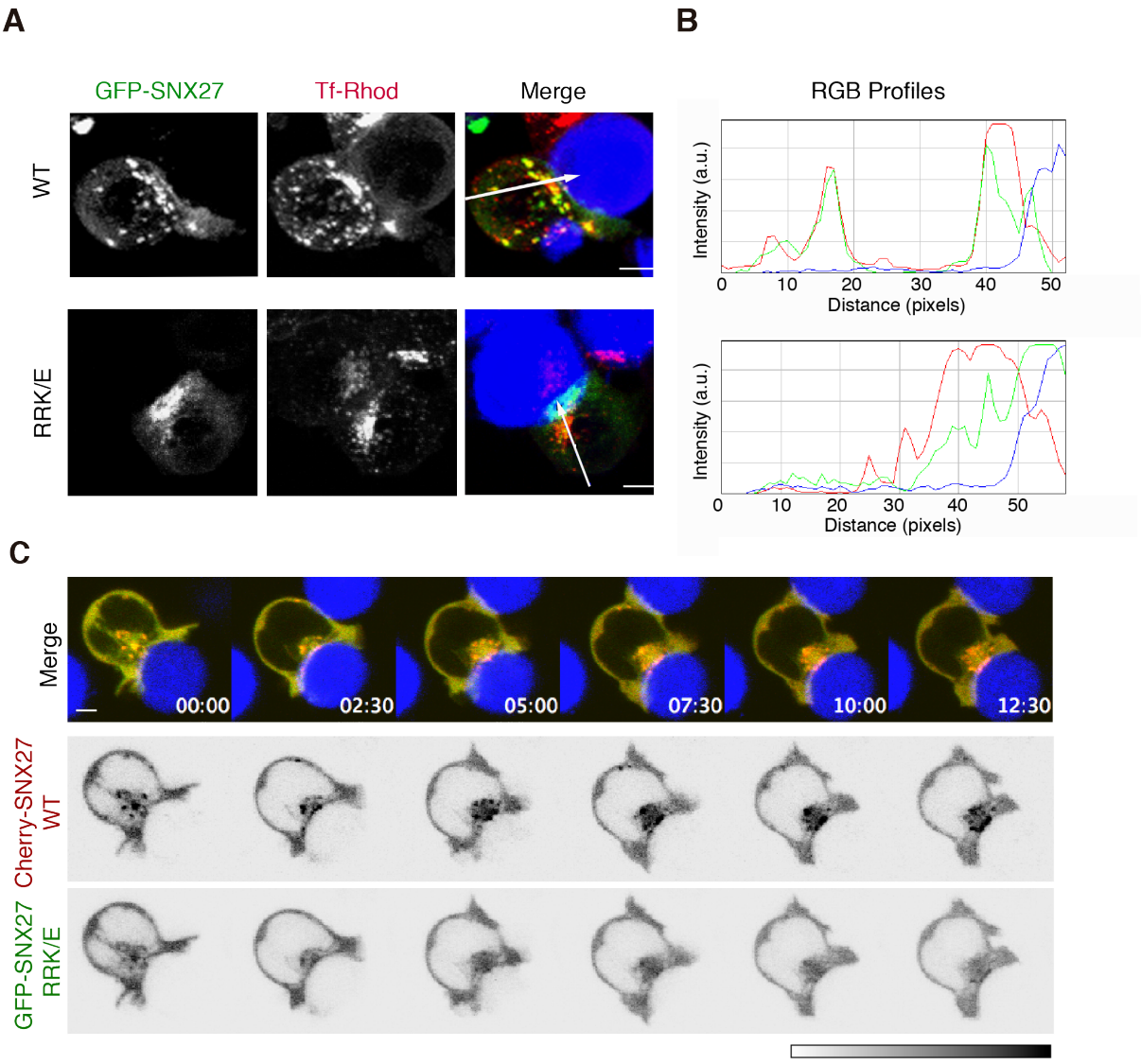

Fig R3. SNX27 recruitment to recycling endosomes is enhanced by PtdInsP binding to the FERM domain

(**A**) Jurkat T cells were transfected with GFP-tagged constructs (green), incubated with Tf-Rhod (red) to visualize Tf-positive recycling endosomes, and stimulated with SEE-pulsed Raji B cells (blue). Cells were methanol-fixed and imaged by confocal microscopy. A Z-stack projection shows that, after synapse formation, WT GFP-SNX27 but not the PtdInsP-binding mutant colocalizes with Tf-Rhod-positive compartments. (**B**) Densitometric analysis of GFP-SNX27 and Tf-Rhod distribution along the white lines in (A). (**C**) The relative dynamics of IS recruitment of SNX27 to the IS were assessed directly by comparing Cherry-SNX27 with GFP-SNX27 RRK/E. Live transfected Jurkat cells were imaged, SEE-pulsed APC were added, and images acquired every 15 s by time-lapse microscopy (see complete video in **Video 1**). Bars in A, C: 3 μm. Color scale of fluorescence intensity (C, bottom).

As mentioned above, the FERM domain lipid-binding site showed a clear preference for bi- and triphosphorylated PtdIns such as PtdIns(4,5)P_2 and PtdIns(3,4,5)P_3. We analyzed the contribution of these lipids to SNX27 recruitment to the IS by studying lipid dynamics using fluorescent probes for these lipids, to track their subcellular distribution in living T cells. PI3K-mediated generation of PtdIns(3,4,5)P_3 at the PM is one of the earliest signals observed in IS formation [138]. Transfection of Jurkat T cells with the PtdIns(3,4,5)P_3-binding AKT pleckstrin homology (PH) domain (DsRed-AKT-PH) allowed distinction between initial and mature stages of IS formation (Fig R4A, B). We confirmed PtdIns(3,4,5)P_3 accumulation at the T cell-APC contact area during early IS formation. At later times, the AKT-PH domain translocated to distal and peripheral areas that correspond to annular PtdIns(3,4,5)P_3 accumulation, which controls actin architecture and thus facilitates cell adhesion and polarized secretion [181]. Cotransfection of the PtdIns(3,4,5)P_3 sensor with WT or the non-lipid-binding SNX27 showed impaired mutant protein colocalization with PtdIns(3,4,5)P_3 during initial recruitment (Fig R4A, B). This result suggests that the early SNX27 translocation to the PM is enhanced by FERM domain binding to lipids.

Together with its phosphorylated product PtdIns(3,4,5)P_3, PtdIns(4,5)P_2 is also recognized as a regulator of polarized trafficking; the spatiotemporal generation and accumulation of this lipid is modulated precisely to activate effectors or signaling molecules (reviewed in [79]). In stimulated T cells, PtdIns(4,5)P_2 is converted to PtdIns(3,4,5)P_3 by PI3K, or is hydrolyzed by PLC to produce Ins(1,4,5)P_3 and DAG. As a result, PtdIns(4,5)P_2 levels decrease substantially following APC contact, and transfection of the GFP-tagged PLCδ PtdIns(4,5)P_2-binding PH domain did not allow clear analysis of PtdIns(4,5)P_2 dynamics in activated T cells (not shown).

As the IS is a focal point not only for endocytosis, but also for exocytosis [128], we considered that vesicle fusion to the PM could result in SNX27 accumulation at the synapse. To track the dynamics of ERC-enriched PtdIns3P, we transfected Jurkat T cells with a sensor composed of two tandem FYVE domains fused to a fluorescent protein (Cherry-FYVE). When T cells were cotransfected with Cherry-FYVE and the SNX27 constructs, both GFP-SNX27 and the GFP-SNX27 RRK/E mutant showed substantial overlap with PtdIns3P-positive intracellular compartments in unstimulated T cells (Fig R5A). APC-challenged T cells did not accumulate PtdIns3P at the synapse; instead, PtdIns3P-enriched vesicles accumulated at discrete locations that delimited the SNX27-positive compartment, often at two foci at the synapse periphery (Fig R5B). These results suggest that SNX27 localization at the IS is not strictly dependent on either PtdIns3P or PtdIns(3,4,5)P_3 association, but that dynamic changes in SNX27 PtdInsP interactions lead to segregation to distinct membrane domains.

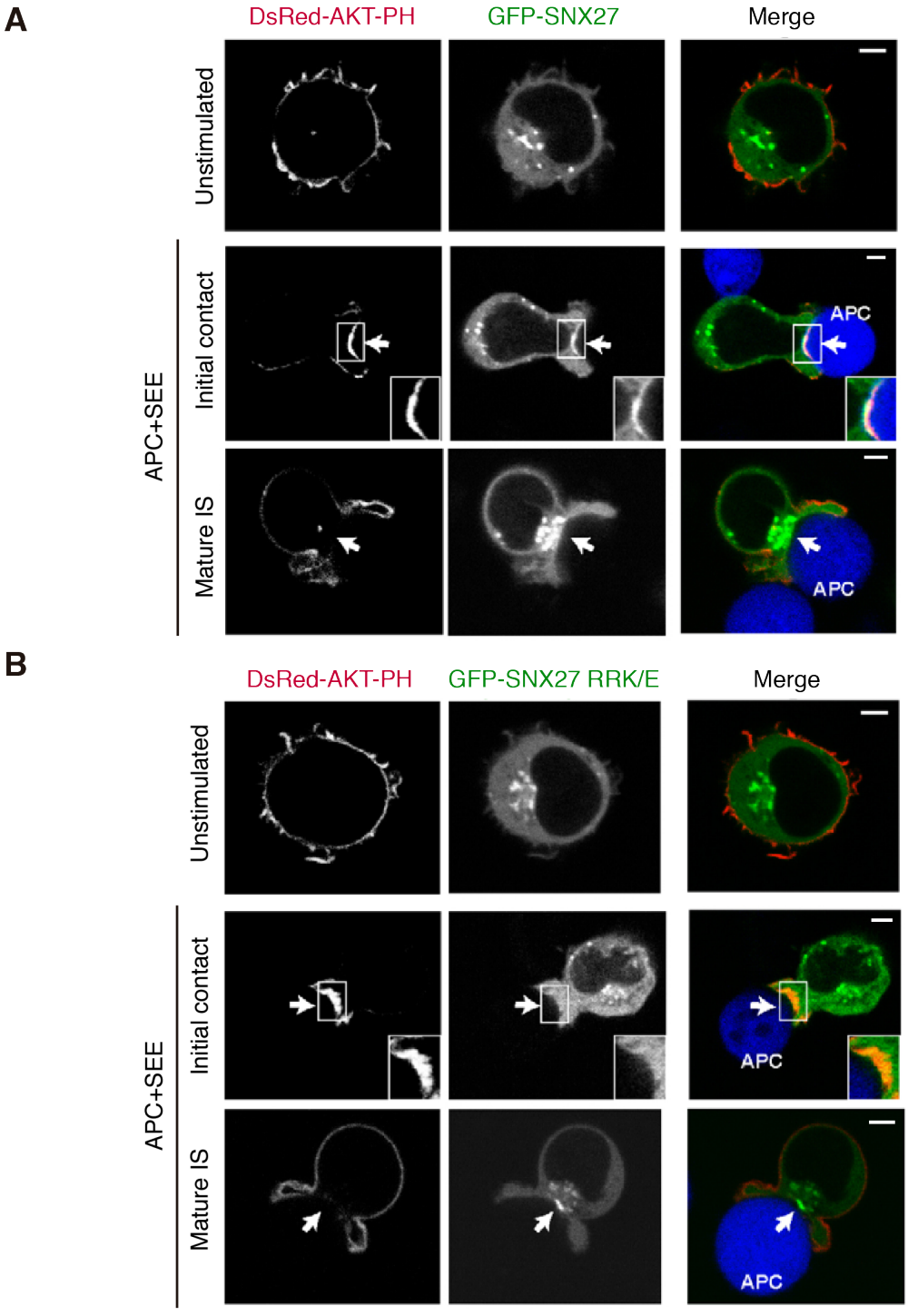

Fig R4. SNX27 accumulates transiently at discrete PtdIns(3,4,5)P_3-enriched sites during T cell-APC contact

Jurkat T cells were stimulated with SEE-pulsed APC (blue) after cotransfection with the PtdIns(3,4,5)P_3-binding probe DsRed2-PH-AKT (red) and WT GFP-SNX27 (**A**) or the RRK/E mutant (**B**). At initial contact, WT GFP-SNX27 overlapped clearly with the PtdIns(3,4,5)P_3 probe, but not at later times, as PtdIns(3,4,5)P_3 redistributed to peripheral IS areas. In contrast, the RRK/E mutant SNX27 showed little colocalization with the PtdIns(3,4,5)P_3 probe at any stage during synapse formation. Arrows indicate IS location; initial contact is shown in insets; bar: 3 μm.

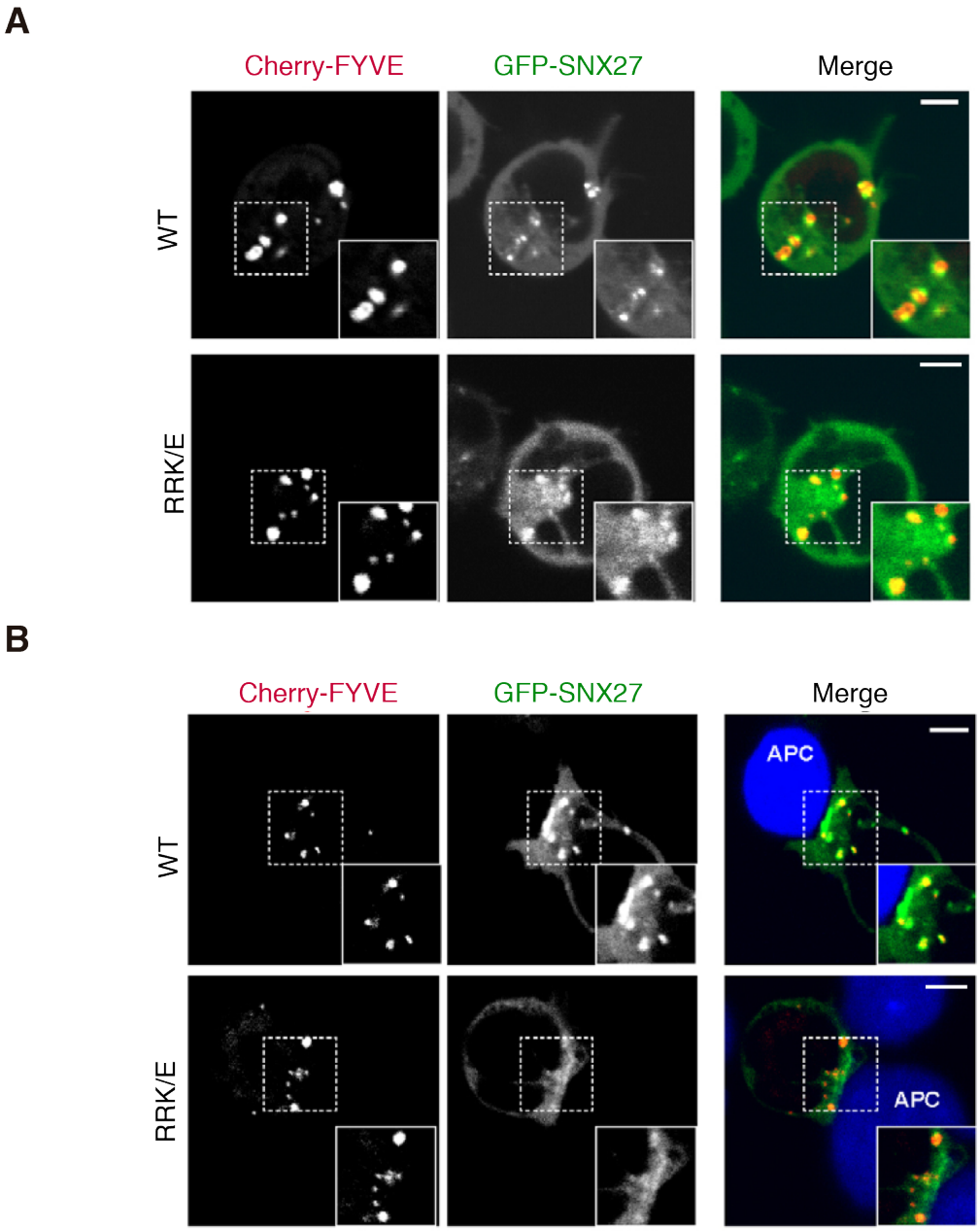

Fig R5. SNX27 accumulates at discrete PtdIns3P-enriched sites during T cell-APC contact

Jurkat T cells were cotransfected with the PtdIns3P-binding probe Cherry-FYVE (red) and GFP-SNX27 or the GFP-SNX27 RRK/E mutant (both green). (**A**) In resting T cells, both of the GFP-SNX27 proteins showed marked colocalization with PtdIns3P-postive intracellular compartments. (**B**) After stimulation with SEE-pulsed APC (blue), intracellular PtdIns3P-postive vesicles localized to the contact area outside the limits of the GFP-SNX27 and GFP-SNX27 RRK/E pools at the IS. Insets show areas with GFP/Cherry colocalization; bar: 3 μm.

1.2. PDZ domain contribution to SNX27 localization at the IS

SNX27 accumulation at the T cell-APC contact area is impaired by deletion of the SNX27 PDZ domain [270], which simultaneously binds to PDZ-bm-containing cargoes and to the retromer component VPS26 [111, 308]. Mutation of L67-74A or H114A residues in SNX27 abolishes its interaction with VPS26 or with PDZ ligands, respectively [111] (Fig R6A). We carried out co-immunoprecipitation analyses of the GFP-SNX27 WT and PDZ mutant proteins expressed in Jurkat T cells. We used as a control the SNX27 PDZ-interacting protein DGKζ [270, 271] and observed that the histidine residue at position 114 of SNX27 is essential for DGKζ interaction, whereas impaired VPS26 interaction (L67-74A mutant) reduces DGKζ recognition (Fig R6B). These experiments showed that VPS26 association cooperates in SNX27 binding to DGKζ, as demonstrated for other PDZ cargoes such as GLUT1, and Kir3.3 [111].

To examine the contribution of these two PDZ subdomains to SNX27 localization at the IS, Jurkat cells were transfected with the GFP-SNX27 constructs and incubated with SEE-loaded APC to allow IS formation. Confocal microscopy analysis showed that the WT GFP-SNX27

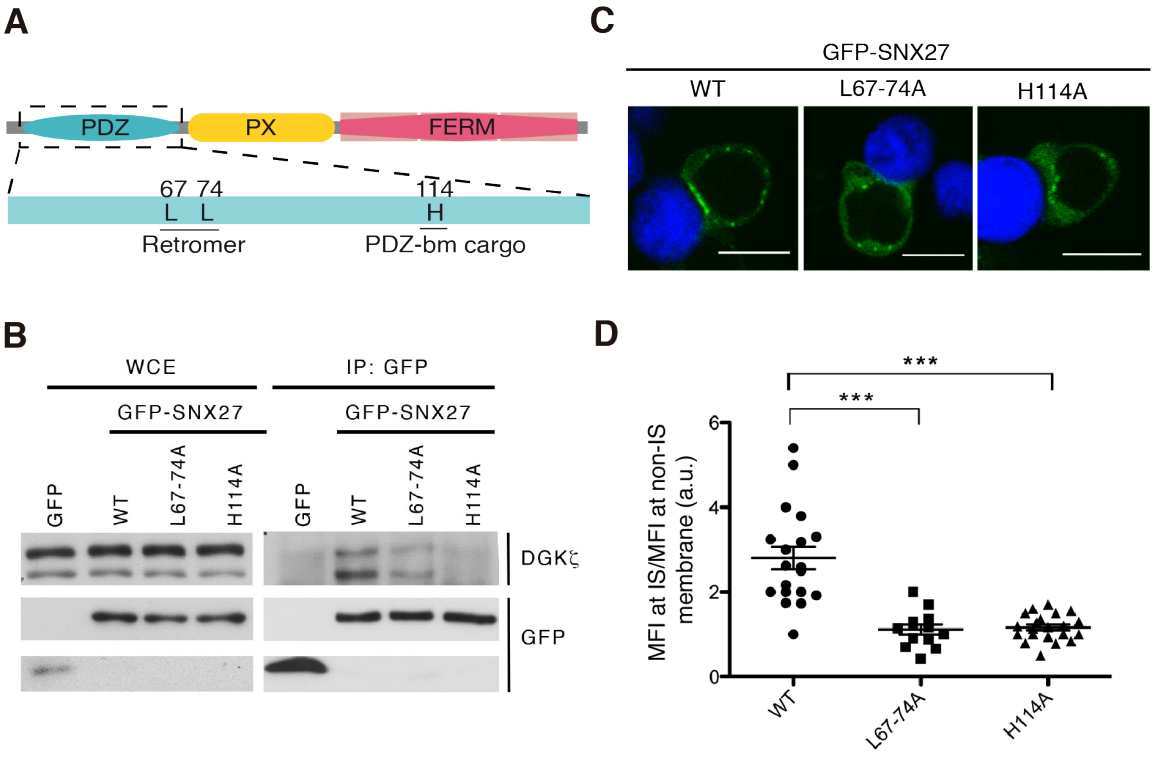

Fig R6. Cargo binding through the SNX27 PDZ domain promotes its accumulation at the immune synapse

(**A**) SNX27 structure, with details of amino acids involved in PDZ domain interactions. (**B**-**D**) Jurkat T cells were transfected with the indicated GFP-tagged constructs. (**B**) GFP immunoprecipitates from whole-cell lysates were analyzed by western blot. DGKζ was used as a control for PDZ-bm-mediated interactions. (**C**, **D**) GFP-SNX27 (green)-transfected Jurkat T cells were stimulated with SEE-pulsed Raji B cells (blue) (15 min) and fixed with cold methanol. (**C**) Representative confocal images; bar: 10 μm. (**D**) Quantitative analysis of WT and mutant GFP-SNX27 accumulation at the IS. Each dot represents the synapse/cytosol mean fluorescence intensity (MFI) ratio of the proteins after APC encounter. Data shown as mean ± SEM; ***p <0.001; one-way ANOVA/Bonferroni post test; $n \geq 19$. A representative experiment is shown.

protein polarized to the IS and accumulated at the T cell-APC area. In contrast, IS localization of the GFP-SNX27 PDZ mutant proteins was impaired (Fig R6C, D). These results showed that a reduced recognition of PDZ ligands by SNX27, directly due to mutation of the PDZ-bm-interacting residues (GFP-SNX27 H114A), or indirectly due to mutation of VPS26-binding residues (GFP-SNX27 L67-74A), prevents SNX27 accumulation at the IS.

To determine PDZ ligand binding contribution to SNX27 localization at the IS and at the early endosomes we immunostained the transfected cells using PKCθ as an IS marker, and EEA1 as an endosomal marker, and analyzed their colocalization with the GFP-SNX27 H114A mutant and the WT proteins. Both proteins colocalized similarly with EEA1-positive vesicles (Fig R7C, D), but only the WT protein accumulated at the PKCθ-positive IS area (Fig R7A,B). This confirmed that impaired cargo interaction mainly affects SNX27 localization to the T cell-APC contact area. To track the simultaneous dynamics of polarization, we cotransfected Cherry-SNX27 WT and GFP-SNX27 H114A. The proteins colocalized in polarized vesicles, although H114A SNX27 did not accumulate at the cell-cell contact area (Fig R7E, F and Video 2). Our results demonstrate the type of interactions necessary for SNX27 localization at the T cell-APC contact area, and support previous data suggesting that PDZ binding to an as yet uncharacterized protein(s) is the main driver of SNX27 accumulation at the IS [270].

1.3. Analysis of the SNX27 interactome during IS formation

SNX27 accumulation at the T cell-APC contact area is lost in the absence of PDZ ligand interaction. To establish the proteins associated with SNX27 during IS formation, we examined the SNX27 interactome and compared it with that of the H114A SNX27 mutant, which has impaired PDZ ligand binding. Conjugates of transfected Jurkat T cells and SEE-loaded APC were lysed, GFP-tagged proteins were immunoprecipitated, and associated proteins analyzed by MS (Fig R8). Immunoprecipitates from empty GFP vector-transfected cells were used as controls. A total of 186 proteins were specific to the SNX27 immunoprecipitates, with proteins that interacted only with WT SNX27 (30 proteins, Supplemental Table S3; see links to all supplemental tables in Appendix 3), the mutant form (31, Supplemental Table S4), or both (125, Supplemental Table S5).

1.3.1. PDZ-independent SNX27 interactions during IS formation

We first explored the PDZ-independent interactome (Supplemental Table S5), shared by WT and H114A GFP-SNX27, to determine the biological role of the identified proteins. Analysis of the Gene Ontology (GO) “Biological Process” terms showed an enrichment in proteins involved in endosomal transport, but also in endocytosis-mediated downregulation of receptor signaling. The large representation of protein binders involved in metabolic process and translation suggests the complexity of SNX27 functions (Fig R9A**,** see data in Supplemental Table S6). The proteins linked to endosomal transport included all the main retromer and WASH complex members as well as some associated regulatory proteins (Fig 9B, Table R1). Noteworthy, we also identified USP7, a deubiquitinating enzyme recently reported to control ubiquitin-dependent

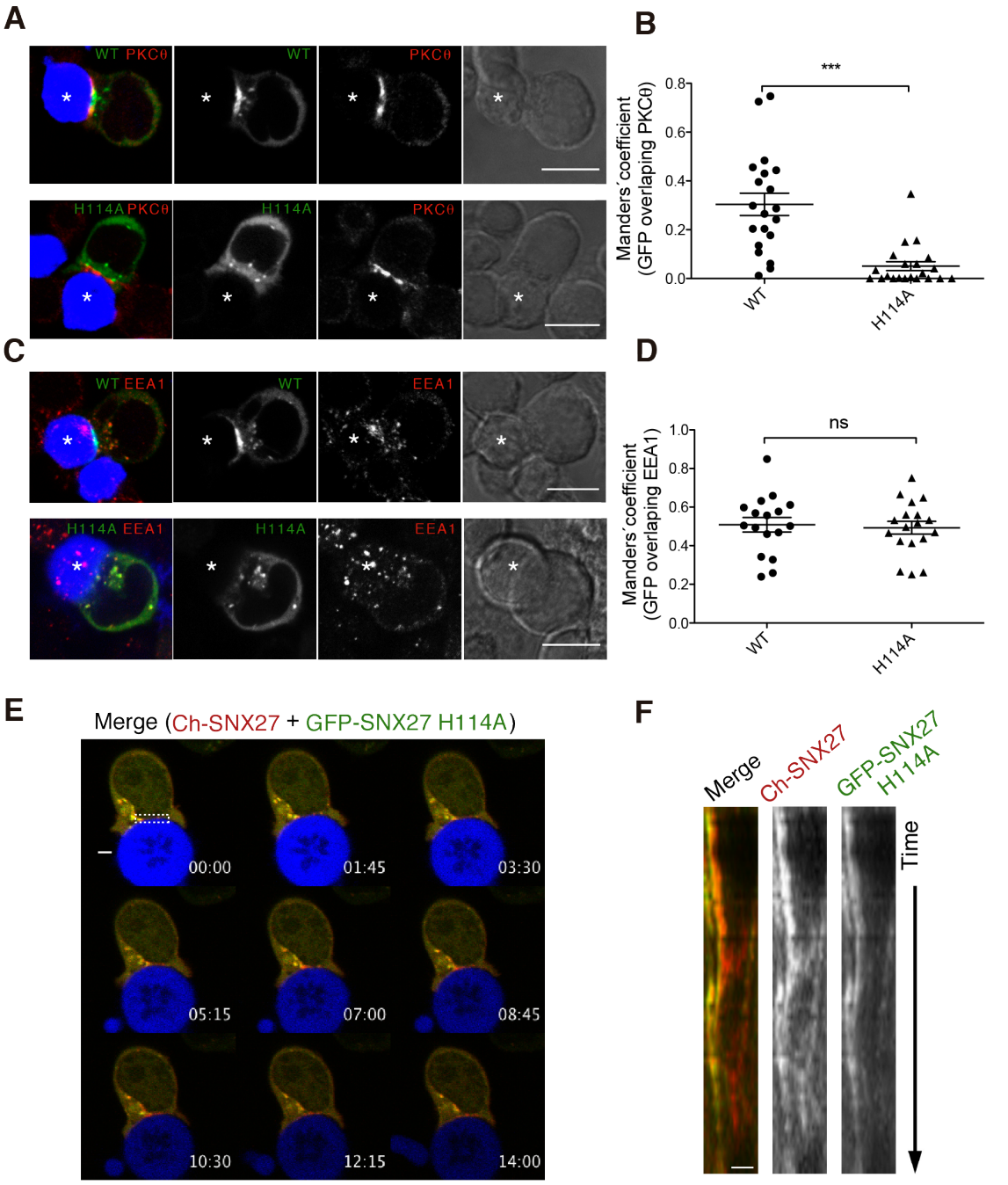

Fig R7. H114A mutation in SNX27 prevents accumulation at the immune synapse

(**A**, **C**) Representative confocal images of GFP-SNX27 (green)-transfected Jurkat T cells stimulated with SEE-loaded Raji cells (blue; white asterisk), then immunostained (red) (**A**) for the PKCθ IS marker or (**C**) for EEA1 to label the endosomal compartment; bar: 10 μm. The WT, but not the PDZ mutant GFP-SNX27, localized to the PKCθ positive area at the T cell-APC contact region. (**B**, **D**) Quantitative analysis of WT and mutant GFP-SNX27 colocalization with (B) PKCθ or (D) EEA1. Manders' overlap coefficient values are represented as dot plots, with each dot representing an individual cell. Data shown as mean ± SEM. (ns, not significant, $p>0.05$; ***$p<0.001$; t-test; $n \geq 20$; a representative experiment is shown). (**E**, **F**) The relative dynamics of SNX27 recruitment to the IS was assessed directly by comparing Cherry-SNX27 (red) with GFP-SNX27 H114A (green) cotransfected in Jurkat T cells. SEE-loaded Raji cells (blue) were added and cells imaged every 15 s by time-lapse microscopy (**E**; see complete video in **Video 2**). (**F**) A composite kymograph of SNX27 construct dynamics were acquired for the dashed area in (E). Bars: 3 μm.

WASH activation [135]. The presence of USP7 in GFP-SNX27 immunoprecipitates suggests its interaction with the SNX27/WASH/retromer multimeric protein complex, and that this ubiquitin-mediated WASH regulatory mechanism operates during IS formation.

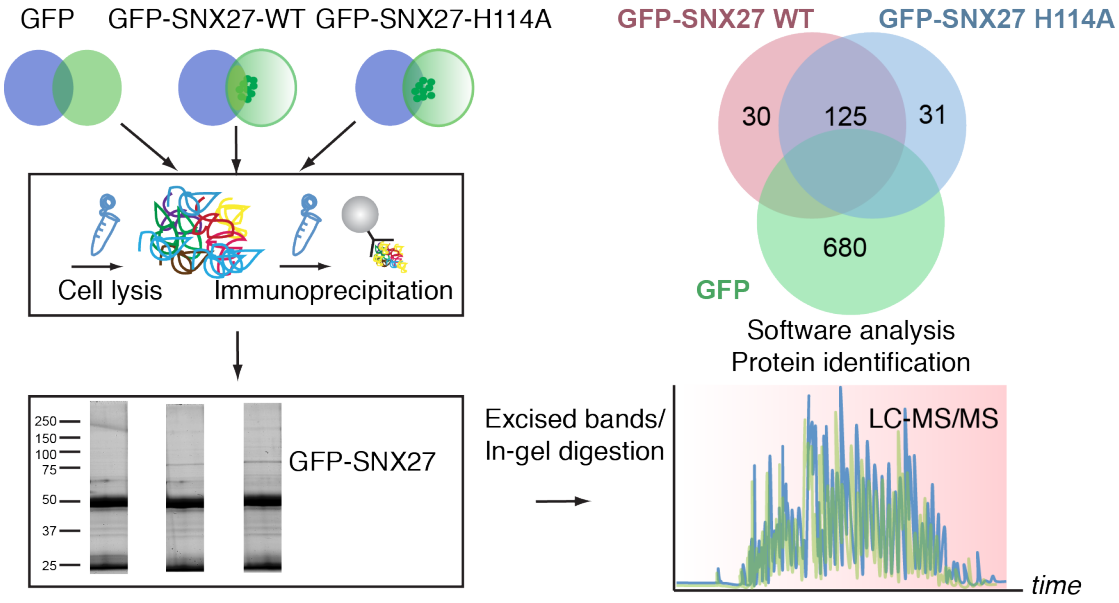

Fig R8. Proteomic analysis of SNX27 interactome during IS formation

Overview of the workflow used. Jurkat T cells were transfected with the indicated GFP-tagged constructs. After 24 h, cells were mixed at a 1:1 ratio with SEE-loaded Raji cells and incubated (15 min). Cells were lysed and GFP immunoprecipitates were analyzed by 1D-gel-MS for protein identification and by western blot for validation.

Protein name	Interactors	References
Retromer complex		
VPS35	VPS29, VPS26, FAM21, TBC1D5, FKBP15	61, 123, 136, 145, 264, 363
VPS29	VPS35	61, 145, 264, 363
VPS26	VPS35, SNX27	111, 123, 145, 264, 308, 363
WASH complex		
WASH1	FAM21, Strumpellin, SWIP, CCDC53	77, 124, 161
FAM21	VPS35, VPS29, FKBP15, SNX27, RME-8, WASH	77, 110, 124, 137, 141, 160, 185, 308
Strumpellin/KIAA0196	SWIP, FAM21, WASH	77, 161
SWIP/KIAA1033	Strumpellin, WASH	77, 161
CCDC53	WASH	77, 161
Associated proteins		
RME-8/DNAJC13	FAM21	110
TBC1D5	VPS35/29/26	136, 260, 287
FKBP15/FKBP133/WAFL	FAM21, VPS35/29/26	136, 137

Table R1. PDZ-independent SNX27 interactome during IS formation

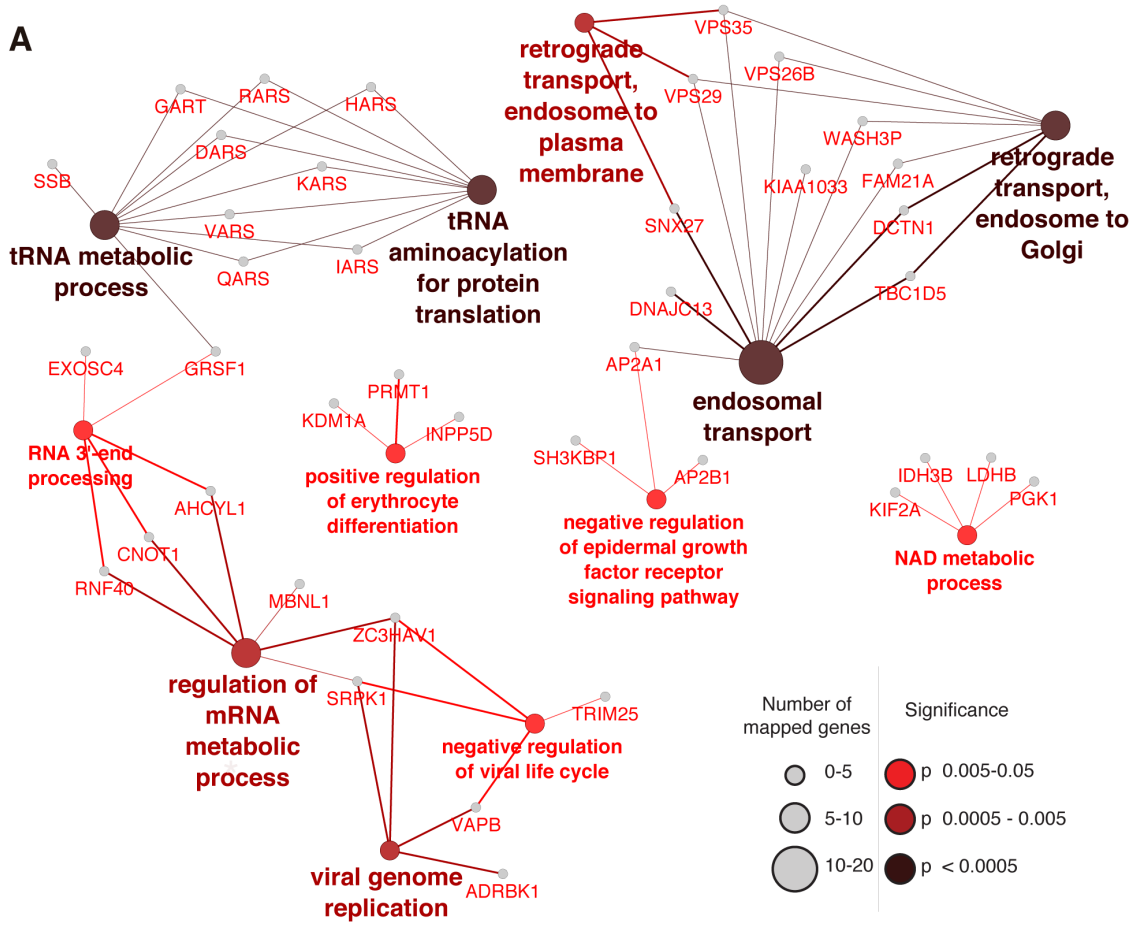

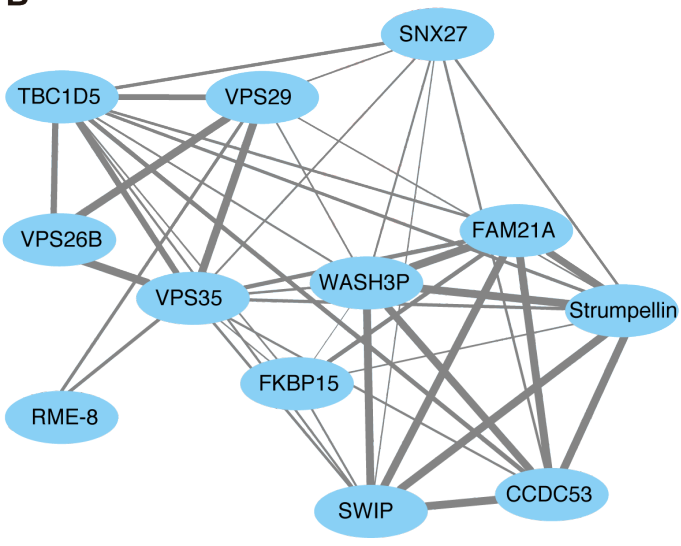

Fig R9. Analysis of PDZ-independent SNX27 interactome

(**A**) Gene Ontology enrichment analysis using the Cytoscape plug-in ClueGO for biological process of the PDZ-independent SNX27 interactome. Proteins associated with clusters with p <0.05 (number of genes mapped and P values, lower right). Heavy lines indicate associations based on experimental evidence. (**B**) Network analysis of PDZ-independent SNX27 interactome components using the STRING database. Heavy lines indicate stronger evidence of association.

Western blot analysis of the GFP-SNX27 immunoprecipitates used for protein identification confirmed that WASH associates to SNX27 independently of PDZ domain integrity (Fig R10A). Immunofluorescence analysis of endogenous proteins during IS formation showed partial WASH colocalization with SNX27 at the IS (Fig R10B, C). The primary role of WASH is to promote the generation of the branched actin networks necessary for endosomal and lysosomal integrity [76, 77, 124, 249]. Although originally considered responsible exclusively for protein degradation, lysosomes are dynamic organelles with secretory function in specialized cell types including T lymphocytes [29]. IS formation leads to rapid polarization of the Golgi and the ERC, and delivery of secretory lysosomes to the point of target recognition [312]. Cotransfection experiments with a plasmid that encodes the secretory lysosome marker GFP-CD63 confirmed its rapid polarization and partial localization with SNX27 (Fig R10D and Video 3). These experiments show that whereas SNX27 is located exclusively in the ERC in non-activated T lymphocytes [271], it also localizes to the polarized secretory compartment after antigen recognition.

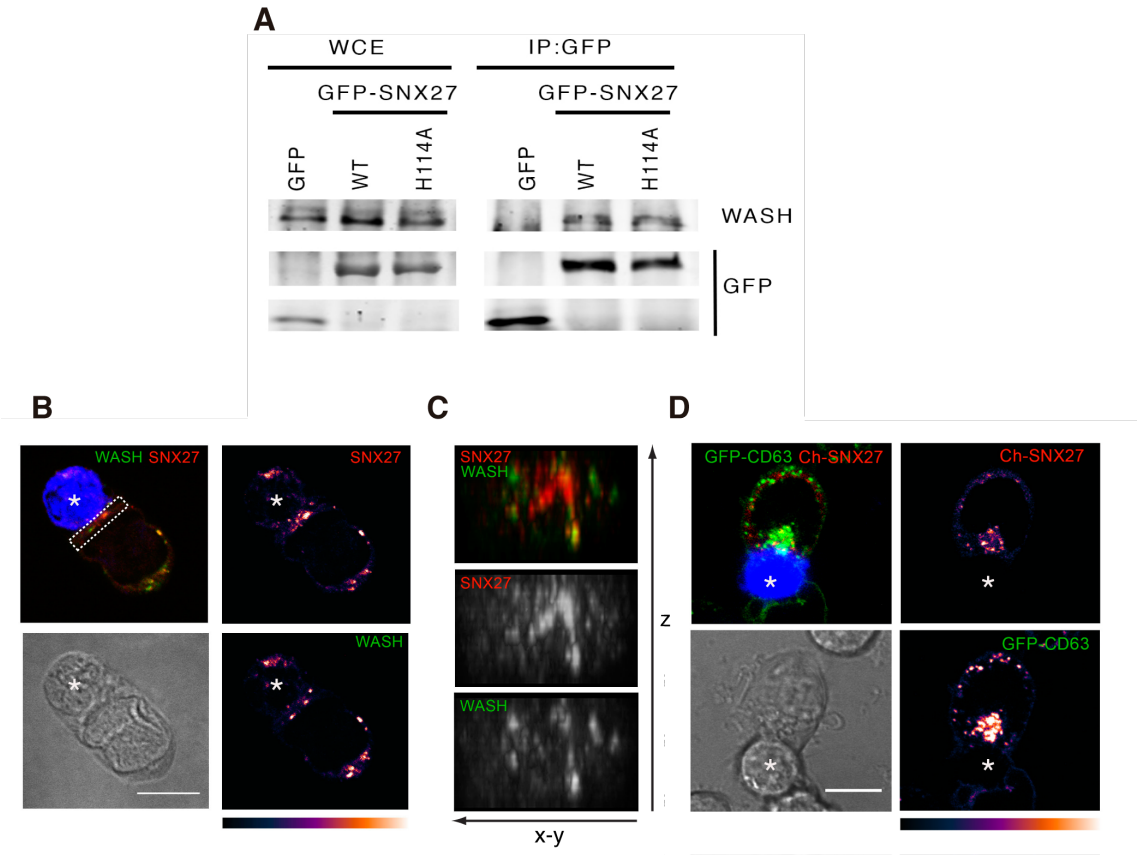

Fig R10. Validation of SNX27/WASH interaction during IS formation

(**A**) GFP immunoprecipitates used for protein identification were validated in western blot. (**B**) Representative confocal images of Jurkat T cells stimulated with SEE-loaded Raji cells (blue; white asterisk) and immunostained for WASH (green) and for SNX27 (red). (**C**) En-face (xy-z) reconstruction of the dashed rectangle in (B) shows protein localization at the T cell-APC contact region. (**D**) Time-lapse microscopy was used to assess the relative dynamics of IS recruitment of Cherry-SNX27 (red) and GFP-CD63 (green) cotransfected in Jurkat cells. SEE-loaded Raji cells (blue; white asterisk) were added and cells imaged every 15 s (see complete video in **Video 3**). Pseudo-color scale of fluorescence intensity (B, D, bottom).

1.3.2. SNX27 role in WASH-mediated transport in T cells

Proteomic data confirmed SNX27 interaction with WASH in Jurkat cells during antigen recognition. Our analysis however does not detect WASH-regulated transmembrane proteins in T cells that include the TCR, CD28, GLUT1 and the integrin LFA-1 (lymphocyte function-associated antigen 1) [256]. We nevertheless identified the TfR (Supplemental Table S5), which requires WASH for efficient recycling in HeLa cells [77]. We thus explored the effects of SNX27 silencing on the turnover of WASH-regulated transmembrane proteins. Western blot analysis in SNX27-silenced cells showed decreased TfR levels and altered GLUT1 expression, with an increase in a slower-migrating band. Inhibition of protein synthesis by cycloheximide (CHX) treatment had no obvious effect on total protein levels in control cells, but induced loss of GLUT1 in SNX27-silenced cells (Fig R11A), which indicated that SNX27 promotes GLUT1 recycling. TfR abundance remained constant in these cells after CHX treatment (Fig R11A), suggesting that SNX27 regulates TfR levels, but not its recycling.

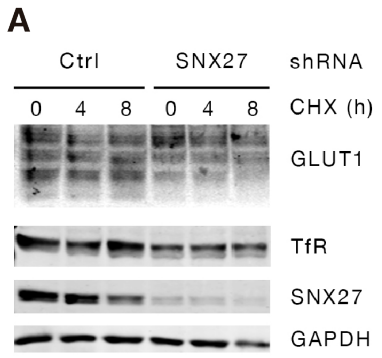

To measure protein recycling to the PM, we compared the effect of CHX treatment on surface expression of TfR (CD71), TCR CD3 epsilon chain (CD3ε) and LFA-1 subunit CD11a in control and SNX27-silenced Jurkat T cells. Flow cytometry analysis showed reduced TfR levels after SNX27 silencing, with no significant differences between

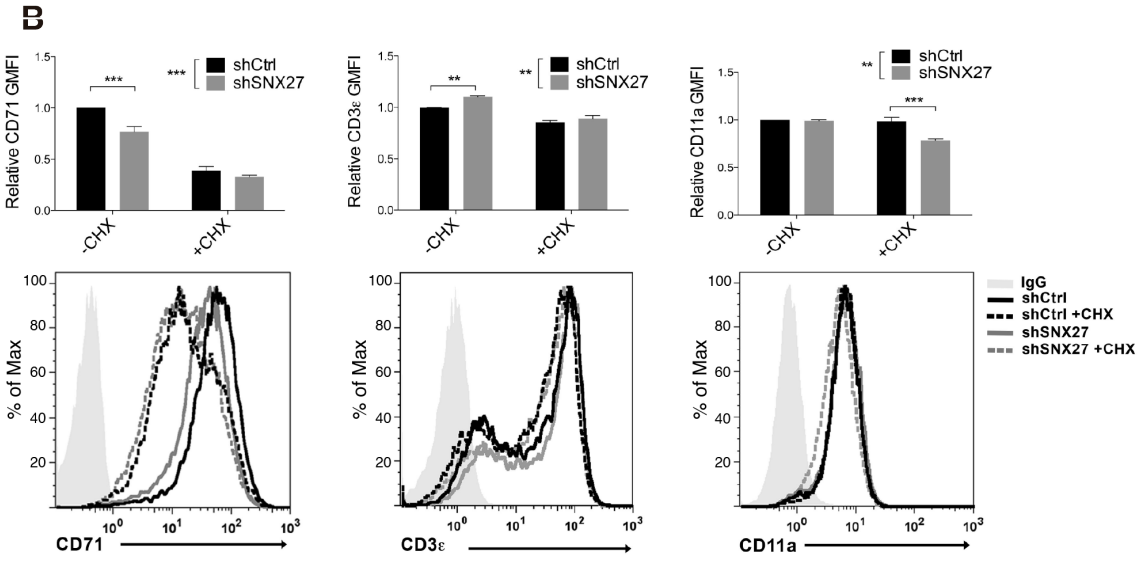

Fig R11. Effect of SNX27 silencing on protein trafficking

shControl and shSNX27 Jurkat T cells were treated with 10 μg/ml cycloheximide (CHX) for the times indicated (**A**) or 4 h (**B**). Total or cell surface levels of the indicated proteins were measured by Western blot (**A**) or by flow cytometry (**B**), respectively. Geometric mean fluorescence intensity (GMFI) was normalized to untreated shControl cells. Data shown as mean ± SEM (**p <0.01, ***p <0.001; two-way ANOVA/Bonferroni post test) from at least three independent experiments. Graphs are shown for a representative experiment.

control and SNX27-silenced cells after CHX treatment (Fig R11B, left). Cell surface abundance of CD3ε was higher as a result of SNX27 silencing, with no further effect after CHX addition (Fig R11B, center); CD11a levels were unaffected by SNX27 silencing in basal conditions, but were significantly reduced by CHX treatment (Fig R11B, right). These studies indicate that SNX27 silencing in T cells decreases TfR abundance and alters GLUT1 and LFA-1 recycling, but not that of CD3ε, partially mimicking WASH loss.

1.3.3. Identification of SNX27 PDZ cargoes during IS formation

The SNX27 PDZ-independent interactome led us to investigate SNX27 role as an adaptor for WASH-mediated trafficking in T cells. The defect of the GFP-SNX27 H114A mutant to accumulate at the IS nonetheless suggested important functions of SNX27 PDZ-bm-containing cargoes at the IS. Proteomic results were thus analyzed to identify putative cargoes; the proteins present only in the GFP-SNX27 WT immunoprecipitates and not those of the H114A mutant form were considered (Supplemental Table S3), and their C-terminal amino acid sequences examined to identify a characteristic type I PDZ-bm (Table R2). We mostly detected cytosolic proteins and only two multipass membrane-associated proteins, the phosphate export mediator XPR1 (xenotropic and polytropic murine leukemia virus receptor) [121] and Kidins220 (kinase D-interacting substrate), which is a receptor scaffolding protein that promotes ERK signaling in neurons [10], and in T and B lymphocytes [78, 100]. Although XPR1 does not bear a canonical type I PDZ-bm, cell surface levels of both proteins decrease after SNX27 silencing in HeLa cells [308].

The PDZ-dependent SNX27 interactome also showed proteins linked to the regulation of

Entry name	Protein	C-terminal
ACOT8	Acyl-coenzyme A thioesterase 8	QVSESKL
ARHG7	Rho guanine nucleotide exchange factor 7 (β-PIX)	AWDETNL
GIT1	ARF GTPase-activating protein GIT1	ITTREKK
GIT2	ARF GTPase-activating protein GIT2	TTKENNN
ARHG6	Rho guanine nucleotide exchange factor 6 (α-PIX)	SKTSILP
CENPJ	Centromere protein J	VLMDTEL
CTRO	Citron Rho-interacting kinase (CRIK)	VWDQSSV
DGKz	Diacylglycerol kinase zeta (DGKζ)	EDQETAV
KDIS	Kinase D-interacting substrate of 220 kDa (KIDINS220)	EERESIL
OTUL	Ubiquitin thioesterase OTULIN	VCEETSL
SHKB1	SH3KBP1-binding protein 1	KLNETSF
ZO-2	Tight junction protein zonula occludens-2	RYRDTEL
CGN	Cingulin	NLQTSSC
XPR1	Xenotropic and polytropic retrovirus receptor 1	TDDEANT

Table R2. PDZ-dependent SNX27 interactome during IS formation. Cargoes with consensus C-terminal PDZ-bm are indicated (bold) (for complete results, see Supplemental Table S3).

receptor endocytosis. The acyl CoA thioesterase 8 (ACOT8) binds to the HIV-1 Nef protein and mediates Nef-induced downregulation of CD4 and MHC-1 [193]. SH3KBP1 binding protein 1 (SHKBP1) interacts with the 85 kDa Cbl-interacting protein (SH3KBP1/CIN85), a known regulator of receptor endocytosis [98] that was indeed identified in our SNX27 PDZ-independent interactome (Supplemental Table S5). In addition to proteins related to receptor transport, we found the deubiquitinase OTULIN, which cleaves Met1-linked ubiquitin chains [89]. This post-translational modification, known as linear ubiquitination, has recently acquired relevance in the regulation of immune responses [155, 293].

SNX27 PDZ interactors in activated T cells also included spindle-associated proteins such as CENPJ/CPAP (centromere associated protein J), a tubulin-binding protein that is essential for centrosome biogenesis [318]. Although does not contain a canonical type 1 PDZ-bm, we also detected CRIK (citron Rho-interacting kinase), a cytokinesis-specific RhoA effector. CRIK controls midbody formation by connecting contractile ring components and MT-associated proteins [19].

In addition, we found validated SNX27 PDZ cargoes such as DGKζ [270, 271], zona occludens-2 (ZO-2) [366] and the p21-activated kinase (PAK)-interactive exchange factor ARHGEF7, also known as β-PIX, as well as the other PIX/GIT complex members α-PIX (ARHGEF6) and GIT1/2 (GPCR kinase-interacting proteins 1 and 2) [328]. For biochemical validation of our proteomics data, we used western blot analysis to test for two selected proteins, β-PIX and ZO-2; we used DGKζ as control (Fig R12A). To determine whether IS formation affects SNX27 interaction with DGKζ, β-PIX or ZO-2, we tested for these proteins in GFP-SNX27 immunoprecipitates from Jurkat cells incubated with Raji B cells, alone or loaded with SEE. Contact with SEE-loaded APC induces activation of TCR-mediated signals as detected by ERK phosphorylation, used as a control of stimulation. The SNX27 interaction with DGKζ, β-PIX and ZO-2 was independent of

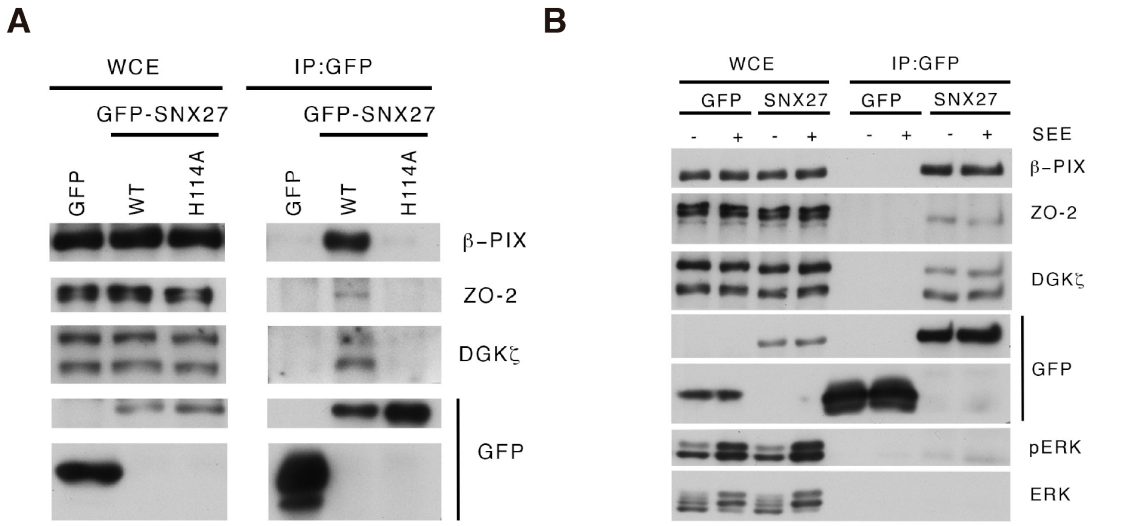

Fig R12. Analysis and validation of SNX27 PDZ ligands during IS formation

(**A**) Western blot analysis of immunoprecipitates confirmed PDZ-bm-dependent interaction of β-PIX and ZO-2 with GFP-SNX27 WT. DGKζ was used as a positive control. (**B**) The interactions in (B) are not markedly regulated by T cell activation with SEE-pulsed APC.

antigen presentation, as binding was also observed after incubation with unloaded APC (Fig R12B).

Whereas DGKζ and β-PIX are known to localize to the T cell IS [120, 254] some of the additionally identified proteins could also contribute to the PDZ-dependent accumulation of SNX27 at the IS. ZO-2 is a member of the membrane-associated guanylate kinase (MAGUK) family of proteins that regulate assembly of tight junctions in epithelial cells [96]. The lack of studies on ZO-2 expression in T lymphocytes, and the presence of its binding partner Cingulin [62] in SNX27 immunoprecipitates prompted us to investigate the possibility of functional localization of ZO-2 at the IS.

1.3.4. Characterization of the ZO-2/SNX27 interaction during IS formation

During IS formation molecules reorganize in supramolecular activation clusters (SMAC) [227]. At the central SMAC (cSMAC), TCR molecules accumulate and deliver signals following antigen recognition. Adhesion molecules distribute at the peripheral SMAC (pSMAC), and promote cell-cell adhesion that "seals" the contact area and allows polarized exchange of information between the contacting cells [84]. Using PKCθ as a cSMAC marker, we examined the location of endogenous ZO-2 in Jurkat T cells incubated with SEE-pulsed APC. ZO-2 was found at the cell-cell contact area, bordering the PKCθ pool (Fig R13A). En-face reconstruction confirmed the peripheral localization of ZO-2 relative to PKCθ (Fig R13B). Comparison of ZO-2 localization with that of the pSMAC marker talin showed that these proteins colocalized at the margin of the contact area (Fig R13C). Reconstruction confirmed peripheral ZO-2 distribution, although colocalization with talin-enriched areas was incomplete (Fig R13D).

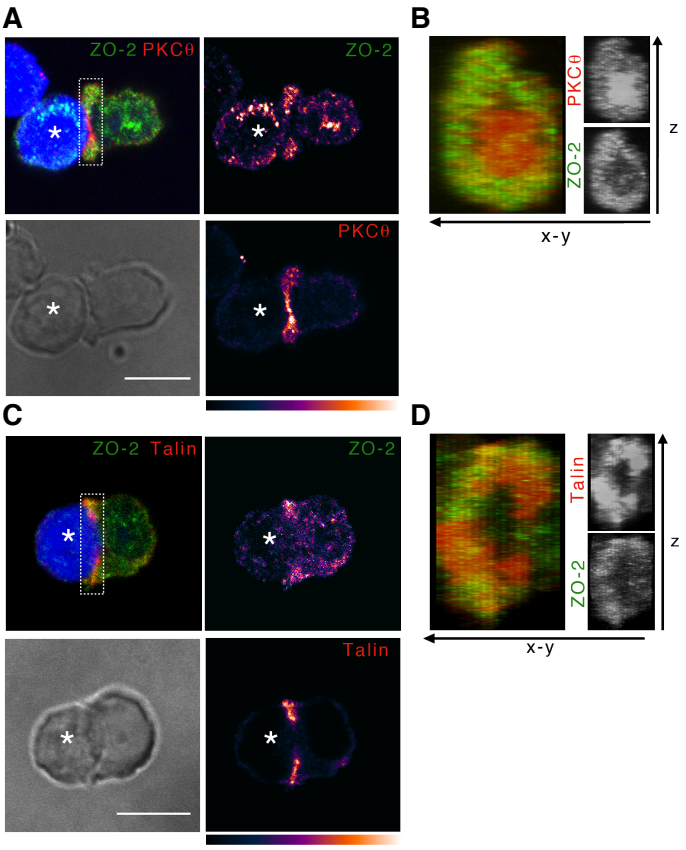

Fig R13. The tight junction protein ZO-2 polarizes to the IS of Jurkat T cells

(**A-D**) Representative confocal images of Jurkat cells stimulated with SEE-loaded Raji cells (blue; white asterisk), then immunostained for ZO-2 (green), and (**A**, **B**) for the PKCθ IS marker (red) or (**C**, **D**) for talin (red) to label the peripheral IS. En-face (xy-z) reconstructions of dashed rectangles in (A) and (C) are shown in (B) and (D), respectively. Pseudo-color scale of fluorescence intensity (A, C, bottom). Representative confocal images are shown; bar: 10 μm

To visualize ZO-2 dynamic distribution early in synapse formation, we transfected Jurkat T cells with a plasmid that encodes GFP-ZO-2, and incubated them with SEE-loaded APC. GFP-ZO-2 accumulated rapidly at the contact area, then redistributed to the pIS, as does the endogenous protein (Fig R14A and Video 4). The GFP-ZO-2 fluorescence intensity ratio at the T cell-APC contact site vs PM outside correlation the contact area showed increased ZO-2 accumulation following antigen recognition (Fig R14B). We used fluorescence recovery after photobleaching (FRAP) to confirm stable ZO-2 localization at the IS and measure its mobility. We calculated GFP-ZO-2 halftime of fluorescence recovery after photobleaching at the membrane, with a mean value of 3.13 s in unstimulated Jurkat cells, which increased to 6.77 s at the IS in conjugates with SEE-loaded APC (Fig R14C). GFP-ZO-2 mobility thus lessens when the IS forms, demonstrating its stable accumulation at the IS.

ZO proteins regulate actin distribution at cell junctions [94]. As IS formation results in rapid actin rearrangement, we examined the correlation between GFP-ZO-2 localization and actin polymerization. The relative F-actin dynamics were tracked by transfection with a construct that encodes a fluorescently labeled Life-act peptide (RFP-LifeAct). In the absence of antigen stimulation, Jurkat cells continuously scan APC without forming stable synapses. GFP-ZO-2 accumulated at membrane ruffles, which are also sites of actin rearrangement (Fig R14D, top). When stable IS formed, GFP-ZO-2 redistributed to and outside those areas in the pIS with intense actin assembly (Fig R14D, bottom). Analysis of GFP-ZO-2 colocalization with drebrin, an F-actin-binding protein that regulates actin polymerization at the IS [253], further confirmed ZO-2 localization at actin cytoskeleton rearrangement sites (Fig R14E). En-face reconstruction showed a similar organization pattern for these proteins, although GFP-ZO-2 localized in part at sites closer to the margin of the T cell-APC contact area (Fig R14F).

Videomicroscopy analysis of live T cells showed that GFP-ZO-2 localization at the IS changed rapidly when T cells contacted a new APC (Video 5). This dynamic relocalization of ZO-2 to new T cell-APC contact areas suggested rapid ZO-2 traffic from and to the synapse as a result of TCR triggering. We cotransfected Jurkat cells with GFP-ZO-2 and Cherry-SNX27 to examine their dynamic distribution during IS formation. Resting cells showed partial ZO-2 localization to SNX27-positive endosomes (Fig R15A, top). After IS formation, most SNX27 was found at the ERC, whereas GFP-ZO-2 redistributed to the edges of the IS (Fig R15A, bottom). Videomicroscopy analysis in real time allowed better visualization of SNX27 and ZO-2 dynamic distribution during IS formation (Fig R15B and Video 6). ZO-1 and ZO-2 share the same domains, although ZO-1 lacks a PDZ-bm [222]. Similar studies in Jurkat T cells using GFP-ZO-1 showed analogous distribution at the IS, with no consistent colocalization with Cherry-SNX27 in any condition (Fig R15C and Video 7). These data confirmed SNX27/ZO-2 interaction at the ERC, and suggest that ZO protein localization to the synapse is not PDZ-bm-dependent. To determine whether SNX27 affects ZO-2 accumulation and/or mobility at the IS, we used videomicroscopy and FRAP experiments. The fluorescence intensity ratio at the T cell-APC

contact site vs. non-IS membrane showed increased ZO-2 accumulation at the IS in SNX27-silenced cells (Fig R15D), in which photobleaching experiments demonstrated reduced GFP-ZO-2 mobility at the IS (Fig R15E). These studies suggest that SNX27 interaction facilitates ZO-2 traffic from the PM, as reported in tight junctions between epithelial cells [366].

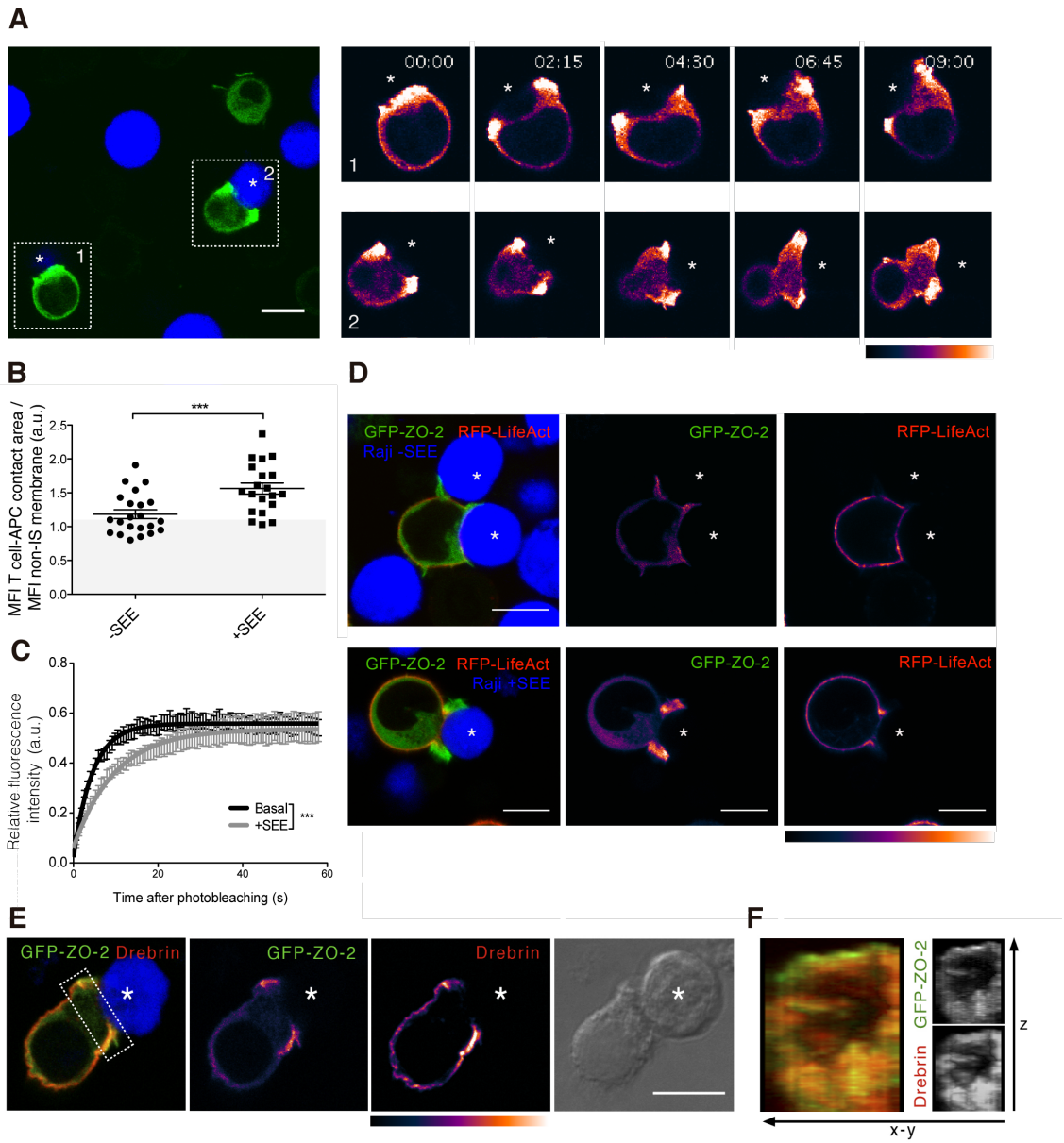

Fig R14. GFP-ZO-2 dynamic distribution during immune synapse formation

Dynamics of IS recruitment of GFP-ZO-2 alone (**A**, green; see **Video 4**) or relative to actin polymerization marked by RFP-LifeAct (**D**, red; see **Video 5**) were assessed by videomicroscopy. Transfected Jurkat cells were imaged every 15 s after the addition of unloaded (top) or SEE-loaded (bottom) Raji cells (blue; white asterisk). (**B**) Quantitative analysis of GFP-ZO-2 accumulation at the T cell-APC contact area. Each dot represents the ZO 2 synapse/cytosol MFI ratio after APC encounter. Data shown as mean ± SEM (***p <0.001; unpaired t-test; n ≥20); a representative experiment is shown. (**C**) FRAP (fluorescence recovery after photobleaching) curves of GFP-ZO-2 normalized fluorescence intensity over a 60-s period after photobleaching. Transfected Jurkat cells were in basal conditions (black line) or stimulated with SEE-loaded APC (grey line). Curves were fitted by one-phase association exponential equations (see Methods). Data shown as mean ± SEM; ***p <0.001; two-way ANOVA; n ≥19. (**E-F**) GFP-ZO-2 (green)-transfected Jurkat T cells stimulated with SEE-loaded Raji cells (blue; white asterisk) were immunostained for the F-actin-binding protein drebrin (red). (F) En-face (y-z) reconstruction of dashed rectangle in (E). (A, D) Representative confocal images are shown; bar: 10 μm; pseudo-color scale of fluorescence intensity.

All together, our results suggest the participation of SNX27 in the regulation of the intracellular transport of cytoskeleton-associated proteins involved in cell-cell contacts formation. Defective traffic of some of these proteins such as LFA-1 results in decreased ability to form T cell-APC conjugates [246]. SNX27-silenced Jurkat cells showed no major synapse

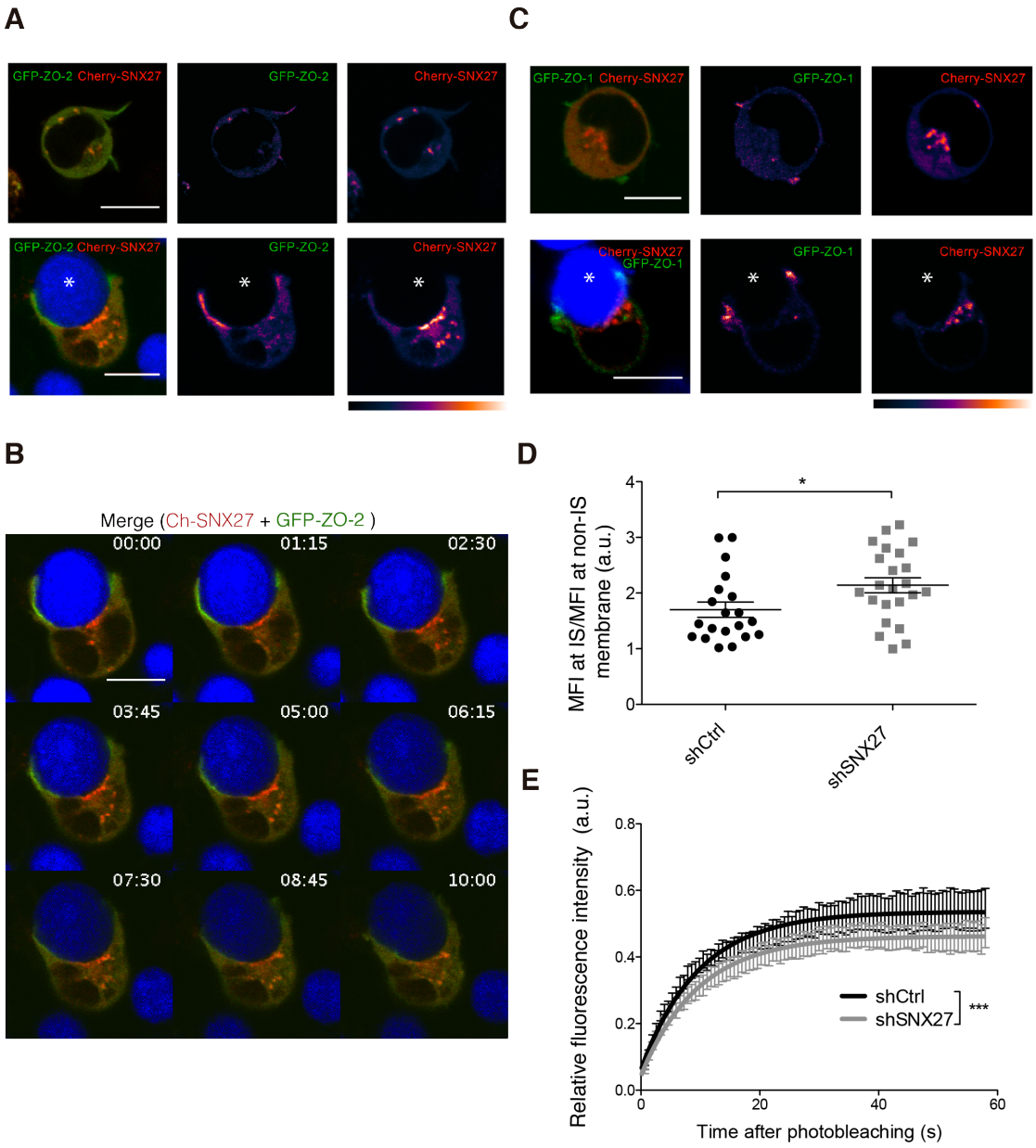

Fig R15. SNX27 colocalizes with GFP-ZO-2 and affects its mobility at the T cell-APC contact area

(**A-C**) Jurkat T cells were transfected with the indicated constructs and stimulated with SEE-loaded Raji cells (blue, asterisk). Videomicroscopy was used for direct assessment of the dynamics of GFP-ZO-2 (**A**, **B**) or GFP-ZO-1 (**C**) (green) localization relative to Cherry-SNX27 (red) polarization to the IS. Cells were imaged every 15 s. Representative confocal images are shown in (A, C); bar: 10 μm (complete videos for A, B) in **Video 6** and for (C) in **Video 7**). (**D**, **E**) shControl or shSNX27 Jurkat T cells expressing GFP-ZO-2 were stimulated with SEE-loaded APC. (D) Quantitative analysis of GFP-ZO-2 accumulation at the T cell-APC contact area. Each dot represents the ZO-2 synapse/cytosol MFI ratio after APC encounter. Data shown as mean ± SEM; *p <0.05; unpaired t-test; n ≥20; a representative experiment is shown. (E) FRAP curves of GFP-ZO-2 normalized fluorescence intensity over a 60-s period after photobleaching. shControl (black line) or shSNX27 (grey line) curves were fitted by one-phase association exponential equations (see Methods). Data shown as mean ± SEM; ***p <0.001; two-way ANOVA; n ≥19. Pseudo-color scale of fluorescence intensity (A, C, bottom).

formation defect, indicated by PKCθ localization to the IS (Fig R16A) and the similar number of conjugates formed after incubation with SEE-loaded APC (Fig R16B, right) compared to controls. SNX27-silenced cells nonetheless showed increased antigen-independent conjugate formation (Fig R16B, left), suggesting a regulatory mechanism of adhesion mediated by SNX27 independently of TCR signaling.

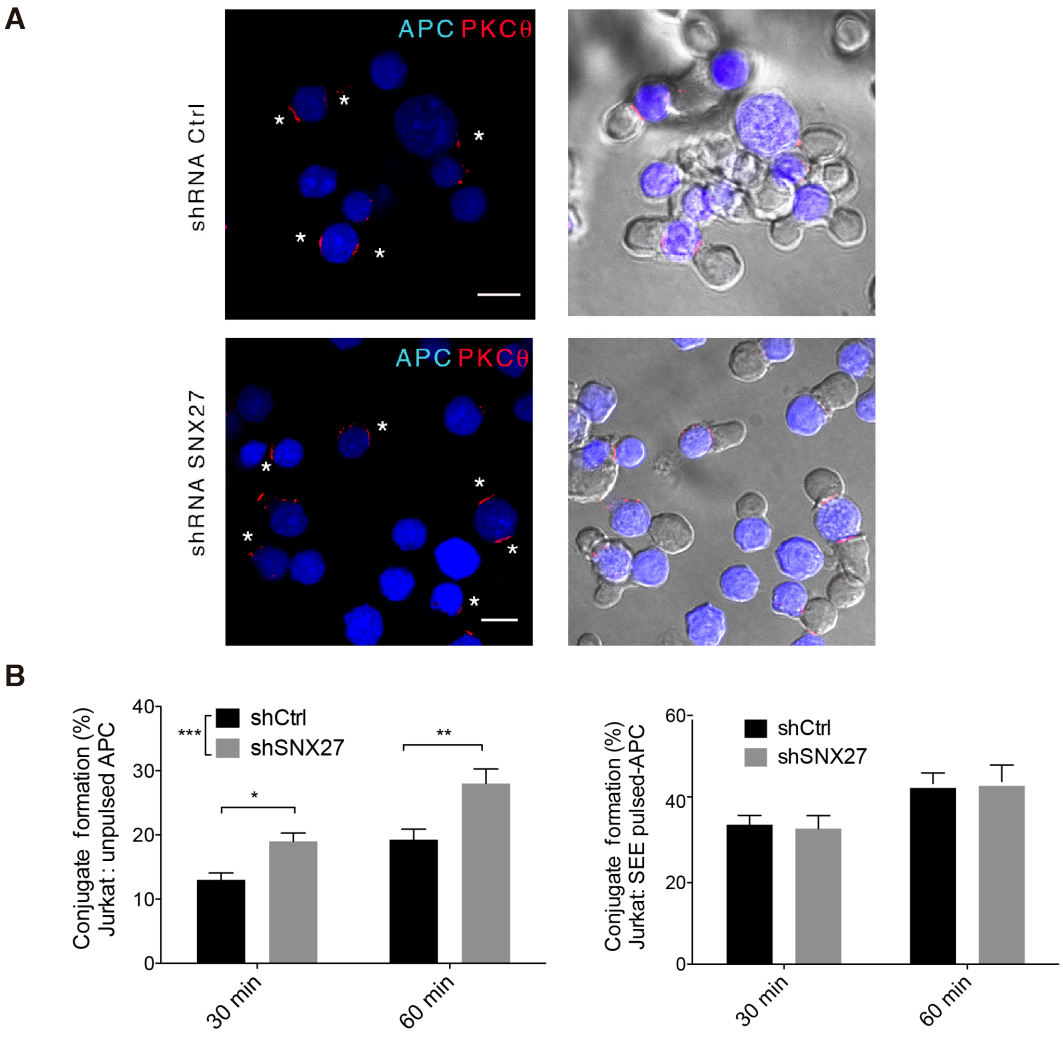

Fig R16. Effect of SNX27 silencing on conjugate formation capacity in Jurkat cells

(**A**) shControl and shSNX27 Jurkat T cells were stimulated with SEE-pulsed APC (blue; white asterisk; 15 min) and immunostained for the PKCθ marker for immune synapse formation (red). Representative confocal images are shown; bar: 10 μm. (**B**) T cell-APC conjugate formation was calculated using flow cytometry (see Experimental Procedures) after T cell stimulation with unpulsed (left) or SEE-pulsed (right) APC for the indicated times. Data shown as mean ± SEM (*p<0.05, **p<0.01; two-way ANOVA/Bonferroni post test; n=4).

2. SNX27 REGULATION OF LIPID SIGNALING

The study of SNX27 dynamics and its interactome at the IS suggested broad functions for SNX27 in T cell intracellular protein trafficking, with various PDZ cargoes identified as cytoskeletal-associated proteins and endocytosis regulators. We also detected SNX27 binding to the lipid signaling modulator DGKζ, which limits activation of the DAG/Ras/ERK pathway after T cell antigen recognition [120]. Our group reported that SNX27 silencing leads to enhanced ERK activation after stimulation with antigen-loaded APC [270], which suggested that DGKζ and SNX27 act in the same pathway. These data concur with the increasing evidence for the participation of intracellular trafficking pathways in the spatiotemporal control of signaling cascades (reviewed in [24, 64, 247]). We decided to examine the possible regulatory mechanisms of DGKζ/SNX27 interaction, and to further study of the role of this interaction in the control of DGKζ functions.

2.1. Analysis of the SNX27/DGKζ PDZ-dependent interaction

The canonical mechanism of PDZ domain interaction involves recognition of cargo proteins through their C-terminal PDZ-bm. Type 1 motifs have the sequence [Ser/Thr]-x-ϕ (ϕ = any hydrophobic residue), such as that of DGKζ (T-A-V). Whereas the C-terminal triplet is essential for binding, specificity is often enhanced by upstream sequences [132, 354]. Dr. Brett Collins's group (Institute for Molecular Bioscience, University of Queensland, Australia) defined the sequence requirements for PDZ-bm binding to SNX27, and showed that there are high- and low-affinity ligands based on the positions of negatively charged acidic side chains upstream of the C-terminal PDZ-bm. High-affinity cargoes require acidic residues located at -3 and -5 positions that are able to clamp a conserved arginine (Arg58) on the SNX27 surface. Some low-affinity cargoes bear amino acids susceptible to phosphorylation that could mimic the acidic side chains necessary for SNX27 high-affinity binding, thus constituting a post-translational regulatory mechanism for PDZ binding ([60] see Appendix 4.4). These data indicated that DGKζ C-terminus, with the E-D-Q-E-T-A-V sequence, is a high-affinity ligand of SNX27.

To confirm the importance of the electrostatic clamp in DGKζ, we collaborated with Collins to test the ability of DGKζ PDZ-bm mutants (Fig R17A) to co-immunoprecipitate SNX27 in Jurkat T cells. While WT GFP-DGKζ precipitated SNX27, constructs modified in their DGKζ PDZ triplet did not (ΔETAV, T927A) (Fig R17B). Mutation of the -3 side chain (E926A) or -3 and -5 side chains (D924A/E926A) abolished the interaction with SNX27, whereas alteration of the -5 side chain only (D924A) reduced but did not abolish binding, which indicated that the -5 acidic side chain has an important but auxiliary role to the essential -3 residue.

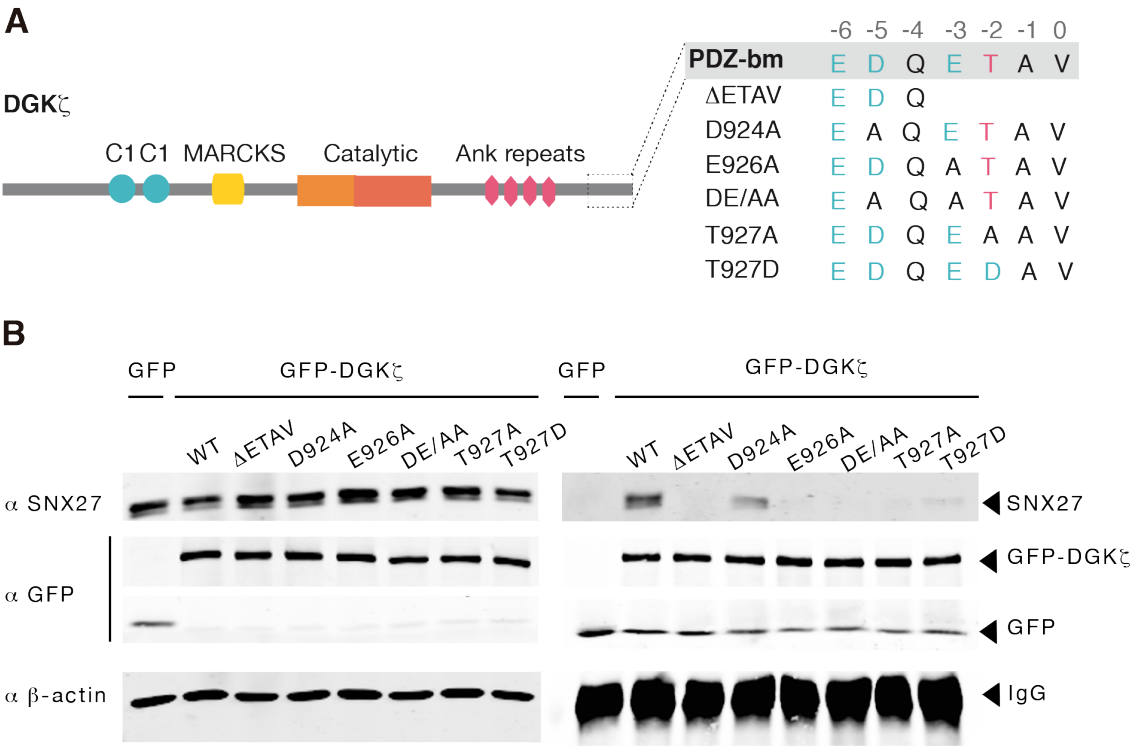

Fig R17. Analysis of the SNX27/DGKζ PDZ-dependent interaction

(**A**) DGKζ structure including MARCKS (myristoylated alanine-rich C-kinase substrate) and ankyrin (Ank) repeat sequences. Amino acids of the DGKζ PDZ-binding motif (PDZ-bm) and the mutants generated are detailed (right); possible phosphorylation sites (pink) and positively charged amino acids (blue) are colored. (**B**) GFP-DGKζ WT and PDZ-bm mutant constructs expressed in Jurkat T cells were analyzed for binding to SNX27 by GFP immunoprecipitation and western blot with the indicated antibodies. A representative experiment is shown ($n = 3$).

DGKζ acidic residues at positions -3, -5 and -6 are not subject to the post-translational regulatory mechanism. Phosphorylation at the -2 residue is nonetheless another regulatory mechanism for PDZ interactions ([114, 362], reviewed in [169, 184]). We thus tested SNX27 binding to the GFP-DGKζ protein with a phosphomimetic mutation at the -2 position (T927D) (Fig R17B). The interaction was barely detected, which confirmed that Thr^{-2} phosphorylation provides a regulatory switch that prevents SNX27 binding to cargo, presumably by causing a steric clash with the SNX27 His114 side chain. To explore the biological relevance of this negative regulatory mechanism, we retrieved experimental data from several web-based bioinformatics resources such as Phosphosite [146]. While phosphoproteomic studies found DGKζ phosphorylated in many residues after various stimuli, there are thus far no reports of PDZ-bm Thr^{-2} phosphorylation (Phosphosite, Acc. nº Q13574). These data are in agreement with our immunoprecipitation studies showing a constitutive DGKζ/SNX27 association after T cell encounter with loaded or unloaded APC (Fig R12B).

2.2. SNX27 contribution to DGKζ stability

Our data indicated that DGKζ is a high-affinity constitutive cargo of SNX27. The best-known function of SNX27 interaction with its cargoes is to facilitate their retrieval from the lysosomal

degradation pathway [308]. We thus examined DGKζ stability in SNX27-silenced Jurkat cells; as a control, we monitored the abundance of the transmembrane proteins GLUT1 and Kidins220, both known SNX27 PDZ cargoes [308]. As previously shown for GLUT1 (Fig R11A), SNX27 silencing in these cells resulted in high levels of both transmembrane cargoes, and protein synthesis inhibition by CHX treatment acutely decreased protein abundance, which was partially rescued after proteasome inhibitor (MG-132) treatment (Fig R18A). These results suggested that in Jurkat cells, protein recycling defects elicit a compensatory feedback mechanism to promote protein synthesis. In contrast, DGKζ did not behave as a classical SNX27 PDZ cargo. SNX27-silenced Jurkat cells showed approximately a 20% reduction in DGKζ levels in untreated cells (Fig R18B), and protein synthesis inhibition alone or combined with proteasome inhibition resulted in modest variations in DGKζ protein abundance. These data suggested that an indirect mechanism decreases DGKζ stability in the absence of SNX27.

In neurons, proteolytic degradation downregulates DGKζ levels in excitotoxic conditions, when DGKζ translocates from the nucleus to cytosol [244]. Subcellular DGKζ localization is controlled by a nuclear localization signal (NLS) that overlaps the myristoylated alanine-rich C-kinase substrate (MARCKS) domain (see DGKζ structure in Fig R17A) [35]; serines within the NLS can be phosphorylated by PKCα [204, 323]. To determine whether PKC-mediated phosphorylation regulates the decrease in DGKζ abundance observed after SNX27 silencing, we treated Jurkat T cells with the classic PKC-selective inhibitor Gö6976 (Gö). We monitored DGKζ protein abundance by western blot, and used an antibody that recognizes phosphorylation of PKC substrates to confirm PKC inhibition. While DGKζ levels remained

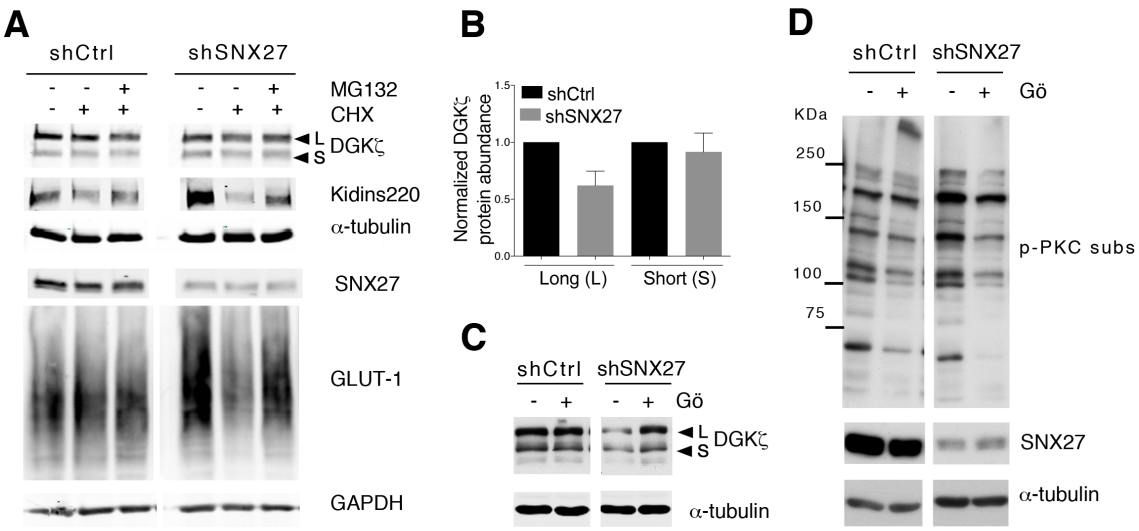

Fig R18. SNX27 silencing triggers PKC activation and subsequent DGKζ degradation in basal conditions

(**A-D**) shControl and shSNX27 Jurkat T cells were treated with the indicated inhibitors (10 μg/ml cycloheximide (CHX); 5μM MG-132; 100nM Gö) for 6 h. Total or cell surface levels of the indicated proteins were measured by western blot. Blots are shown from a representative experiment. (**B**) Quantification of DGKζ (top) long (L) and (bottom) short (S) splicing isoforms levels 72-96 h after shRNA transfection. Data shown as mean ± SEM from at least three independent experiments. Graphs are shown for a representative experiment.

constant in shRNA control cells following Gö treatment, they were rescued in SNX27-silenced cells (Fig R18C). Accordingly, we observed that in untreated cells the phospho-PKC substrate antibody signal was higher in SNX27-silenced cells than in controls (Fig R18D). These data indicated that PKC-mediated regulation of DGKζ protein levels also occurs in T cells, and that SNX27 silencing triggers PKC activation and subsequent DGKζ degradation in basal conditions.

2.3. Analysis of DAG signaling in SNX27-silenced activated T cells

DGKζ-MARCKS phosphorylation by PKCα not only regulates DGKζ localization and stability, but also its activity [203, 204, 323], and DGKζ limits PKCα activity by attenuating local DAG accumulation. This is a mutual regulatory mechanism in which DGKζ phosphorylation following PKC activation leads to disruption of PKC/DGKζ association [203]. The spatial organization of this signaling complex allows to precisely modulate local DAG signaling. Our results suggested that SNX27 contributes to sustain this complex, as silencing SNX27 in Jurkat T cells increases PKC activity in basal conditions. Our laboratory previously showed that SNX27 silencing mimicked that of DGKζ, and resulted in enhanced ERK activation after T cell triggering by antigen-loaded APC [270], which suggested that SNX27 also controls DGKζ-dependent negative regulation of the PKC/Ras/ERK pathway after stimulation.

DAG generation downstream of TCR triggering promotes Ras/ERK activation and AP-1 transcription [86]. The activation of this pathway can be monitored by measuring surface abundance of CD69, a C-type lectin that is transcriptionally upregulated shortly after TCR stimulation [280]. To test whether SNX27 silencing leads to enhanced, functional Ras/ERK activation, we measured CD69 surface abundance after incubation of Jurkat T cells with agonist antibodies. We used soluble anti-CD3 for TCR triggering alone, or in combination with soluble anti-CD28 for costimulation. Whereas unstimulated Jurkat T cells expressed low CD69 levels, CD3 stimulation resulted in a large cell population with high surface CD69 levels ($CD69^{hi}$) that increased following CD28 costimulation. In SNX27-silenced cells, the number of $CD69^{hi}$ cells was significantly higher than in controls (Fig R19A,B), which concurs with findings in DGKζ-depleted cells [365]. CD3 and CD3/CD28 costimulation also led to an increase in the geometric mean fluorescence intensity (GMFI) of the $CD69^{hi}$ population, with SNX27-silenced cells showing a significantly higher value after T cell stimulation (Fig R19A-C). To confirm that CD69 upregulation in SNX27-silenced cells was caused by hyperactivation of the Ras/ERK/AP-1 pathway, we measured the promoter activity of the AP-1-binding site in the CD69 promoter [45]. AP-1 activity after CD3 stimulation was higher in SNX27-silenced compared to control cells, and CD28 markedly augmented this difference (Fig R19D), which correlated well with the effect observed on CD69 induction.

In DGKζ-silenced activated Jurkat T cells, the absence of the mutual DGKζ/PKCα regulation leads to PKCα-dependent Ras hyperactivation [119]. To dissect PKC and ERK signaling input to CD69 transcriptional upregulation, cells were pretreated with pharmacological inhibitors before stimulation; we used Gö for classic PKC inhibition, and the MEK (MAPK/ERK kinase) inhibitor

PD98059 for ERK pathway blockade. Gö treatment reduced AP-1 activity following anti-CD3 stimulation in test and control cells. SNX27-silenced cells nonetheless showed higher promoter activity than controls, which suggested additional gain of function effects on AP-1 regulated transcription. After PD treatment, AP-1 activity levels decreased to similar extent in SNX27-silenced cells and controls (Fig R19D), which indicated that the additional gain of AP-1 activity in SNX27-silenced cells was probably related to direct DAG-dependent RasGRP1/Ras hyperactivation. Our results thus demonstrated that CD3 stimulation after SNX27 silencing results in Ras/ERK pathway hyperactivation that is partially PKCα-dependent. AP-1 promoter activity in CD3/CD28-stimulated cells was also sensitive to PKC and MEK inhibition, but enhanced AP-1 activity was still observed in SNX27-silenced cells compared to controls, which implied a contribution by additional signaling pathways (Fig R19D).

PKCθ is the main PKC isoform that acts downstream of CD28 to amplify early TCR signaling pathways [274]. PKCθ activation not only promotes ERK-dependent AP-1 transcription, but also activates the NF-κB-mediated transcription program (reviewed in [157]). Recent results from our laboratory indeed suggest a role for DGKζ in the control of PKCθ/PDK-1/NF-κB activation downstream of CD3/CD28 stimulation (Avila-Flores *et al.*, unpublished data). Analyses of the promoter activity of the NF-κB binding site in the CD69 promoter [197] showed that signaling in this

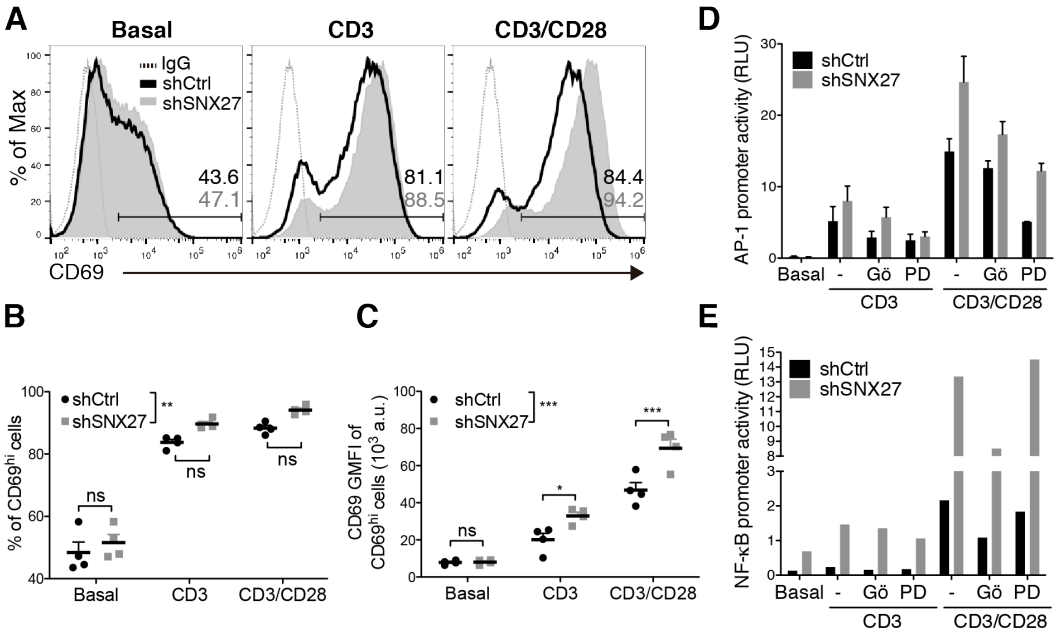

Fig R19. Stimulation of SNX27-silenced Jurkat cells results in Ras/ERK/AP-1 and NF-κB pathway hyperactivation

shRNA-transfected Jurkat T cells were stimulated (6h) with soluble anti-CD3 alone or with anti-CD28 for costimulation. Where indicated, cells were pretreated with Gö6976 or PD98059 for classic PKC or MEK inhibition, respectively. (**A**-**C**) Cells were stained for CD69 surface marker and, using flow cytometry, $CD69^{hi}$ cells were gated, and (**B**) the percentage and (**C**) geometric mean fluorescence intensity (GMFI) of $CD69^{hi}$ cells were calculated. (**A**) Representative flow cytometry plots with $CD69^{hi}$ gate shown. (**B**, **C**) Data shown as mean ± SEM (ns, not significant, $p>0.05$; *$p<0.05$; **$p<0.01$; ***$p<0.001$; paired t-test; $n = 4$). (**D**-**E**) Luciferase assays were performed to calculate (**D**) AP-1 or (**E**) NF-κB promoter activity. (D) Data shown as mean ± SEM ($n = 2$). (E) Data shown as mean, a representative experiment is shown ($n = 3$). RLU, relative luciferase units (see Methods).

pathway is also augmented in SNX27-silenced cells, and that PKCα activity contributes only partially to NF-κB promoter activity (Fig R19E). Further studies are required to determine whether PKCθ hyperactivation promotes NF-κB activity after SNX27 silencing.

2.4. Analysis of TCR signaling in SNX27-silenced T cells

Our results demonstrated that stimulation of SNX27-silenced Jurkat T cells results in Ras/ERK/AP-1 and NF-κB pathway hyperactivation and suggest that enhanced activation of DAG-regulated signals mediates this effect. We performed a detailed biochemical analysis to examine the activation of well-characterized signaling molecules that participate in the transmission of TCR activation signals and could contribute to an enhanced T cell response.

PKC activation was monitored using an anti-phospho-PKC substrates antibody; SNX27-silenced cells showed increased phosphorylation of PKC substrates compared to controls (Fig R20A). PKC activation promotes phosphorylation and degradation of the NF-κB inhibitor IκB, which releases NF-κB into the nucleus, where it activates its target genes [213]. In accordance with the enhanced NF-κB promoter activity, SNX27 silencing led to increased IκB degradation compared to controls (Fig R20B). We also analyzed PKD activation, which is a dual, direct and PKC-mediated DAG effector that is phosphorylated on its PKC-regulated residue (Ser744/748) in response to TCR stimulation (reviewed in [214]). CD3/CD28 stimulation triggered transitory PKD phosphorylation, which was enhanced and sustained in SNX27-silenced cells (Fig R20B). These data thus supported the hypothesis that PKC-mediated functions downstream of CD28 costimulation are enhanced after SNX27 silencing.

SNX27-silenced cells showed increased Ras/ERK pathway activation, measured as CD69

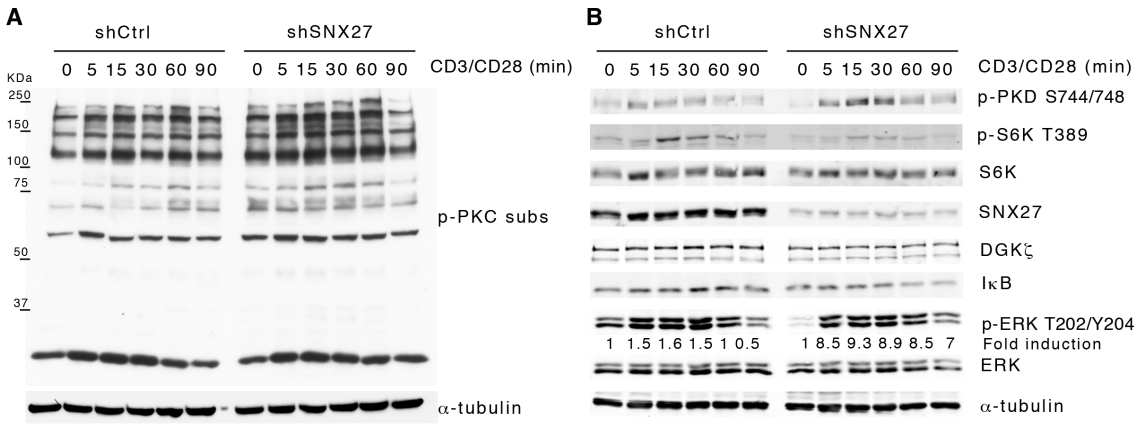

Fig R20. Effect of SNX27 silencing on DAG-dependent signaling after CD3/CD28 costimulation

shControl and shSNX27 Jurkat T cells were stimulated with soluble anti-CD3 and anti-CD28 for costimulation for the times indicated. Western blot analysis of cell lysates showed (**A**) phosphorylation of PKC substrates (p-PKC subs) and (**B**) phospho- and total protein abundance of the indicated proteins. Phospho-ERK signals were normalized to total ERK abundance, and results for each time point were also normalized to unstimulated cells to calculate fold induction. Blots and graphs are for a representative experiment.

induction and AP-1 activity. When we monitored ERK phosphorylation directly, however, we found unpredicted lower ERK phosphorylation in unstimulated SNX27-silenced Jurkat cells than in controls. Although these data require further study, when ERK phosphorylation after TCR triggering was quantified and normalized to unstimulated cells, SNX27-silenced cells showed the predicted marked increase in ERK phosphorylation (Fig R20B), which coincides with our earlier findings.

CD28 engagement also activates PI3K, and subsequent PtdIns(3,4,5)P_3 production allows PDK-1 and AKT recruitment and activation, which in turn assists activation of the metabolic regulator mTOR and its substrates, including the S6 kinase (S6K) ([59] reviewed in [33, 338]). Analysis of mTOR activation by determining S6K phosphorylation at the Thr389 residue, showed reduced activation in SNX27-silenced cells (Fig R20B). This implied that in contrast to the enhanced activation of PKC- and ERK-regulated signals, SNX27 silencing decreases mTORC1 activation downstream of CD3/CD28 triggering.

2.5. Analysis of DGKζ function in SNX27-silenced T cells

Our results showed that SNX27 silencing in T cells was reminiscent of that of DGKζ, and led to enhanced activation of DAG-effectors like PKC and RasGRP as well as a subsequent increase in AP-1/CD69 upregulation and NF-κB transcriptional activity (sections 2.3 and 2.4). We also found that although SNX27 silencing partially decreased DGKζ abundance due to PKC hyperactivation, DGKζ expression was not completely abolished (section 2.2). To examine whether the residual DGKζ is able to control these pathways when SNX27 expression is reduced, we analyzed CD69 upregulation and NF-κB promoter activity in cells expressing shRNA sequences against SNX27 and DGKζ (Fig R21A). The combined downmodulation of the two proteins did not have an additive effect, as CD69 induction did not increase substantially compared to silencing of SNX27 or DGKζ individually. When PKC and ERK contributions were assessed using Gö and PD inhibitors, we obtained similar results in SNX27-, DGKζ-, and SNX27/DGKζ-silenced cells (Fig R21B, C). Induction of NF-κB promoter activity after costimulation was also similar in SNX27- and in DGKζ-silenced cells, although double shRNA-silenced cells appeared to be resistant to Gö treatment (Fig R21D).

Our results demonstrate that SNX27 participates in DAG lipid signaling through DGKζ interaction in both basal and stimulation conditions, and suggest that the effects after SNX27 silencing are due mainly to a combination of decreased abundance, activity, and/or mislocalization of DGKζ, which are all causally related. Further experiments are needed to address this hypothesis.

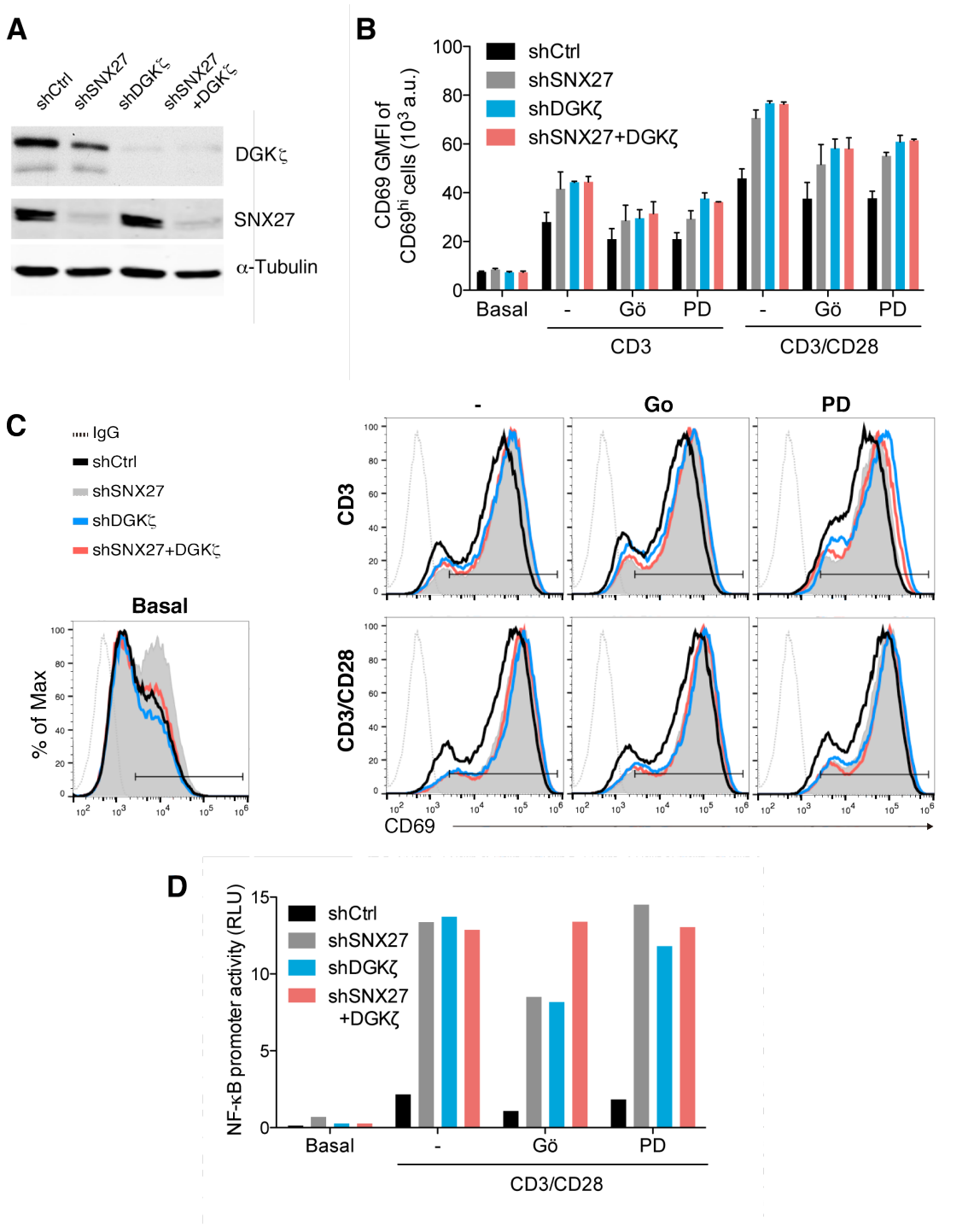

Fig R21. SNX27 participates in DAG lipid signaling through DGKζ interaction

(**A**) Total abundance of the indicated proteins in shRNA-transfected Jurkat T cells were analyzed by western blot. (**B-D**) shRNA-transfected cells were stimulated (6h) with soluble anti-CD3 alone or with anti-CD28 for costimulation. Where indicated, cells were pretreated with Gö6976 or PD98059 for classic PKC or MEK inhibition, respectively. (**B**, **C**) Cells were stained for CD69 surface marker and, using flow cytometry, the CD69^{hi} population were gated, and the geometric mean fluorescence intensity (GMFI) of CD69^{hi} cells were calculated. (B) Data shown as mean ± SEM (n = 2). (C) Representative flow cytometry plots with CD69^{hi} gate shown. (**D**) Luciferase assays were performed to calculate NF-κB promoter activity. Data shown as mean, a representative experiment is shown (n = 2). RLU, relative luciferase units (see Methods).

3. EFFECT OF SNX27 DEFICIENCY ON PRIMARY T CELL FUNCTION

Our studies in Jurkat T cells indicate that SNX27/DGKζ interaction regulates DGKζ-dependent DAG metabolism downstream of TCR triggering and costimulation. DGKζ-deficient primary T cells are hyperresponsive to TCR stimulation [365], which suggests that DGKζ limits the DAG signaling threshold for activation. SNX27 depletion in primary T cells could thus mimic that of DGKζ to promote DAG-regulated functions. The defective function of additional SNX27 interactors could nonetheless also affect T cell activation. To determine whether SNX27 plays a role in naïve T cell activation, we characterized primary T cell development and function in SNX27 KO mice (*Snx27*$^{-/-}$). *Snx27*$^{-/-}$ mice were originally reported to die at 4 weeks post-partum due to postnatal growth defects [40]. Optimization of housing and feeding conditions by Dr G Kinna (in Dr. B Collins's and Dr. R Teasdale's groups) nonetheless allowed us to analyze mice from 6 to 12 weeks old. Crossing *Snx27*$^{+/-}$ heterozygotes on C57BL/6 and 129SV mixed backgrounds [40] generated F1 hybrid background *Snx27*$^{+/+}$ and *Snx27*$^{-/-}$ mice and enabled paired analysis of littermates.

3.1. T cell development analysis

Committed lymphoid progenitor cells arise in the bone marrow and migrate to the thymus. Thymocytes differentiate into mature T lymphocytes after the processes of death by neglect, negative and positive selection, and lineage-specific development (reviewed in [115]). T lymphocytes are then borne in the blood to the peripheral lymphoid tissues in the spleen and lymph node organs (reviewed in [199]). We analyzed total cellularity of the thymus, spleen and lymph nodes (LN) in *Snx27*$^{-/-}$ mice and observed a significant decrease in spleen cellularity compared to littermate controls (Fig R22A); this decrease correlated with a smaller organ (Fig R22B). This was consistent with previous reports showing that *Snx27* deletion in mice

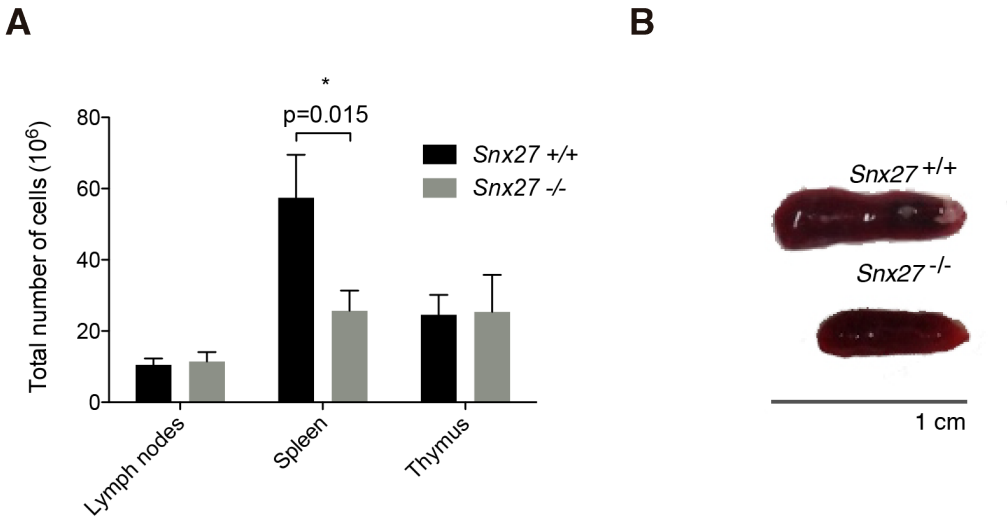

Fig R22. *Snx27*$^{-/-}$ mice show reduced spleen cellularity

(**A**) WT and *Snx27*$^{-/-}$ littermate-matched pairs of mice were sacrificed and total cellularity was recorded of the thymus, spleen and lymph nodes following erythrocyte lysis. Data shown as mean ± SEM (*p<0.05; paired t-test; *n* = 7). (**B**) Spleens from a littermate pair are shown. Bar: 1 cm.

results in smaller animals with reduced organ size [40, 51]. Thymus and LN cellularity were nonetheless unaltered in *Snx27*$^{-/-}$ mice (Fig R22A).

T cell development and maturation takes place in the thymus; thymocyte populations at different stages are identified by cell surface marker expression. Early committed T cells lack expression of the TCR and of the CD4 and CD8 coreceptors, and are termed double negative thymocytes (DN; CD4^{-}CD8^{-}). DN thymocytes can be subdivided into four differentiation stages defined by CD44 and CD25 expression (DN1, CD44^{+}CD25^{-}; DN2, CD44^{+}CD25^{+}; DN3, CD44^{-}CD25^{+}; DN4, CD44^{-}CD25^{-}) [122]. Throughout these stages, cells undergo β-selection, a process that involves apoptosis of thymocytes that do not express a productive pre-TCR. Selected thymocytes proliferate extensively during DN3-DN4 stages and mature into double positive thymocytes (DP; CD4^{+}CD8^{+}) that replace their pre-TCR to yield a complete αβTCR. Subsequent positive and negative selection determines thymocyte commitment to the CD4 or CD8 lineages (reviewed in [115]) (Fig R23A).

Using flow cytometry, we analyzed cell surface expression of CD4, CD8, CD44 and CD25 markers in thymocytes and calculated the percentage of cells found at each stage of T cell development. The analysis of thymocyte distribution in DN stages showed a decrease in the DN1 population and an increase in DN4 cells in *Snx27*$^{-/-}$ mice, both significant compared to WT controls (Fig R23B). The DN4 stage is defined by cells negative for CD44 (the hyaluronic acid receptor) and CD25 (the interleukin-2 (IL-2) receptor α chain). Both of these receptors are prone to recycling [91, 142], so an enlarged CD44^{-}CD25^{-} population could be the result of defective CD44 or CD25 protein trafficking. We thus analyzed the percentage of this population in other developmental stages, and found that the number of CD44^{-}CD25^{-} cells gated in CD4^{+}, CD8^{+} and DP thymocytes was within the normal ranges (not shown). These data suggest that there is no general CD44 or CD25 protein trafficking defect in *Snx27*$^{-/-}$ thymocytes. We also determined that the larger DN4 population in *Snx27*$^{-/-}$ mice was not a result of elevated TCRγδ expression, as the DN population included a similar percentage of TCRγδ^{+} cells in WT and *Snx27*$^{-/-}$ mice (Fig R23C). As accumulation of previously selected mature thymocytes that downregulated expression of CD4 and CD8 coreceptors might also explain our data, we analyzed DN thymocytes for maturation indicators such as smaller cell size and/or TCRαβ expression. While DN4 *Snx27*$^{-/-}$ thymocytes showed a tendency towards smaller cell size (Fig R23D), the percentage of TCRαβ^{+} DN cells was similar to WT thymocytes (Fig R23C). Although additional studies are needed, our results suggest enhanced proliferation of *Snx27*$^{-/-}$ thymocytes at the DN4 stage during development. Analysis of DP and CD4^{+} or CD8^{+} single positive (SP) thymocyte populations showed no significant differences, although we observed a slight tendency towards increased numbers of SP cells in *Snx27*$^{-/-}$ thymocytes (Fig R23E).

Mature T lymphocytes exit the thymus and migrate to peripheral lymphoid sites in the spleen and LN, where mature B cells also reside (reviewed in [182, 199]). We quantified the percentages of lymphocyte populations in cell suspensions from WT and *Snx27*$^{-/-}$ spleen and LN as above;

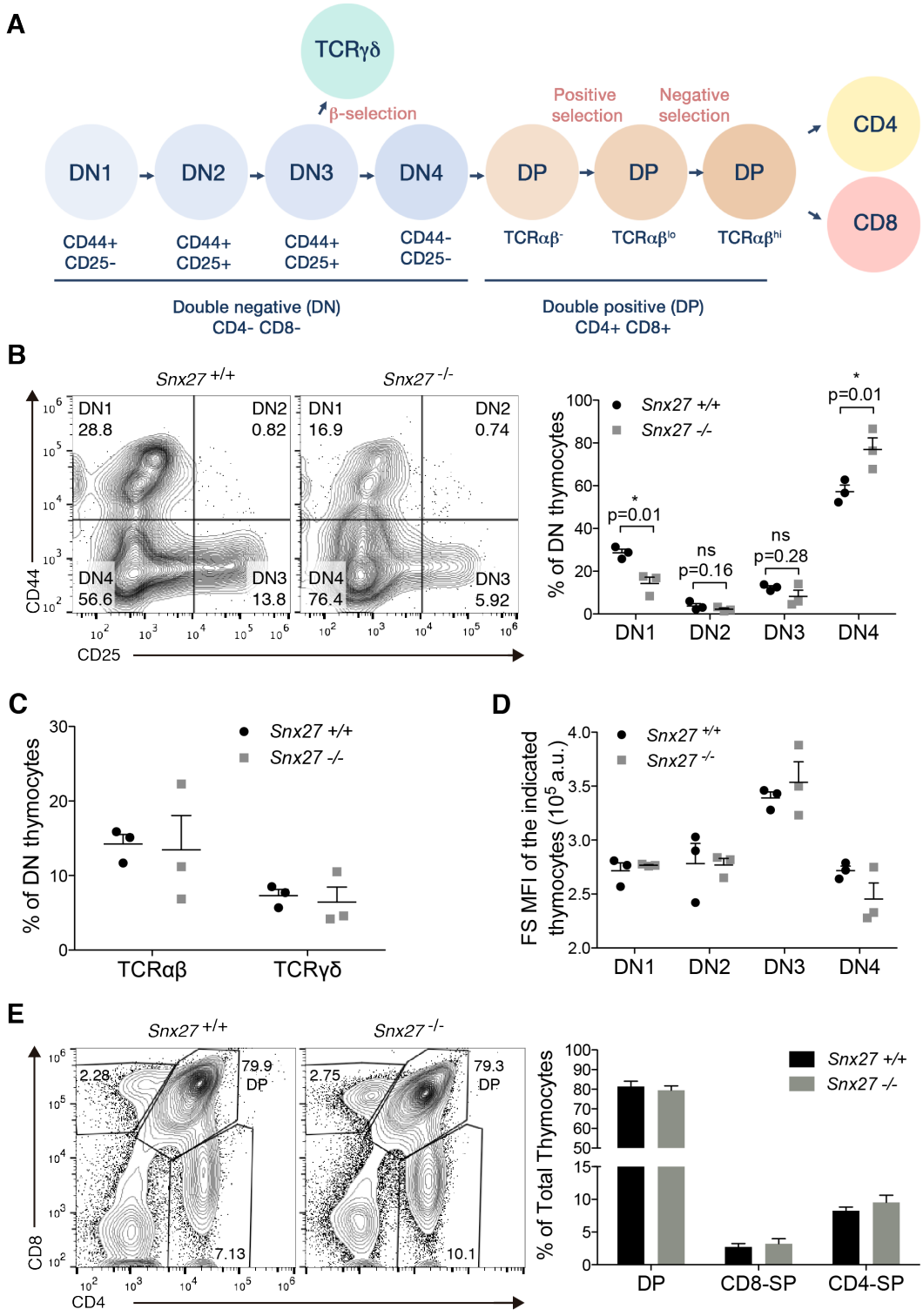

Fig R23. Analysis of T cell development in WT and *Snx27*$^{-/-}$ mice

(**A**) Stages in T cell development (see text for details). (**B-E**) Thymocytes from WT and *Snx27*$^{-/-}$ littermate pairs were stained for the indicated cell surface markers and analyzed by flow cytometry. (**B-D**) Double negative thymocytes (DN,CD4$^-$CD8$^-$) were gated and (**B**) cell percentage and (**D**) size in the four developmental stages was calculated (DN1, CD44$^+$CD25$^-$; DN2, CD44$^+$CD25$^+$; DN3, CD44$^-$CD25$^+$; DN4, CD44$^-$CD25$^-$); (**C**) percentage of cells expressing TCRαβ or TCRγδ was also calculated. (**E**) The percentage of total double-positive (DP, CD4$^+$CD8$^+$) and single positive (SP, CD4$^+$CD8$^-$ or CD4$^-$CD8$^+$) thymocytes was calculated. (**B**, **E**) Representative flow cytometry plots are shown (left). Data shown as mean ± SEM [*p<0.05; paired t-test; (**B-D**) $n = 3$ (**E**) $n = 7$] (right). a.u., arbitrary units.

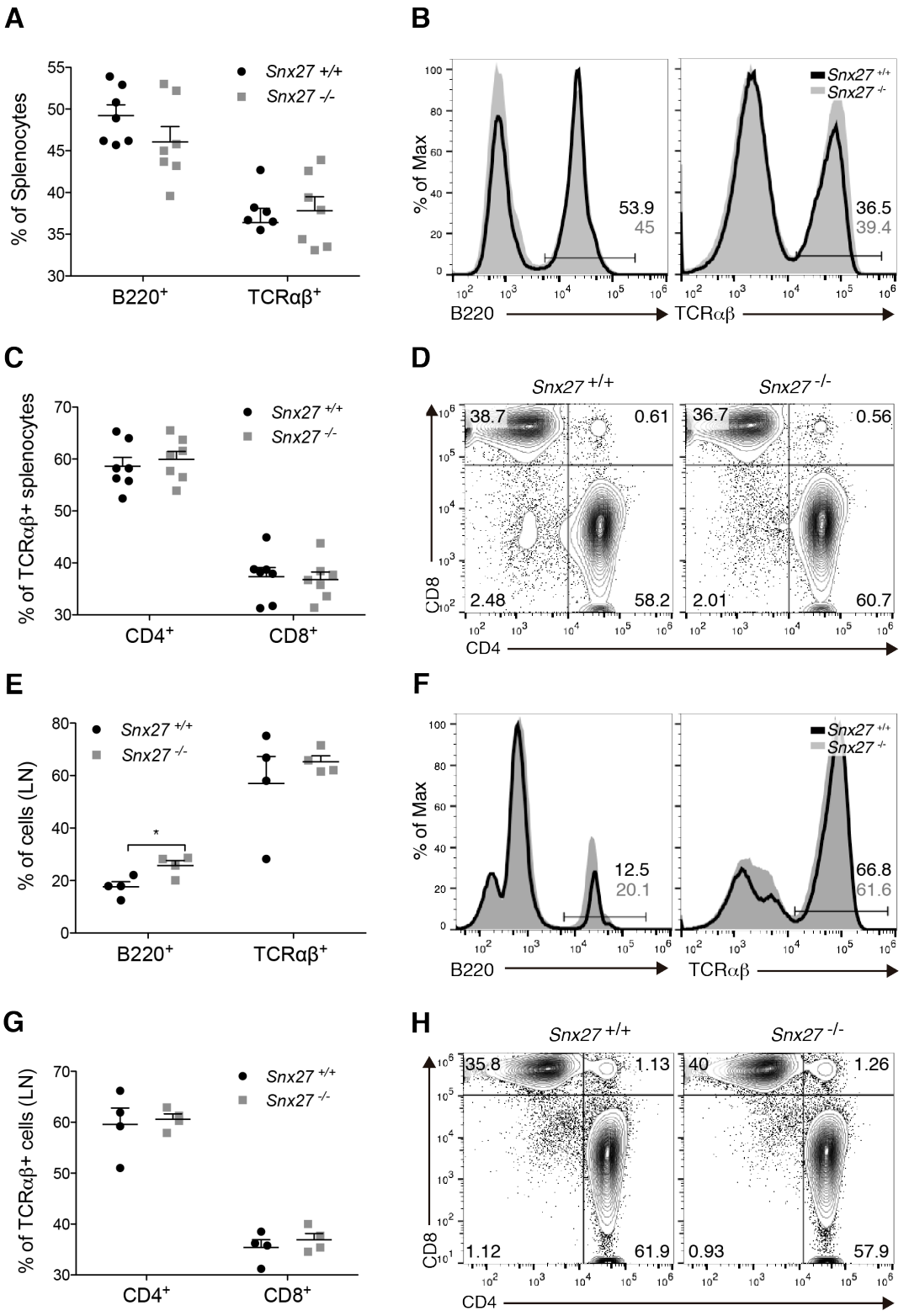

Fig R24. *Snx27*$^{-/-}$ mice show normal T cell populations in peripheral lymphoid tissue

(**A**-**D**) Splenocytes and (**E**-**H**) lymph node (LN) cells from WT and *Snx27*$^{-/-}$ littermate pairs were stained for the indicated cell surface markers and analyzed by flow cytometry. (**A**, **B**, **E**, **F**) The percentage of B220^{+} and TCRαβ^{+} cells was calculated. (**C**, **D**, **G**, **H**) TCRαβ^{+} cells were gated and the percentages of CD4^{+} and CD8^{+} cells were calculated. (**A**, **C**, **E**, **G**) Data shown as mean ± SEM [*p<0.05; paired t-test; (**A**, **C**) $n = 7$ (**E**, **G**) $n = 4$]. (**B**, **D F**, **H**) Representative flow cytometry plots are shown.

B cells were detected by surface expression of B220, an isoform of the tyrosine phosphatase CD45 expressed at all B lymphocyte stages.

Compared to WT controls, there were no gross differences in the number of *Snx27*$^{-/-}$ TCR$\alpha\beta^+$ cells in spleen or LN (Fig R24A, B, E, F) or in the percentages of CD4$^+$ and CD8$^+$ cells gated in TCR$\alpha\beta^+$ (Fig R24C, D, G, H). Analysis of the B220$^+$ cell population in LN nonetheless showed increased numbers in *Snx27*$^{-/-}$ mice (Fig R24E); further studies are needed to confirm these data.

3.2. T cell activation analysis

Snx27 deletion in mice did not markedly alter T cell development. The normal cellularity of *Snx27*$^{-/-}$ mouse thymus contrasted with a substantial decrease in spleen. *Snx27*$^{-/-}$ mice nonetheless maintained peripheral T cell populations similar to WT littermates, which allowed us to compare the activation of spleen T cells from WT and *Snx27*$^{-/-}$ mice. To trigger T cell activation *in vitro*, we stimulated splenocytes for 48 h with agonistic antibodies; we used plate-bound anti-CD3 for TCR triggering alone, or combined with soluble anti-CD28 for costimulation. Using flow cytometry, we measured cell surface expression of several activation markers in CD4$^+$ or CD8$^+$ cells, as well as their proliferation and growth.

3.2.1. Induction of T cell activation markers

TCR triggering and costimulation in SNX27-silenced Jurkat T cells resulted in hyperactivation of DAG/PKC/Ras-dependent pathways, as shown by the increase in the number of cells that upregulated CD69, as well as in enhanced CD69 expression per cell. We thus analyzed CD69 upregulation in WT and *Snx27*$^{-/-}$ activated T cells. At 48 h after stimulation with anti-CD3 antibody, the percentage of CD69$^+$ cells was higher in *Snx27*$^{-/-}$ CD4$^+$ and CD8$^+$ cells compared to those in WT mice (Fig R25A-D). This is reminiscent of the larger proportion of CD69$^+$ T cells observed after anti-CD3 stimulation of DGK$\zeta^{-/-}$ mouse T cells [365], and suggests that SNX27 limits the Ras signaling threshold for activation in primary mouse T cells. The GMFI of the CD69$^+$ cells was nonetheless similar in WT and *Snx27*$^{-/-}$ cells (Fig R25E, F), resembling that described for ERK phosphorylation in DGK$\zeta^{-/-}$ mice [268].

Whereas CD69 upregulation is a very sensitive, transient measure of antigen recognition, CD44 expression is also induced after antigen recognition, and remains high on all antigen-experienced cells [34]. We thus analyzed *Snx27*$^{-/-}$ T cell activation by measuring CD44 upregulation in CD4$^+$ and CD8$^+$ cells. Naïve CD4$^+$ T cells express low levels of CD44 [34]; *Snx27*$^{-/-}$ CD4$^+$ splenocytes showed normal amounts of surface CD44, as indicated by CD44 GMFI in basal conditions (Fig R26A, B). TCR activation nonetheless resulted in a marked reduction in CD44 levels in *Snx27*$^{-/-}$ CD4$^+$ T cells, which was significant compared to controls after CD3/CD28 costimulation (Fig R26B). Naïve CD8$^+$ T cells do not express CD44, and we could thus distinguish the proportion of responsive T cells. As shown in CD69 analysis (Fig R25), a larger proportion of *Snx27*$^{-/-}$ T cells responded to anti-CD3 stimulation compared to

controls (Fig R26C, D) confirming that SNX27 limits the threshold for responsive cells. CD44 GMFI was nonetheless reduced in *Snx27*$^{-/-}$ activated CD8^{+} T cells (Fig R26); this suggests a general defect in *Snx27*$^{-/-}$ T cells in achieving high CD44 levels, which is aggravated by CD3/CD28 costimulation.

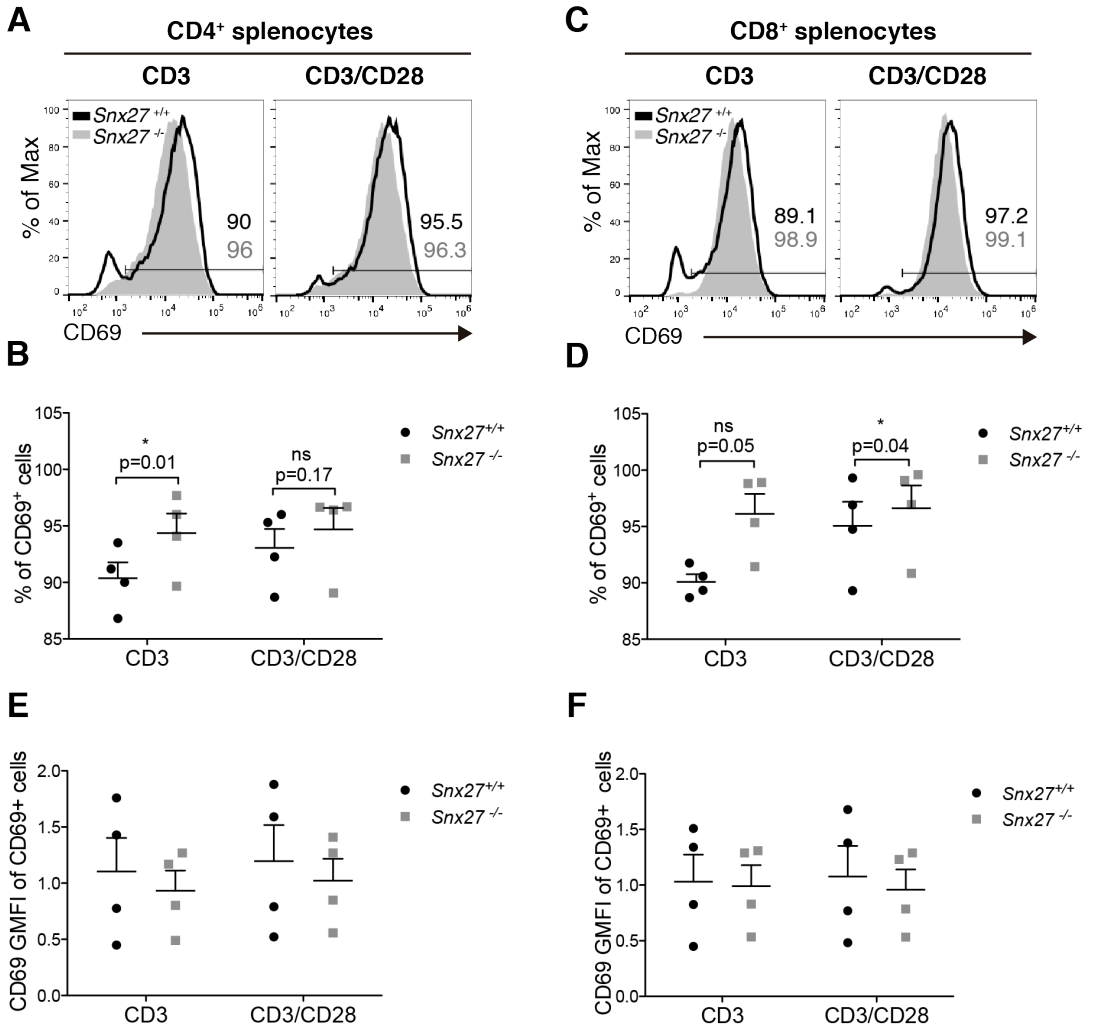

Fig R25. Analysis of CD69 induction in *Snx27*$^{-/-}$ splenocytes

(**A**-**F**) Splenocytes from WT and *Snx27*$^{-/-}$ littermate pairs were stimulated (48 h) with plate-bound anti-CD3 alone or with soluble anti-CD28 for costimulation, and stained for the indicated cell surface markers. Using flow cytometry, (**A**, **B**, **E**) CD4^{+} or (**C**, **D**, **F**) CD8^{+} cells were gated, and (**B**, **E**) the percentage and (**E**, **F**) geometric mean fluorescence intensity (GMFI) of CD69^{+} cells were calculated. (**B**, **D**, **E**, **F**) Data shown as mean ± SEM (ns, not significant, p>0.05; *p<0.05; paired t-test; *n* = 4). (**A**, **C**) Representative flow cytometry plots are shown.

3.2.2. Induction of T cell growth and proliferation

Snx27$^{-/-}$ mice showed a larger population of responsive T cells, whereas low cell surface CD44 abundance suggested a *Snx27*$^{-/-}$ T cell impairment in achieving a full activation phenotype. During naïve T cell activation, quiescent lymphocytes enter the cell cycle. Full activation of primary T cells not only elicits proliferation signals, but also triggers metabolic reprogramming to

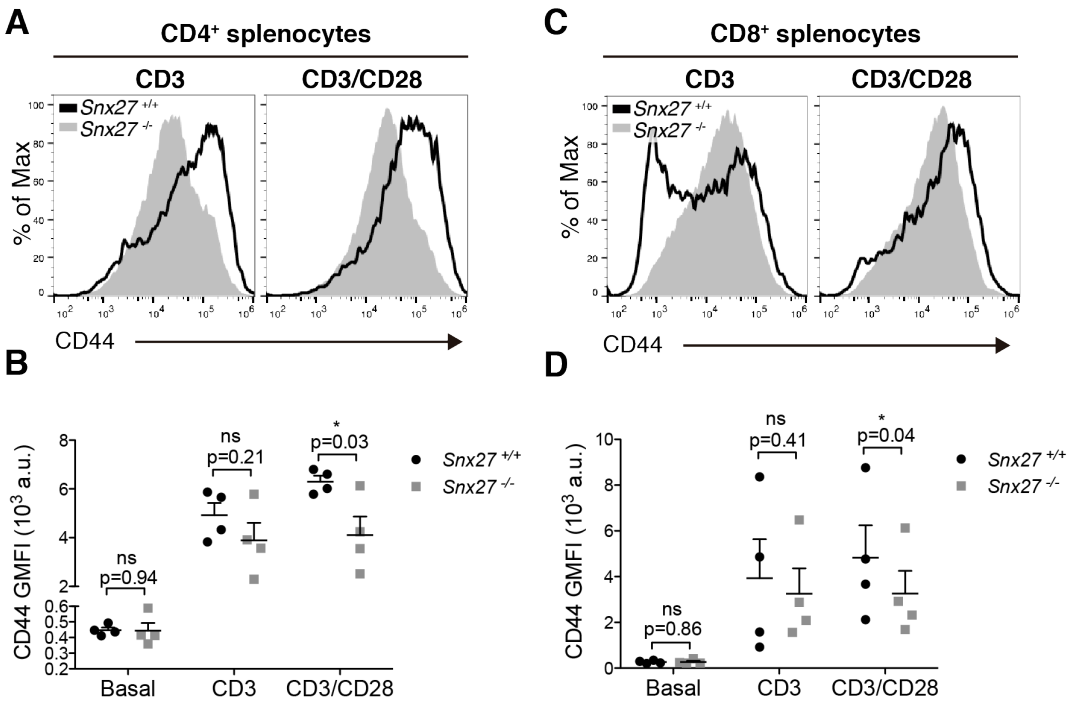

Fig R26. Analysis of CD44 induction in *Snx27*$^{-/-}$ splenocytes

Splenocytes from WT and *Snx27*$^{-/-}$ littermate pairs were stimulated (48 h) with plate-bound anti-CD3 alone or with soluble anti-CD28 and stained for the indicated cell surface markers. Using flow cytometry, (**A**, **B**) CD4^{+} or (**C**, **D**) CD8^{+} cells were gated, and the CD44 GMFI was calculated. (**B**, **D**) Data shown as mean ± SEM (ns, not significant, p>0.05; *p<0.05; paired t-test; $n = 4$). (**A**, **C**) Representative flow cytometry plots are shown. a.u., arbitrary units.

support cell growth. Binding of costimulatory molecules activates PI3K and the metabolic regulator mTOR (reviewed in [33, 338]). As recently reported, mTOR activity downstream of TCR triggering is indicated by cell size [259]. When we monitored T cell size by flow cytometry using forward scatter (FSC), we observed naïve cell growth after CD3 stimulation, with a larger number of cells that increased in size in response to CD28 costimulation (Fig R27A, E).

Abundance of cell surface CD44 in naïve T cells is also an mTOR activity reporter [147], as described in cancer cells [67]. The putative correlation between mTOR activity and CD44 expression following T cell activation has nonetheless not yet been addressed. We thus examined cell surface CD44 abundance relative to cell size, a known mTOR activation marker in T cells. We calculated the CD44 GMFI of cells from four distinctly sized populations [from the smallest FSC MFI population ("size 1"; S1) to the largest ("size 4"; S4) (Fig R27 A, E)], and used cell surface TCRβ expression as a control. Our results showed that while TCRβ GMFI remained constant independently of cell size, CD44 GMFI was directly proportional to FSC MFI in CD4^{+} and CD8^{+} cells after CD3 or CD3/CD28 stimulation (FigR27C, D). These data suggest mTOR-dependent control of CD44 upregulation after T cell activation, and that the *Snx27*$^{-/-}$ T cell defect in achieving high CD44 levels could be a result of poor mTOR activation and cell growth.

To determine whether SNX27 deficiency affects cell growth, we measured cell size in WT and *Snx27*$^{-/-}$ mouse T cells. *Snx27*$^{-/-}$ cell size was normal in basal conditions (Fig R28B, E), but was smaller than WT controls after CD3 or CD3/CD28 stimulation; differences were significant for CD4^{+} cells, and for CD8^{+} cells only following CD3/CD28 stimulation (Fig R28B, E). When we calculated cell distribution among distinctly sized populations (gates shown in Fig R28 A, D), we observed that CD3-stimulated T cells were found mostly in the smaller S1 and S2 populations, with no gross differences between WT and *Snx27*$^{-/-}$ T cells. Following

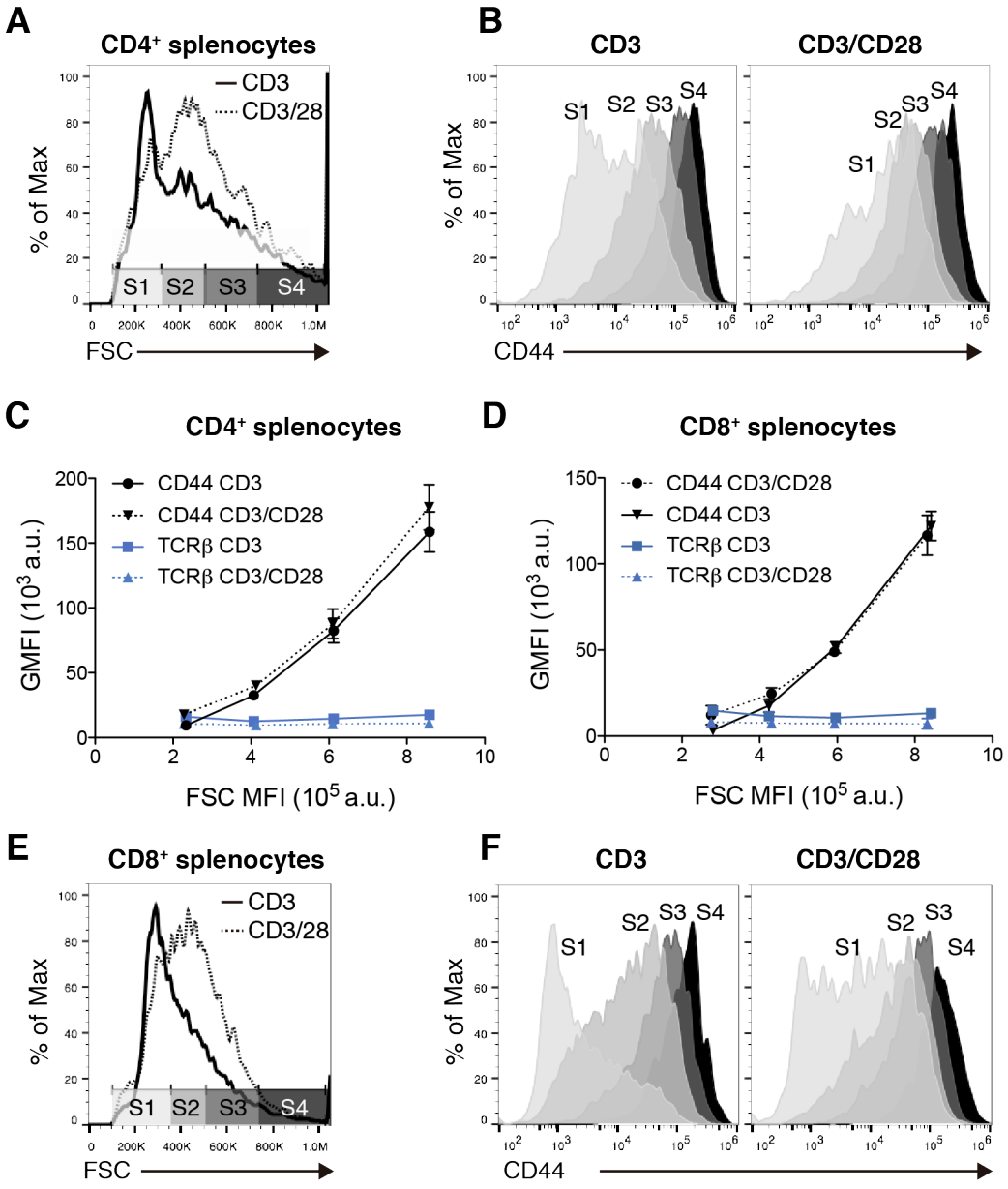

Fig R27. Correlation between cell size and CD44 expression in activated T cells

Splenocytes from WT mice were stimulated (48 h) with plate-bound anti-CD3 alone or with soluble anti-CD28 and stained for the indicated cell surface markers. Using flow cytometry, (**A**-**C**) CD4^{+} or (**D**-**F**) CD8^{+} cells were gated and the MFI of CD44 (black) and TCRβ (blue) were calculated in cells from the four distinctly sized populations (S1, S2, S3, S4; gates shown in **A**, **E**). (**C**, **D**) Data shown as mean ± SEM (n = 2). (**B**, **F**) Representative flow cytometry plots are shown. a.u., arbitrary units.

CD28 costimulation, the percentage of WT T cells in the larger sized populations S3 and S4 increased, whereas the percentage of S3 and S4 populations in $CD4^+$ and $CD8^+$ *Snx27*$^{-/-}$ cells remained low (Fig R28 C, F). This growth defect was independent of Ras activation, as most *Snx27*$^{-/-}$ cells upregulated CD69 after TCR triggering. The lower CD44 abundance observed in *Snx27*$^{-/-}$ T cells could be explained by this growth defect, as our previous analyses showed that S3 and S4 populations are those with the highest CD44 levels (Fig R27).

T cell growth following stimulation is linked to subsequent proliferation; the expression of T cell activation markers including CD44 increases further after cell division [97]. To determine

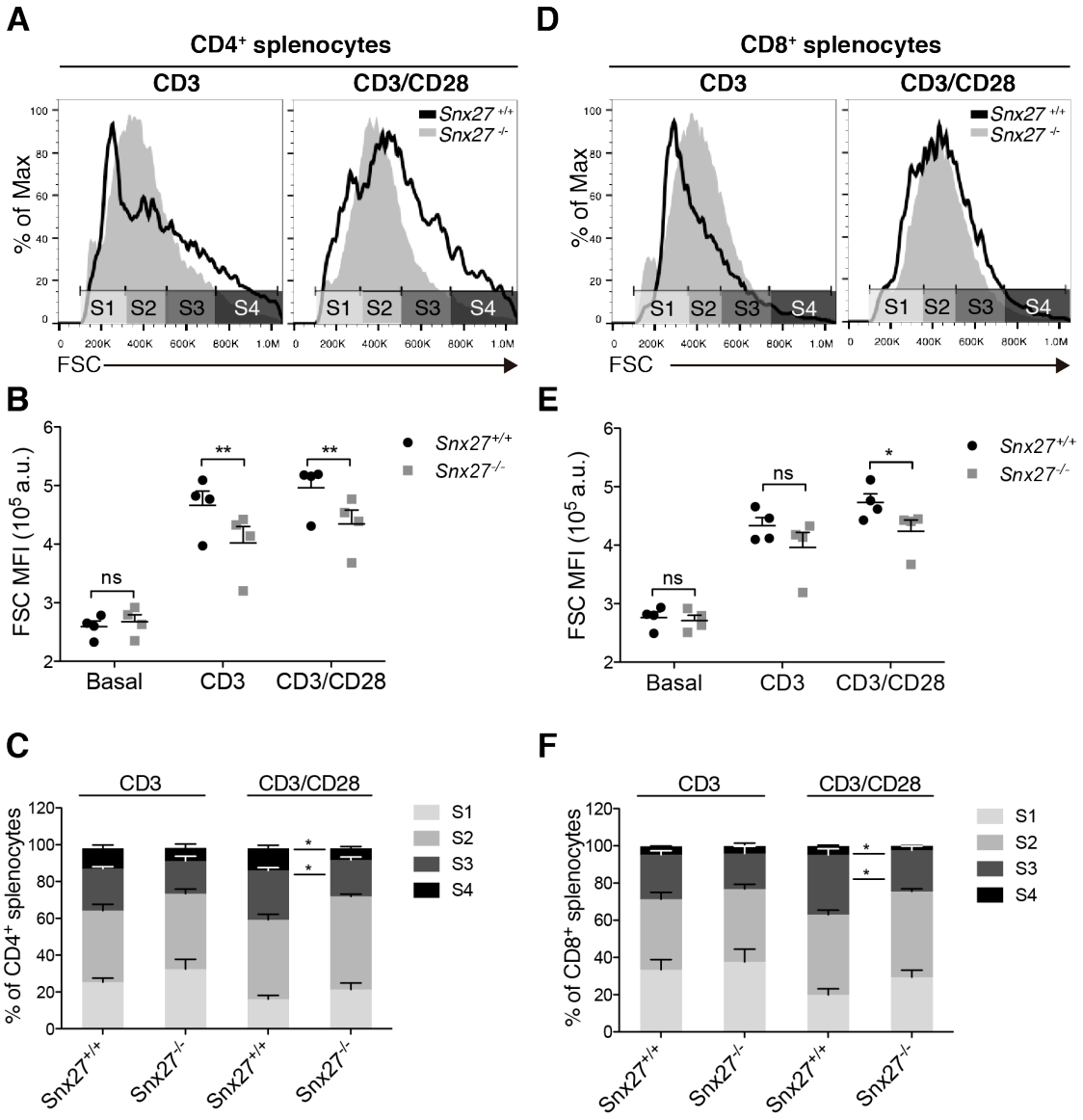

Fig R28. *Snx27*$^{-/-}$ splenocytes showed reduced growth after activation

(**A**-**F**) Splenocytes from WT and *Snx27*$^{-/-}$ littermate pairs were stimulated (48 h) with plate-bound anti-CD3 alone or with soluble anti-CD28 for costimulation, and cell size was calculated using flow cytometry. (**A**-**C**) $CD4^+$ or (**D**-**F**) $CD8^+$ cells were gated, and (**B**, **E**) MFI of the forward scatter (FSC) was calculated, as well as (**C**, **G**) the percentage of cells in four distinctly sized populations (S1, S2, S3, S4; gates shown in **A**, **D**). (**B**, **C**, **E**, **F**) Data shown as mean ± SEM (ns, not significant, $p>0.05$; *$p<0.05$; **$p<0.01$; paired t-test; $n = 4$). (**A**, **D**) Representative flow cytometry plots are shown. a.u., arbitrary units.

whether SNX27 depletion in T cells also affects proliferative responses, we monitored cell proliferation by flow cytometry. Before stimulation, WT and *Snx27*$^{-/-}$ splenocytes were stained with CellTrace, and at 48 h after stimulation, generations of proliferating cells were identified by dye dilution. Proliferation of anti-CD3 antibody-treated *Snx27*$^{-/-}$ CD4^{+} and CD8^{+} T cells was normal (Fig R29). CD28 costimulation further promoted division in WT and *Snx27*$^{-/-}$ cells, although analysis of flow cytometry plots indicated a low proportion of cells with a higher division rate in *Snx27*$^{-/-}$ splenocytes (Fig R29). To determine whether *Snx27*$^{-/-}$ cells have an intrinsic defect that prevents a high division index, we turned to less physiological but more potent proliferative stimuli. We used phorbol 12-myristate 13-acetate (PMA, 0.1 μg/ml) and ionomycin (Io, 1nM) for pharmacological TCR stimulation, or the T cell mitogen concanavalin A (ConA), a lectin that crosslinks glycosylated surface receptors including the TCR. These treatments indeed resulted in a more productive response; cell proliferation and CD44 abundance increased (not shown). *Snx27*$^{-/-}$ T cells maintained low surface CD44 abundance compared to controls (not shown), whereas the number of WT and *Snx27*$^{-/-}$ splenocyte divisions was similar (Fig R29). Overall, our data showed no gross *Snx27*$^{-/-}$ T cell proliferation defects, and suggest impaired capacity for full mTOR activation as a cause of reduced CD44 expression after activation.

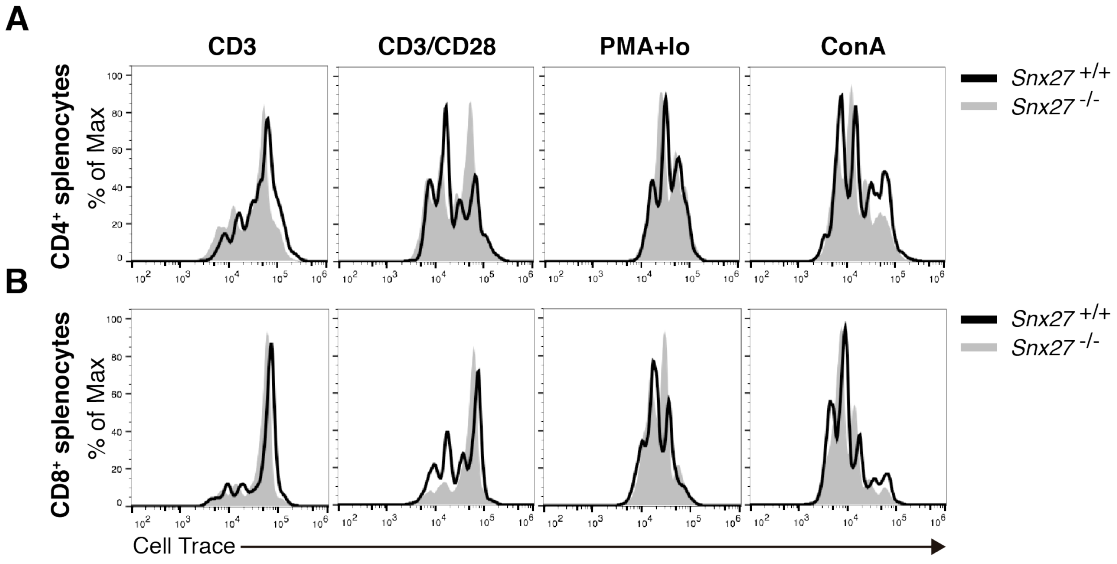

Fig R29. Dye dilution analysis of T cell division

Splenocytes from WT and *Snx27*$^{-/-}$ littermate pairs were labeled with CellTrace and stimulated (48 h) with plate-bound anti-CD3 alone or with soluble anti-CD28 for costimulation, with concanavalin A (ConA, 5 μg/ml) or phorbol 12-myristate 13-acetate (PMA, 0.1 μg/ml) and ionomycin (Io, 1 nM). Cells were then stained for CD4 and CD8 surface markers and analyzed by flow cytometry. (**A**, **B**) CD4^{+} or (**C**, **D**) CD8^{+} cells were gated, and representative flow cytometry plots of Cell Trace intensity were analyzed. Data shown are representative of three experiments.

3.2.3. mTOR activation in T cells

mTOR activation and metabolic reprogramming in T cells leads to enhanced expression of nutrient receptors and transporters, including TfR and GLUT1, to allow rapid growth ([109, 364], reviewed in [33, 338]). To confirm decreased mTOR activation in *Snx27*$^{-/-}$ cells, we analyzed surface expression of these receptors after T cell stimulation. Available anti-GLUT1 antibodies react poorly with GLUT1 extracellular domains, and data on cell surface GLUT1 abundance were thus inconclusive (not shown). Analysis of surface TfR abundance on activated T cells was possible using a fluorescently labeled anti-CD71 antibody. CD71 expression increased after anti-CD3 stimulation in WT T cells, with a further increase after anti-CD28 costimulation (Fig R30). *Snx27*$^{-/-}$ T cells also upregulated CD71, although it was less abundant than in WT controls; differences were substantial after CD28 costimulation (Fig R30).

Our flow cytometry data strongly suggested impaired mTOR activation in SNX27-depleted T cells. In a biochemical analysis, we directly assessed mTOR activation in splenocytes after TCR triggering and costimulation elicited by ConA treatment. To examine early signaling up to 1 h post-activation, we analyzed rps6 (ribosomal protein S6) phosphorylation at Ser235/6, which is downstream of the mTORC1/S6K pathway; we also tested mTORC2-dependent AKT phosphorylation at Ser473, as well as ERK phosphorylation as a control for Ras/ERK pathway

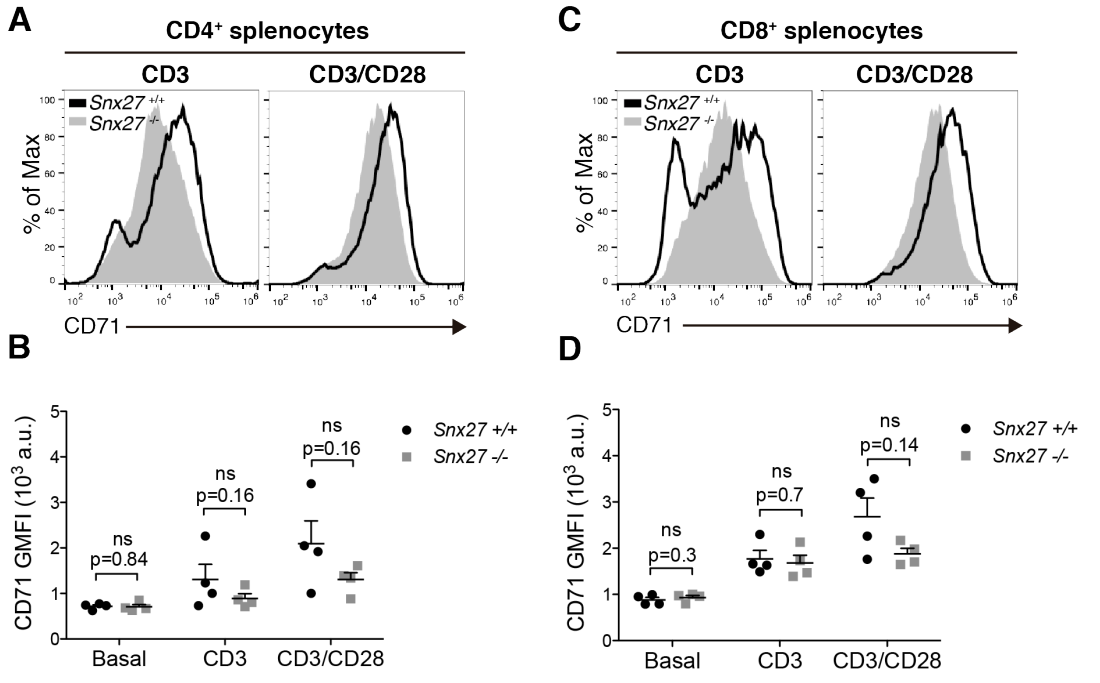

Fig R30. Analysis of CD71 induction in *Snx27*$^{-/-}$ splenocytes

Splenocytes from WT and *Snx27*$^{-/-}$ littermate pairs were stimulated (48 h) with plate-bound anti-CD3 alone or with soluble anti-CD28 for costimulation, and stained for the indicated cell surface markers. Using flow cytometry, (**A**, **B**) CD4^{+} or (**C**, **D**) CD8^{+} cells were gated, and the CD71 GMFI was calculated. (**B**, **D**) Data shown as mean ± SEM (ns, not significant, p>0.05; paired t-test; $n = 4$). (**A**, **C**) Representative flow cytometry plots are shown.

activation. Whereas ERK phosphorylation proceeded normally in *Snx27*$^{-/-}$ splenocytes, rps6 phosphorylation was delayed (Fig R31). AKT Ser473 phosphorylation was also reduced in *Snx27*$^{-/-}$ splenocytes at later times, which indicated alterations in mTORC2 pathway downstream of TCR triggering. These data indicate that impaired mTOR activation is concomitant with the inability of SNX27-depleted T cells to grow normally or to express high CD44 and TfR levels.

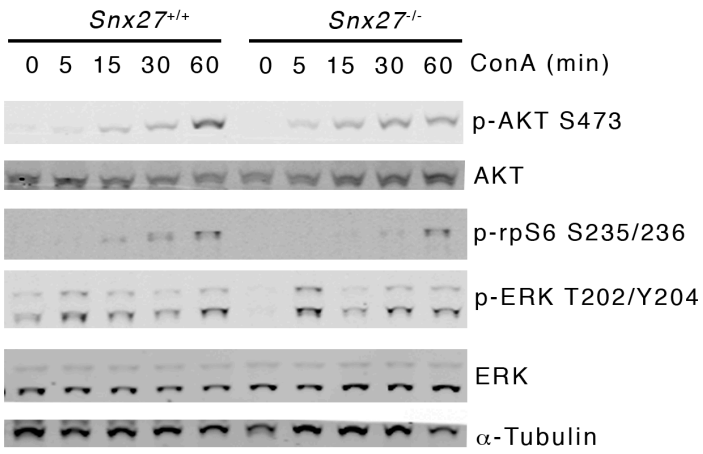

Fig R31. *Snx27*$^{-/-}$ splenocytes show reduced mTOR activation

Splenocytes from a WT and *Snx27*$^{-/-}$ littermate pair were stimulated with ConA for the indicated times. AKT, rpsS6 and ERK phosphorylation and total abundance were evaluated by western blot in total cell lysates. Tubulin was used as a loading control. A representative experiment is shown.

3.2.4. Analysis of surface levels of putative SNX27 cargoes

SNX27-depleted T cells responded to activation by CD3/CD28 costimulation, and proliferated with no gross defects, whereas they did not grow normally in response to stimulation. Weak mTOR pathway activation due to altered TCR-mediated signaling or metabolic defects could explain the smaller cell size. Indeed, SNX27 is known mainly for its implication the PDZ-dependent trafficking of nutrient receptors and transporters such as GLUT1 [308]. The NPxY-binding capacity of the SNX-FERM proteins, including SNX27, could also mediate recycling of proteins important for T cell function such as LFA-1 and the TCR complex protein CD3ε. WASH KO primary T cells have low levels of cell surface LFA-1 in basal conditions and of TCRβ after activation [256], and our data in Jurkat cells indicated that SNX27 silencing affects LFA-1 stability. To determine whether SNX27 depletion alters cell surface abundance of these two proteins in primary T cells in basal or stimulation conditions, we monitored the signal of fluorescently labeled anti-CD11a and -CD3ε antibodies by flow cytometry.

In contrast to WASH-depleted T cells, *Snx27*$^{-/-}$ cells showed normal CD11a levels in basal conditions compared to controls (Fig R32). After TCR triggering, cell surface CD11a was low in *Snx27*$^{-/-}$ T cells, which was significant compared to controls after CD3/CD28 costimulation (Fig R32B,D). When we analyzed CD3ε expression in the same conditions, we found no defects in *Snx27*$^{-/-}$ T cells; the activation-dependent downmodulation of CD3ε was indeed less pronounced in *Snx27*$^{-/-}$ T cells and led to a small increase in cell surface CD3ε that was

significant in activated CD8$^+$ T cells (Fig R33). Similar analysis of these two proteins in unstimulated SNX27-silenced Jurkat cells showed significant differences in LFA-1 levels after protein synthesis inhibition, whereas cell surface CD3ε abundance remained normal or higher than controls in all conditions (Fig R11B in section 3.2). These results suggest that whereas SNX27 is not necessary for TCR recycling, it participates in maintaining cell surface LFA-1 levels.

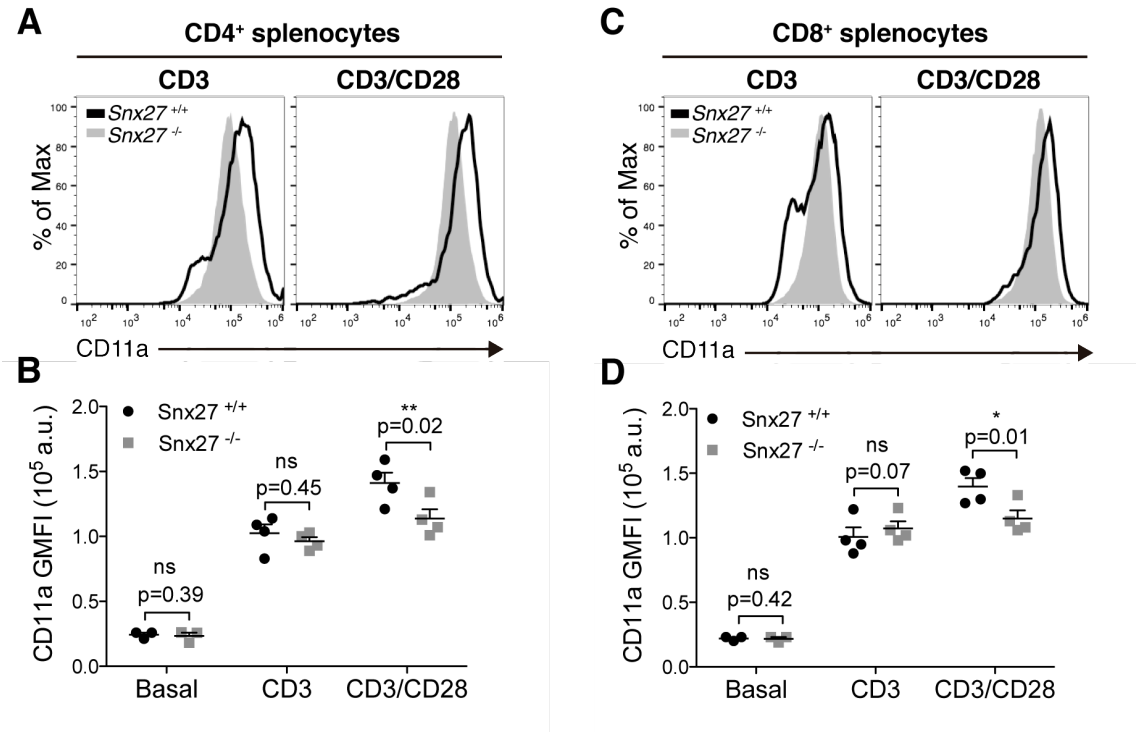

Fig R32. Analysis of LFA-1 (CD11a subunit) abundance in *Snx27*$^{-/-}$ splenocytes

Splenocytes from WT and *Snx27*$^{-/-}$ littermate pairs were stimulated (48 h) with plate-bound anti-CD3 alone or with soluble anti-CD28, and stained for the indicated cell surface markers. Using flow cytometry, (**A**, **B**) CD4$^+$ or (**C**, **D**) CD8$^+$ cells were gated, and the CD11a GMFI was calculated. (**B**, **D**) Data shown as mean ± SEM (ns, not significant, p>0.05; *p<0.05; **p<0.01; paired t-test; $n = 4$). (**A**, **C**) Representative flow cytometry plots are shown.

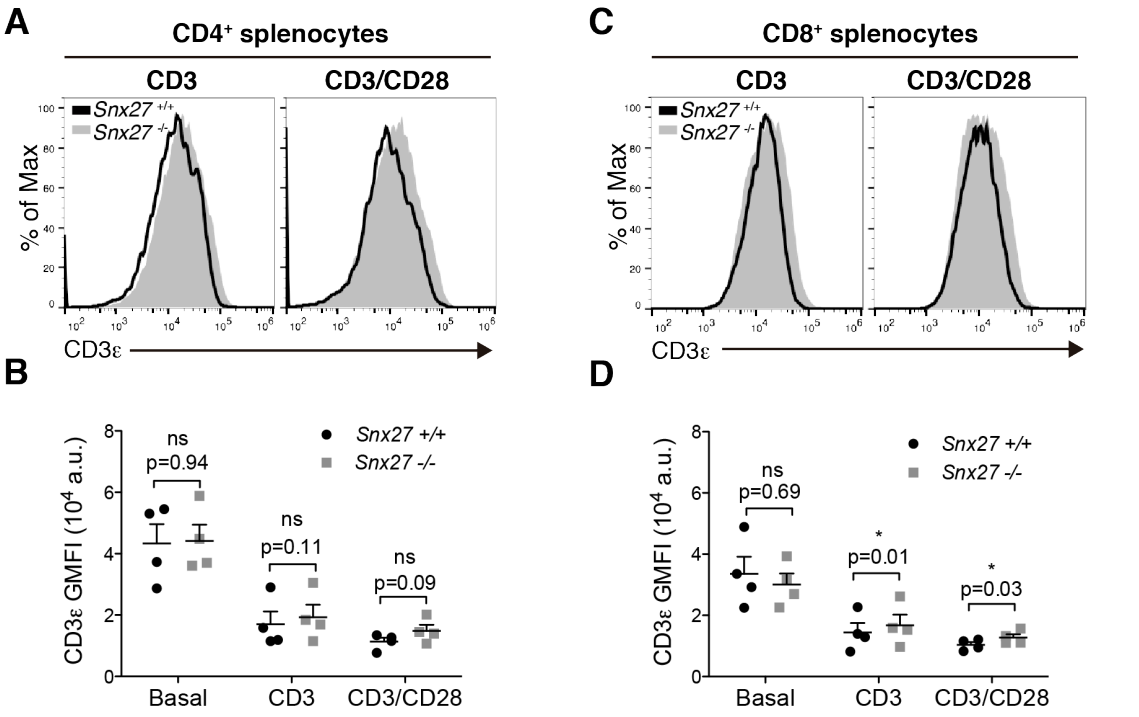

Fig R33. Analysis of CD3ε cell surface abundance in *Snx27*$^{-/-}$ splenocytes

Splenocytes from WT and *Snx27*$^{-/-}$ littermate pairs were stimulated (48 h) with plate-bound anti-CD3 alone or with soluble anti-CD28, and stained for the indicated cell surface markers. Using flow cytometry, (**A**, **B**) CD4^{+} or (**C**, **D**) CD8^{+} cells were gated, and the CD3ε GMFI was calculated. (**B**, **D**) Data shown as mean ± SEM (ns, not significant, p>0.05; *p<0.05; **p<0.01; paired t-test; $n = 4$). (**A**, **C**) Representative flow cytometry plots are shown.

4. SNX27 ROLE DURING INVASION

Proteomic and subcellular localization studies demonstrated SNX27/WASH interaction in T cells. We showed partial colocalization of SNX27 with WASH and CD63, which suggested SNX27 participation in WASH-mediated polarized secretion after antigen recognition, and requires further study. In cancer cells, WASH also colocalizes with CD63-positive late endosomes [360], and controls actin assembly to facilitate integrin and metalloproteinase secretion [228, 360]. The putative participation of SNX27 in WASH-regulated tumor cell polarized trafficking and exocytosis, however, has not yet been explored.

The MDA-MB-231 human invasive breast adenocarcinoma cell line is used as a model to study invadopodia formation and MT1-MMP delivery to these structures. When MDA-MB-231 cells are cultured on cross-linked gelatin as a matrix, the majority of intracellular MT1-MMP is located at late endosomes [307], where the WASH/exocyst complex assist in MMP trafficking and exocytosis to the invadopodial PM [228]. To determine whether SNX27 participates in these processes, we first examined SNX27 dynamics relative to actin polymerization in MDA-MB-231 cells plated on cross-linked gelatin. Live-cell imaging after cotransfection of the F-actin probe RFP-LifeAct with GFP-SNX27 showed that SNX27-positive endosomes moved rapidly and accumulated at actin cytoskeleton remodeling areas (Video 8, yellow arrows). In spreading cells, these endosomes localized at stable ring-shaped punctuate structures, some of which showed tubules that were reminiscent of linear invadopodia [163] (Video 8, blue arrows).

To determine whether the observed structures were MT1-MMP PM delivery sites [228], Cherry-SNX27 (Ch-SNX27)-transfected cells were immunostained for WASH and MT1-MMP endogenous proteins, and F-actin was labeled with fluorescent phalloidin. Densitometric analyses of protein distribution showed that Ch-SNX27 colocalized with WASH at MT1-MMP-positive F-actin-rich structures (Fig R34A-C), which was confirmed by quantitative colocalization analyses (Fig R34C). Immunostaining of the endogenous SNX27 and WASH proteins in cells transfected with the MT1-MMPmCherry (MT1-MMPCh) construct further confirmed colocalization of both proteins in MT1-MMPCh-positive endosomes. The amount of SNX27 accumulated at these sites inversely correlated with the size of the MT1-MMP-positive area (Fig R34D), which concurs with WASH localization at invadopodia during early stages of their formation [228]. Z projections and orthogonal views reconstructed from confocal images of the MT1-MMP-enriched sites showed that, while SNX27 localized at the top region of the MT1-MMP endosomes, WASH was closer to the region adjacent to the PM (Fig R34E). Although total internal reflection fluorescence (TIRF) and super-resolution microscopy are required to confirm these data, our results suggested that SNX27 is an adaptor for cargoes that participate in early stages of invadopodium formation.

To further explore the role of SNX27 during invadopodium formation, we established stable MDA-MB-231-derived cell lines that expressed shRNA against the previously validated SNX27 mRNA sequence (shSNX27 cells) or a non-targeting one (shCtrl cells) in a doxycycline (Dox)-

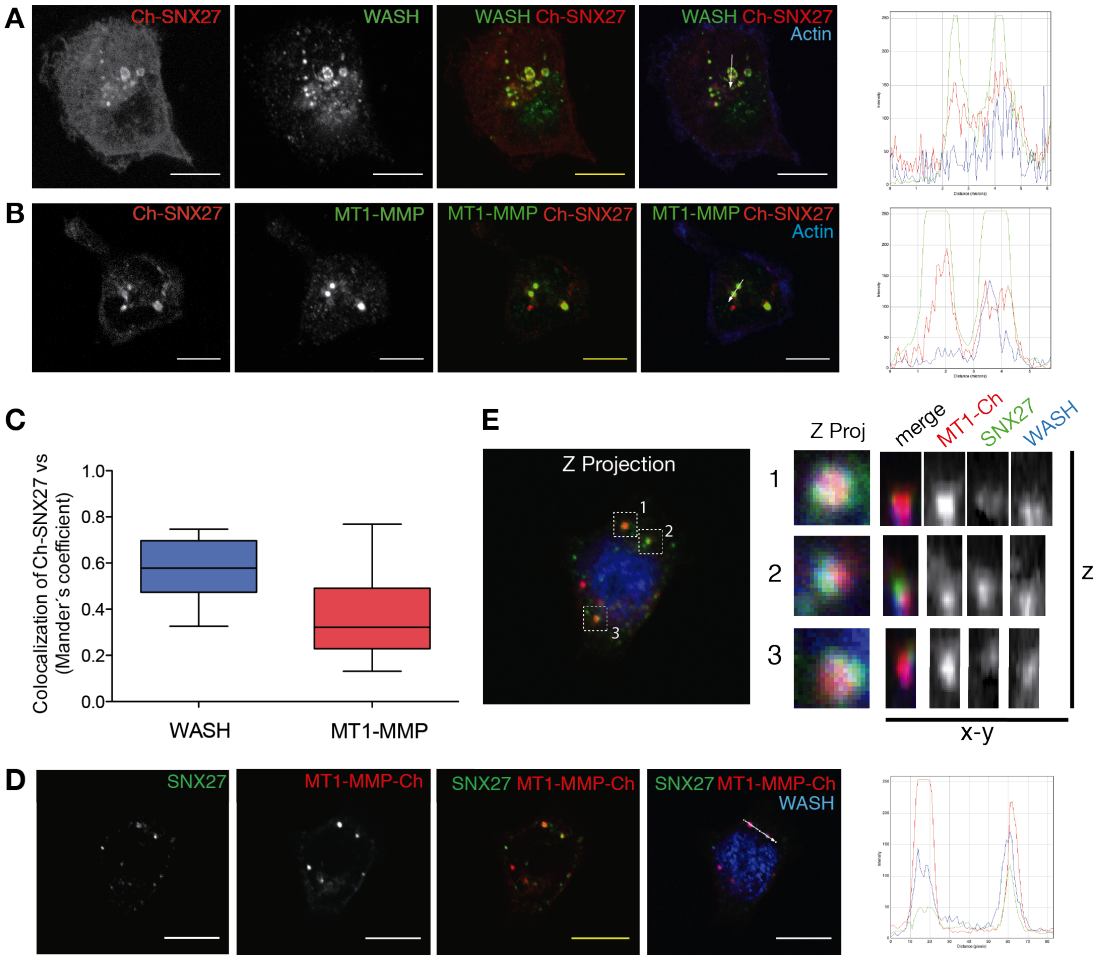

Fig R34. SNX27 colocalizes with WASH on MT1-MMP-positive endosomes in invasive cells

MDA-MB-231 cells were transfected with the indicated Cherry-tagged constructs, plated on cross-linked gelatin, stained with antibodies for the indicated proteins and, where indicated, also for F-actin using phalloidin. (**A**, **B**, **D**) Representative confocal images are shown; bar: 10μm. Densitometric analyses of protein distribution along the white line are shown on RGB profiles on the right. (**C**) Quantitative analysis of Cherry-SNX27 colocalization with WASH and MT1-MMP. Manders' overlap coefficient values for each cell were calculated and represented as box plots. (**E**) Z-projection of the cell shown in D (left), orthogonal views of the boxed regions (right) were generated using Image J.

dependent manner. After 72-96 h Dox treatment, SNX27 protein abundance in shCtrl cells remained constant, while it was reduced to 40% in shSNX27 cells (Fig R35A,B).

WASH complex components stability depends on the expression of core subunits including Strumpellin, FAM21 or SWIP [77, 161]. Protein abundance of WASH1 and Strumpellin in Dox-treated shSNX27 cells was normal (Fig R35B), which indicated that in MDA-MB-231 cells, SNX27 might be a WASH complex adaptor, but it is not a core component. MT1-MMP levels in Dox-treated shSNX27 cells were also unchanged, suggesting that SNX27 is not needed for MT1-MMP recycling in MDA-MB-231 cells (Fig R35B). We nonetheless analyzed MT1-MMP-positive endosomes morphology in these cells plated on cross-linked gelatin. In control shSNX27 cells (no Dox addition), MT1-MMP accumulated at small vesicles associated to well

organized WASH-positive puncta (Fig R35C, top). In Dox-treated cells, however, we observed large MT1-MMP-positive aggregations inside and outside WASH-delimited endosomes (Fig R35C, bottom), which suggested that SNX27 participates in MT1-MMP PM delivery regulation. Quantitative analyses of the MT1-MMP-positive area per cell showed an increased area in Dox-treated shSNX27 cells (Fig R35D), which correlated with the alterations in MT1-MMP-positive endosomes morphology.

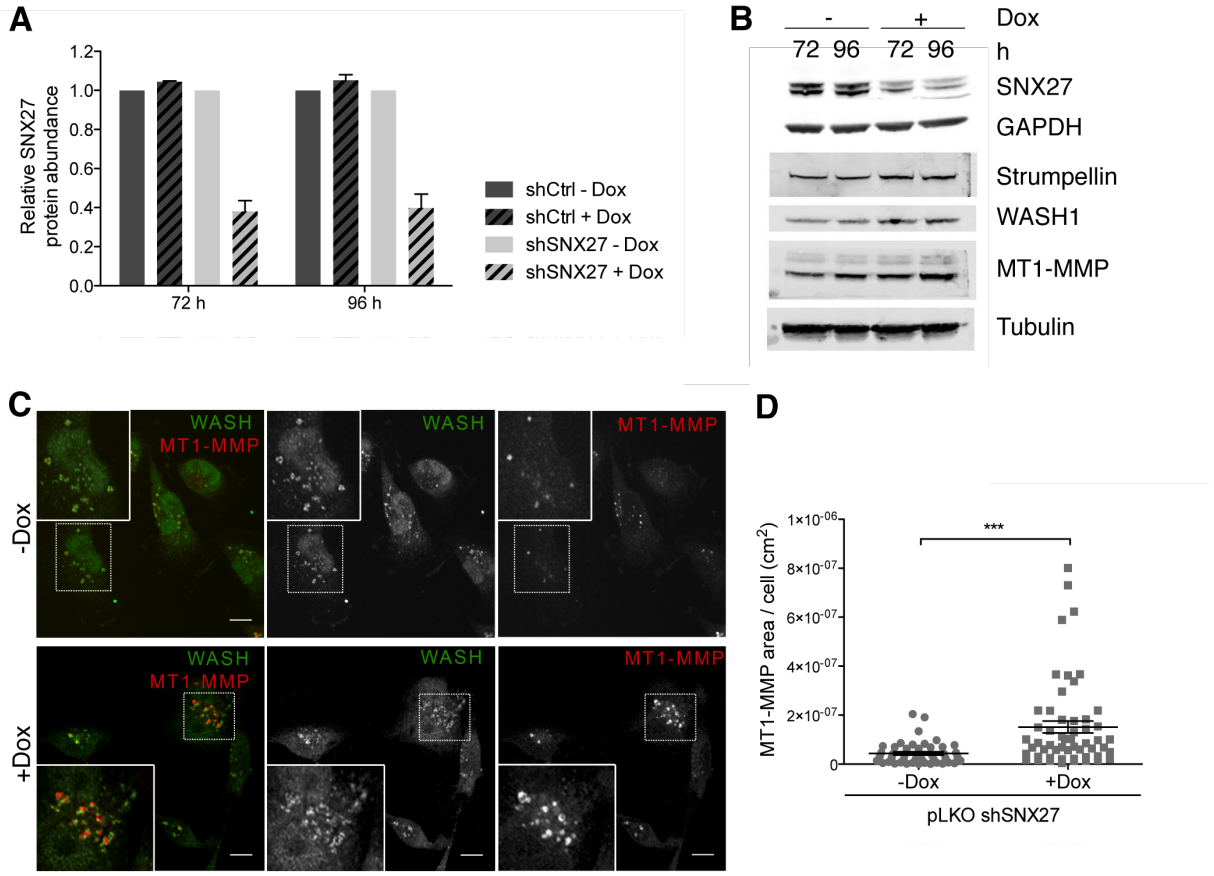

Fig R35. SNX27 silencing alters MT1-MMP morphology at WASH-positive endosomes

For SNX27 silencing, MDA-MB-231 cells stably expressing the pLKO-Tet-on-shSNX27 construct were treated with 1 mg/ml doxycycline (Dox) for 72-96 h to induce shRNA expression. (**A**, **B**) Protein abundance of SNX27 and the indicated proteins in cell lysates was analyzed by western blot using the corresponding antibodies. (A) Quantification showed SNX27 silencing after 72h of Dox treatment (n=2). No differences in SNX27 levels were detected in Dox-treated control cells (shCtrl). (**C**, **D**) Cells were plated on cross-linked gelatin, stained with antibodies for the indicated proteins, and imaged using a confocal microscope; bar: 10μm. Insets show WASH/MT1-MMP-positive endosomes. (D) MT1-MMP-positive area per cell was calculated using ImageJ. Each dot represents an individual cell, data shown as mean ± SEM (t-test,***P<0.001)..

Our studies in 2D invadopodia-forming cells allowed us to examine SNX27 dynamics and localization at these invasive protrusions. Nonetheless, cells in tumors invade into 3D extracellular matrices (ECM). To study SNX27 role during cell invasion in matrix we used circular invasion assays (CIA; see Material and Methods section), which closely mimic 3D invasion while allowing live-cell and immunofluorescence microscopy analyses. Imaging of GFP-SNX27-transfected live cells during invasion into matrigel showed that GFP-SNX27

clustered in small puncta near the tips of invading pseudopods (Video 9, yellow arrows). SNX27-positive vesicles also moved throughout the cell body or were organized in ring-shaped punctuate structures similar to those observed in 2D invadopodia assays (Video 9, blue arrows). Immunostaining of endogenous SNX27 in non-transfected untreated shSNX27 cells confirmed its accumulation at the F-actin-enriched tips of invasive protrusions, where it colocalized with endogenous WASH protein (Fig R36A top, yellow arrows). Anti-MT1-MMP antibody detected poorly the MMP in Matrigel-embedded cells, so its location could not be examined in these assays. Our data nonetheless suggested functional accumulation of SNX27 at the tips of invading pseudopods.

In agreement with previous data, SNX27 knockdown after Dox treatment did not prevent WASH location at endosomes or its localization to invading pseudopods (Fig R36A bottom, yellow arrows). Quantification of the area invaded in CIA nonetheless showed a tendency towards reduced invasion of Dox-treated cells compared to untreated controls (Fig R36B). During CIA, cells invade in a protease-dependent manner and assemble focal adhesions and invadopodia similar to those of Matrigel-embedded cells [359]. To confirm the effect of SNX27 silencing on tumor cell invasion into the ECM, we analyzed MDA-MB-231 cells ability to invade into 3D Matrigel matrices using inverted invasion assays (see Methods). Dox-treated or untreated shSNX27 cells were allowed to invade into Matrigel for 96 h. We calculated the relative invasion area, and showed that it was reduced after SNX27 knockdown (Fig R36C-D). Our data suggested that SNX27 assists WASH functions promoting tumor cell invasion. SNX27 controlled MT1MMP1-positive endosomes morphology, but it did not regulate MT1-MMP protein abundance, indicating that other putative SNX27 cargoes must participate in PM MT1-MMP delivery.

Clustered and aggregated MT1-MMP-positive endosomes are also found in MDA-MB-231 cells after silencing of WASH-associated exocyst complex components [228]. PIP5K-dependent PtdIns(4,5)P_2 production regulates exocyst complex assembly as well as its function promoting integrin trafficking in MDA-MB-231 cells [322]. The PIP5K isoform β bears a PDZ-bm [211], and thus we hypothesized that its binding to SNX27 could control local PtdIns(4,5)P_2 production and assist exocyst function. In collaboration with our colleague Dr. Rosa Ana Lacalle from Dr. Santos Mañes's group (Centro Nacional de Biotecnología-CSIC, Madrid) we tested the ability of SNX27 to bind PIP5Kβ. We used a splice variant of the PIP5Kγ isoform (PIP5Kγi2) as a non-PDZ-binding control. Co-immunoprecipitation analyses of Myc-tagged SNX27 and FLAG-tagged PIP5K expressed in HEK293T cells (see Fig R37A) did not detect Myc-SNX27 interaction with PIP5Kβ (data not shown). Instead, we observed an unpredicted SNX27/PIP5Kγi2 association (Fig R37B). PIP5Kγi2 was nonetheless absent in immunoprecipitates of a Myc-SNX27 that lacks the FERM domain (SNX27-NT) (Fig R37B), which indicates that SNX27 FERM domain is essential for SNX27/PIP5Kγi2 binding. These results were confirmed by testing the interaction between *in vitro*-translated full-length SNX27

(FL) or SNX27-NT proteins and FLAG-PIP5Kγi2 immunoprecipitated from HEK293T lysates (Fig R37C). Moreover, GST pull-down assays indicated direct physical interaction between GST-SNX27 and PIP5Kγi2 purified proteins (Fig R37D).

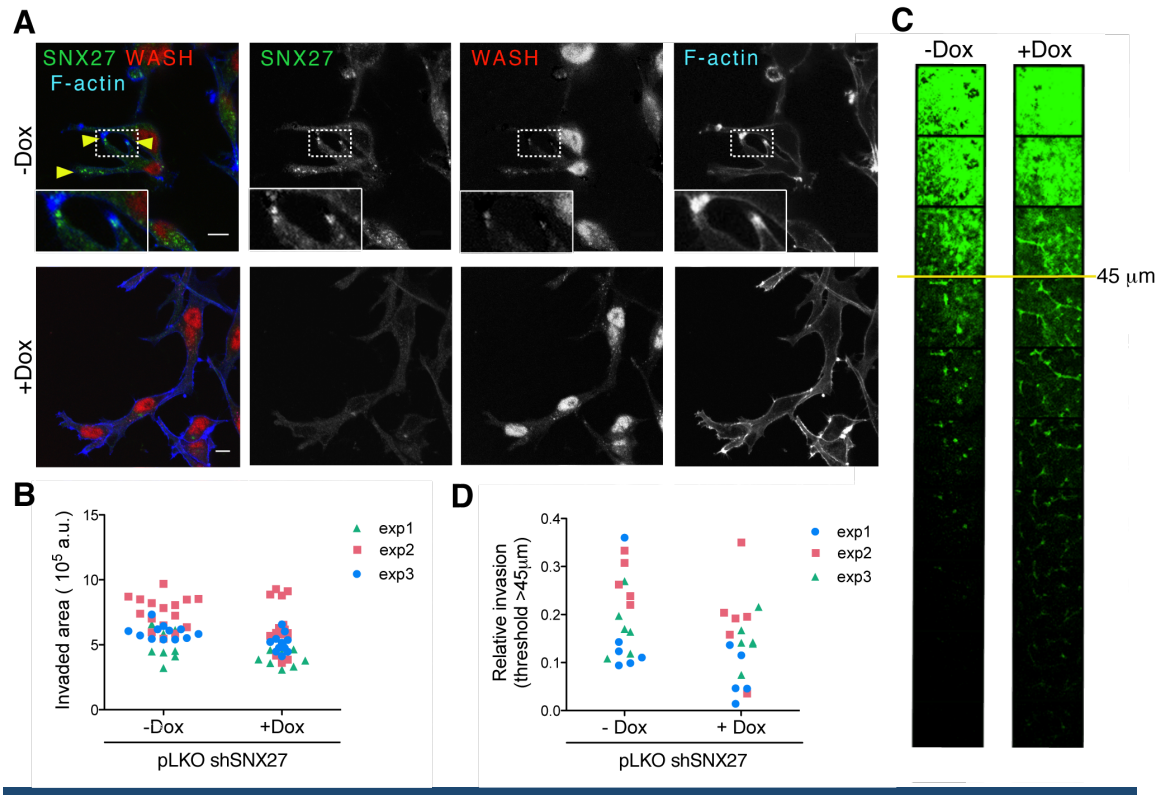

Fig R36. SNX27 silencing affects the invasive capacity of MDA-MB-231 cells

(**A**,**B**) Matrigel circular invassion assays (CIA) were performed (see Methods). Untreated and Dox-treated shSNX27 MDA-MB-231 cells were allowed to invade for 12 h, (A) fixed, and stained for SNX27 and WASH by immunofluorescence. F-actin was detected using fluorescent phalloidin. Insets show SNX27/WASH-positive endosomes localized at actin-puncta within invading pseudopods. Images are from a representative experiment; bar: 10μm. (B) Total invaded area was calculated using ImageJ. Results from three independent experiments are shown on the dot plot. (**C**-**D**) Matrigel inverted invasion assays were performed (see Methods). (C) Untreated and Dox-treated shSNX27 MDA-MB-231 cells were allowed to invade for 96 h, and serial optical sections were captured at 15-μm intervals. Relative invasion was calculated using ImageJ considering cells that invaded 45μm or more. (D) Each dot represents repeated values obtained within an experiment. Results from three independent experiments in duplicate are shown.

PIP5Kγi2 (also termed PIP5Kγ661) compared to other variants has an extended C-terminal region essential for talin interaction (Fig R37B); talin-FERM domain binds PIP5Kγi2 through the same binding site that mediates its NPxY-dependent association with β-integrins (reviewed in [330]). We thus hypothesized that the molecular mechanism for PIP5Kγi2 association with SNX27 FERM domain could be analogous to that with talin-FERM domain. We tested the ability of a SNX27 mutant with impaired NPxY-binding (Myc-SNX27 WA) to co-immunoprecipitate with PIP5Kγi2. SNX27 WA mutation however did not prevent PIP5Kγi2 binding (Fig R37E). Moreover, SNX27 also co-immunoprecipitated with the PIP5Kγ isoform splice variant 1 (PIP5Kγi1) that lacks the talin-binding site (Fig R37F). These data suggested an alternative mechanism for SNX27/PIP5Kγi2 interaction.

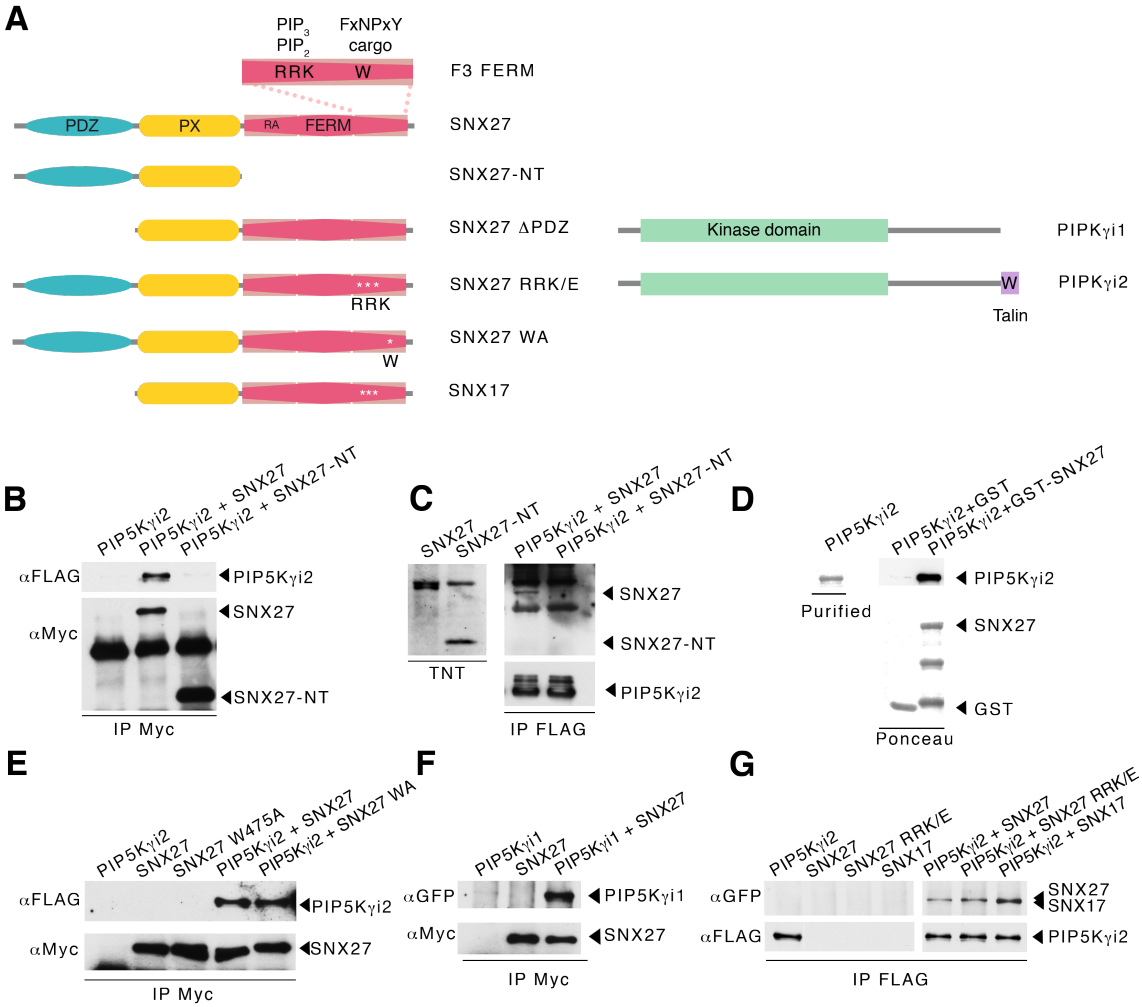

H

	SNX27	SNX27ΔPDZ	SNX27-NT	SNX27 RRK/E	SNX27 W475A	SNX17
PIPKγi1	+					
PIPKγi2	+	+	–	+	+	+
PIPKγi2 KD	+					
PIPKγi2 WF	+					

Fig R37. SNX27 directly binds PIP5Kγ through FERM domain

(**A**) Scheme of proteins used, domains and interaction sites are shown (tags not shown) (**B**,**E-G**) Myc-, FLAG- or GFP-tagged proteins expressed in HEK293 cells were tested for binding by co-immunoprecipitation. Results were analyzed by western blot. (**C**) SNX27 and SNX27-NT proteins were *in vitro*-translated using the TNT system and tested for co-immunoprecipitation with FLAG-PIPKγi2 in a HEK293 cell lysate. (**D**) Physical interaction between the two proteins was confirmed by GST-pull down assay using GST-SNX27 and purified PIPKγi2. (**H**) Summary of the results of immunoprecipitation and pull-down assays.

PIP5Kα interaction with β-arrestin is dependent on PtdIns(4,5)P_2/PtdIns(3,4,5)P_3 recognition through a PtdIns-binding pocket (Arg234, Arg238, and Lys252; RRK residues) [238] analogous to that located at the SNX27 FERM domain [118]. To examine whether SNX27/PIP5Kγi2 interaction is PtdIns-binding dependent, we used the SNX27 RRK/E mutant in our co-immunoprecipitation analyses. RRK/E mutation in SNX27 did not prevent PIP5Kγi2 interaction; indeed, SNX17,

which lacks the PtdIns-binding pocket, also interacted with PIP5Kγi2 (Fig R37G). Our results indicate a unique SNX FERM association to PIP5Kγ that is different from that described for other proteins structurally similar to SNX27, which will require further studies for its characterization. This previously unreported association could be important to control endosomal PtdIns(4,5)P_2 production and couple lipid signaling to intracellular protein trafficking and exocytosis.

Discussion

VI. DISCUSSION

1. ROLE OF SNX27 IN T CELLS

1.1. SNX27 at the immune synapse

1.1.1. FERM domain lipid binding contributes to SNX27 localization

The PtdIns3P-binding PX domain promotes SNX endosomal membrane recruitment (reviewed in [319]). SNX27, SNX17 and SNX31 bear a FERM-like domain that interacts with cargoes containing NPxY/NPxxY motifs [116]. Coordinated binding to phosphoinositides and cargo enhances membrane attachment of many trafficking proteins through the process termed coincidence detection (reviewed in [42]). Ghai *et al*. showed that the contribution of NPxY/NPxxY interactions to endosomal localization is nonetheless different for SNX17 and SNX27. Whereas mutation of the residue that mediates this type of interaction in SNX17 (W321A) profoundly affects its endosomal localization, the analogous mutation in SNX27 (W475A) has no impact on SNX27 localization to vesicles in epithelial-like cells [116]. In accordance, our results in Jurkat T cells showed that, like the WT protein, GFP-SNX27 W475A localized to the ERC and to the T cell-APC contact area, which indicates that binding to the NPxY/NPxxY motif affects neither ERC nor IS recruitment of SNX27.

Ghai *et al*. suggested that the lower sensitivity of SNX27 membrane recruitment to NPxY/NxxY cargo engagement can be explained in part by membrane localization enhanced via PDZ domain interaction with cargoes [116]. The low endosomal association of SNX17 shown here, and the limited vesicle localization of a mutant SNX27 protein lacking the PDZ domain reported previously [270, 271] support this hypothesis. In addition to PDZ-based interactions, PtdIns-binding sites alternative to that at the PX domain can also explain the enhanced membrane affinity of SNX27. In collaboration with Ghai *et al*., we defined a PtdIns-binding site at the SNX27 FERM domain that was absent in SNX17 and SNX31 [118]. This PtdInsP-binding pocket is adjacent to the NPxY/NxxY cargo recognition site [118], which might allosterically regulate FERM domain binding to cargo and to PtdInsP.

Localization analyses in HeLa cells suggested that the FERM-located PtdIns-binding site is not necessary for SNX27 accumulation at the ERC (see [118] in Appendix 4.1). This coincides with results from Tseng *et al*. in the same cell type; they compared SNX27 vesicle-binding ability to that of SNX17 and SNX31, and suggested an additional lipid-binding site in SNX27 that was apparent only in cells treated with the PI3K inhibitor wortmannin, or when the PX domain was mutated [326]. In contrast to the modest effect in untreated HeLa cells, endosomal localization of the SNX27 FERM non-PtdIns-binding mutant was markedly altered in Jurkat cells; poor vesicle association was evident in basal conditions, and this phenotype was more pronounced in Jurkat cells challenged by superantigen-loaded APC. This suggests the need for lipid binding through the FERM domain for correct SNX27 localization during polarized vesicle traffic. The reduced SNX17 vesicle localization in unstimulated Jurkat cells, and its notably enhanced cytosolic localization after stimulation with APC also concur with this hypothesis. The combined results

from both of these cell models leads us to conclude that the additional lipid anchor in SNX27 assists its continuity at the ERC when ERC lipid composition is altered by inhibitor treatment or after transition to an activated state.

Using fluorescent-tagged lipid binding domains, we were able to examine SNX27 partitioning between different membrane domains in APC-stimulated T cells in greater detail. The initial IS recruitment of WT GFP-SNX27 correlated with transient IS location of a PtdIns(3,4,5)P_3-binding probe (Fig D1A); however, the SNX27 FERM mutant did not colocalize with the lipid-binding probe at this stage. To determine whether this initial PM accumulation of the WT GFP-SNX27 originates directly from vesicles or if it is driven by PM lateral movement will require further study. At the mature IS, when the PtdIns(3,4,5)P_3-binding probe localized to peripheral IS, both WT and the FERM mutant SNX27 accumulated normally at the central IS (Fig D1A). These data are in agreement with our current and previous studies showing that PM localization of SNX27 during IS formation is PDZ domain-dependent [270]. The reduced retrieval of the FERM mutant protein into endosomal compartments after IS maturation nonetheless suggests that recognition of bi- and triphosphorylated PtdIns derivatives aids SNX27 transport back to the ERC (see model in Fig D1B). The contribution of this additional lipid-binding site to SNX27 localization thus correlates with its preference for lipid derivatives known to be involved in endocytosis [118].

1.1.2. PDZ ligand binding mediates SNX27 accumulation at the immune synapse

SNX27 does not accumulate at the IS after deletion of its PDZ domain [270], which binds simultaneously to PDZ-bm-containing cargoes and to the retromer component VPS26 [111, 308]. Distinct point mutants prevent SNX27 binding to the retromer or to PDZ-bm; impaired SNX27/retromer association nonetheless affects PDZ ligand binding [111], and the precise contribution of retromer binding to SNX27 IS localization thus could not be determined in these experimental conditions. Our protein localization studies allowed us to demonstrate that SNX27 IS accumulation is mediated through its association to PDZ-bm, as the non-PDZ-bm-binding mutant (H114A) did not accumulate at the T cell-APC contact area. The mutant protein overlapped at the ERC with EEA1, and also with the WT protein when cotransfected; the IS localization defect was thus not a result of mutant protein mislocalization to a different endosome subset, but of a lack of interaction with PDZ ligands.

To identify the SNX27 interactome during IS formation, we performed a proteomic analysis to compare proteins associated to the WT SNX27 and to the point mutant with impaired PDZ-cargo recognition (H114A). This strategy allowed discrimination between PDZ-dependent and -independent SNX27 interactomes. Although it was not anticipated, we detected proteins specifically associated with the mutant form; further studies are needed to determine whether mutation of the PDZ ligand-binding site in SNX27 directly promotes binding to alternative cargoes or is a result of defective mutant localization to the IS.

Analysis of the PDZ-dependent SNX27 interactome identified several proteins with a canonical type I PDZ-bm. Structural studies by Clairfeuille *et al.* recently defined PDZ-bm

subcategories based on amino acid sequences upstream of the PDZ-bm, and predicted their binding affinity to the SNX27 PDZ domain; an acidic residue at the -3 position is essential for association, whereas acidic residues in -5/6 positions enhance interaction affinity. Phosphorylated residues can substitute for acidic amino acids and act as a regulatory switch for SNX27 binding to ligands ([60] see Appendix 4.4). Most proteins in our PDZ-dependent interactome analysis bear an acidic residue at the -3 position (see Table R2), and some have acidic residues in -5/6 positions. None of the proteins identified have Ser or Thr in -5/6 positions, which indicates that they are not subject to PDZ-bm regulatory switching. Our biochemical analyses validated the PDZ-mediated interaction of SNX27 with DGKζ, β-PIX and ZO-2, and showed that these interactions occur in resting cells or cells challenged with SEE-

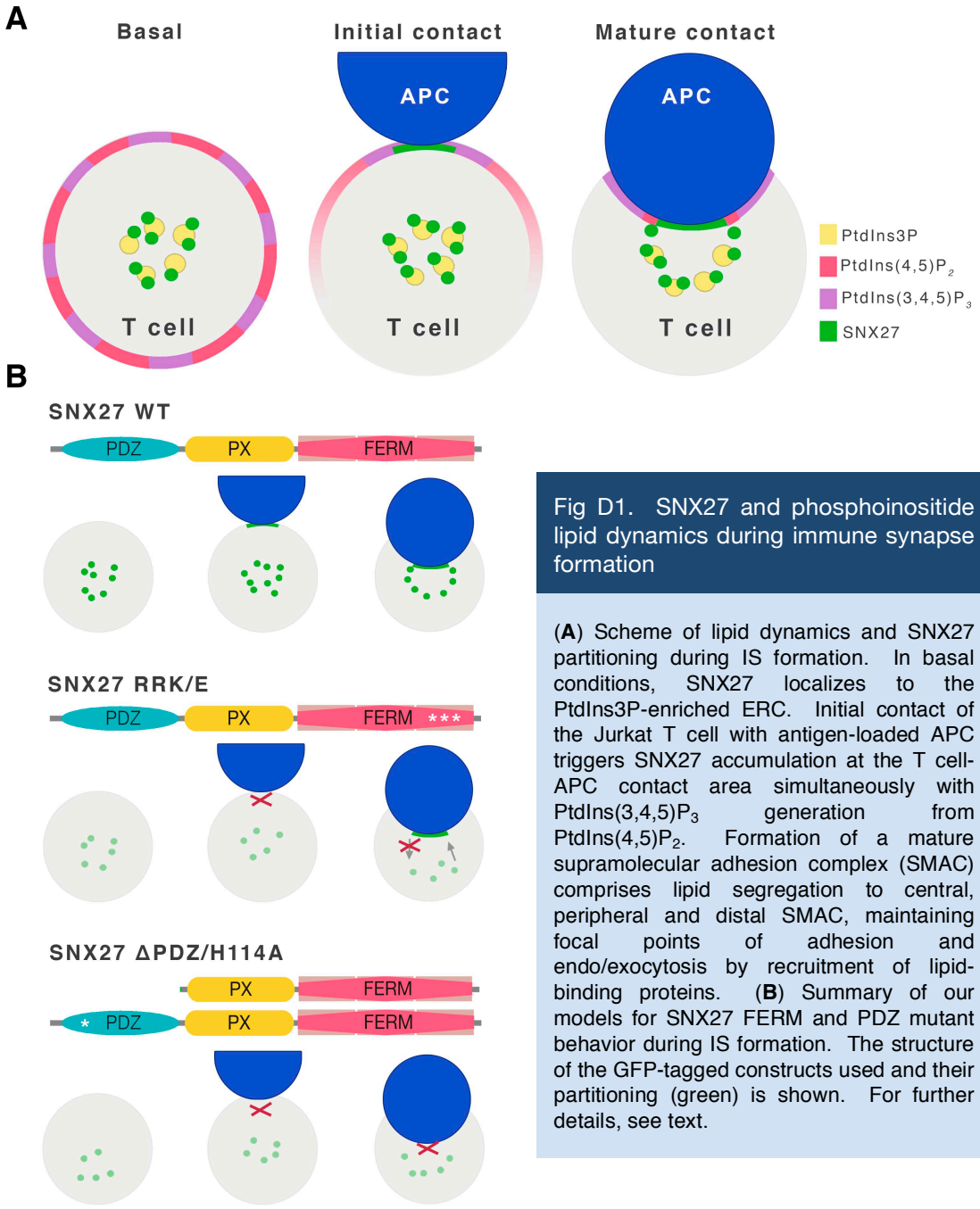

Fig D1. SNX27 and phosphoinositide lipid dynamics during immune synapse formation

(**A**) Scheme of lipid dynamics and SNX27 partitioning during IS formation. In basal conditions, SNX27 localizes to the PtdIns3P-enriched ERC. Initial contact of the Jurkat T cell with antigen-loaded APC triggers SNX27 accumulation at the T cell-APC contact area simultaneously with PtdIns(3,4,5)P_3 generation from PtdIns(4,5)P_2. Formation of a mature supramolecular adhesion complex (SMAC) comprises lipid segregation to central, peripheral and distal SMAC, maintaining focal points of adhesion and endo/exocytosis by recruitment of lipid-binding proteins. (**B**) Summary of our models for SNX27 FERM and PDZ mutant behavior during IS formation. The structure of the GFP-tagged constructs used and their partitioning (green) is shown. For further details, see text.

loaded APC, findings that coincide with the strong constitutive association to SNX27 predicted by Clairfeuille *et al.* [60]. These data suggest that the PDZ-dependent IS localization of SNX27 is not mediated by binding to specific cargoes only in stimulation conditions. Alternatively, IS recruitment of cargoes constitutively bound to SNX27 could drive SNX27 IS localization. Our identification of ZO-2 as an IS component, and the translocation of DGKζ and β-PIX to the synapse [120, 254] support this hypothesis. SNX27 interaction with Kidins220, which is constitutively associated with the TCR [78], and with CENPJ, which forms part of the centrosome that moves to and contacts the PM at the IS [311], could also contribute to PDZ-dependent IS localization.

1.1.3. SNX27 controls ZO-2 dynamic redistribution at the immune synapse

The strict organization of the IS resembles the ordered regulation of cytosolic proteins in the vicinity of transmembrane proteins in polarized epithelial cells. Several cell polarity proteins indeed localize to the IS [201]. The ZO proteins act as scaffolds to facilitate interaction between transmembrane proteins and cytoskeletal components, and are reported to be important in epithelial cell-cell junctions [94]. Identification of ZO-2 as a SNX27 partner in T lymphocytes was therefore not predicted. The presence of cingulin, a ZO-2 interactor in tight junctions, indicated a conserved role for ZO-2 at the IS. Cingulin is a RhoA signaling regulator that links ZO-2 to the actomyosin cytoskeleton [62] and indeed, our immunofluorescence analyses showed ZO-2 at the peripheral/distal SMAC, the site of actin retrograde flow and actomyosin contraction during IS formation [355].

Gap junctions (GJ) mediate direct transfer of small molecules between adjacent cells; ions, metabolites, and second messengers such as Ca^{2+} and $InsP_3$ as well as siRNA are permeable to GJ (reviewed in [74, 90]). This type of junction is observed at the peripheral SMAC [88, 219], where the GJ channel-forming protein connexin 43 (Cx43) mediates bidirectional communication between APC and T cells in murine and human systems [219]. Cx43-associated proteins include ZO-2 and ZO-1 [299] as well as drebrin, which maintains functional Cx43-containing GJ in epithelial cells and astrocytes [37]. A very recent report describes the formation of these supramolecular complexes through non-overlapping binding sites for drebrin and ZO-1 in Cx43 [6]. In Jurkat T cells, ZO-1 (data not shown), ZO-2 and drebrin colocalized at the IS (see model in Fig D2), but Cx43 expression was not detected (not shown). Although Cx43 is the most ubiquitous Cx, 21 Cx genes have been found in humans, with Cx30 and Cx32 also expressed in T cells (reviewed in [237]). Cx30 and Cx32 indeed associate with ZO-2 during mammary epithelial cell differentiation ([316], reviewed in [74]). Further studies are thus needed to assess the details of ZO-2 participation in T cell GJ formation.

To detect antigens, T lymphocytes scan cell surfaces continuously; this results in the formation/disruption of cell-cell contacts that culminate in stable, polarized synapses. We showed that during sequential contact with APC, ZO-2 rapidly relocalized from one cell-cell contact area to a new one, which correlated with localized actin rearrangement. SNX27 and ZO-2 colocalized at endosomal compartments, and FRAP studies demonstrated that SNX27

silencing decreases ZO-2 mobility at the synapse. These studies suggest that SNX27-mediated interaction facilitates dynamic ZO-2 traffic to and from cell-cell contacts (see model in Fig D2), consistent with the reported function of SNX27 [366]. Our observations not only coincide with ZO function in epithelial cells, but also in neuronal dendrites. ZO proteins control the accumulation of adhesive components at filopodia to stabilize the transient interactions between dendrites [172]. ZO localization to regulate dendritic filopodial dynamics is reminiscent of our videomicroscopy observations, and further suggests that ZO proteins could be important in stabilizing cell-cell connections in T cells. Our study thus indicates conservation in the pathways that delimit polarized structures in both nervous and epithelial systems during IS formation.

1.2. SNX27 as an adaptor for WASH-mediated trafficking

WASH mediates actin polymerization on vesicles involved in recycling and exocytosis [77, 124, 249]. During IS formation, the T cell-APC contact zone becomes a focal area for endo- and exocytosis [29]. WASH-positive endosomes polarize to the IS [124], where we showed partial colocalization of SNX27 with WASH and CD63, which suggests SNX27 participation in WASH-mediated polarized secretion after antigen recognition. Whereas the WASH role in T cell protein secretion has not been studied, its function in protein recycling has been addressed; WASH KO in mouse CD4 T cells leads to low cell surface levels of LFA-1 in basal conditions, and of TCR and GLUT1 after activation [256].

SNX27 is widely accepted as an adaptor for WASH-mediated trafficking of PDZ-bm-containing cargo including GLUT1 [308]. In agreement, Jurkat T cells showed decreased GLUT1

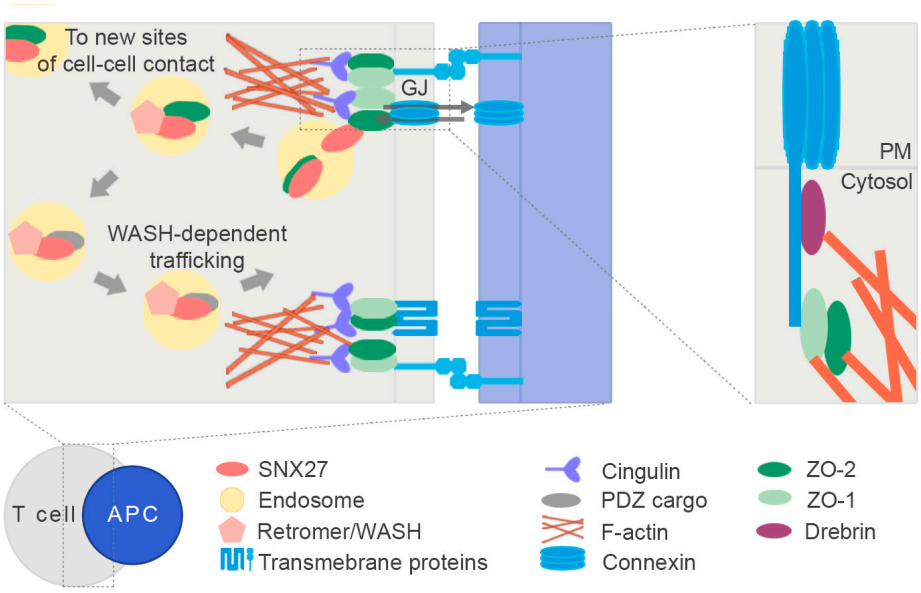

Fig D2. Model for SNX27 role in protein transport at the immune synapse

In T cells, SNX27 acts as an adaptor for WASH-mediated transport mainly for PDZ cargoes, some of which are recruited to the immune synapse (IS) and promote SNX27 accumulation at this site. These include the cell-cell adhesion and communication protein ZO-2, which localizes to actin rearrangement sites where it is subject to SNX27-mediated trafficking. ZO-2 colocalizes with the F-actin-binding protein that regulates actin polymerization at the IS. The complex formed by ZO proteins and drebrin bound to the gap junction (GJ) channel-forming proteins termed connexins could mediate bidirectional communication between antigen-presenting cells (APC) and T cells.

stability after SNX27 silencing. Although the LFA-1 integrin and the TCR do not have a PDZ-bm, the cytoplasmic tails of subunits in both protein complexes have amino acid sequences that potentially bind the SNX FERM domain. The LFA-1 integrin β2 subunit, also termed CD18, bears an NPxF motif (reviewed in [317]), and the TCR complex protein CD3ε has the NPxY consensus sequence. Nevertheless, neither SNX27 silencing in Jurkat T cells, nor its depletion in primary mouse T cells decreased CD3ε cell surface abundance in any conditions, which suggests that the WASH functions that stabilize the TCR at the PM do not require SNX27 interaction. Recent data identified SNX17 as a regulator of TCR and LFA-1 traffic in activated T lymphocytes [246]. SNX17 silencing in Jurkat and human primary T cells decreases surface TCRαβ levels [246], indicating that SNX17 and SNX27 functions are not redundant, and SNX17 has a prominent role controlling TCRαβ recycling.

LFA-1 trafficking in Jurkat cells is affected by SNX17 and SNX27 knockdown. Nonetheless, we showed that SNX27 silencing lowered LFA-1 abundance only after inhibition of protein synthesis, whereas Osborne e*t al.* found reduced LFA-1 levels in untreated, unstimulated SNX17-silenced cells [246]. This coincides with results in other cell types, in which SNX27 depletion has a mild effect on integrin recycling, at difference from the clear integrin-protective function of SNX17 and SNX31 [309, 326]. LFA-1 is essential for T cell-APC conjugate formation [230], and SNX17 knockdown results in fewer conjugates than in controls [246]. SNX27 silencing did not alter conjugate formation, which further supports the prominent role of SNX17 in LFA-1 trafficking. The alteration of TCR levels on the SNX17-silenced cell surface could nonetheless explain the defects reported in antigen-dependent conjugate formation [246].

In primary T cells, our results and those of Osborne e*t al.* showed that SNX17 or SNX27 depletion affects LFA-1 levels, mainly after T cell activation. SNX27 binds preferentially to NPxY phosphorylated at Y_0 [116], and binding of various proteins to integrin β tails is regulated by phosphorylation (reviewed by [186]). While this regulatory mechanism could operate for SNX27 binding to β integrins, the NPxF of β2 integrins is a non-phosphorylatable motif; activation-induced phosphorylation of the binding motif thus does not explain the stimulation-dependent decrease in LFA-1 surface abundance in *Snx27*$^{-/-}$ T cells. A recent study of docking protein 1 (Dok1) binding to CD18 showed that NPxF adjacent phosphorylation sites (Ser745 and Ser756) regulate Dok1/CD18 association [130]. Phorbol esters and CD3 ligation induce CD18 phosphorylation on these Ser residues by activating PKC isoforms α and η [92]. This phosphorylation-based regulatory mechanism could thus operate after T cell activation, leading to conformational changes in the LFA-1 heterodimer that promote SNX-FERM/NPxF motif interaction for SNX17- or SNX27-mediated integrin recycling.

Based on current knowledge, we suggest that SNX27 is specialized and directs PDZ cargoes to the WASH/retromer pathway, while the other SNX-FERM proteins make a larger contribution to NPxY-containing cargo traffic to this transport pathway. This might be explained by the structural differences of SNX FERM domains (detailed in section 1.1), and concurs with

unaltered dynamics of the non-NPxY-binding mutant GFP-SNX27 W475A during IS formation. As SNX17 does not interact with the WASH/retromer transport machinery, however, it must use an indirect mechanism to stabilize integrins and TCR components.

Studies in HeLa cells indicate that TfR recycling needs WASH function [77], but not that of SNX27 [308]. We identified the TfR in the PDZ-independent SNX27 interactome, and showed that SNX27 silencing results in a marked decrease in total and cell surface TfR levels in Jurkat cells. At difference from the SNX27 PDZ partner GLUT1, TfR abundance was not further reduced after protein synthesis inhibition. These data coincide with the HeLa cells studies and indicate that, in T lymphocytes, SNX27 controls TfR expression via a mechanism that differs from that of the conventional recycling pathway of PDZ cargoes. Our analysis of *Snx27*$^{-/-}$ primary mouse T cells, which showed decreased TfR expression after TCR triggering, helped to explain Jurkat data and will be discussed (section 1.3.2).

1.3. SNX27 modulates lipid and metabolic signaling pathways

SNX27 PDZ and FERM-like domains are known scaffolds for signaling complexes. The RA domain in the SNX27 FERM-like domain associates with H-Ras [117] and K-Ras [196]. The SNX27 PDZ domain binds CASP, which regulates signaling through the Arf family of small GTPases [209], as well as Kidins220 [308], a scaffold that promotes ERK signaling [10, 78, 100]. Our proteomic analysis confirmed SNX27 PDZ association to additional scaffolds and signaling complexes such as ZO-2 [366] and the PIX/GIT complex [328]. Furthermore, our laboratory identified SNX27 PDZ domain association to DGKζ and suggested that SNX27 also participates in DAG-dependent signaling pathways [270, 271].

1.3.1. DGKζ/SNX27 association regulates DAG signaling in T cells

SNX27-mediated regulation of PKC activity

DGKζ has a central role in the control of DAG signaling after T cell activation (reviewed in [220]), and we demonstrated that this contribution is strictly dependent on SNX27 interaction. SNX27 showed strong constitutive interaction with DGKζ, and SNX27 silencing affected DGKζ protein stability in Jurkat cells. The SNX27 contribution to DGKζ stability nonetheless differed from its function in stabilizing transmembrane PDZ cargoes such as GLUT1 and Kidins220, which use SNX27-mediated transport to recycle after internalization [308]. In T cells, SNX27 silencing potentiates DGKζ degradation in a PKC-dependent manner, similar to that described in neurons [244].

DGKζ and PKCα are subject to reciprocal regulation; DGKζ-mediated DAG consumption limits PKCα function, whereas PKCα-dependent DGKζ phosphorylation at the MARCKS domain disrupts PKCα/DGKζ association [203, 204, 323]. At neuronal synapses, the PDZ-containing scaffold protein PSD-95 (postsynaptic density protein 95) enables this regulatory mechanism in basal conditions [183]. In neuromuscular junctions, the PDZ proteins syntrophins facilitate PKC-dependent localization of DGKζ to junctions [1]. In T cells, where reciprocal PKCα/DGKζ modulation also occurs [119], SNX27 acts an endosomal scaffold for DGKζ to control basal PKC

activity. Disruption of SNX27/DGKζ association leads to PKC hyperactivation and subsequent DGKζ-MARCKS domain phosphorylation and degradation (Fig D3, left).

Analysis of DGKζ in endogenous SNX27 and GFP-SNX27 immunoprecipitates showed both long and short alternative splicing DGKζ isoforms, which concurs with their common C-terminal domain [81]. Decreased DGKζ protein abundance after SNX27 silencing was nonetheless more apparent for the long isoform, which has an extended N-terminal region that bears several Akt phosphorylation consensus sequences (R-X-R-X-X-S/T). Whether the two DGKζ isoforms have distinct regulatory mechanisms and functions in the immune system remains to be determined. Based on experimental data in the Phosphosite repository [146] (Phosphosite, acc. nº Q13574), these sites can be phosphorylated in Jurkat cells. These post-translational modifications could also contribute to the protein stability changes observed after SNX27 silencing.

The reciprocal PKC/DGKζ regulatory mechanism is PKCα-specific [203, 204, 323]. PKCα bears a C-terminal PDZ-bm [306] that, although it is not predicted to bind SNX27 ([60] see Appendix 4.4), is needed for the abovementioned PSD-95 scaffolding functions [183]. We thus hypothesized that the effects of SNX27 silencing on DAG signaling pathways are PKCα-dependent. In agreement, after inhibition of classic PKC, TCR-triggered AP-1 promoter activity and CD69 upregulation in SXN27-silenced cells were similar to controls.

Novel PKC, including PKCθ, are also regulated by the DAG produced after TCR triggering [80]. PKCθ is the main PKC isoform that operates downstream of CD28 (reviewed in [157]) and interacts with PDK-1 to promote NF-κB activation [250]. Data from our laboratory showed that DGKζ silencing enhanced PKCθ membrane stability and promoted PDK-1 scaffolding functions; DGKζ therefore not only limits DAG signaling, but also its crosstalk with PtdIns(3,4,5)P_3 pathways downstream of TCR triggering and costimulation (Avila-Flores *et al.*, unpublished data). When SNX27-silenced cells were co-stimulated, the enhanced NF-κB and AP-1 promoter activity and high CD69 expression were reduced only in part by inhibition of classical PKC, suggesting the participation of additional DAG effectors. Further studies are needed to determine whether enhanced PKCθ activity mediates the effects observed in SNX27-silenced cells after CD3/CD28 costimulation.

We found a minor fraction of DGKζ associated with endogenous SNX27 (data not shown), and SNX27 silencing led to only a 20% decrease in DGKζ total protein abundance. The hyperactive phenotype of SNX27-silenced cells nonetheless mimicked that of DGKζ-silenced cells, which suggests that the DGKζ fraction that remains after SNX27 silencing does not control DAG-dependent pathways. Although additional studies are needed to assess this question, PKC-mediated DGKζ phosphorylation and inactivation would explain these data in agreement with the model proposed by Luo *et al.* [203, 204]. SNX27 silencing might also lead to DGKζ mislocalization to subcellular compartments where it is not functional. Fractionation experiments or immunofluorescence analyses with antibodies that detect endogenous DGKζ would be needed to determine its subcellular localization in the absence of SNX27.

The effects of silencing SNX27 and DGKζ on CD69 upregulation and NF-κB activity were not enhanced in double-silenced T cells, which supports the hypothesis that SNX27 controls DAG signaling through DGKζ interaction. SNX27 nonetheless has other putative PDZ cargoes also related to DAG and PtdIns(3,4,5)P_3 signaling pathways such as the PH domain and leucine-rich repeat protein phosphatase (PHLPP). PHLPP suppresses lipid second messenger signaling directly by dephosphorylating and inactivating Akt, PKC, and S6K at their hydrophobic phosphorylation motifs (reviewed in [240]). The role of PHLPP in immune cells has only been addressed in regulatory T cells, where it limits Akt activity [251]. PHLPP1 and PHLPP2 PDZ ligands bind SNX27 *in vitro* ([60] see Appendix 4.4), and SNX27/PHLPP interaction was observed in proteomics analyses [304]. Although PHLPP2 was not identified in our interactome analysis, preliminary data from our laboratory confirmed PDZ-dependent SNX27/PHLPP2 association in Jurkat T cells (not shown). Further studies are needed to determine whether this interaction contributes to signaling downstream of TCR triggering and CD28 costimulation.

SNX27-mediated regulation of RasGRP

DAG generation after TCR triggering controls the Ras/ERK/AP-1 pathway by promoting PKC activity [119, 274] and also through direct RasGRP1 binding [86]. Inhibition of classic PKC in SXN27-silenced cells reduced in part AP-1 transcription, whereas MEK inhibition decreased AP-1 activity to a similar level in both SNX27-silenced and control cells. These data suggest that SNX27 silencing leads to TCR-triggered hyperactivation of the Ras/ERK/AP-1 pathway both through direct and PKC-mediated RasGRP1 regulation. This coincides with data in DGKζ-silenced T cells [119, 274], and correlates with studies in non-T cells that reported DGKζ interaction

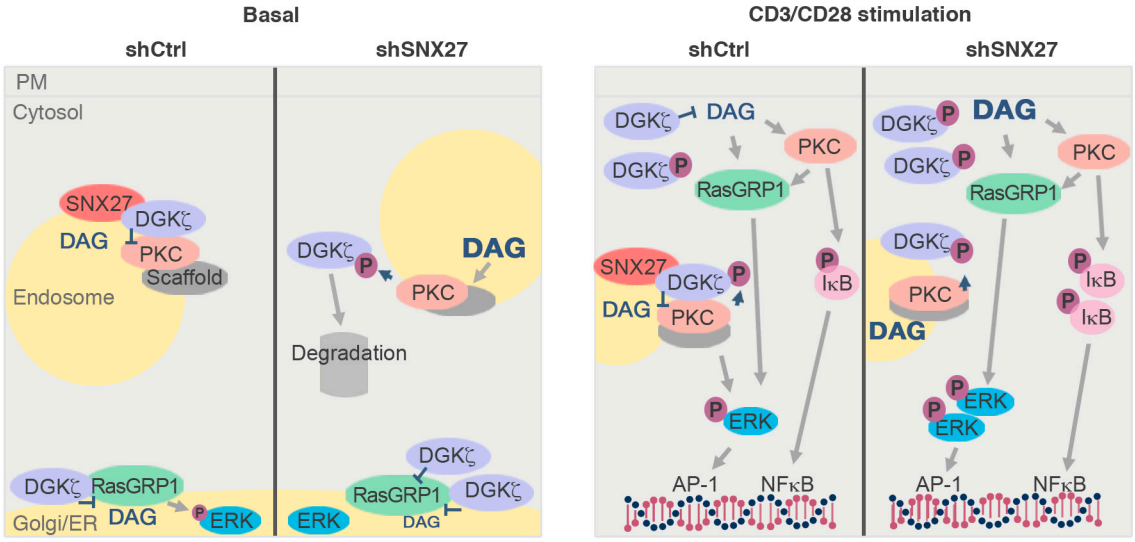

Fig D3. Model for SNX27 role as a scaffold for lipid signaling

In T cells, SNX27 is an endosomal PDZ scaffold for DGKζ-mediated control of DAG effectors activation. SNX27 allows DGKζ/PKCα reciprocal regulation, and thus SNX27 silencing leads to PKC hyperactivation and subsequent DGKζ-MARCKS domain phosphorylation and degradation. SNX27 silencing in (right) stimulated T cells leads to both PKC and RasGRP1/ERK pathways hyperactivation; in contrast, SNX27 silencing in (left) basal conditions prevents DGKζ-mediated PKC modulation while it promotes DGKζ stabilization in the RasGRP1 signaling complex.

not only with PKCα [203], but also with RasGRP1 [324]. This dual role of DGKζ and the hypothesized function for SNX27 as a constitutive scaffold for DGKζ, concur with a model where SNX27 silencing would eliminate the DGKζ-mediated restriction for DAG access to PKC and RasGRP1. Increasing evidence indeed supports the relevance of the spatial control of Ras activation (reviewed in [164]).

Biochemical analyses confirmed that fold induction of ERK phosphorylation after CD3- (data not shown) and CD3/CD28-triggering relative to unstimulated cells was higher in SNX27-silenced cells than in controls. Nonetheless, basal ERK activation, at difference of that observed upon DGKζ silencing [119], was lower in SNX27-silenced cells compared to controls. Basal Ras activity in unstimulated T cells, referred to as constitutive or tonic signaling, is the consequence of RasGRP1 activity; RasGRP1 facilitates SOS (son of sevenless)/RasGTP priming that is further activated upon TCR triggering in a tyrosine kinase-dependent manner [275]. As DGKζ also acts as a negative regulator of basal RasGRP1/ERK activation [275], our data suggest a role for SNX27 coupling tonic PKC and Ras activation in endosomes. On the one hand, SNX27 could scaffold DGKζ association with PKC and not with RasGRP in basal conditions; SNX27 silencing would thus prevent DGKζ-mediated PKC signaling modulation, while promoting DGKζ stabilization in the RasGRP signaling complex (Fig D3, right). On the other hand, SNX27 scaffolding functions for Ras proteins [117, 196] might contribute to PKC/Ras signal transduction in unstimulated T cells.

Both hypotheses could explain low constitutive ERK activation after SNX27 dowmodulation; however, there are results inconsistent with a putative low basal RasGRP1 activation. Several studies indicate that DAG/RasGRP1 tonic signals control TCR expression [212, 274], and we found significant upregulation of TCR surface abundance in SNX27-silenced Jurkat cells compared to controls. Moreover, constitutive RasGRP1 activity controls mTOR-dependent CD44 expression, and *Rasgrp1*$^{-/-}$ mice show low CD44 levels in DP and SP thymocytes [67]; in contrast, although we showed low CD44 induction linked to defective mTOR triggering in activated *Snx27*$^{-/-}$ T cells (see section 1.3.2), *Snx27*$^{-/-}$ thymocytes had normal CD44 surface abundance. Further studies are thus needed to confirm whether SNX27 downmodulation or depletion results in low RasGRP1 activation as well as to elucidate the molecular details that facilitate SNX27 control of the Ras/ERK axis under different stimulation conditions.

1.3.2. SNX27 silencing or depletion in T cells affects mTOR activation

mTOR is a major regulator of T cell metabolism whose activation promotes high expression of nutrient receptors and transporters to support cell growth (reviewed in [33, 338]). In this study we demonstrated SNX27 contribution to full mTOR activation in T cells. TfR upregulation in *Snx27*$^{-/-}$ activated T cells was reduced compared to controls, and our results in Jurkat T cells suggested that this was not due to defective TfR recycling. *Snx27*$^{-/-}$ activated T cells and SNX27-silenced Jurkat cells (data not shown) were smaller than controls, and biochemical analyses of both SNX27-silenced Jurkat and primary *Snx27*$^{-/-}$ activated T cells confirmed

defective mTOR activation following TCR/CD28 costimulation. Furthermore, we found that T cell size after TCR triggering and costimulation not only correlates with mTOR activity [259], but also with CD44 cell surface abundance, which is an mTOR activity reporter in naïve T cells [147]. In accordance, we showed low surface levels of CD44 in *Snx27*$^{-/-}$ activated T cells. CD44 levels were not monitored in Jurkat T cells due to lack of expression of this protein.

mTOR is a nutrient sensor activated by amino acids and glucose, and also by lipids necessary for membrane biosynthesis during cell growth. PA is a central metabolite for membrane phospholipids synthesis and participates in mTOR signaling ([12, 324, 357], reviewed in [107]). Data in T cells lacking DGKα and DGKζ, however, suggest an inhibitory role for DGK activity on mTOR signaling [126] (Avila-Flores *et al.*, unpublished data). Our data indicate that, contrary to DGK silencing, abnormal control of DAG/PA production as a result of DGKζ malfunction or mislocalization in SNX27-silenced and -depleted T cells could lead to impaired mTOR activation.

SNX27 binding to other cargoes could nonetheless explain the defects in TCR-mediated mTOR activation. Amino acid and glucose uptake contribute to mTOR activation in T lymphocytes (reviewed in [258]). On the one hand, GLUT1 is the major glucose transporter in T cells (reviewed in [248]), where its deficiency impairs sustained mTORC1 signaling and efficient upregulation of TfR and CD98 expression [208]. On the other hand, TCR triggering induces leucine uptake via a System L amino-acid transporter that is composed of CD98 and SLC1A5 (also termed ASCT2) [298], which is needed for mTORC1 activation in naïve T cells after TCR/CD28 costimulation [235]. SNX27 regulated GLUT1 levels in Jurkat T cells and, although we did not monitor CD98 cell surface expression, SLC1A5 also bears a PDZ-bm at the C-terminus and is a putative SNX27 cargo [308]. These data indicate that SNX27-mediated trafficking of GLUT1 facilitates mTOR signaling in T lymphocytes, and suggest that SNX27-dependent regulation of the amino acid transporter levels, directly through SLC1A5 recycling, or indirectly by the control of GLUT1 levels, could also contribute to mTOR activation after TCR triggering.

Irrespective of the identity of cargoes involved, our studies strongly indicate defective mTOR activation after SNX27 downmodulation or depletion. Additional data supporting this hypothesis come from studies in mice; low or null expression of the proteins that participate in the mTOR signaling pathway results in small animals with reduced organ size (reviewed in [353]), and *Snx27*$^{-/-}$ mice are indeed smaller than controls [40, 51]. Nevertheless, while we observed decreased spleen cellularity in *Snx27*$^{-/-}$ animals compared to controls, thymus and lymph node (LN) cellularity were unaltered. Normal thymus and LN cellularity concur with no gross defects in T cell development; however, if we considered their relative size to that of the animal, their cellularity would be proportionally higher in *Snx27*$^{-/-}$ mice than in controls. LN cellularity data could be variable due to the laborious process for their extraction from small mice. Further analyses are required to rule out *Snx27*$^{-/-}$ mice alterations in LN cellularity determinants such as lymphocyte homing (reviewed in [337]). Thymic size and thymopoiesis capacity are determined by

thymic niche availability and by T cell progenitor dosage, which depends on cell proliferation and apoptosis during development and thymic involution (reviewed in [129]). Although additional studies are needed, the increase in *Snx27*$^{-/-}$ DN4 progenitors suggests enhanced thymocyte proliferation at the DN4 stage, which could contribute to maintain a normal-sized thymus.

Defects in cell growth seem to counteract cell proliferation; cell growth and cell cycle progression are nonetheless distinct processes in mammalian cells [101]. In T lymphocytes, mTOR promotes cell cycle progression but is not strictly necessary for proliferation (reviewed in [56]). *Snx27*$^{-/-}$ cells, with a clear defect in cell growth, were indeed able to proliferate normally. SNX27 binding to cargoes with diverse functions might account for the opposed effects of SNX27 depletion on T cell activation; while downregulation of mTOR signaling-related cargoes explains growth defects, proliferation and CD69 expression data concur with a defective DGKζ function [365]. These effects might compensate for each other and, depending of each cell type demands, become more apparent in primary mouse T cells or Jurkat cells. Whereas small cell size was observed in primary cells only after activation, when they have high metabolic demands, it was reproduced in the human leukemic cell line Jurkat (data not shown). This correlates with the elevated basal activation of PI3K-dependent pathways in Jurkat cells, which lack the PtdIns(3,4,5)P_3 phosphatase PTEN (phosphatase and tensin homolog) [290] and whose growth is also PI3K/Akt axis-dependent [349]. Cell growth defects in this cell line did not impair the positive outcome of DAG signaling hyperactivation after TCR triggering; however, severe growth limitations in *Snx27*$^{-/-}$ T cells could result in alterations in T cell differentiation and expansion of effector populations and must be preventing further effects on CD69 upregulation and cell proliferation.

2. ROLE OF SNX27 IN CANCER CELL INVASION

The WASH and exocyst complexes have an important role during tumor cell invasion; they coordinate to allow the formation of late endosomes-to-PM connections that facilitate focal delivery of invasion-related proteins to the ECM [228]. WASH-dependent actin polymerization generates the forces required to form these endosomal membrane extensions [76, 77, 125], while the exocyst assists membrane tethering and promotes vesicle fusion through SNARE complex regulation (reviewed in [140]). In MDA-MB-231 cells, the WASH/exocyst association regulates MT1-MMP exocytosis at invadopodia [228]. Our studies, carried out in these cells during invasion into 2D and 3D matrices, indicated a dynamic localization of SNX27 at these structures that correlated with actin cytoskeleton rearrangements. We demonstrated consistent colocalization of SNX27 with WASH at MT1-MMP-positive endosomes, which showed altered morphology after SNX27 silencing. These data, and the tendency of SNX27-silenced cells towards reduced invasion in 2D and 3D assays, suggest the participation of SNX27 in the regulation of WASH-dependent transport during cancer cell invasion.

SNX27 acts as a WASH adaptor for PDZ-binding cargoes including the GLUT1 and the monocarboxylate transporter (MCT1) [308], which have been associated with cancer cell

invasion [105, 158]. Nevertheless, most reports on SNX27 PDZ cargoes in cancer cells indicate their contribution to cell growth and chemoresistance; MRP4 [139] is an ATP-binding cassette (ABC) transporter that promotes tumor drug resistance [102], and alterations in GLUT1, MCT1 or SLC1A5 expression are linked to the metabolic reprogramming in tumors that supports cell growth (reviewed in [27, 133]). The so termed "Warburg effect" and "glutamine addition" in tumor cells are indeed proved targets for cancer treatment (for more information see [27, 52, 133]). SNX27 downmodulation in highly metastatic cells, like in primary activated T cells, could thus affect metabolic signaling pathways activation and interfere with cell growth, which provides a reason for further studies.

Metabolic defects can contribute to reduce tumor cell invasion [134]. Aggressive tumor cell lines like MDA-MB-231 are nonetheless resistant to metabolic signaling pathways inhibition [194], which suggests that alterations in other signaling or trafficking pathways reduce the invasion of SNX27-silenced cells. We found morphological changes in WASH/MT1-MMP-positive structures after SNX27 silencing, indicating its participation in MT1-MMP trafficking. This concurs with results from Steinberg *et al.* in HeLa cells; they found MT1-MMP in SNX27 interactome, and showed increased MT1-MMP surface abundance in SNX27-silenced cells, which they proposed was caused by unbalanced sorting processes [308]. SNX27 PDZ is not predicted to bind MT1-MMP C-terminus (RSLLDKV) ([60]; see Appendix 4.4), and thus it is unlikely that SNX27 acts as a direct adaptor for MT1-MMP/WASH complex association. Alternatively, SNX27 might bind to regulatory proteins that control WASH-mediated MT1-MMP transport during invasion.

WASH-associated machinery not only facilitates MT1-MMP delivery to invadopodia, the exocyst is presented as a regulatory complex that restricts and prevents excessive diffusion of MT1-MMP to ensure its efficient focal delivery; direct interaction between WASH and the exocyst components Exo84 and Sec3 negatively controls WASH functions [228]. Our finding that SNX27 interacts with PIP5Kγ, a known exocyst regulator [322], suggests a role for SNX27 facilitating lipid-mediated control of the WASH/exocyst complex. As the PA produced by DGKζ regulates PIP5K activity [205], the respective binding of PIP5K and DGKζ to SNX27 FERM and PDZ domains would add another level of complexity to this regulatory mechanism (Fig D4). Nevertheless, we cannot rule out the contribution of other PDZ interactions, some components of the exocyst complex including the Exo70 and the WASH-interacting subunit Exo84 were detected in SNX27 interactome analyses and bear a PDZ-bm predicted to bind SNX27 ([60, 308]).

Additional experiments are required to confirm the formation of these multiprotein complexes in invasive tumor cells and to define their molecular details. We nonetheless hypothesize that SNX27 scaffolding functions ensure a correct activation of exocyst and WASH complexes through the modulation of endosomal lipid composition. This model is in agreement with our results and those from Steinberg *et al.* [308] that suggest that SNX27 silencing leads to unbalanced MT1-MMP trafficking, but does not impair MT1-MMP delivery.

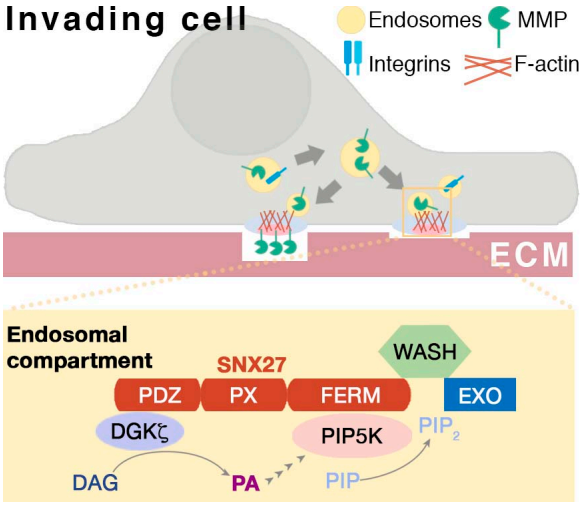

Fig D4. Model for SNX27 role as a scaffold for lipid signaling in invasive cells

The WASH-associated exocyst complex (EXO) regulates MT1-MMP focal delivery to invadopodia. PIP5Kγ regulates exocyst function through PtdIns(4,5)P_2 (PIP_2) production. SNX27 interacts with PIP5Kγ and with DGKζ, which generates the phosphatidic acid (PA) that regulates PIP5K activity. Respective binding of PIP5K and DGKζ to SNX27 FERM and PDZ domains suggests a lipid-based regulatory mechanism to control protein trafficking to invadopodia.

The assays used in this study examine the MMP-dependent invasion capacity of MDA-MB-231 cells [359]. WASH-dependent integrin recycling contributes to enhance this capacity [360], and exocyst regulation by PIP5K controls integrin recycling in this cell type [322]. SNX27 and WASH colocalized in α5 integrin-positive endosomes adjacent to focal adhesions when MDA-MB-231 cells were plated on fibronectin, with a localization pattern similar to that shown in MT1-MMP-positive structures (data not shown). Although additional studies are needed, SNX27 could thus participate in the formation of this type of structures irrespectively of vesicle content, which varies depending on cell requirements during a particular physiological process.

3. SNX27: A HUB FOR ENDOSOMAL SIGNALING AND PROTEIN TRANSPORT IN POLARIZED CELLS

In this study, we aimed to determine the role of SNX27 in two polarized cell models, activated T cells and invasive tumor cells. Our data suggest that whereas the well-known function of SNX27 in the recycling of nutrient receptors and transporters is crucial for primary T cell growth, there is a major contribution of SNX27 role as a cytoskeleton regulator and lipid signaling scaffold during IS and invadopodia formation. We hypothesize that SNX27 acts as an endosomal hub to assist local lipid modulation in both cell models. In T cells, where DAG-regulated pathways are crucial to delimit cell functions (reviewed in [220]), SNX27 controls DAG signals through DGKζ binding. In cancer cells, where PA production regulates membrane remodeling [176, 205, 352], SNX27 binding to DGKζ and PIP5K could contribute to the formation of invasive structures. Both at the IS and at the invadopodium, lipid modulation is linked to cytoskeletal remodeling (reviewed in [345]). DGKζ could couple lipid signaling to actin reorganization through PIP5K activity modulation [272], and through Rac1 and RhoA regulation [2, 9].

DGKζ and PIP5K expression augment in several types of metastatic cancer [39, 315]. Although SNX27 expression has not been studied, its chromosome localization (1q21.3) in humans is frequently amplified in different types of invasive cancer (reviewed in [55, 229]). This coincides with data from bioinformatics resources such as the cBioPortal for Cancer Genomics [49, 113] (see Appendix 1). Other genes within 1q21 amplicon have been associated with poor prognosis [207, 361], enhanced SNX27 expression could contribute to promote oncogenic traits in tumor cells.

In contrast to SNX27 amplification in cancer cells, diminished expression and/or mutation of SNX27 and its interactors are linked to neurodegenerative diseases (Table D1). Emerging evidence indicates that sufferers of a neurodegenerative disorder have reduced incidence for most cancers [152]. Our studies in tumor cells thus help to illustrate how the alteration of a molecular pathway linked to neurodegenerative diseases could exert a protective role against cancer development.

Our proteomic study in T cells identified SNX27 interactors linked to neurological diseases (Table D1), which suggests close analogy between neurological function and immune system regulation. Moreover, the hypothesized scaffolding role of SNX27 for local lipid signaling modulation in T cells is reminiscent of that reported for other PDZ-containing proteins in neurons; DGKζ localizes to neuronal synapses through direct interaction with PSD-95, and regulates dendritic spine maintenance by promoting DAG-to-PA conversion downstream of NMDAR activation (for more information see [170, 183, 288]). These receptors are known SNX27 cargoes [40, 342], and thus the molecular organization of these proteins in SNX27-positive endosomes could be similar to that found at the synaptic PM. Studies of SNX27 at the neuronal synapse have been mainly focused on SNX27 role in the recycling of PDZ-interacting receptors [40, 150, 162, 196, 342]. Our data indicate that SNX27 could integrate sorting events with lipid signaling to control signal transduction of these receptors. Furthermore, NMDAR trafficking and surface abundance is controlled by PKC activation [54], which suggest participation of SNX27 in this feedback mechanism that ensures receptor availability at the cell surface. In addition to NMDAR signal transduction, DGKζ modulation of the DAG/PKC pathway is involved in GPCR signal transduction [72, 239, 241, 281], and thus DGKζ deregulation in *Snx27*$^{-/-}$ mice might account for some of the observed effects in PTHR signaling hyperactivation [51].

This study broadens our knowledge of the SNX27 function in T lymphocytes and invasive tumor cells, and suggests that our findings on SNX27-mediated coordination of lipid signaling with polarized vesicular trafficking and cytoskeletal dynamics could be extrapolated to other models of intense polarized trafficking.

Protein names	Neurological disorders	References
SNX27	Down syndrome, Alzheimer disease, myoclonic epilepsy	70, 341, 342
VPS26	Alzheimer disease	301
VPS35	Alzheimer disease, Parkinson disease	200, 301, 335
SWIP	Intellectual disability	276
RME-8	Parkinson disease	334
Strumpellin	Hereditary spastic paraplegia	329
USP7	Intellectual disability and autism spectrum disorder	135
CENPJ	Primary microcephaly, Seckel syndrome	31, 218
XPR1	Primary familial brain calcification	187
Kidins220	Alzheimer disease	198

Table D1. Proteins found in SNX27 interactome associated with neurological disorders

Conclusions
Conclusiones

VII. CONCLUSIONS

1. The SNX27 FERM domain recognizes membrane phosphoinositides. FERM domain lipid recognition mediates early SNX27 translocation to the immune synapse (IS) and enhances its recruitment to the endocytic recycling compartment during IS formation, but is nonetheless dispensable for SNX27 recruitment to the mature IS of Jurkat T cells.

2. PDZ ligand recognition is necessary for SNX27 accumulation at the IS, which suggests that cargoes recruited to the IS could contribute to this localization. Proteomic analysis of PDZ-interacting cargoes identified the cell-cell junction protein ZO-2 as a SNX27 partner during IS formation. ZO-2 localizes to the actin cytoskeleton rearrangement sites at the peripheral IS of Jurkat T cells, where its dynamics are regulated by SNX27/ZO-2 interaction.

3. The constitutive interaction of DGKζ with SNX27 facilitates DGKζ-dependent regulation of DAG-based signals both in basal and stimulating conditions. SXN27 silencing reduced DGKζ protein levels as a result of PKC activation in basal conditions; after TCR triggering, enhanced activation of classical PKC promoted Ras/ERK/AP-1 hyperactivation. Co-stimulation further augmented Ras/ERK/AP-1 signals and enhanced NF-κB activation in SNX27-silenced cells, which suggests participation of additional DAG effectors.

4. *Snx27* deletion in mice does not grossly alter T cell development. Activation-induced CD69 expression was normal in *Snx27*$^{-/-}$ primary mouse T cells and their proliferation was not substantially altered. *Snx27*$^{-/-}$ T cells nonetheless showed growth defects and lower CD44 surface abundance compared to controls. This correlated with a decrease in CD71 levels and in mTOR activation after TCR triggering, which was also apparent in SNX27-silenced Jurkat T cells.

5. SNX27 interacts with the retromer/WASH complex in Jurkat T cells. WASH localizes to CD63-positive endosomes and colocalizes with endosomal SNX27 at the IS. SNX27 acts in part as an adaptor for WASH-mediated transport in T cells; it is essential for the recycling of its PDZ cargo GLUT1, and participates in maintaining cell surface LFA-1 levels in Jurkat cells and in activated mouse T cells. SNX27 is not necessary for TCR recycling.

6. In MDA-MB-231 invasive breast cancer cells, SNX27 colocalized with WASH- and MT1-MMP-positive endosomes located at invadopodia; when these cells invaded 3D matrices, SNX27 localized at the front of the invading pseudopods. SNX27 downmodulation in MDA-MB-231 cells altered MT1-MMP accumulation at invadopodia and its depletion reduced invasive cell migration. The previously unreported SNX27 association to PIP5Kγ, a PtdIns(4,5)P_2-synthesizing enzyme that modulates exocyst function and promotes cancer cell migration, could contribute to the effects observed on cell invasion.

VII. CONCLUSIONES

1. El dominio FERM de SNX27 reconoce fosfoinositidos de membrana. Dicho reconocimiento facilita la translocación inicial de SNX27 a la sinapsis inmune (SI) y promueve su localización en el compartimento endocítico durante la formación de la SI. Sin embargo, es dispensable para su reclutamiento a la sinapsis madura de células Jurkat.

2. El reconocimiento de cargos de PDZ es necesario para la acumulación de SNX27 en la SI, lo que sugiere el reclutamiento de dichos cargos. Empleando un análisis proteómico identificamos cargos que emplean o no el dominio PDZ para unir SNX27 durante la formación de la SI. Entre ellos cabe destacar la proteína de las uniones intercelulares ZO-2, cuya asociación con SNX27 le permite regular sus dinámicas de localización en la SI.

3. La interacción constitutiva DGKζ/SNX27 facilita la regulación de las señales de DAG dependientes de DGKζ. El silenciamiento de SNX27 en condiciones basales reduce los niveles de proteína DGKζ por la activación de PKC; tras la estimulación del TCR, la activación aumentada de PKC clásicas resulta en la hiperactivación de la ruta de Ras/ERK/AP-1; la coestimulación promueve un aumento aún mayor de la señalización de esta ruta así como de la de NF-κB, lo que sugiere la participación de otros efectores del DAG.

4. La deleción de *Snx27* en ratones no afecta notablemente al desarrollo de células T. Tras la activación de las células T primarias *Snx27*$^{-/-}$ la expresión de CD69 es normal y su proliferación no está alterada sustancialmente. Sin embargo, dichas células comparadas con los controles, muestran defectos en crecimiento y bajos niveles de CD44 en superficie. Esto correlaciona con una baja expresión de CD71 y una menor activación de mTOR tras la estimulación, lo cual también se observó en células Jurkat silenciadas para SNX27.

5. SNX27 interacciona con el complejo retrómero/WASH en células Jurkat. WASH se localiza en endosomas positivos para CD63 y colocaliza con la fracción endosomal de SNX27 en la SI. SNX27 funciona en parte como un adaptador para el transporte mediado por WASH en células T; es esencial para el reciclaje de cargos de PDZ como GLUT1, y participa en mantener LFA-1 en superficie tanto en células Jurkat como en células T primarias de ratón activadas. SNX27 no es necesaria para el reciclaje del TCR.

6. En la línea celular de cáncer de mama invasivo MDA-MB-231, SNX27 colocaliza con endosomas positivos para WASH y MT1-MMP en los invadopodios; durante la invasión en matrices 3D, SNX27 localiza al frente de los pseudópodos invasivos. El silenciamiento de SNX27 en MDA-MB-231 altera la acumulación de MT1-MMP en los invadopodios y reduce la capacidad migratoria invasiva de estas células. La asociación previamente no reportada de SNX27 a PIP5Kγ, una enzima lipídica que modula la función del exocisto y promueve la migración de las células tumorales, podría contribuir a los efectos observados en la invasión celular.

References

VIII. REFERENCES

1. Abramovici, H., et al., *Diacylglycerol kinase-zeta localization in skeletal muscle is regulated by phosphorylation and interaction with syntrophins.* Mol Biol Cell, 2003. **14**(11): p. 4499-511.
2. Abramovici, H., et al., *Diacylglycerol kinase zeta regulates actin cytoskeleton reorganization through dissociation of Rac1 from RhoGDI.* Mol Biol Cell, 2009. **20**(7): p. 2049-59.
3. Alonso, M.A. and J. Millan, *The role of lipid rafts in signalling and membrane trafficking in T lymphocytes.* J Cell Sci, 2001. **114**(Pt 22): p. 3957-65.
4. Alonso, R., et al., *Diacylglycerol kinase alpha regulates the formation and polarisation of mature multivesicular bodies involved in the secretion of Fas ligand-containing exosomes in T lymphocytes.* Cell Death Differ, 2011. **18**(7): p. 1161-73.
5. Alvi, F., et al., *Regulation of membrane trafficking and endocytosis by protein kinase C: emerging role of the pericentrion, a novel protein kinase C-dependent subset of recycling endosomes.* Cell Mol Life Sci, 2007. **64**(3): p. 263-70.
6. Ambrosi, C., et al., *Connexin43 Forms Supramolecular Complexes through Non-Overlapping Binding Sites for Drebrin, Tubulin, and ZO-1.* PLoS One, 2016. **11**(6): p. e0157073.
7. Angus, K.L. and G.M. Griffiths, *Cell polarisation and the immunological synapse.* Curr Opin Cell Biol, 2013. **25**(1): p. 85-91.
8. Anitei, M. and B. Hoflack, *Bridging membrane and cytoskeleton dynamics in the secretory and endocytic pathways.* Nat Cell Biol, 2012. **14**(1): p. 11-9.
9. Ard, R., et al., *Diacylglycerol kinase zeta regulates RhoA activation via a kinase-independent scaffolding mechanism.* Mol Biol Cell, 2012. **23**(20): p. 4008-19.
10. Arevalo, J.C., et al., *A unique pathway for sustained neurotrophin signaling through an ankyrin-rich membrane-spanning protein.* EMBO J, 2004. **23**(12): p. 2358-68.
11. Asp, L., et al., *Early stages of Golgi vesicle and tubule formation require diacylglycerol.* Mol Biol Cell, 2009. **20**(3): p. 780-90.
12. Avila-Flores, A., et al., *Modulation of the mammalian target of rapamycin pathway by diacylglycerol kinase-produced phosphatidic acid.* J Biol Chem, 2005. **280**(11): p. 10091-9.
13. Bailey, T.A., et al., *A kinase inhibitor screen reveals protein kinase C-dependent endocytic recycling of ErbB2 in breast cancer cells.* J Biol Chem, 2014. **289**(44): p. 30443-58.
14. Balana, B., et al., *Ras-association domain of sorting Nexin 27 is critical for regulating expression of GIRK potassium channels.* PLoS One, 2013. **8**(3): p. e59800.

15. Balana, B., et al., *Mechanism underlying selective regulation of G protein-gated inwardly rectifying potassium channels by the psychostimulant-sensitive sorting nexin 27.* Proc Natl Acad Sci U S A, 2011. **108**(14): p. 5831-6.
16. Balla, T., *Inositol-lipid binding motifs: signal integrators through protein-lipid and protein-protein interactions.* J Cell Sci, 2005. **118**(Pt 10): p. 2093-104.
17. Barclay, J.W., et al., *Phosphorylation of Munc18 by protein kinase C regulates the kinetics of exocytosis.* J Biol Chem, 2003. **278**(12): p. 10538-45.
18. Baron, C.L. and V. Malhotra, *Role of diacylglycerol in PKD recruitment to the TGN and protein transport to the plasma membrane.* Science, 2002. **295**(5553): p. 325-8.
19. Bassi, Z.I., et al., *Citron kinase controls a molecular network required for midbody formation in cytokinesis.* Proc Natl Acad Sci U S A, 2013. **110**(24): p. 9782-7.
20. Batista, A., et al., *Recruitment of transferrin receptor to immunological synapse in response to TCR engagement.* J Immunol, 2004. **172**(11): p. 6709-14.
21. Batista, F.D., D. Iber, and M.S. Neuberger, *B cells acquire antigen from target cells after synapse formation.* Nature, 2001. **411**(6836): p. 489-94.
22. Bauch, C., et al., *Subcellular sorting of the G-protein coupled mouse somatostatin receptor 5 by a network of PDZ-domain containing proteins.* PLoS One, 2014. **9**(2): p. e88529.
23. Becker, K.P. and Y.A. Hannun, *cPKC-dependent sequestration of membrane-recycling components in a subset of recycling endosomes.* J Biol Chem, 2003. **278**(52): p. 52747-54.
24. Benzing, C., J. Rossy, and K. Gaus, *Do signalling endosomes play a role in T cell activation?* FEBS J, 2013. **280**(21): p. 5164-76.
25. Betz, A., et al., *Munc13-1 is a presynaptic phorbol ester receptor that enhances neurotransmitter release.* Neuron, 1998. **21**(1): p. 123-36.
26. Betz, C. and M.N. Hall, *Where is mTOR and what is it doing there?* J Cell Biol, 2013. **203**(4): p. 563-74.
27. Bhutia, Y.D., et al., *Amino Acid transporters in cancer and their relevance to "glutamine addiction": novel targets for the design of a new class of anticancer drugs.* Cancer Res, 2015. **75**(9): p. 1782-8.
28. Billcliff, P.G. and M. Lowe, *Inositol lipid phosphatases in membrane trafficking and human disease.* Biochem J, 2014. **461**(2): p. 159-75.
29. Blott, E.J. and G.M. Griffiths, *Secretory lysosomes.* Nat Rev Mol Cell Biol, 2002. **3**(2): p. 122-31.
30. Bolte, S. and F.P. Cordelieres, *A guided tour into subcellular colocalization analysis in light microscopy.* J Microsc, 2006. **224**(Pt 3): p. 213-32.
31. Bond, J., et al., *A centrosomal mechanism involving CDK5RAP2 and CENPJ controls brain size.* Nat Genet, 2005. **37**(4): p. 353-5.

32. Bonello, G., et al., *Dynamic recruitment of the adaptor protein LAT: LAT exists in two distinct intracellular pools and controls its own recruitment.* J Cell Sci, 2004. **117**(Pt 7): p. 1009-16.
33. Buck, M.D., D. O'Sullivan, and E.L. Pearce, *T cell metabolism drives immunity.* J Exp Med, 2015. **212**(9): p. 1345-60.
34. Budd, R.C., et al., *Distinction of virgin and memory T lymphocytes. Stable acquisition of the Pgp-1 glycoprotein concomitant with antigenic stimulation.* J Immunol, 1987. **138**(10): p. 3120-9.
35. Bunting, M., et al., *Molecular cloning and characterization of a novel human diacylglycerol kinase zeta.* J Biol Chem, 1996. **271**(17): p. 10230-6.
36. Burgstaller, G. and M. Gimona, *Podosome-mediated matrix resorption and cell motility in vascular smooth muscle cells.* Am J Physiol Heart Circ Physiol, 2005. **288**(6): p. H3001-5.
37. Butkevich, E., et al., *Drebrin is a novel connexin-43 binding partner that links gap junctions to the submembrane cytoskeleton.* Curr Biol, 2004. **14**(8): p. 650-8.
38. Byfield, M.P., J.T. Murray, and J.M. Backer, *hVps34 is a nutrient-regulated lipid kinase required for activation of p70 S6 kinase.* J Biol Chem, 2005. **280**(38): p. 33076-82.
39. Cai, K., et al., *Increased diacylglycerol kinase zeta expression in human metastatic colon cancer cells augments Rho GTPase activity and contributes to enhanced invasion.* BMC Cancer, 2014. **14**: p. 208.
40. Cai, L., et al., *Deficiency of sorting nexin 27 (SNX27) leads to growth retardation and elevated levels of N-methyl-D-aspartate receptor 2C (NR2C).* Mol Cell Biol, 2011. **31**(8): p. 1734-47.
41. Caldieri, G., et al., *Polarised apical-like intracellular sorting and trafficking regulates invadopodia formation and degradation of the extracellular matrix in cancer cells.* Eur J Cell Biol, 2012. **91**(11-12): p. 961-8.
42. Carlton, J.G. and P.J. Cullen, *Coincidence detection in phosphoinositide signaling.* Trends Cell Biol, 2005. **15**(10): p. 540-7.
43. Carman, C.V., et al., *Transcellular diapedesis is initiated by invasive podosomes.* Immunity, 2007. **26**(6): p. 784-97.
44. Carrasco, S. and I. Merida, *Diacylglycerol, when simplicity becomes complex.* Trends Biochem Sci, 2007. **32**(1): p. 27-36.
45. Castellanos, M.C., et al., *Expression of the leukocyte early activation antigen CD69 is regulated by the transcription factor AP-1.* J Immunol, 1997. **159**(11): p. 5463-73.
46. Caswell, P. and J. Norman, *Endocytic transport of integrins during cell migration and invasion.* Trends Cell Biol, 2008. **18**(6): p. 257-63.
47. Caswell, P.T., et al., *Rab-coupling protein coordinates recycling of alpha5beta1 integrin and EGFR1 to promote cell migration in 3D microenvironments.* J Cell Biol, 2008. **183**(1): p. 143-55.

48. Caswell, P.T., S. Vadrevu, and J.C. Norman, *Integrins: masters and slaves of endocytic transport.* Nat Rev Mol Cell Biol, 2009. **10**(12): p. 843-53.
49. Cerami, E., et al., *The cBio cancer genomics portal: an open platform for exploring multidimensional cancer genomics data.* Cancer Discov, 2012. **2**(5): p. 401-4.
50. Chakraborty, A.K. and A. Weiss, *Insights into the initiation of TCR signaling.* Nat Immunol, 2014. **15**(9): p. 798-807.
51. Chan, A.S., et al., *Sorting nexin 27 couples PTHR trafficking to retromer for signal regulation in osteoblasts during bone growth.* Mol Biol Cell, 2016. **27**(8): p. 1367-82.
52. Chan, D.A., et al., *Targeting GLUT1 and the Warburg effect in renal cell carcinoma by chemical synthetic lethality.* Sci Transl Med, 2011. **3**(94): p. 94ra70.
53. Chemin, K., et al., *Cytokine secretion by CD4+ T cells at the immunological synapse requires Cdc42-dependent local actin remodeling but not microtubule organizing center polarity.* J Immunol, 2012. **189**(5): p. 2159-68.
54. Chen, B.S. and K.W. Roche, *Regulation of NMDA receptors by phosphorylation.* Neuropharmacology, 2007. **53**(3): p. 362-8.
55. Chen, L., T.H. Chan, and X.Y. Guan, *Chromosome 1q21 amplification and oncogenes in hepatocellular carcinoma.* Acta Pharmacol Sin, 2010. **31**(9): p. 1165-71.
56. Chi, H., *Regulation and function of mTOR signalling in T cell fate decisions.* Nat Rev Immunol, 2012. **12**(5): p. 325-38.
57. Chia, J., et al., *RNAi screening reveals a large signaling network controlling the Golgi apparatus in human cells.* Mol Syst Biol, 2012. **8**: p. 629.
58. Choudhuri, K., et al., *Polarized release of T-cell-receptor-enriched microvesicles at the immunological synapse.* Nature, 2014. **507**(7490): p. 118-23.
59. Chung, J., et al., *Rapamycin-FKBP specifically blocks growth-dependent activation of and signaling by the 70 kd S6 protein kinases.* Cell, 1992. **69**(7): p. 1227-36.
60. Clairfeuille, T., et al., *A molecular code for endosomal recycling of phosphorylated cargos by the SNX27-retromer complex.* Nat Struct Mol Biol, in press.
61. Collins, B.M., et al., *Vps29 has a phosphoesterase fold that acts as a protein interaction scaffold for retromer assembly.* Nat Struct Mol Biol, 2005. **12**(7): p. 594-602.
62. Cordenonsi, M., et al., *Cingulin contains globular and coiled-coil domains and interacts with ZO-1, ZO-2, ZO-3, and myosin.* J Cell Biol, 1999. **147**(7): p. 1569-82.
63. Costello, P.S., M. Gallagher, and D.A. Cantrell, *Sustained and dynamic inositol lipid metabolism inside and outside the immunological synapse.* Nat Immunol, 2002. **3**(11): p. 1082-9.
64. Cullen, P.J., *Endosomal sorting and signalling: an emerging role for sorting nexins.* Nat Rev Mol Cell Biol, 2008. **9**(7): p. 574-82.
65. Cullen, P.J., *Phosphoinositides and the regulation of tubular-based endosomal sorting.* Biochem Soc Trans, 2011. **39**(4): p. 839-50.

66. Cullen, P.J. and H.C. Korswagen, *Sorting nexins provide diversity for retromer-dependent trafficking events.* Nat Cell Biol, 2012. **14**(1): p. 29-37.

67. Daley, S.R., et al., *Rasgrp1 mutation increases naive T-cell CD44 expression and drives mTOR-dependent accumulation of Helios(+) T cells and autoantibodies.* Elife, 2013. **2**: p. e01020.

68. Dall'Armi, C., K.A. Devereaux, and G. Di Paolo, *The role of lipids in the control of autophagy.* Curr Biol, 2013. **23**(1): p. R33-45.

69. Dall'Armi, C., et al., *The phospholipase D1 pathway modulates macroautophagy.* Nat Commun, 2010. **1**: p. 142.

70. Damseh, N., et al., *A defect in the retromer accessory protein, SNX27, manifests by infantile myoclonic epilepsy and neurodegeneration.* Neurogenetics, 2015. **16**(3): p. 215-21.

71. Das, V., et al., *Activation-induced polarized recycling targets T cell antigen receptors to the immunological synapse; involvement of SNARE complexes.* Immunity, 2004. **20**(5): p. 577-88.

72. Davidson, L., et al., *Gonadotropin-releasing hormone-induced activation of diacylglycerol kinase-zeta and its association with active c-src.* J Biol Chem, 2004. **279**(12): p. 11906-16.

73. Davis, D.M., et al., *The human natural killer cell immune synapse.* Proc Natl Acad Sci U S A, 1999. **96**(26): p. 15062-7.

74. Dbouk, H.A., et al., *Connexins: a myriad of functions extending beyond assembly of gap junction channels.* Cell Commun Signal, 2009. **7**: p. 4.

75. De Matteis, M.A. and A. Godi, *PI-loting membrane traffic.* Nat Cell Biol, 2004. **6**(6): p. 487-92.

76. Derivery, E., et al., *Actin polymerization controls the organization of WASH domains at the surface of endosomes.* PLoS One, 2012. **7**(6): p. e39774.

77. Derivery, E., et al., *The Arp2/3 activator WASH controls the fission of endosomes through a large multiprotein complex.* Dev Cell, 2009. **17**(5): p. 712-23.

78. Deswal, S., et al., *Kidins220/ARMS associates with B-Raf and the TCR, promoting sustained Erk signaling in T cells.* J Immunol, 2013. **190**(5): p. 1927-35.

79. Di Paolo, G. and P. De Camilli, *Phosphoinositides in cell regulation and membrane dynamics.* Nature, 2006. **443**(7112): p. 651-7.

80. Diaz-Flores, E., et al., *Membrane translocation of protein kinase Ctheta during T lymphocyte activation requires phospholipase C-gamma-generated diacylglycerol.* J Biol Chem, 2003. **278**(31): p. 29208-15.

81. Ding, L., et al., *Alternative splicing of the human diacylglycerol kinase zeta gene in muscle.* Proc Natl Acad Sci U S A, 1997. **94**(11): p. 5519-24.

82. Dobrowolski, R. and E.M. De Robertis, *Endocytic control of growth factor signalling: multivesicular bodies as signalling organelles.* Nat Rev Mol Cell Biol, 2012. **13**(1): p. 53-60.
83. Douglass, A.D. and R.D. Vale, *Single-molecule microscopy reveals plasma membrane microdomains created by protein-protein networks that exclude or trap signaling molecules in T cells.* Cell, 2005. **121**(6): p. 937-50.
84. Dustin, M.L., *Signaling at neuro/immune synapses.* J Clin Invest, 2012. **122**(4): p. 1149-55.
85. Dustin, M.L., A.K. Chakraborty, and A.S. Shaw, *Understanding the structure and function of the immunological synapse.* Cold Spring Harb Perspect Biol, 2010. **2**(10): p. a002311.
86. Ebinu, J.O., et al., *RasGRP, a Ras guanyl nucleotide- releasing protein with calcium- and diacylglycerol-binding motifs.* Science, 1998. **280**(5366): p. 1082-6.
87. Ehrlich, L.I., et al., *Dynamics of p56lck translocation to the T cell immunological synapse following agonist and antagonist stimulation.* Immunity, 2002. **17**(6): p. 809-22.
88. Elgueta, R., et al., *Gap junctions at the dendritic cell-T cell interface are key elements for antigen-dependent T cell activation.* J Immunol, 2009. **183**(1): p. 277-84.
89. Elliott, P.R. and D. Komander, *Regulation of Met1-linked polyubiquitin signalling by the deubiquitinase OTULIN.* FEBS J, 2016. **283**(1): p. 39-53.
90. Evans, W.H. and P.E. Martin, *Gap junctions: structure and function (Review).* Mol Membr Biol, 2002. **19**(2): p. 121-36.
91. Eyster, C.A., et al., *Discovery of new cargo proteins that enter cells through clathrin-independent endocytosis.* Traffic, 2009. **10**(5): p. 590-9.
92. Fagerholm, S., et al., *Phosphorylation of the cytoplasmic domain of the integrin CD18 chain by protein kinase C isoforms in leukocytes.* J Biol Chem, 2002. **277**(3): p. 1728-38.
93. Fang, Y., et al., *Phosphatidic acid-mediated mitogenic activation of mTOR signaling.* Science, 2001. **294**(5548): p. 1942-5.
94. Fanning, A.S. and J.M. Anderson, *Zonula occludens-1 and -2 are cytosolic scaffolds that regulate the assembly of cellular junctions.* Ann N Y Acad Sci, 2009. **1165**: p. 113-20.
95. Fanning, A.S., T.Y. Ma, and J.M. Anderson, *Isolation and functional characterization of the actin binding region in the tight junction protein ZO-1.* FASEB J, 2002. **16**(13): p. 1835-7.
96. Fanning, A.S., C.M. Van Itallie, and J.M. Anderson, *Zonula occludens-1 and -2 regulate apical cell structure and the zonula adherens cytoskeleton in polarized epithelia.* Mol Biol Cell, 2012. **23**(4): p. 577-90.
97. Fazekas de St Groth, B., A.L. Smith, and C.A. Higgins, *T cell activation: in vivo veritas.* Immunol Cell Biol, 2004. **82**(3): p. 260-8.

98. Feng, L., et al., *SH3KBP1-binding protein 1 prevents epidermal growth factor receptor degradation by the interruption of c-Cbl-CIN85 complex.* Cell Biochem Funct, 2011. **29**(7): p. 589-96.

99. Fernandez-Ulibarri, I., et al., *Diacylglycerol is required for the formation of COPI vesicles in the Golgi-to-ER transport pathway.* Mol Biol Cell, 2007. **18**(9): p. 3250-63.

100. Fiala, G.J., et al., *Kidins220/ARMS binds to the B cell antigen receptor and regulates B cell development and activation.* J Exp Med, 2015. **212**(10): p. 1693-708.

101. Fingar, D.C., et al., *Mammalian cell size is controlled by mTOR and its downstream targets S6K1 and 4EBP1/eIF4E.* Genes Dev, 2002. **16**(12): p. 1472-87.

102. Fletcher, J.I., et al., *ABC transporters in cancer: more than just drug efflux pumps.* Nat Rev Cancer, 2010. **10**(2): p. 147-56.

103. Fletcher, S.J. and J.Z. Rappoport, *Moving forward: polarised trafficking in cell migration.* Trends Cell Biol, 2010. **20**(2): p. 71-8.

104. Flinn, R.J., et al., *The late endosome is essential for mTORC1 signaling.* Mol Biol Cell, 2010. **21**(5): p. 833-41.

105. Fogarty, F.M., et al., *HRG-1 enhances cancer cell invasive potential and couples glucose metabolism to cytosolic/extracellular pH gradient regulation by the vacuolar-H(+) ATPase.* Oncogene, 2014. **33**(38): p. 4653-63.

106. Fooksman, D.R., et al., *Functional anatomy of T cell activation and synapse formation.* Annu Rev Immunol, 2010. **28**: p. 79-105.

107. Foster, D.A., *Phosphatidic acid and lipid-sensing by mTOR.* Trends Endocrinol Metab, 2013. **24**(6): p. 272-8.

108. Fox, C.J., P.S. Hammerman, and C.B. Thompson, *Fuel feeds function: energy metabolism and the T-cell response.* Nat Rev Immunol, 2005. **5**(11): p. 844-52.

109. Frauwirth, K.A., et al., *The CD28 signaling pathway regulates glucose metabolism.* Immunity, 2002. **16**(6): p. 769-77.

110. Freeman, C.L., G. Hesketh, and M.N. Seaman, *RME-8 coordinates the activity of the WASH complex with the function of the retromer SNX dimer to control endosomal tubulation.* J Cell Sci, 2014. **127**(Pt 9): p. 2053-70.

111. Gallon, M., et al., *A unique PDZ domain and arrestin-like fold interaction reveals mechanistic details of endocytic recycling by SNX27-retromer.* Proc Natl Acad Sci U S A, 2014. **111**(35): p. E3604-13.

112. Gallon, M. and P.J. Cullen, *Retromer and sorting nexins in endosomal sorting.* Biochem Soc Trans, 2015. **43**(1): p. 33-47.

113. Gao, J., et al., *Integrative analysis of complex cancer genomics and clinical profiles using the cBioPortal.* Sci Signal, 2013. **6**(269): p. pl1.

114. Gardiol, D., et al., *Oncogenic human papillomavirus E6 proteins target the discs large tumour suppressor for proteasome-mediated degradation.* Oncogene, 1999. **18**(40): p. 5487-96.

115. Germain, R.N., *T-cell development and the CD4-CD8 lineage decision.* Nat Rev Immunol, 2002. **2**(5): p. 309-22.
116. Ghai, R., et al., *Structural basis for endosomal trafficking of diverse transmembrane cargos by PX-FERM proteins.* Proc Natl Acad Sci U S A, 2013. **110**(8): p. E643-52.
117. Ghai, R., et al., *Phox homology band 4.1/ezrin/radixin/moesin-like proteins function as molecular scaffolds that interact with cargo receptors and Ras GTPases.* Proc Natl Acad Sci U S A, 2011. **108**(19): p. 7763-8.
118. Ghai, R., et al., *Phosphoinositide binding by the SNX27 FERM domain regulates its localization at the immune synapse of activated T-cells.* J Cell Sci, 2015. **128**(3): p. 553-65.
119. Gharbi, S.I., et al., *Transient PKCalpha shuttling to the immunological synapse is governed by DGKzeta and regulates L-selectin shedding.* J Cell Sci, 2013. **126**(Pt 10): p. 2176-86.
120. Gharbi, S.I., et al., *Diacylglycerol kinase zeta controls diacylglycerol metabolism at the immunological synapse.* Mol Biol Cell, 2011. **22**(22): p. 4406-14.
121. Giovannini, D., et al., *Inorganic phosphate export by the retrovirus receptor XPR1 in metazoans.* Cell Rep, 2013. **3**(6): p. 1866-73.
122. Godfrey, D.I., et al., *A developmental pathway involving four phenotypically and functionally distinct subsets of CD3-CD4-CD8- triple-negative adult mouse thymocytes defined by CD44 and CD25 expression.* J Immunol, 1993. **150**(10): p. 4244-52.
123. Gokool, S., et al., *Identification of a conserved motif required for Vps35p/Vps26p interaction and assembly of the retromer complex.* Biochem J, 2007. **408**(2): p. 287-95.
124. Gomez, T.S. and D.D. Billadeau, *A FAM21-containing WASH complex regulates retromer-dependent sorting.* Dev Cell, 2009. **17**(5): p. 699-711.
125. Gomez, T.S., et al., *Trafficking defects in WASH-knockout fibroblasts originate from collapsed endosomal and lysosomal networks.* Mol Biol Cell, 2012. **23**(16): p. 3215-28.
126. Gorentla, B.K., C.K. Wan, and X.P. Zhong, *Negative regulation of mTOR activation by diacylglycerol kinases.* Blood, 2011. **117**(15): p. 4022-31.
127. Graham, T.R. and C.G. Burd, *Coordination of Golgi functions by phosphatidylinositol 4-kinases.* Trends Cell Biol, 2011. **21**(2): p. 113-21.
128. Griffiths, G.M., A. Tsun, and J.C. Stinchcombe, *The immunological synapse: a focal point for endocytosis and exocytosis.* J Cell Biol, 2010. **189**(3): p. 399-406.
129. Gui, J., et al., *Thymus Size and Age-related Thymic Involution: Early Programming, Sexual Dimorphism, Progenitors and Stroma.* Aging Dis, 2012. **3**(3): p. 280-90.
130. Gupta, S., et al., *An Alternative Phosphorylation Switch in Integrin beta2 (CD18) Tail for Dok1 Binding.* Sci Rep, 2015. **5**: p. 11630.
131. Gwack, Y., et al., *Signalling to transcription: store-operated Ca2+ entry and NFAT activation in lymphocytes.* Cell Calcium, 2007. **42**(2): p. 145-56.

132. Hall, R.A., et al., *The beta2-adrenergic receptor interacts with the Na+/H+-exchanger regulatory factor to control Na+/H+ exchange.* Nature, 1998. **392**(6676): p. 626-30.

133. Hamanaka, R.B. and N.S. Chandel, *Targeting glucose metabolism for cancer therapy.* J Exp Med, 2012. **209**(2): p. 211-5.

134. Han, T., et al., *How does cancer cell metabolism affect tumor migration and invasion?* Cell Adh Migr, 2013. **7**(5): p. 395-403.

135. Hao, Y.H., et al., *USP7 Acts as a Molecular Rheostat to Promote WASH-Dependent Endosomal Protein Recycling and Is Mutated in a Human Neurodevelopmental Disorder.* Mol Cell, 2015. **59**(6): p. 956-69.

136. Harbour, M.E., et al., *The cargo-selective retromer complex is a recruiting hub for protein complexes that regulate endosomal tubule dynamics.* J Cell Sci, 2010. **123**(Pt 21): p. 3703-17.

137. Harbour, M.E., S.Y. Breusegem, and M.N. Seaman, *Recruitment of the endosomal WASH complex is mediated by the extended 'tail' of Fam21 binding to the retromer protein Vps35.* Biochem J, 2012. **442**(1): p. 209-20.

138. Harriague, J. and G. Bismuth, *Imaging antigen-induced PI3K activation in T cells.* Nat Immunol, 2002. **3**(11): p. 1090-6.

139. Hayashi, H., et al., *Sorting nexin 27 interacts with multidrug resistance-associated protein 4 (MRP4) and mediates internalization of MRP4.* J Biol Chem, 2012. **287**(18): p. 15054-65.

140. Heider, M.R. and M. Munson, *Exorcising the exocyst complex.* Traffic, 2012. **13**(7): p. 898-907.

141. Helfer, E., et al., *Endosomal recruitment of the WASH complex: active sequences and mutations impairing interaction with the retromer.* Biol Cell, 2013. **105**(5): p. 191-207.

142. Hemar, A., et al., *Endocytosis of interleukin 2 receptors in human T lymphocytes: distinct intracellular localization and fate of the receptor alpha, beta, and gamma chains.* J Cell Biol, 1995. **129**(1): p. 55-64.

143. Hennigan, R.F., K.L. Hawker, and B.W. Ozanne, *Fos-transformation activates genes associated with invasion.* Oncogene, 1994. **9**(12): p. 3591-600.

144. Hesketh, G.G., et al., *VARP is recruited on to endosomes by direct interaction with retromer, where together they function in export to the cell surface.* Dev Cell, 2014. **29**(5): p. 591-606.

145. Hierro, A., et al., *Functional architecture of the retromer cargo-recognition complex.* Nature, 2007. **449**(7165): p. 1063-7.

146. Hornbeck, P.V., et al., *PhosphoSitePlus, 2014: mutations, PTMs and recalibrations.* Nucleic Acids Res, 2015. **43**(Database issue): p. D512-20.

147. Hsieh, A.C., et al., *The translational landscape of mTOR signalling steers cancer initiation and metastasis.* Nature, 2012. **485**(7396): p. 55-61.

148. Huse, M., *Lymphocyte polarity, the immunological synapse and the scope of biological analogy.* Bioarchitecture, 2011. **1**(4): p. 180-185.
149. Huse, M., et al., *T cells use two directionally distinct pathways for cytokine secretion.* Nat Immunol, 2006. **7**(3): p. 247-55.
150. Hussain, N.K., et al., *Sorting Nexin 27 regulates basal and activity-dependent trafficking of AMPARs.* Proc Natl Acad Sci U S A, 2014. **111**(32): p. 11840-5.
151. Hutagalung, A.H. and P.J. Novick, *Role of Rab GTPases in membrane traffic and cell physiology.* Physiol Rev, 2011. **91**(1): p. 119-49.
152. Ibanez, K., et al., *Molecular evidence for the inverse comorbidity between central nervous system disorders and cancers detected by transcriptomic meta-analyses.* PLoS Genet, 2014. **10**(2): p. e1004173.
153. Idkowiak-Baldys, J., et al., *Sustained receptor stimulation leads to sequestration of recycling endosomes in a classical protein kinase C- and phospholipase D-dependent manner.* J Biol Chem, 2009. **284**(33): p. 22322-31.
154. Iglesias, T., et al., *Identification and cloning of Kidins220, a novel neuronal substrate of protein kinase D.* J Biol Chem, 2000. **275**(51): p. 40048-56.
155. Ikeda, F., *Linear ubiquitination signals in adaptive immune responses.* Immunol Rev, 2015. **266**(1): p. 222-36.
156. Insall, R.H. and L.M. Machesky, *Actin dynamics at the leading edge: from simple machinery to complex networks.* Dev Cell, 2009. **17**(3): p. 310-22.
157. Isakov, N. and A. Altman, *PKC-theta-mediated signal delivery from the TCR/CD28 surface receptors.* Front Immunol, 2012. **3**: p. 273.
158. Izumi, H., et al., *Monocarboxylate transporters 1 and 4 are involved in the invasion activity of human lung cancer cells.* Cancer Sci, 2011. **102**(5): p. 1007-13.
159. Jain, J., et al., *Nuclear factor of activated T cells contains Fos and Jun.* Nature, 1992. **356**(6372): p. 801-4.
160. Jia, D., et al., *Multiple repeat elements within the FAM21 tail link the WASH actin regulatory complex to the retromer.* Mol Biol Cell, 2012. **23**(12): p. 2352-61.
161. Jia, D., et al., *WASH and WAVE actin regulators of the Wiskott-Aldrich syndrome protein (WASP) family are controlled by analogous structurally related complexes.* Proc Natl Acad Sci U S A, 2010. **107**(23): p. 10442-7.
162. Joubert, L., et al., *New sorting nexin (SNX27) and NHERF specifically interact with the 5-HT4a receptor splice variant: roles in receptor targeting.* J Cell Sci, 2004. **117**(Pt 22): p. 5367-79.
163. Juin, A., et al., *Physiological type I collagen organization induces the formation of a novel class of linear invadosomes.* Mol Biol Cell, 2012. **23**(2): p. 297-309.
164. Jun, J.E., I. Rubio, and J.P. Roose, *Regulation of ras exchange factors and cellular localization of ras activation by lipid messengers in T cells.* Front Immunol, 2013. **4**: p. 239.

165. Jurdic, P., et al., *Podosome and sealing zone: specificity of the osteoclast model.* Eur J Cell Biol, 2006. **85**(3-4): p. 195-202.

166. Kaizuka, Y., et al., *Mechanisms for segregating T cell receptor and adhesion molecules during immunological synapse formation in Jurkat T cells.* Proc Natl Acad Sci U S A, 2007. **104**(51): p. 20296-301.

167. Kalaidzidis, I., et al., *APPL endosomes are not obligatory endocytic intermediates but act as stable cargo-sorting compartments.* J Cell Biol, 2015. **211**(1): p. 123-44.

168. Kikuchi, K. and K. Takahashi, *WAVE2- and microtubule-dependent formation of long protrusions and invasion of cancer cells cultured on three-dimensional extracellular matrices.* Cancer Sci, 2008. **99**(11): p. 2252-9.

169. Kim, E. and M. Sheng, *PDZ domain proteins of synapses.* Nat Rev Neurosci, 2004. **5**(10): p. 771-81.

170. Kim, K., J. Yang, and E. Kim, *Diacylglycerol kinases in the regulation of dendritic spines.* J Neurochem, 2010. **112**(3): p. 577-87.

171. Kim, Y.C. and K.L. Guan, *mTOR: a pharmacologic target for autophagy regulation.* J Clin Invest, 2015. **125**(1): p. 25-32.

172. Komaki, R., H. Togashi, and Y. Takai, *Regulation of dendritic filopodial interactions by ZO-1 and implications for dendrite morphogenesis.* PLoS One, 2013. **8**(10): p. e76201.

173. Kong, K.F., et al., *A motif in the V3 domain of the kinase PKC-theta determines its localization in the immunological synapse and functions in T cells via association with CD28.* Nat Immunol, 2011. **12**(11): p. 1105-12.

174. Krauss, M. and V. Haucke, *Phosphoinositide-metabolizing enzymes at the interface between membrane traffic and cell signalling.* EMBO Rep, 2007. **8**(3): p. 241-6.

175. Krummel, M.F. and I. Macara, *Maintenance and modulation of T cell polarity.* Nat Immunol, 2006. **7**(11): p. 1143-9.

176. Ktistakis, N.T., et al., *Phospholipase D1 and potential targets of its hydrolysis product, phosphatidic acid.* Biochem Soc Trans, 2003. **31**(Pt 1): p. 94-7.

177. Kumari, S., et al., *Actin foci facilitate activation of the phospholipase C-gamma in primary T lymphocytes via the WASP pathway.* Elife, 2015. **4**.

178. Kupfer, A. and S.J. Singer, *The specific interaction of helper T cells and antigen-presenting B cells. IV. Membrane and cytoskeletal reorganizations in the bound T cell as a function of antigen dose.* J Exp Med, 1989. **170**(5): p. 1697-713.

179. Lacalle, R.A., et al., *Type I phosphatidylinositol 4-phosphate 5-kinase controls neutrophil polarity and directional movement.* J Cell Biol, 2007. **179**(7): p. 1539-53.

180. Lauffer, B.E., et al., *SNX27 mediates PDZ-directed sorting from endosomes to the plasma membrane.* J Cell Biol, 2010. **190**(4): p. 565-74.

181. Le Floc'h, A., et al., *Annular PIP3 accumulation controls actin architecture and modulates cytotoxicity at the immunological synapse.* J Exp Med, 2013. **210**(12): p. 2721-37.

182. LeBien, T.W. and T.F. Tedder, *B lymphocytes: how they develop and function.* Blood, 2008. **112**(5): p. 1570-80.
183. Lee, D., et al., *Functional and Physical Interaction of Diacylglycerol Kinase zeta with Protein Kinase Calpha Is Required for Cerebellar Long-Term Depression.* J Neurosci, 2015. **35**(46): p. 15453-65.
184. Lee, H.J. and J.J. Zheng, *PDZ domains and their binding partners: structure, specificity, and modification.* Cell Commun Signal, 2010. **8**: p. 8.
185. Lee, S., J. Chang, and C. Blackstone, *FAM21 directs SNX27-retromer cargoes to the plasma membrane by preventing transport to the Golgi apparatus.* Nat Commun, 2016. **7**: p. 10939.
186. Legate, K.R. and R. Fassler, *Mechanisms that regulate adaptor binding to beta-integrin cytoplasmic tails.* J Cell Sci, 2009. **122**(Pt 2): p. 187-98.
187. Legati, A., et al., *Mutations in XPR1 cause primary familial brain calcification associated with altered phosphate export.* Nat Genet, 2015. **47**(6): p. 579-81.
188. Lillemeier, B.F., et al., *TCR and Lat are expressed on separate protein islands on T cell membranes and concatenate during activation.* Nat Immunol, 2010. **11**(1): p. 90-6.
189. Lin, T.B., et al., *VPS26A-SNX27 Interaction-Dependent mGluR5 Recycling in Dorsal Horn Neurons Mediates Neuropathic Pain in Rats.* J Neurosci, 2015. **35**(44): p. 14943-55.
190. Lin, Y.H., et al., *Diacylglycerol lipase regulates lifespan and oxidative stress response by inversely modulating TOR signaling in Drosophila and C. elegans.* Aging Cell, 2014. **13**(4): p. 755-64.
191. Litvak, V., et al., *Maintenance of the diacylglycerol level in the Golgi apparatus by the Nir2 protein is critical for Golgi secretory function.* Nat Cell Biol, 2005. **7**(3): p. 225-34.
192. Liu, J. and W. Guo, *The exocyst complex in exocytosis and cell migration.* Protoplasma, 2012. **249**(3): p. 587-97.
193. Liu, L.X., et al., *Mutation of a conserved residue (D123) required for oligomerization of human immunodeficiency virus type 1 Nef protein abolishes interaction with human thioesterase and results in impairment of Nef biological functions.* J Virol, 2000. **74**(11): p. 5310-9.
194. Logue, J.S. and D.K. Morrison, *Complexity in the signaling network: insights from the use of targeted inhibitors in cancer therapy.* Genes Dev, 2012. **26**(7): p. 641-50.
195. Lokuta, M.A., et al., *Type Igamma PIP kinase is a novel uropod component that regulates rear retraction during neutrophil chemotaxis.* Mol Biol Cell, 2007. **18**(12): p. 5069-80.
196. Loo, L.S., et al., *A role for sorting nexin 27 in AMPA receptor trafficking.* Nat Commun, 2014. **5**: p. 3176.

197. Lopez-Cabrera, M., et al., *Transcriptional regulation of the gene encoding the human C-type lectin leukocyte receptor AIM/CD69 and functional characterization of its tumor necrosis factor-alpha-responsive elements.* J Biol Chem, 1995. **270**(37): p. 21545-51.

198. Lopez-Menendez, C., et al., *Kidins220 accumulates with tau in human Alzheimer's disease and related models: modulation of its calpain-processing by GSK3beta/PP1 imbalance.* Hum Mol Genet, 2013. **22**(3): p. 466-82.

199. Love, P.E. and A. Bhandoola, *Signal integration and crosstalk during thymocyte migration and emigration.* Nat Rev Immunol, 2011. **11**(7): p. 469-77.

200. Lucin, K.M., et al., *Microglial beclin 1 regulates retromer trafficking and phagocytosis and is impaired in Alzheimer's disease.* Neuron, 2013. **79**(5): p. 873-86.

201. Ludford-Menting, M.J., et al., *A network of PDZ-containing proteins regulates T cell polarity and morphology during migration and immunological synapse formation.* Immunity, 2005. **22**(6): p. 737-48.

202. Lunn, M.L., et al., *A unique sorting nexin regulates trafficking of potassium channels via a PDZ domain interaction.* Nat Neurosci, 2007. **10**(10): p. 1249-59.

203. Luo, B., S.M. Prescott, and M.K. Topham, *Association of diacylglycerol kinase zeta with protein kinase C alpha: spatial regulation of diacylglycerol signaling.* J Cell Biol, 2003. **160**(6): p. 929-37.

204. Luo, B., S.M. Prescott, and M.K. Topham, *Protein kinase C alpha phosphorylates and negatively regulates diacylglycerol kinase zeta.* J Biol Chem, 2003. **278**(41): p. 39542-7.

205. Luo, B., S.M. Prescott, and M.K. Topham, *Diacylglycerol kinase zeta regulates phosphatidylinositol 4-phosphate 5-kinase Ialpha by a novel mechanism.* Cell Signal, 2004. **16**(8): p. 891-7.

206. Ma, J.S., T.F. Haydar, and S. Radoja, *Protein kinase C delta localizes to secretory lysosomes in CD8+ CTL and directly mediates TCR signals leading to granule exocytosis-mediated cytotoxicity.* J Immunol, 2008. **181**(7): p. 4716-22.

207. Ma, N.F., et al., *Isolation and characterization of a novel oncogene, amplified in liver cancer 1, within a commonly amplified region at 1q21 in hepatocellular carcinoma.* Hepatology, 2008. **47**(2): p. 503-10.

208. Macintyre, A.N., et al., *The glucose transporter Glut1 is selectively essential for CD4 T cell activation and effector function.* Cell Metab, 2014. **20**(1): p. 61-72.

209. MacNeil, A.J., M. Mansour, and B. Pohajdak, *Sorting nexin 27 interacts with the Cytohesin associated scaffolding protein (CASP) in lymphocytes.* Biochem Biophys Res Commun, 2007. **359**(4): p. 848-53.

210. MacNeil, A.J. and B. Pohajdak, *Polarization of endosomal SNX27 in migrating and tumor-engaged natural killer cells.* Biochem Biophys Res Commun, 2007. **361**(1): p. 146-50.

211. Manes, S., et al., *An isoform-specific PDZ-binding motif targets type I PIP5 kinase beta to the uropod and controls polarization of neutrophil-like HL60 cells.* FASEB J, 2010. **24**(9): p. 3381-92.
212. Markegard, E., et al., *Basal LAT-diacylglycerol-RasGRP1 signals in T cells maintain TCRalpha gene expression.* PLoS One, 2011. **6**(9): p. e25540.
213. Matsumoto, R., et al., *Phosphorylation of CARMA1 plays a critical role in T Cell receptor-mediated NF-kappaB activation.* Immunity, 2005. **23**(6): p. 575-85.
214. Matthews, S.A., et al., *Spatial and temporal regulation of protein kinase D (PKD).* EMBO J, 2000. **19**(12): p. 2935-45.
215. Mazzeo, C., et al., *Protein kinase D1/2 is involved in the maturation of multivesicular bodies and secretion of exosomes in T and B lymphocytes.* Cell Death Differ, 2016. **23**(1): p. 99-109.
216. McGarvey, J.C., et al., *Actin-Sorting Nexin 27 (SNX27)-Retromer Complex Mediates Rapid Parathyroid Hormone Receptor Recycling.* J Biol Chem, 2016. **291**(21): p. 10986-1002.
217. McGough, I.J., et al., *Identification of molecular heterogeneity in SNX27-retromer-mediated endosome-to-plasma-membrane recycling.* J Cell Sci, 2014. **127**(Pt 22): p. 4940-53.
218. McIntyre, R.E., et al., *Disruption of mouse Cenpj, a regulator of centriole biogenesis, phenocopies Seckel syndrome.* PLoS Genet, 2012. **8**(11): p. e1003022.
219. Mendoza-Naranjo, A., et al., *Functional gap junctions accumulate at the immunological synapse and contribute to T cell activation.* J Immunol, 2011. **187**(6): p. 3121-32.
220. Merida, I., et al., *Redundant and specialized roles for diacylglycerol kinases alpha and zeta in the control of T cell functions.* Sci Signal, 2015. **8**(374): p. re6.
221. Merida, I., A. Avila-Flores, and E. Merino, *Diacylglycerol kinases: at the hub of cell signalling.* Biochem J, 2008. **409**(1): p. 1-18.
222. Metais, J.Y., et al., *hScrib interacts with ZO-2 at the cell-cell junctions of epithelial cells.* FEBS Lett, 2005. **579**(17): p. 3725-30.
223. Michell, R.H., et al., *Phosphatidylinositol 3,5-bisphosphate: metabolism and cellular functions.* Trends Biochem Sci, 2006. **31**(1): p. 52-63.
224. Mitchell, C.A., et al., *Inositol polyphosphate 5-phosphatases: lipid phosphatases with flair.* IUBMB Life, 2002. **53**(1): p. 25-36.
225. Mittelbrunn, M., et al., *Unidirectional transfer of microRNA-loaded exosomes from T cells to antigen-presenting cells.* Nat Commun, 2011. **2**: p. 282.
226. Miura, S. and Y. Mishina, *Hepatocyte growth factor-regulated tyrosine kinase substrate (Hgs) is involved in BMP signaling through phosphorylation of SMADS and TAK1 in early mouse embryo.* Dev Dyn, 2011. **240**(11): p. 2474-81.
227. Monks, C.R., et al., *Three-dimensional segregation of supramolecular activation clusters in T cells.* Nature, 1998. **395**(6697): p. 82-6.

228. Monteiro, P., et al., *Endosomal WASH and exocyst complexes control exocytosis of MT1-MMP at invadopodia.* J Cell Biol, 2013. **203**(6): p. 1063-79.

229. Morgan, G.J., B.A. Walker, and F.E. Davies, *The genetic architecture of multiple myeloma.* Nat Rev Cancer, 2012. **12**(5): p. 335-48.

230. Morgan, M.M., et al., *Superantigen-induced T cell:B cell conjugation is mediated by LFA-1 and requires signaling through Lck, but not ZAP-70.* J Immunol, 2001. **167**(10): p. 5708-18.

231. Munoz, M.B. and P.A. Slesinger, *Sorting nexin 27 regulation of G protein-gated inwardly rectifying K(+) channels attenuates in vivo cocaine response.* Neuron, 2014. **82**(3): p. 659-69.

232. Murphy, D.A. and S.A. Courtneidge, *The 'ins' and 'outs' of podosomes and invadopodia: characteristics, formation and function.* Nat Rev Mol Cell Biol, 2011. **12**(7): p. 413-26.

233. Nagaya, H., et al., *Diacylglycerol kinase delta suppresses ER-to-Golgi traffic via its SAM and PH domains.* Mol Biol Cell, 2002. **13**(1): p. 302-16.

234. Nakagawa, T. and M. Asahi, *beta1-adrenergic receptor recycles via a membranous organelle, recycling endosome, by binding with sorting nexin27.* J Membr Biol, 2013. **246**(7): p. 571-9.

235. Nakaya, M., et al., *Inflammatory T cell responses rely on amino acid transporter ASCT2 facilitation of glutamine uptake and mTORC1 kinase activation.* Immunity, 2014. **40**(5): p. 692-705.

236. Nazarewicz, R.R., et al., *Early endosomal antigen 1 (EEA1) is an obligate scaffold for angiotensin II-induced, PKC-alpha-dependent Akt activation in endosomes.* J Biol Chem, 2011. **286**(4): p. 2886-95.

237. Neijssen, J., B. Pang, and J. Neefjes, *Gap junction-mediated intercellular communication in the immune system.* Prog Biophys Mol Biol, 2007. **94**(1-2): p. 207-18.

238. Nelson, C.D., et al., *Beta-arrestin scaffolding of phosphatidylinositol 4-phosphate 5-kinase Ialpha promotes agonist-stimulated sequestration of the beta2-adrenergic receptor.* J Biol Chem, 2008. **283**(30): p. 21093-101.

239. Nelson, C.D., et al., *Targeting of diacylglycerol degradation to M1 muscarinic receptors by beta-arrestins.* Science, 2007. **315**(5812): p. 663-6.

240. Newton, A.C. and L.C. Trotman, *Turning off AKT: PHLPP as a drug target.* Annu Rev Pharmacol Toxicol, 2014. **54**: p. 537-58.

241. Niizeki, T., et al., *Diacylglycerol kinase zeta rescues G alpha q-induced heart failure in transgenic mice.* Circ J, 2008. **72**(2): p. 309-17.

242. Niu, Y., et al., *PtdIns(4)P regulates retromer-motor interaction to facilitate dynein-cargo dissociation at the trans-Golgi network.* Nat Cell Biol, 2013. **15**(4): p. 417-29.

243. Oka, T., et al., *Functional complexes between YAP2 and ZO-2 are PDZ domain-dependent, and regulate YAP2 nuclear localization and signalling.* Biochem J, 2010. **432**(3): p. 461-72.

244. Okada, M., et al., *DGKzeta is degraded through the cytoplasmic ubiquitin-proteasome system under excitotoxic conditions, which causes neuronal apoptosis because of aberrant cell cycle reentry.* Cell Signal, 2012. **24**(8): p. 1573-82.
245. Onnis, A., F. Finetti, and C.T. Baldari, *Vesicular Trafficking to the Immune Synapse: How to Assemble Receptor-Tailored Pathways from a Basic Building Set.* Front Immunol, 2016. **7**: p. 50.
246. Osborne, D.G., et al., *SNX17 affects T cell activation by regulating TCR and integrin recycling.* J Immunol, 2015. **194**(9): p. 4555-66.
247. Palfy, M., A. Remenyi, and T. Korcsmaros, *Endosomal crosstalk: meeting points for signaling pathways.* Trends Cell Biol, 2012. **22**(9): p. 447-56.
248. Palmer, C.S., et al., *Glucose metabolism regulates T cell activation, differentiation, and functions.* Front Immunol, 2015. **6**: p. 1.
249. Park, L., et al., *Cyclical action of the WASH complex: FAM21 and capping protein drive WASH recycling, not initial recruitment.* Dev Cell, 2013. **24**(2): p. 169-81.
250. Park, S.G., et al., *The kinase PDK1 integrates T cell antigen receptor and CD28 coreceptor signaling to induce NF-kappaB and activate T cells.* Nat Immunol, 2009. **10**(2): p. 158-66.
251. Patterson, S.J., et al., *Cutting edge: PHLPP regulates the development, function, and molecular signaling pathways of regulatory T cells.* J Immunol, 2011. **186**(10): p. 5533-7.
252. Pelkmans, L., et al., *Genome-wide analysis of human kinases in clathrin- and caveolae/raft-mediated endocytosis.* Nature, 2005. **436**(7047): p. 78-86.
253. Perez-Martinez, M., et al., *F-actin-binding protein drebrin regulates CXCR4 recruitment to the immune synapse.* J Cell Sci, 2010. **123**(Pt 7): p. 1160-70.
254. Phee, H., R.T. Abraham, and A. Weiss, *Dynamic recruitment of PAK1 to the immunological synapse is mediated by PIX independently of SLP-76 and Vav1.* Nat Immunol, 2005. **6**(6): p. 608-17.
255. Pim, D., et al., *A Novel PDZ Domain Interaction Mediates the Binding between Human Papillomavirus 16 L2 and Sorting Nexin 27 and Modulates Virion Trafficking.* J Virol, 2015. **89**(20): p. 10145-55.
256. Piotrowski, J.T., et al., *WASH knockout T cells demonstrate defective receptor trafficking, proliferation, and effector function.* Mol Cell Biol, 2013. **33**(5): p. 958-73.
257. Poincloux, R., F. Lizarraga, and P. Chavrier, *Matrix invasion by tumour cells: a focus on MT1-MMP trafficking to invadopodia.* J Cell Sci, 2009. **122**(Pt 17): p. 3015-24.
258. Pollizzi, K.N. and J.D. Powell, *Integrating canonical and metabolic signalling programmes in the regulation of T cell responses.* Nat Rev Immunol, 2014. **14**(7): p. 435-46.
259. Pollizzi, K.N., et al., *Cellular size as a means of tracking mTOR activity and cell fate of CD4+ T cells upon antigen recognition.* PLoS One, 2015. **10**(4): p. e0121710.

260. Popovic, D., et al., *Rab GTPase-activating proteins in autophagy: regulation of endocytic and autophagy pathways by direct binding to human ATG8 modifiers.* Mol Cell Biol, 2012. **32**(9): p. 1733-44.

261. Prevostel, C., et al., *Protein kinase C(alpha) actively downregulates through caveolae-dependent traffic to an endosomal compartment.* J Cell Sci, 2000. **113 (Pt 14)**: p. 2575-84.

262. Quann, E.J., et al., *Localized diacylglycerol drives the polarization of the microtubule-organizing center in T cells.* Nat Immunol, 2009. **10**(6): p. 627-35.

263. Rainero, E., et al., *Diacylglycerol kinase alpha controls RCP-dependent integrin trafficking to promote invasive migration.* J Cell Biol, 2012. **196**(2): p. 277-95.

264. Restrepo, R., et al., *Structural features of vps35p involved in interaction with other subunits of the retromer complex.* Traffic, 2007. **8**(12): p. 1841-53.

265. Rhee, J.S., et al., *Beta phorbol ester- and diacylglycerol-induced augmentation of transmitter release is mediated by Munc13s and not by PKCs.* Cell, 2002. **108**(1): p. 121-33.

266. Ridley, A.J., et al., *Cell migration: integrating signals from front to back.* Science, 2003. **302**(5651): p. 1704-9.

267. Riedl, J., et al., *Lifeact: a versatile marker to visualize F-actin.* Nat Methods, 2008. **5**(7): p. 605-7.

268. Riese, M.J., et al., *Decreased diacylglycerol metabolism enhances ERK activation and augments CD8+ T cell functional responses.* J Biol Chem, 2011. **286**(7): p. 5254-65.

269. Riha, P. and C.E. Rudd, *CD28 co-signaling in the adaptive immune response.* Self Nonself, 2010. **1**(3): p. 231-240.

270. Rincon, E., et al., *Translocation dynamics of sorting nexin 27 in activated T cells.* J Cell Sci, 2011. **124**(Pt 5): p. 776-88.

271. Rincon, E., et al., *Proteomics identification of sorting nexin 27 as a diacylglycerol kinase zeta-associated protein: new diacylglycerol kinase roles in endocytic recycling.* Mol Cell Proteomics, 2007. **6**(6): p. 1073-87.

272. Roach, A.N., et al., *Phosphatidic acid regulation of PIPKI is critical for actin cytoskeletal reorganization.* J Lipid Res, 2012. **53**(12): p. 2598-609.

273. Robinson, F.L. and J.E. Dixon, *Myotubularin phosphatases: policing 3-phosphoinositides.* Trends Cell Biol, 2006. **16**(8): p. 403-12.

274. Roose, J.P., et al., *A diacylglycerol-protein kinase C-RasGRP1 pathway directs Ras activation upon antigen receptor stimulation of T cells.* Mol Cell Biol, 2005. **25**(11): p. 4426-41.

275. Roose, J.P., et al., *Unusual interplay of two types of Ras activators, RasGRP and SOS, establishes sensitive and robust Ras activation in lymphocytes.* Mol Cell Biol, 2007. **27**(7): p. 2732-45.

276. Ropers, F., et al., *Identification of a novel candidate gene for non-syndromic autosomal recessive intellectual disability: the WASH complex member SWIP.* Hum Mol Genet, 2011. **20**(13): p. 2585-90.
277. Sakane, F., et al., *Diacylglycerol kinases as emerging potential drug targets for a variety of diseases.* Curr Drug Targets, 2008. **9**(8): p. 626-40.
278. Sakurai-Yageta, M., et al., *The interaction of IQGAP1 with the exocyst complex is required for tumor cell invasion downstream of Cdc42 and RhoA.* J Cell Biol, 2008. **181**(6): p. 985-98.
279. Sancak, Y., et al., *The Rag GTPases bind raptor and mediate amino acid signaling to mTORC1.* Science, 2008. **320**(5882): p. 1496-501.
280. Sancho, D., M. Gomez, and F. Sanchez-Madrid, *CD69 is an immunoregulatory molecule induced following activation.* Trends Immunol, 2005. **26**(3): p. 136-40.
281. Santos, T., et al., *Dynamics of diacylglycerol kinase zeta translocation in living T-cells. Study of the structural domain requirements for translocation and activity.* J Biol Chem, 2002. **277**(33): p. 30300-9.
282. Schafer, I.B., et al., *The binding of Varp to VAMP7 traps VAMP7 in a closed, fusogenically inactive conformation.* Nat Struct Mol Biol, 2012. **19**(12): p. 1300-9.
283. Schenck, A., et al., *The endosomal protein Appl1 mediates Akt substrate specificity and cell survival in vertebrate development.* Cell, 2008. **133**(3): p. 486-97.
284. Schoumacher, M., et al., *Actin, microtubules, and vimentin intermediate filaments cooperate for elongation of invadopodia.* J Cell Biol, 2010. **189**(3): p. 541-56.
285. Schu, P.V., et al., *Phosphatidylinositol 3-kinase encoded by yeast VPS34 gene essential for protein sorting.* Science, 1993. **260**(5104): p. 88-91.
286. Scita, G. and P.P. Di Fiore, *The endocytic matrix.* Nature, 2010. **463**(7280): p. 464-73.
287. Seaman, M.N., et al., *Membrane recruitment of the cargo-selective retromer subcomplex is catalysed by the small GTPase Rab7 and inhibited by the Rab-GAP TBC1D5.* J Cell Sci, 2009. **122**(Pt 14): p. 2371-82.
288. Seo, J., et al., *Regulation of hippocampal long-term potentiation and long-term depression by diacylglycerol kinase zeta.* Hippocampus, 2012. **22**(5): p. 1018-26.
289. Shahnazari, S., et al., *A diacylglycerol-dependent signaling pathway contributes to regulation of antibacterial autophagy.* Cell Host Microbe, 2010. **8**(2): p. 137-46.
290. Shan, X., et al., *Deficiency of PTEN in Jurkat T cells causes constitutive localization of Itk to the plasma membrane and hyperresponsiveness to CD3 stimulation.* Mol Cell Biol, 2000. **20**(18): p. 6945-57.
291. Sharma, V.P., et al., *Tks5 and SHIP2 regulate invadopodium maturation, but not initiation, in breast carcinoma cells.* Curr Biol, 2013. **23**(21): p. 2079-89.
292. Sherman, E., et al., *Functional nanoscale organization of signaling molecules downstream of the T cell antigen receptor.* Immunity, 2011. **35**(5): p. 705-20.

293. Shimizu, Y., L. Taraborrelli, and H. Walczak, *Linear ubiquitination in immunity.* Immunol Rev, 2015. **266**(1): p. 190-207.

294. Shin, H.W., et al., *An enzymatic cascade of Rab5 effectors regulates phosphoinositide turnover in the endocytic pathway.* J Cell Biol, 2005. **170**(4): p. 607-18.

295. Shisheva, A., *PIKfyve: Partners, significance, debates and paradoxes.* Cell Biol Int, 2008. **32**(6): p. 591-604.

296. Sigismund, S., et al., *Endocytosis and signaling: cell logistics shape the eukaryotic cell plan.* Physiol Rev, 2012. **92**(1): p. 273-366.

297. Siliceo, M. and I. Merida, *T cell receptor-dependent tyrosine phosphorylation of beta2-chimaerin modulates its Rac-GAP function in T cells.* J Biol Chem, 2009. **284**(17): p. 11354-63.

298. Sinclair, L.V., et al., *Control of amino-acid transport by antigen receptors coordinates the metabolic reprogramming essential for T cell differentiation.* Nat Immunol, 2013. **14**(5): p. 500-8.

299. Singh, D., et al., *Connexin 43 interacts with zona occludens-1 and -2 proteins in a cell cycle stage-specific manner.* J Biol Chem, 2005. **280**(34): p. 30416-21.

300. Singh, V., et al., *Sorting nexin 27 regulates basal and stimulated brush border trafficking of NHE3.* Mol Biol Cell, 2015. **26**(11): p. 2030-43.

301. Small, S.A., et al., *Model-guided microarray implicates the retromer complex in Alzheimer's disease.* Ann Neurol, 2005. **58**(6): p. 909-19.

302. Soares, H., et al., *Regulated vesicle fusion generates signaling nanoterritories that control T cell activation at the immunological synapse.* J Exp Med, 2013. **210**(11): p. 2415-33.

303. Sorkin, A. and M. von Zastrow, *Endocytosis and signalling: intertwining molecular networks.* Nat Rev Mol Cell Biol, 2009. **10**(9): p. 609-22.

304. Sowa, M.E., et al., *Defining the human deubiquitinating enzyme interaction landscape.* Cell, 2009. **138**(2): p. 389-403.

305. Stahelin, R.V., et al., *Mechanism of membrane binding of the phospholipase D1 PX domain.* J Biol Chem, 2004. **279**(52): p. 54918-26.

306. Staudinger, J., J. Lu, and E.N. Olson, *Specific interaction of the PDZ domain protein PICK1 with the COOH terminus of protein kinase C-alpha.* J Biol Chem, 1997. **272**(51): p. 32019-24.

307. Steffen, A., et al., *MT1-MMP-dependent invasion is regulated by TI-VAMP/VAMP7.* Curr Biol, 2008. **18**(12): p. 926-31.

308. Steinberg, F., et al., *A global analysis of SNX27-retromer assembly and cargo specificity reveals a function in glucose and metal ion transport.* Nat Cell Biol, 2013. **15**(5): p. 461-71.

309. Steinberg, F., et al., *SNX17 protects integrins from degradation by sorting between lysosomal and recycling pathways.* J Cell Biol, 2012. **197**(2): p. 219-30.

310. Stinchcombe, J.C. and G.M. Griffiths, *Communication, the centrosome and the immunological synapse.* Philos Trans R Soc Lond B Biol Sci, 2014. **369**(1650).
311. Stinchcombe, J.C., et al., *Centrosome polarization delivers secretory granules to the immunological synapse.* Nature, 2006. **443**(7110): p. 462-5.
312. Stinchcombe, J.C., et al., *Centriole polarisation to the immunological synapse directs secretion from cytolytic cells of both the innate and adaptive immune systems.* BMC Biol, 2011. **9**: p. 45.
313. Sun, L., et al., *Sorting nexin 27 interacts with Fzd7 and mediates Wnt signalling.* Biosci Rep, 2016. **36**(1).
314. Sun, Y., et al., *Phosphatidylinositol (4,5) bisphosphate controls T cell activation by regulating T cell rigidity and organization.* PLoS One, 2011. **6**(11): p. e27227.
315. Sun, Y., et al., *Type I gamma phosphatidylinositol phosphate kinase modulates invasion and proliferation and its expression correlates with poor prognosis in breast cancer.* Breast Cancer Res, 2010. **12**(1): p. R6.
316. Talhouk, R.S., et al., *Heterocellular interaction enhances recruitment of alpha and beta-catenins and ZO-2 into functional gap-junction complexes and induces gap junction-dependant differentiation of mammary epithelial cells.* Exp Cell Res, 2008. **314**(18): p. 3275-91.
317. Tan, S.M., *The leucocyte beta2 (CD18) integrins: the structure, functional regulation and signalling properties.* Biosci Rep, 2012. **32**(3): p. 241-69.
318. Tang, C.J., et al., *CPAP is a cell-cycle regulated protein that controls centriole length.* Nat Cell Biol, 2009. **11**(7): p. 825-31.
319. Teasdale, R.D. and B.M. Collins, *Insights into the PX (phox-homology) domain and SNX (sorting nexin) protein families: structures, functions and roles in disease.* Biochem J, 2012. **441**(1): p. 39-59.
320. Tello-Lafoz, M., et al., *A role for novel lipid interactions in the dynamic recruitment of SNX27 to the T-cell immune synapse.* Bioarchitecture, 2014. **4**(6): p. 215-20.
321. Temkin, P., et al., *SNX27 mediates retromer tubule entry and endosome-to-plasma membrane trafficking of signalling receptors.* Nat Cell Biol, 2011. **13**(6): p. 715-21.
322. Thapa, N., et al., *Phosphoinositide signaling regulates the exocyst complex and polarized integrin trafficking in directionally migrating cells.* Dev Cell, 2012. **22**(1): p. 116-30.
323. Topham, M.K., et al., *Protein kinase C regulates the nuclear localization of diacylglycerol kinase-zeta.* Nature, 1998. **394**(6694): p. 697-700.
324. Topham, M.K. and S.M. Prescott, *Diacylglycerol kinase zeta regulates Ras activation by a novel mechanism.* J Cell Biol, 2001. **152**(6): p. 1135-43.
325. Torres-Ayuso, P., et al., *Diacylglycerol kinase-zeta regulates mTORC1 and lipogenic metabolism in cancer cells through SREBP-1.* Oncogenesis, 2015. **4**: p. e164.

326. Tseng, H.Y., et al., *Sorting nexin 31 binds multiple beta integrin cytoplasmic domains and regulates beta1 integrin surface levels and stability.* J Mol Biol, 2014. **426**(18): p. 3180-94.

327. Ulrich, F. and C.P. Heisenberg, *Trafficking and cell migration.* Traffic, 2009. **10**(7): p. 811-8.

328. Valdes, J.L., et al., *Sorting nexin 27 protein regulates trafficking of a p21-activated kinase (PAK) interacting exchange factor (beta-Pix)-G protein-coupled receptor kinase interacting protein (GIT) complex via a PDZ domain interaction.* J Biol Chem, 2011. **286**(45): p. 39403-16.

329. Valdmanis, P.N., et al., *Mutations in the KIAA0196 gene at the SPG8 locus cause hereditary spastic paraplegia.* Am J Hum Genet, 2007. **80**(1): p. 152-61.

330. van den Bout, I. and N. Divecha, *PIP5K-driven PtdIns(4,5)P2 synthesis: regulation and cellular functions.* J Cell Sci, 2009. **122**(Pt 21): p. 3837-50.

331. Varma, R., et al., *T cell receptor-proximal signals are sustained in peripheral microclusters and terminated in the central supramolecular activation cluster.* Immunity, 2006. **25**(1): p. 117-27.

332. Vicente-Manzanares, M., C.K. Choi, and A.R. Horwitz, *Integrins in cell migration--the actin connection.* J Cell Sci, 2009. **122**(Pt 2): p. 199-206.

333. Vicinanza, M., et al., *Function and dysfunction of the PI system in membrane trafficking.* EMBO J, 2008. **27**(19): p. 2457-70.

334. Vilarino-Guell, C., et al., *DNAJC13 mutations in Parkinson disease.* Hum Mol Genet, 2014. **23**(7): p. 1794-801.

335. Vilarino-Guell, C., et al., *VPS35 mutations in Parkinson disease.* Am J Hum Genet, 2011. **89**(1): p. 162-7.

336. Vizcaino, J.A., et al., *2016 update of the PRIDE database and its related tools.* Nucleic Acids Res, 2016. **44**(D1): p. D447-56.

337. von Andrian, U.H. and T.R. Mempel, *Homing and cellular traffic in lymph nodes.* Nat Rev Immunol, 2003. **3**(11): p. 867-78.

338. Waickman, A.T. and J.D. Powell, *Mammalian target of rapamycin integrates diverse inputs to guide the outcome of antigen recognition in T cells.* J Immunol, 2012. **188**(10): p. 4721-9.

339. Wang, C., et al., *Regulation of Integrin beta 1 recycling to lipid rafts by Rab1a to promote cell migration.* J Biol Chem, 2010. **285**(38): p. 29398-405.

340. Wang, R., et al., *Lipid rafts control human melanoma cell migration by regulating focal adhesion disassembly.* Biochim Biophys Acta, 2013. **1833**(12): p. 3195-205.

341. Wang, X., et al., *Sorting nexin 27 regulates Abeta production through modulating gamma-secretase activity.* Cell Rep, 2014. **9**(3): p. 1023-33.

342. Wang, X., et al., *Loss of sorting nexin 27 contributes to excitatory synaptic dysfunction by modulating glutamate receptor recycling in Down's syndrome.* Nat Med, 2013. **19**(4): p. 473-80.

343. Wang, Y.B., et al., *Adaptor protein APPL1 couples synaptic NMDA receptor with neuronal prosurvival phosphatidylinositol 3-kinase/Akt pathway.* J Neurosci, 2012. **32**(35): p. 11919-29.

344. Wen, P.J., et al., *Ca2+-regulated pool of phosphatidylinositol-3-phosphate produced by phosphatidylinositol 3-kinase C2alpha on neurosecretory vesicles.* Mol Biol Cell, 2008. **19**(12): p. 5593-603.

345. Wernimont, S.A., et al., *Adhesions ring: a structural comparison between podosomes and the immune synapse.* Eur J Cell Biol, 2008. **87**(8-9): p. 507-15.

346. Wiederschain, D., et al., *Single-vector inducible lentiviral RNAi system for oncology target validation.* Cell Cycle, 2009. **8**(3): p. 498-504.

347. Wierda, K.D., et al., *Interdependence of PKC-dependent and PKC-independent pathways for presynaptic plasticity.* Neuron, 2007. **54**(2): p. 275-90.

348. Xie, S., N. Naslavsky, and S. Caplan, *Diacylglycerol kinase alpha regulates tubular recycling endosome biogenesis and major histocompatibility complex class I recycling.* J Biol Chem, 2014. **289**(46): p. 31914-26.

349. Xu, Z., et al., *The inducible expression of the tumor suppressor gene PTEN promotes apoptosis and decreases cell size by inhibiting the PI3K/Akt pathway in Jurkat T cells.* Cell Growth Differ, 2002. **13**(7): p. 285-96.

350. Yamaguchi, H. and T. Oikawa, *Membrane lipids in invadopodia and podosomes: key structures for cancer invasion and metastasis.* Oncotarget, 2010. **1**(5): p. 320-8.

351. Yamaguchi, H., et al., *Phosphoinositide 3-kinase signaling pathway mediated by p110alpha regulates invadopodia formation.* J Cell Biol, 2011. **193**(7): p. 1275-88.

352. Yang, J.S., et al., *A role for phosphatidic acid in COPI vesicle fission yields insights into Golgi maintenance.* Nat Cell Biol, 2008. **10**(10): p. 1146-53.

353. Yang, X. and T. Xu, *Molecular mechanism of size control in development and human diseases.* Cell Res, 2011. **21**(5): p. 715-29.

354. Ye, F. and M. Zhang, *Structures and target recognition modes of PDZ domains: recurring themes and emerging pictures.* Biochem J, 2013. **455**(1): p. 1-14.

355. Yi, J., et al., *Actin retrograde flow and actomyosin II arc contraction drive receptor cluster dynamics at the immunological synapse in Jurkat T cells.* Mol Biol Cell, 2012. **23**(5): p. 834-52.

356. Yoon, M.S., et al., *Class III PI-3-kinase activates phospholipase D in an amino acid-sensing mTORC1 pathway.* J Cell Biol, 2011. **195**(3): p. 435-47.

357. You, J.S., J.W. Frey, and T.A. Hornberger, *Mechanical stimulation induces mTOR signaling via an ERK-independent mechanism: implications for a direct activation of mTOR by phosphatidic acid.* PLoS One, 2012. **7**(10): p. e47258.

358. You, J.S., et al., *The role of diacylglycerol kinase zeta and phosphatidic acid in the mechanical activation of mammalian target of rapamycin (mTOR) signaling and skeletal muscle hypertrophy.* J Biol Chem, 2014. **289**(3): p. 1551-63.

359. Yu, X. and L.M. Machesky, *Cells assemble invadopodia-like structures and invade into matrigel in a matrix metalloprotease dependent manner in the circular invasion assay.* PLoS One, 2012. **7**(2): p. e30605.

360. Zech, T., et al., *The Arp2/3 activator WASH regulates alpha5beta1-integrin-mediated invasive migration.* J Cell Sci, 2011. **124**(Pt 22): p. 3753-9.

361. Zhan, F., et al., *CKS1B, overexpressed in aggressive disease, regulates multiple myeloma growth and survival through SKP2- and p27Kip1-dependent and -independent mechanisms.* Blood, 2007. **109**(11): p. 4995-5001.

362. Zhang, Y., et al., *Structural and functional analysis of the ligand specificity of the HtrA2/Omi PDZ domain.* Protein Sci, 2007. **16**(8): p. 1738-50.

363. Zhao, X., et al., *Dominant-negative behavior of mammalian Vps35 in yeast requires a conserved PRLYL motif involved in retromer assembly.* Traffic, 2007. **8**(12): p. 1829-40.

364. Zheng, Y., et al., *A role for mammalian target of rapamycin in regulating T cell activation versus anergy.* J Immunol, 2007. **178**(4): p. 2163-70.

365. Zhong, X.P., et al., *Enhanced T cell responses due to diacylglycerol kinase zeta deficiency.* Nat Immunol, 2003. **4**(9): p. 882-90.

366. Zimmerman, S.P., et al., *Sorting nexin 27 (SNX27) associates with zonula occludens-2 (ZO-2) and modulates the epithelial tight junction.* Biochem J, 2013. **455**(1): p. 95-106.

367. Zoncu, R., et al., *A phosphoinositide switch controls the maturation and signaling properties of APPL endosomes.* Cell, 2009. **136**(6): p. 1110-21.

Appendix

IX. APPENDIX

1. SNX27 data from cBioPortal for Cancer Genomics [49, 113]

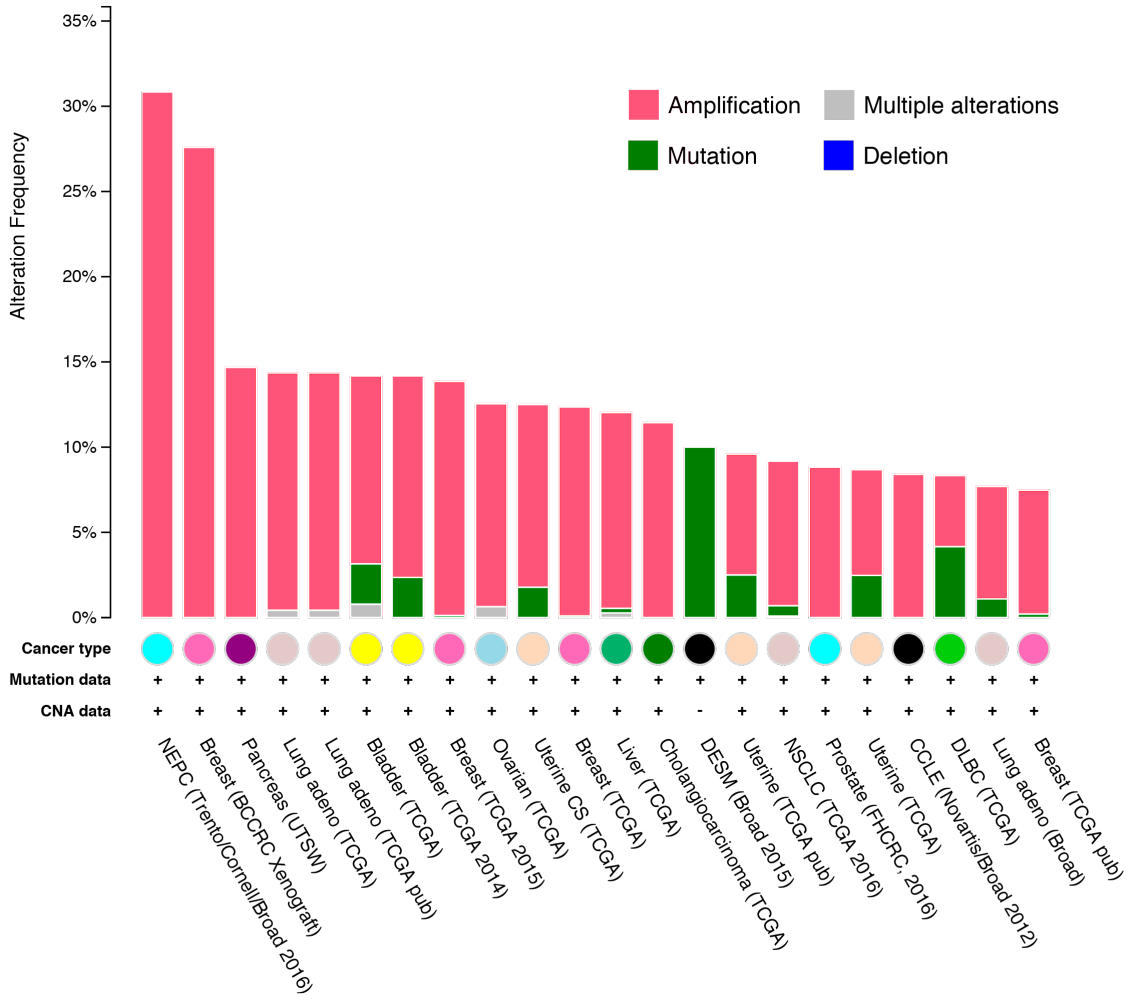

2. Analysis of SNX27 PtdInsP-binding capacity [118]

Thermodynamic parameters for the binding of PtdInsPs with SNX27 by ITC[a]

Protein	PI lipid[b]	K_d (μM)	ΔH (kcal/mol)	$T\Delta S$ (kcal/mol)	ΔG (kcal/mol)	N[d]
SNX27	PI3*P*	7.0 ± 4.0	−3.8 ± 1.9	2.2 ± 1.0	−6.0 ± 0.9	0.9 ± 0.5
	PI(3,4)P_2	4.6 ± 0.5	−3.2 ± 0.4	3.9 ± 0.11	−4.0 ± 0.7	1.0 ± 0.0
	PI(3,5)P_2	3.0 ± 0.1	−1.9 ± 1.4	5.5 ± 1.3	−7.4 ± 0.0	1.0
	PI(4,5)P_2	3.6 ± 3.3	−3.1 ± 1.2	4.3 ± 1.8	−7.4 ± 0.6	1.1 ± 0.2
	PI(3,4,5)P_3	3.8 ± 0.1	−2.6 ± 0.1	4.7 ± 0.0	−7.3 ± 0.0	1.1 ± 0.1
SNX27ΔPDZ	PI3*P*	3.4 ± 0.3	−3.7 ± 0.1	3.6 ± 0.6	−7.3 ± 0.5	1.0
	PI(3,4)P_2	11.5 ± 2.2	−6.7 ± 1.7	1.26 ± 0.3	−7.5 ± 1.2	1.0
	PI(3,5)P_2	15.0 ± 2.7	−4.5 ± 4.8	3.2 ± 2.9	−7.7 ± 1.9	1.0
	PI(4,5)P_2	11.4 ± 7.1	−5.7 ± 1.8	1.1 ± 2.0	−6.8 ± 0.2	1.1 ± 0.1
	PI(3,4,5)P_3	11.4 ± 3.0	−4.5 ± 3.3	2.2 ± 3.2	−6.7 ± 0.2	1.0
SNX27 FERM	PI3*P*	> 100	−1.7 ± 0.2	1.3 ± 1.4	−3.0 ± 1.7	1.0 ± 0.0
	PI(3,4)P_2	3.4 ± 1.4	−2.7 ± 0.0	4.7 ± 0.2	−7.4 ± 0.2	1.1 ± 0.1
	PI(3,5)P_2	2.8 ± 0.6	−1.4 ± 0.1	5.4 ± 0.7	−6.8 ± 0.5	1.0
	PI(4,5)P_2	4.9 ± 0.3	−3.9 ± 1.2	3.2 ± 1.2	−7.2 ± 0.0	1.0
	PI(3,4,5)P_3	4.0 ± 0.7	−2.7 ± 0.0	4.5 ± 0.1	−7.3 ± 0.1	1.0
SNX27(R490E)	PI3*P*	4.1 ± 2.0	−4.2 ± 1.0	3.1 ± 0.7	−7.3 ± 0.2	1.0 ± 0.1
	PI(3,4)P_2	NB[c]				
	PI(3,5)P_2	NB[c]				
	PI(4,5)P_2	NB[c]				
	PI(3,4,5)P_3	NB[c]				
SNX27(R496E)	PI3*P*	2.2 ± 0.2	−4.8 ± 1.8	6.5 ± 8.1	−14.6 ± 10.2	1.1 ± 0.1
	PI(3,4)P_2	NB[c]				
	PI(3,5)P_2	NB[c]				
	PI(4,5)P_2	NB[c]				
	PI(3,4,5)P_3	NB[c]				
SNX27(RRK/E)	PI3*P*	2.1 ± 1.3	−4.0 ± 0.9	2.4 ± 2.1	−7.7 ± 0.1	1.1 ± 0.1
	PI(3,4)P_2	NB[c]				
	PI(3,5)P_2	NB[c]				
	PI(4,5)P_2	NB[c]				
	PI(3,4,5)P_3	NB[c]				
SNX27(R1196A/Y197A)	PI3*P*	NB[c]				
	PI(3,4,5)P_3	7.7 ± 0.5	−1.6 ± 0.3	5.1 ± 1.7	6.7 ± 2.1	1.1 ± 0.2

a. Each experiment was perfomed at least 2-3 times. Errors show standard deviation (SD).
b. PIs incorporated a water soluble diC8 acyl chain.
c. NB = no binding detectable.
d. In cases where no error is given for the stoichiometry, it has been fixed as 1.0 to prevent over-fitting of the data.

3. Links to videos and supplemental tables

Video 1 related to Figure R3: Relative dynamics of IS recruitment of GFP-SNX27 and the RRK/E mutant

https://www.dropbox.com/s/rdc4bfc7q8x9tfk/video1.mov?dl=0

Video 2 related to Figure R7: Relative dynamics of IS recruitment of GFP-SNX27 and the PDZ mutant

https://www.dropbox.com/s/xwgeege3m4tlotn/video2.mov?dl=0

Video 3 related to Figure R10: Relative dynamics of IS recruitment of Cherry-SNX27 and GFP-CD63

https://www.dropbox.com/s/xapnkqxthnta8vt/video3.mov?dl=0

Video 4 related to Figure R14: Dynamics of IS recruitment of GFP-ZO-2

https://www.dropbox.com/s/pnnnevpwyjgo23q/video4.mov?dl=0

Video 5 related to Figure R14: Dynamics of IS recruitment of GFP-ZO2 relative to actin polymerization

https://www.dropbox.com/s/u22t54zsx4m7cu2/video5.mov?dl=0

Video 6 related to Figure R15: Relative dynamics of IS recruitment of GFP-ZO-2 and Cherry-SNX27

https://www.dropbox.com/s/s1ce8s8cbqucyls/video6.mov?dl=0

Video 7 related to Figure R15: Relative dynamics of IS recruitment of GFP-ZO-1 and Cherry-SNX27

https://www.dropbox.com/s/m28k7hps09ids9r/video7.mov?dl=0

Video 8 related to Results section 4: Dynamics of GFP-SNX27 relative to actin polymerization in invadopodia-forming MDA-MB-231 cells

https://www.dropbox.com/s/lg4q78kvusf65qd/Video8.avi?dl=0

Video 9 related to Results section 4: Dynamics of GFP-SNX27 in MDA-MB-231 cells invading during CIA assay

https://www.dropbox.com/s/rbvm5vuv8xc21qo/Video9.avi?dl=0

Supplemental Tables S1-S6 related to Figure R8

Sheet1: Table S1. Complete report of identified proteins in all samples

Sheet2: Table S2. Identified proteins in GFP control samples

Sheet3: Table S3. Identified proteins in GFP-SNX27 WT samples

Sheet4: Table S4. Identified proteins in GFP-SNX27 H114A

Sheet5: Table S5. Identified proteins in both GFP-SNX27 WT and H114A samples

Sheet6: Table S6. Gene Ontology (GO) enrichment analysis of PDZ-independent SNX27 interactors

https://www.dropbox.com/s/bba6n7kg80c1b8x/Supplemental%20Tables%20S1-S6.xlsx?dl=0

4. Published articles

4.1. Ghai *et al*, 2015[118]

4.2. Tello-Lafoz *et al*, 2015[320]

4.3. Torres-Ayuso *et al*, 2015[325]

4.4. Clairfeuille *et al*, 2016 [60]